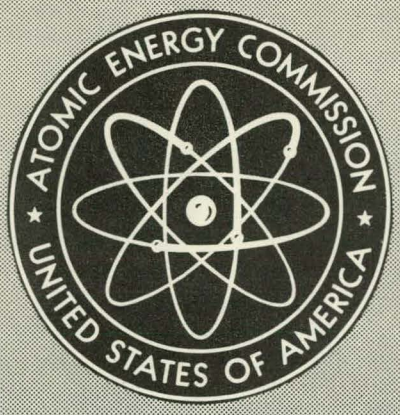

GEAP-4024

NUCLEAR SUPERHEAT PROJECT TENTH QUARTERLY PROGRESS REPORT, OCTOBER–DECEMBER 1961

By
R. T. Pennington

July 1962
[DTI Issuance Date]

Atomic Power Equipment Department
General Electric Company
San Jose, California

UNITED STATES ATOMIC ENERGY COMMISSION • DIVISION OF TECHNICAL INFORMATION

DISCLAIMER

LEGAL NOTICE

USAEC Division of Technical Information Extension, Oak Ridge, Tennessee

GEAP-4024

REACTOR TECHNOLOGY

NUCLEAR SUPERHEAT PROJECT

TENTH QUARTERLY PROGRESS REPORT

October - December, 1961

prepared for

THE U.S. ATOMIC ENERGY COMMISSION

under

CONTRACT NO. AT(04-3)-189, PROJECT AGREEMENT #13

by

R. T. Pennington

Atomic Power Equipment Department

GENERAL ELECTRIC COMPANY

San Jose, California

CONTRIBUTORS

R. T. Pennington — Project Engineer
Nuclear Superheat Project

S. F. Armour
H. N. Bass
R. F. Boyle
F. J. Brutschy
G. Brynsvold
J. T. Cochran
C. O. Coffer
R. M. Cohen
F. A. Comprelli
M. L. Couchman
D. Douglass
E. L. Esch
T. F. Evans
M. D. Fitzsimmons
G. G. Gaul
R. Hackney
V. E. Hazel
K. Hikido
R. L. Holladay
H. F. Johnston
R. F. Kirby
S. Levy
M. F. Lyons
J. McClaughry
I. L. Marburger
T. B. Murdock
W. L. Pearl
G. T. Peterson
E. E. Polomik
W. R. Raymont
H. P. Rebman
A. B. Reynolds
G. F. Rieger
J. I. Riesland
D. R. Riley
J. E. Rinde
C. H. Robbins
J. M. Roberts
J. F. Rowe
R. A. Schmidt
C. M. Shields
M. Siegler
C. N. Spalaris
A. Silvester
J. Taylor
F. G. Warzek
B. Wolfe

TABLE OF CONTENTS

			Page No.
1.0		INTRODUCTION AND SUMMARY	1
1.1		Introduction	1
1.2		Summary	3
	1.2.1	Task A - Conceptual Design and Program Evaluation	3
	1.2.2	Task B - Fuel Technology	3
	1.2.3	Task C - Materials Development	4
	1.2.4	Task D - Experimental Physics	5
	1.2.5	Task E - Coolant Chemistry	5
	1.2.6	Task F - Heat Transfer	6
	1.2.7	Task G - Mechanical Development	6
	1.2.8	Task H - SADE and E-SADE	6
	1.2.9	Task J - Mixed Spectrum Superheat Study	7
2.0		TASK A - CONCEPTUAL DESIGN AND PROGRAM EVALUATION	9
2.1		Program Evaluation	
	2.1.1	Introduction	9
	2.1.2	Results by Tasks	9
2.2		Conceptual Design Studies	16
	2.2.1	Engineering Physics Analysis	16
	2.2.2	Reactor Conceptual Design Studies	19
3.0		TASK B - FUEL TECHNOLOGY	26
3.1		Irradiation Tests	26
3.2		Post-Irradiation Examinations	31
	3.2.1	SH-4 Evaluations	31
	3.2.2	SH-4C Evaluations	32
3.3		Fuel Design and Fabrication	34
	3.3.1	Fuel for SADE, SH-6	34
	3.3.2	Fuel Design for E-SADE, ESH-2	48
	3.3.3	Fuel Fabrication for ESH-1	51
	3.3.4	Pellet Fabrication	51
	3.3.5	Non-Destructure Inspection	53
	3.3.6	Fretting Corrosion Tests	53
4.0		TASK C - MATERIALS DEVELOPMENT	54
4.1		Alternate Clad Program	
	4.1.1	Phase I - Literature Survey	54
	4.1.2	Conclusions of the Literature Survey	58
	4.1.3	Procurement of Alternate Cladding Materials	61
	4.1.4	Evaluation of 300 Series Stainless Steel Tubing	62
	4.1.5	Fabricability Testing for Alternate Cladding Materials	63
4.2		Strain Cycling Experiments	63
	4.2.1	Strain Cycle Tests - Laboratory Experiments	63
	4.2.2	Strain Cycling Under Irradiation	64

TABLE OF CONTENTS (CON'D)

			Page No.
5.0		TASK D - EXPERIMENTAL PHYSICS	69
5.1		AEC Superheat Critical Experiments	69
	5.1.1	Summary from GEAP-3882	69
5.2		ESADA-VESR Preliminary Critical Experiment Program	74
	5.2.1	Summary	74
	5.2.2	Comparison of Experimental Results with Predictions	74
6.0		TASK E - COOLANT CHEMISTRY	77
6.1		Out-of-Pile Evaluations	77
	6.1.1	General Corrosion	77
	6.1.2	Chloride Stress Corrosion Studies	77
	6.1.3	Inspection of Stress Corrosion Samples	80
	6.1.4	Oxygen-Hydrogen Recombination Studies	94
6.2		SADE Evaluations	94
	6.2.1	Summary	94
	6.2.2	In-Pile Evaluations on SH-5A	94
7.0		TASK F - HEAT TRANSFER	98
7.1		Summary	98
7.2		Task F-2, Heat Transfer to Superheated Steam	98
7.3		Fretting Corrosion	100
7.4		Superheated Steam Pressure Drops - E-SADE Element	101
7.5		Superheated Steam Pressure Drops - Dummy Cluster (3 Wire) Element	101
8.0		TASK G - MECHANICAL DEVELOPMENT	102
8.1		Steam Separator Development	102
	8.1.1	Summary	102
	8.1.2	Discussion	102
	8.1.3	Test Program	103
8.2		Seal Development	103
	8.2.1	Leak Test of Superheat Seal	103
	8.2.2	Leak Test of Superheat Seal	104
	8.2.3	Corrosion Test	104
9.0		TASK H - SADE AND E-SADE	106
9.1		SADE	106
	9.1.1	Summary	106
	9.1.2	SH-4C Irradiation	106
	9.1.3	SH-5A	106
	9.1.4	NUSU Irradiation	114
	9.1.5	SH-1 Irradiation	126
	9.1.6	SH-6 Design Conditions	129
9.2		E-SADE	133
	9.2.1	E-SADE Installation and Construction Status	133
	9.2.2	E-SADE Fuel Bundles	136

TABLE OF CONTENTS (CON'D)

			Page No.
	9.2.3	Power Scalloping - ESH-1 Fuel Bundle	137
	9.2.4	E-SADE Special Handling Equipment	142
	9.2.5	E-SADE Safeguards Status	162
10.0		TASK J - MIXED SPECTRUM SUPERHEATER DESIGN STUDY	165
10.1		Prototype Design	165
10.2		Safety-Core Meltdown Studies	167
10.3		Test Reactor Meltdown Excursions and Resultant Energy Releases (FARM I)	167
	10.3.1	Introduction	167
	10.3.2	Problem	168
	10.3.3		
	10.3.4	Problem Approximation	168
	10.3.5	Equations	170
	10.3.6	Initial and Boundary Conditions	183
	10.3.7	Notation	186
10.4		Critical Facility Design	188
10.5		Mixed Spectrum Superheater Critical Experiment Preliminary Hazards Evaluation	188
	10.5.1	Description of the Core	188
	10.5.2	Differences Between the New Core and the Old Core	193
	10.5.3	Excursion Types	194
	10.5.4	Calculated Excursions	196
	10.5.5	Maximum Credible Accident	197
	10.5.6	Conclusions	200

LIST OF ILLUSTRATIONS

Figure No.	Title	Page No.
2.1	Single Pass Superheat Reactor	21
3.1	Warpage Measurements SH-4C	35
3.2	I.D. Measurements SH-4C	36
3.3	O.D. Measurements SH-4C	37
3.4	Circumferential Crack SH-4C	38
3.5	Intergranular Attack of Clad	39
3.6	Intergranular Attack of Clad	40
3.7	"Gumdrop" Monitor for UO_2 Expansion	41
3.8	Fuel Assembly, Lower End	46
3.9	Fuel Assembly, Upper End	46
3.10	Scalloped Liner	46
3.11	Flow Tube with Liner	46
	142F170	43
	142F141	44
	141F979	49
	762D660	50
4.1	Strain Cycle Tests	65
6.1	Corrosion of Type 316 Stainless Steel	81
6.2	Corrosion of Type 316 Stainless Steel	81
6.3	Corrosion of Type 347 Stainless Steel	82
6.4	Corrosion of Type 347 Stainless Steel	82
6.5	Corrosion of Type 406 Stainless Steel	83
6.6	Corrosion of Type 406 Stainless Steel	83
6.7	Corrosion of Incoloy Alloy	84
6.8	Corrosion of Incoloy Alloy	84
6.9	Corrosion of Type 406 Stainless Steel	85

LIST OF ILLUSTRATIONS (CON'D)

Figure No.	Title	Page No.
6.10	Corrosion of Type 406 Stainless Steel	85
6.11	Type RA-330 Surface Condition	88
6.12	Type RA-330 Surface Condition	88
6.13	Incoloy Surface Condition	89
6.14	Incoloy Surface Condition	89
6.15	Incoloy Scale Formation	90
6.16	Incoloy Microstructure	90
6.17	Type 406 Surface Condition	91
6.18	Type 406 Scale Formation	91
6.19	Type 406 Microstructure	92
9.1	Fuel Element SH-5A	111
9.2	Process Tube	112
9.3	SH-5A Element Power Plot	113
9.4	NUSU Element Power Plot	117
9.5	NUSU Design Values	118
9.6	NUSU Superheat Experiment	121
9.7	NUSU Superheat Experiment	122
9.8	SH-1 Element Power Plot	128
9.9	SH-1 Element Temperature Distribution	130
9.10	SH-1 Element Heat Loss	131
9.11	Fuel Rod Cluster SH-6	134
9.12	Fuel Assembly SH-6	135
9.13	Nine Element Fuel Assembly	138
9.14	SHNEE Test Coupling	139
9.15	Nine Element Fuel Assembly	140

LIST OF ILLUSTRATIONS (CON'D)

Figure No.	Title	Page No.
9.16	VBWR Core Configuration, ESH-1	141
9.17	ESH-1 Power Distribution - Position A Outside Surface	143
9.18	ESH-1 Power Distribution - Position A Inside Surface	144
9.19	ESH-1 Power Distribution - Position B Outside Surface	145
9.20	ESH-1 Power Distribution - Position B Inside Surface	146
9.21	ESH-1 Power Distribution - Position C Outside Surface	147
9.22	ESH-1 Power Distribution - Position C Inside Surface	148
9.23	ESH-1 Power Distribution - Position D Outside Surface	149
9.24	ESH-1 Power Distribution - Position D Inside Surface	150
9.25	ESH-1 Power Distribution - Position E Outside Surface	151
9.26	ESH-1 Power Distribution - Position E Inside Surface	152
9.27	ESH-1 Power Distribution - Position F Outside Surface	153
9.28	ESH-1 Power Distribution - Position F Inside Surface	154
9.29	ESH-1 Power Distribution - Position G Outside Surface	155
9.30	ESH-1 Power Distribution - Position G Inside Surface	156
9.31	ESH-1 Power Distribution - Position H Outside Surface	157
9.32	ESH-1 Power Distribution - Position H Inside Surface	158
9.33	ESH-1 Power Distribution - Position I Outside Surface	159
9.34	ESH-1 Power Distribution - Position I Inside Surface	160
9.35	ESH 1 Thermal Neutron Flux	161
9.36	SHNEE Hoist	163
9.37	SHNEE Transfer Track	164
10.1	Incremental Vaporization Process	174
10.2	MSSR Critical Facility	190
10.3	MSSR Core Cross Section	191
10.4	MSSR Fast Core Fuel Element Schematic	192

LIST OF TABLES

Table No.	Title	Page No.
3.1	Design and Fabrication SH-5A	27
3.2	Irradiation History SH-5A	30
3.3	Corrosion Film and Crud Analysis SH-4 Fuel	32
4.1	Alternate Cladding Material Availability	62
4.2	Irradiation Schedule - Strain Cycle Tests	67
5.1	Comparison of Model Predictions with Experiment	71
5.2	Thermal Utilization	74
6.1	Superheat Exposures in CL-1	78
6.2	Stress Failures in CL-1 Heater Sheaths	79
6.3	Stress Corrosion Tests	80
6.4	Tubular Constant Stress Fixtures Exposed to Nuclear Superheat Environment	86
6.5	Weight Gains for Corrosion Coupons	87
7.1	Heat Transfer Data	99
7.2	Exposure Conditions for E-SADE Prototype	100
9.1	SH-5A Design Operating Conditions	109
9.2	NUSU Design Operating Conditions	119
9.3	NUSU Alarm and Scram Settings	120
9.4	SH-1 Design Operating Conditions	127
9.5	SH-6 Design Operating Conditions	132
9.6	SH-6 Alarm and Scram Settings	133
10.1	75 MWe MSSR Reactor Data	165

1.0 INTRODUCTION AND SUMMARY

1.1 Introduction

This is the tenth of a series of quarterly reports which will cover the progress and results from the conceptual design, economic evaluations and research and development work performed by the General Electric Company as part of the Nuclear Superheat Project under Contract AT(04-3)-189, Project Agreement No. 13. The following list of progress reports and topical reports have been published as a result of thie work.

GEAP-3290, First Quarterly Progress Report, July - September, 1959

GEAP-3319, Superheat Process Tube Heat Transfer Tests

GEAP-3371, Second Quarterly Progress Report, October - December, 1959

GEAP-3387, Fabrication, Irradiation and Evaluation of Superheat Fuel Elements

GEAP-3468, Third Quarterly Progress Report, January - March, 1960

GEAP-3538, Fourth Quarterly Progress Report, April - June, 1960

GEAP-3563, Interim Report on Steam Dryer Development

GEAP-3564, Results of Air-Water Steam-Water Tests on Primary Steam Separators - October, 1960

GEAP-3581, Fifth Quarterly Progress Report, July - September, 1960

GEAP-3589, Economic Study for 300 MW(e) Separate Superheat Reactor

GEAP-3590, Economic Study of the Mixed Spectrum Superheater

GEAP-3591, Manufacture of the Adhesive Bonded AEC Superheat Critical Fuel

GEAP-3633, Economic Study for 300 MW(e) Once-Through Superheat Reactor

GEAP-3686, Sixth Quarterly Progress Report, October - December, 1960

GEAP-3698, Erosion Experiments of Powder Compacted Uranium Dioxide Under Dynamic Steam Flow

GEAP-3703, Heat Transfer Coefficients with Annular Flow During "Once-Through" Boiling of Water to 100 Per Cent Quality at 800, 1100, and 1400 psi

GEAP-3724, Seventh Quarterly Progress Report, January - March, 1961

GEAP-3737, Flood Safety of The Mixed Spectrum Superheater

GEAP-3739, Plastic Strain in Thin Fuel Element Cladding Due to UO_2 Thermal Expansion

GEAP-3778, A Simulated Superheat Reactor Corrosion Facility

GEAP-3785, Eighth Quarterly Progress Report June - August, 1961

GEAP-3787, Results of Air-Water and Steam-Water Tests on Radial Vane Steam Separator Models

GEAP-3796, Design, Fabrication and Irradiation of Superheat Fuel Element SH-4B in VBWR

GEAP-3779, Corrosion of Type 304 Stainless Steel in Simulated Superheat Reactor Environments

GEAP-3875, Materials for Nuclear Superheat Applications, A Literature Survey

GEAP-3877, Ninth Quarterly Progress Report, July - September, 1961

Section I of the First Quarterly Report (GEAP-3290) presented a description of the Nuclear Superheat Project including objectives, approach to the problem and expected results by individual task. The following tabulation of task titles is listed for easy reference.

TASK A - Conceptual Design and Program Evaluation

TASK B - Fuel Technology

TASK C - Materials Development

TASK D - Experimental Physics

TASK E - Coolant Chemistry

TASK F - Heat Transfer

TASK G - Mechanical Development

TASK H - SADE & E-SADE

TASK J - Mixed Spectrum Superheat Study

1.2 Summary

The following section provides a brief summary of significant results by task for this reporting period. Section 2.1 provides a brief summary of significant results by task for the total program since the initiation of the Nuclear Superheat Project.

1.2.1 TASK A - Conceptual Design and Program Evaluation

Conceptual design effort has concentrated on the design of a large separate superheat reactor for a 600 MWe plant. The reactor design concept is based on the use of either a single-pass annular fuel element or a 7-rod cluster fuel element. Plant and reactor data summary is listed is Section 2.2.

1.2.2 TASK B - Fuel Technology

During this reporting period a 0.016" thick stainless steel clad annular fuel element was irradiated in the SADE loop. A maximum exit temperature recorded was 845°F with a maximum power of 83 KW(t). Activity release measurements during irradiation in the SADE loop were a factor of at least 300 less than those found in SH-4B or SH-4C, indicating that there is a very small leak in the cladding or a slight UO_2 surface contamination. Comparison of SH-5A operation with former in-service failures of superheat fuel elements indicates that if a clad defect exists it is not similar in nature to the large gross defects observed in SH-4B or SH-4C.

Post-irradiation examinations of SH-4 fuel element indicate that there was a significant amount of chloride deposited in the corrosion film on the fuel element. Since the SH-4 fuel element did not develop a clad defect, one may conclude that chloride stress cracking may have occurred during subsequent irradiation and that chloride stress cracking is highly statistical in nature.

Post-irradiation examination of SH-4C fuel element, which developed a defect on the inside clad surface, indicates that there is no evidence of fretting corrosion between the fuel cladding and the wire wrapped spacer. In addition, post-irradiation examinations indicated that chlorides were found in the vicinity of the failed portion, that the wire wrapped spacer had failed either during irradiation or during removal of the fuel, and that there was a significant increase in length of the fuel element. This fuel element growth has not been observed in previous irradiations.

1.2.3 TASK C - Materials Development

A topical report, "Materials for Nuclear Superheat Applications, A Literature Survey," GEAP 3875, was completed. This literature survey was initiated to investigate the possibility of developing an alternate cladding material for superheat fuel application. The results of this literature survey were listed in Section 4.1. Based on this survey, two possible directions seem to be apparent for reducing the susceptibility of superheat fuel cladding to chloride stress cracking. These are to reduce the impurity level in stainless steel and to utilize cladding

materials having either a very low or very high nickel content.

Bench tests were completed for eleven specimens utilizing the equipment intended to perform strain cycling of Type 304 stainless steel in the GETR reactor.

1.2.4 TASK D - Experimental Physcis

A topical report, GEAP 3882, "AEC Superheat Critical - A Comparison of Experiment and Theory of Uniform Lattices," is in the final stages of preparation.

The experimental measurements on the ESADA-VESR Preliminary Critical Experiment Program were completed. The work during this period consisted of analyzing data and preparation of a topical report.

1.2.5 TASK E - Coolant Chemistry

A topical report, GEAP 3779, "Corrosion of Type 304 Stainless Steel in Simulated Superheat Reactor Environments" has been issued. The series of chloride stress corrosion tests initiated in September with 1.5 ppm of sodium chloride in the circulating water and stressed heater sheaths has been continued. Two stress cracking failures have occurred in the superheated steam corrosion test loop; however, both of these failures occurred on stressed heater sheaths in low temperature regions. As a result of these two failures and since it has not been possible to reproduce chloride stress cracking in the high temperature sheaths, the superheat corrosion test loop is being programmed

to operate under simulated SADE exposure conditions which will provide temperature and moisture cycling in the heater sheaths.

Isothermal coupons have been exposed to nuclear superheat environment in the corrosion test loop. The materials exposed are Types 304, 316, 347 and 406 stainless steel, Incoloy and RA-330.

Radiochemistry measurements were made on the SADE loop operating with SH-5A fuel element. These measurements indicate that the leakage of fission gases from the SADE fuel element has been less than 0.5 μc/sec and the carryover of the reactor water to the SADE loop, based on NA-24 tracer techniques, has been less than 1.5000.

1.2.6 TASK F - Heat Transfer

Heat transfer tests were performed at high Reynolds numbers. Twenty additional heat transfer data runs were made, however, difficulties were experienced in obtaining steady heater temperature measurements.

1.2.7 TASK G -Mechanical Development

During this report period, efforts were devoted to procurement and air-water testing of a full circle radial separator model.

Six test runs were conducted in the leak test facility on the temperature actuated superheat seal. The results of these tests indicated that the seal concept is feasible.

1.2.8 TASK H - SADE and E-SADE

1.2.8.1 SADE

The SADE irradiation during this reporting period was limited to SH-5A. Because of concern about chloride stress corrosion, modifications to the SADE in-core facility were made to minimize in-leakage of reactor water. These consisted of utilizing a mass spectrometer type in-reactor facility and seal welding of the underwater flange.

The NUSU fuel element was received on December 23, 1961. This fuel element, which is a combination boiling on the outside - superheat on the inside - fuel element, was fabricated by the General Nuclear Engineering Corporation. SADE loop operating conditions and modifications for the NUSU test are detailed in Section 9.1.4.

1.2.8.2 E-SADE

Installation work was performed on E-SADE during VBWR shutdown. The loop installation is approximately 60% completed. However, installation difficulties are anticipated due to higher basement activity in the VBWR enclosure than were formerly anticipated.

1.2.9 TASK J - Mixed Spectrum Superheat Study

The primary effort during this reporting period has been in accumulation of the design, performance and cost information for a 75 MWe MSSR prototype.

A conceptual design of the proposed critical facility for the MSSR concept has been completed and a preliminary hazards review has been held with the Vallecitos Safeguards Council. The conceptual design concept is discussed in detail in Section 10.5.

2.0 TASK A - CONCEPTUAL DESIGN AND PROGRAM EVALUATION

2.1 Program Evaluation

2.1.1 Introduction

The following section is intended to provide a high light summary of the significant results by task on the Nuclear Superheat Project. Progress reports and topical reports initiated as a result of this work are listed in Section 1.0.

2.1.2 Results by Tasks

2.1.2.1 Task A - Conceptual Design

This work has involved conceptual design studies of integral thermal superheat reactors, once-through superheat reactors and separate superheat reactors under Task A and a Mixed Spectrum Superheat Reactor under Task J. The design activity including reactor mechanical design; nuclear physics, hydraulic and thermodynamic analysis; and safety analysis, has established detailed development test requirements for associated Nuclear Superheat Project development activities.

2.1.2.2 Task B - Fuel Technology

Fuel technology work areas have involved design, fabrication and post-irradiation evaluations of fuel elements and fuel capsules to determine performance characteristics under nuclear superheat conditions, and development of fuel fabrication techniques, processs tubes and non-free standing stainless steel fuel cladding. The following significant results have been obtained:

(a) Irradiation of six fuel prototypes, shown in Tablee 3.1 and 3.2.

(b) Fabrication of large quantities of high density, high integrity UO_2 pellets having annular geometry. Development of well controlled techniques for pressing and sintering annular pellets to size.

(c) Fabrication of thin-clad, non self supporting fuel element which was operated successfully at high temperatures for at least 35 days. (SH-5A)

(d) Recognitition of an operational limit for stainless clad fuel elements in steam containing relatively high moisture and slight chloride impurities.

(e) Investigated and determined clad strain levels in annular and rod type fuel elements under short time irradiation, as a function of clad thickness, fabrication parameters and power generation (heat flux).

(f) Developed two promising concepts of process tubes, which are essential in the design of efficient nuclear superheat power plants.

(g) Irradiated three fuel elements at high heat fluxes with clad failures in the VBWR without seriously affecting the reactor operational routine.

2.1.2.3 Task C - Materials Development

Materials Development activities have involved investigations of the basic properties of commercially available stainless steels and conduct of a literature survey to

provide the AEC with a technical basis for selection of alternate cladding materials for nuclear superheat application. The following significant results have been obtained:

(a) A literature survey on alternate cladding materials was completed and the results have been included in a report now in preparation. The conclusions from this report were included in Section 4.1.

(b) An apparatus was designed to study the strain cycle properties of materials in the laboratory and in the reactor at 1300°F. The first reactor experiment is scheduled to begin during the first week in January 1962. Laboratory tests have been carried out successfully using the method developed.

(c) Non destructive techniques were developed to examine incoming tubing for possible flaws which may be the result of fabrication or handling. A statistical evaluation has been completed which relates the degree and number of tubing defects with various types of 300 series austenitic alloys. A limited study was also completed to determine the effect of various tubing flaws and cold work upon the burst strength of tubing.

2.1.2.4 Task D - Experimental Physics

The experimental physics evaluations have included measurements on uniform arrays of annular fuel at several water to fuel ratios as part of Task D and in addition,

performance of a critical experiment for the EVESR reactor. The EVESR critical was performed at no cost to the AEC. The following significant results were obtained:

(a) Significant discrepancies were found between experimental measurements and predictions made utilizing engineering design models that had formerly demonstrated reasonable accuracy in treating boiling water and pressurized water lattices.

(b) These discrepancies were traced to omission of spatial dependence of the thermal spectrum in the boiling water reactor model.

(c) A semi-empirical technique to account for spatial variation of thermal spectrum when normalized to detailed calculations and lattice measurements provided excellent agreement with reactivity and reactivity coefficient measurements.

2.1.2.5 Task E - Coolant Chemistry

The work under Task E has involved in-pile evaluations with the SADE loop and out-of-pile evaluations with the Superheated Steam Corrosion Test Loop.

In-Pile

In-pile coolant chemistry evaluations have included measurement of radiation levels, radiochemical analysis of inlet and outlet steam samples from the SADE loop during operation of sound superheat elements and in-serivce failures. Measurements have also been taken on

coupons installed in the exit steam system of the SADE loop. The accumulation of fission product release data was restricted prior to the irradiation of fuel element SH-5A (see Table 3.2) because the SADE license modification to permit continued operation with defective superheat fuel was not obtained until November 2, 1961. The significant results from the in-pile coolant chemistry evaluations are:

(a) The SADE loop and VBWR reactor were operated within license limits in terms of activity release after loss of cladding integrity for SH-2, SH-4B and SH-4C fuel failures. This conclusion is based on measurements made to identify fuel defect prior to reactor shutdown.

(b) Gaseous fission product release from SH-4C was about 40 microcuries per second and was the same order of magnitude of release measured for boiling water fuel element defects.

(c) Radiochemical analysis of activity on SADE loop coupons indicated that iodine activity was predominant contributor as compared to corrosion product activity in boiling water reactor systems.

Out-of-Pile

The out-of-pile corrosion evaluations have involved experimental determination of corrosion performance for superheat cladding materials under simulated superheat conditions. The first phase of the program resulted in

general corrosion evaluations on Type 304 stainless steel under typical superheat conditions of steam velocity, steam temperature, heat flux and hydrogen and oxygen containing steam. The second phase of the program provides for local corrosion evaluations on Type 304 stainless steel and alternate cladding materials. The loop operating conditions were changed for second phase testing to include 1.5 ppm Cl^- in the circulating water and stressed heater sheaths. During both phases above, isothermal coupons were exposed to 1050°F steam and evaluated. The significant results of the work are as follows:

(a) Table 6.1 summarizes the performance for superheat exposures through December 31, 1962 for the entire program.

(b) During the general corrosion evaluations ten cycles of various duration were accumulated prior to August 25, 1961. During the second phase of the program, six cycles of various duration were performed in an attempt to reproduce chloride stress cracking in the heater sheaths. For each run, test conditions were changed, as compared to the preceding run, in order to enhance susceptibility to chloride stress cracking.

(c) The uniform corrosion rate for Type 304 stainless steel was determined to be satisfactory for superheat application.

(d) The oxygen and hydrogen levels in the loop could not be controlled by batch addition due to recombination

at the heaters. A continuous hydrogen, oxygen decomposer was added to the system.

(e) Chloride stress cracking such as was observed in fuel element testing in SADE, has not been reproduced in the out-of-pile loop with Cl^- addition of 1.5 ppm, specimen stress levels of 25,000 psi and specimen surface temperatures up to 1300°F.

(f) Corrosion screening studies in static and dynamic environments were initiated, using 300 series as well as alternate materials. Experimental results show that under constant stress the uniform corrosion rate of Type 304 stainless at 1050°F steam is 2-4 times greater than the rate of unstressed specimens. AISI 406 exhibited uniform corrosion rates similar to those found for 304, and Incoloy was found to have uniform corrosion rates of about 35 to 40 times less than 304, based upon the weight gain.

2.1.2.6 Task F - Heat Transfer

The work under Task F has involved experimental determination of heat transfer coefficients in an out-of-pile heat transfer loop. The significant results are:

(a) Determination of a semi-empirical relationship to predict heat transfer coefficients in the region of high steam quality.

(b) Determination of a semi-empirical relationship to predict heat transfer coefficients in the region of very high Reynolds numbers (>500,000).

2.1.2.7 Task G - Mechanical Development

Mechanical development work has been involved with two major hardware items. These are steam separators and mechanical, removable seals. In addition, fabrication development work and prototype 9-element tube bundle tests were performed at the Moss Landing Station of P.G. & E. The significant results are:

(a) Performance testing and development work was completed on steam demisters.

(b) Performance testing and development work was done on radial separators. The performance of this type of separator provides a significant improvement over other separators tested.

2.1.2.8 Task H - SADE and E-SADE

A total of six annular fuel elements was irradiated in the SADE loop as shown on Table 3.2. Design and procurement of equipment was completed for the E-SADE facility. Installation of equipment was initiated and is continuing during routine VBWR shutdowns.

2.1.2.9 Task J - Mixed Spectrum Superheat Reactor Study

Design work and analytical work was completed which provides a technical basis for establishing cost incentives and definition of problem areas for the concept.

2.2 Conceptual Design Studies

2.2.1 Engineering Physics Analysis

2.2.1.1 Separate Superheat Power Shaping Studies

During the quarter, a one-dimensional burn-up study of a single-batch core was performed to investigate the feasibility of maintaining a flat radial power profile by means of regional variations in fuel enrichment and erbium content. In this concept the entire batch of fuel would remain fixed in position throughout the fuel life. The key advantage of this concept would be the elimination of frequent fuel movement (with associated steam pipe coupling and de-coupling) that multi-batch reloading would require. This simplification, and possible improvements in power flattening, would be counter-balanced by a fuel cost penalty due to the higher enrichments required for single-batch operation.

The following table summarizes the results of a one-dimensional burn-up analysis for a 12,000 MWD/T single-batch core. This particular case had eight concentric radial fuel zones with a total of four different fuel concentrations. Enrichments varied from 2.6% to 4.5%. The volume-averaged enrichment and erbium to uranium atom ratio were 3.23% and 0.00199, respectively.

MWD/T Burn-up	k_{eff}	Peak-Average Radial Power
0	1.037	1.21
4000	1.062	1.20
8000	1.041	1.13
12000	0.999	1.22

This study pointed out the feasibility of maintaining a reasonably flat radial power distribution in a single-

batch core. Slight variations in erbium distribution were found to have a marked effect on the power shape, however, and fuel concentrations would have to be carefully controlled if this scheme were used. For the same equilibrium discharge exposure, the fuel in a multi-batch core (with partial re-loading) need be enriched to approximately 2.6%. Because of the enrichment penalty (about 0.6%), the single-batch approach was abandoned in the re-design of the large separate superheat reactor.

2.2.1.2 Separate Superheat Re-design

Fuel element size, process tube spacing, and lattice type for the re-designed separate superheat reactor have been tentatively determined using a 16 fuel rod bundle. The control elements, in a "D" type lattice, are on a center-to-center spacing of 9.646 inches, yielding an unflooded water-to-fuel volume ratio of 2.22 and a flooded water-to fuel-ratio of 3.10 with control rods and poison curtains removed. The material for the control rods and poison curtains has been changed from stainless steel to Inconel to obtain the desired shutdown margin.

An initial enrichment of 3.2% U-235 has been chosen which necessitates the use of the poison curtains in the initial core in addition to the 0.1% atom fraction of erbium that is included in the fuel. Maximum cold unflooding reactivity (controls withdrawn) was found to be less than 1% Δk while the maximum hot flooding effect (controls ganged)

was calculated to be in excess of 5.0% Δk. Further optimization of the lattice to minimize the flooding-unflooding accident problem will be attempted. Work is also in progress to determine the core burn-up characteristics and to evaluate the temperature and void coefficients.

2.2.2 Reactor Conceptual Design Studies

2.2.2.1 Summary

Conceptual design effort has concentrated on the design of a large Separate Superheater for a 600 MWE plant. This reactor design is based on the use of a single pass annular fuel element. Another reactor design will be made for a seven rod cluster fuel element. These two designs, their performance and estimated plant costs, will be reported in a separate topical report.

2.2.2.2 Size Selection

The boiling water-separate superheat reactor can be used for very large power plants. The size has been selected on the basis of using the largest boiling water reactor that can be built with today's reactor technology. This maximum size is approximately equivalent to a 400 MWE boiling water reactor plant. When a separate superheat reactor is added, the combined unit rating is 600 MWE.

The boiling water reactor is a single cycle, forced recirculation reactor with internal steam separation.

2.2.2.3 Turbine Selection

The steam turbine will be a 1800 RPM unit with four flow exhaust. The last stage buckets size is 38 in. A two shaft, cross-compound, unit, will be used. A tandem compound unit for throttle conditions of 900°F, 965 psia, and 4,970,000 #/hr steam flow, must be designed for large clearances to accommodate the expansion of its longer shaft.

A cross-compound unit with shorter shafts, can employ lower clearances and hence its operation efficiency is higher. A cross-compound unit for 900°F steam will have a turbine heat rate of 9,010 Btu/hr.

2.2.2.4 Separate Superheat Reactor

The separate superheat reactor is a single pass reactor. Saturated steam flows from the top of the vessel down pass the fuel elements. The superheated steam is collected in a large steam plenum at the bottom of the reactor and exits through nozzles in the side of the reactor vessel. The preliminary design of this reactor is shown on Drawing 56064-847, Figure 2.1.

This reactor design differs from previous designs in the following ways:

(a) The saturated steam entrance pipe is an integral part of the fuel assembly; former designs used a clamp type seal. The elimination of the entrance seals prevents leakage of water into the fuel element.

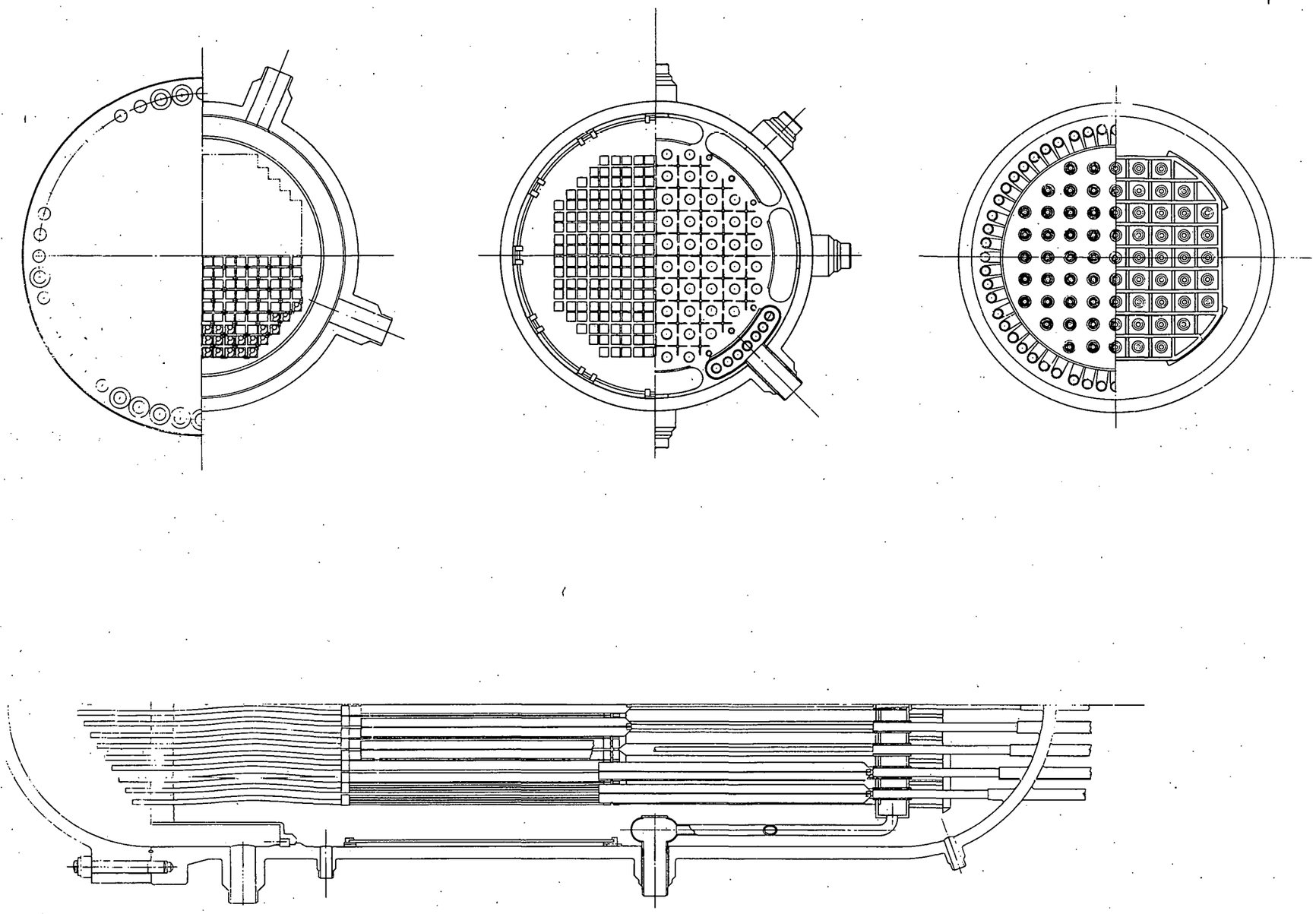

Figure 2.1

The only seal is located downstream of the fuel element; such leakage will not produce corrosion problems.

(b) The fuel element bundle size has been reduced from a 7 by 7 array of annular elements to a 4 by 4 array. The 4 by 4 bundle is approximately $4\frac{1}{2}$ inches square. The small fuel bundle reduces the importance of any refueling accidents.

(c) The control rods have been changed to small cruciform shaped control rods in order to reduce the severity of any control rod accidents.

(d) The exit steam plenum has been changed from multi-six inch pipes to one large steam plenum. This larger plenum can handle the high steam flow with lower steam pressure drop; the large steam plenum also permits the vessel height to be reduced.

(e) The reactor design is based on the use of a single annular, single-pass fuel element. With the type of fuel element, the division of heat between the inner and outer steam flow passages is a major design problem. The division of heat between inner and outer steam passages will change with time for several reasons. One reason is that more plutonium is created at the outside edge of the fuel pellet and the center of heat generation must shift toward the outer edge of the fuel pellet. A second reason is that the gap between the fuel pellet and the

inside cladding will change with creep of the inner cladding. These factors were sufficiently important to initiate the study of a fuel element composed of seven solid rods.

2.2.2.5 Plant and Reactor Data Summary

(1) General Data

(a)	Reactor types	Single cycle boiling water reactor is pressure vessel and superheat reactor in separate pressure vessel
(b)	Nuclear moderator	Light water
(c)	Fuel	UO_2 pellets
(d)	Cladding	Stainless steel
(e)	Coolant	Light water and steam

(2) Plant Data

(a)	Gross electrical output	600 MWE
(b)	Net electrical output	582 MWE
(c)	Turbine throttle pressure	965 psia
(d)	Turbine throttle temp.	900°F
(e)	Turbine throttle flow	4,948,000 #/hr
(f)	Net plant heat rate	9,443 Btu/KWH
(g)	Net plant efficiency	36.2%

(3) Boiling Water Reactor

(a)	Total thermal power	1202.0 MW
(b)	Core height	135 in.
(c)	Core equivalent diameter	138 in.

(d) Average core power density 36.3 KW/l

(e) Reactor vessel

Height	53.4 ft.
Inside diameter	192 in.

(f) Steam separator — Internal, radial flow

(g) Recirculation

Type	Forced
Flow	49,700,000 #/hr.
Number of loops	5

(h) Steam flow — 4,977,000 #/hr.

(i) Water/fuel ratio — 2.6

(j) Fuel bundle

Number	594
Size	4.6 in. x 4.6 in.
Rods per bundle	49

(k) Fuel Rod

Type	UO_2 pellets
Pellet diameter	0.420 in.
Clad O.D.	0.443 in.
Clad material	Stainless steel

(l) Control rods

Number	145
Shape	Cruciform
Size	8 in. x 3/8 in.

(4) <u>Superheat Reactor</u>

(a) Total thermal power — 408.3 MW

(b) Core height — 96 in.

(c) Equivalent core diameter — 95 in.

(d) Average core power density — 37.3 KW/l

(e) Reactor vessel

Height	38.5 ft.
Inside diameter	126 in.

(f) Fuel bundle

Number	284
Size	4.5 x 4.5 in.
Rods per bundle	16

(g) Fuel rod

Type	UO_2 annular pellets
Pellet diameter	.700 in. O.D.
	.260 in. I.D.
Clad material	Stainless steel

(h) Control rods

Number	69
Shape	Cruciform
Size	8 in. x 3/8 in.

3.0 TASK B - FUEL TECHNOLOGY

3.1 Irradiation Tests

Fuel element SH-5A, a .016" clad, annular design swaged over the pellets for support, was irradiated during this period. The flow passages between the fuel walls and the surrounding process tube are maintained by point spacers attached to the process tube by plug welding. The instrument tube is identical to that used with SH-4C, filled with specimens selected, cut and premachined to study material physical properties as a function of irradiation exposure to high temperature steam. The plenum support for this fuel element was designed and fabricated in such a way as to provide clad support even in the event the fuel loading moves in relation to the clad.

The fuel element was inserted in SADE loop November 11 and the irradiation testing began November 13. The maximum exit steam temperature recorded was 845°F, maximum power 83 KW, and the length of irradiation as of December 31 was approximately 770 hours. The number of power cycles from 40 KW or greater was 24 throughout December for a total of 34 throughout the run. Activity release measurements were a factor of at least 300 less than those found in SH-4B or SH-4C, showing that either there is a very small leak in the cladding which did not progress with power cycling, or slight UO_2 surface contamination. Apparently, if a type of clad defect exists, it is not similar in nature to the large defects found in SH-4B and SH-4C, as it does not interfere with the normal reactor startup or routine operations.

Details of the irradiation performance of SH-5A are shown in Tables 3.1 and 3.2.

TABLE 3.1

DESIGN AND FABRICATION DATA

	SH-1	SH-2	SH-4B	SH-4	SH-4C	SH-5A
Process tube	304	304	304	304	304	304
O.D.	1.660"	1.660"	1.660"	1.660"	1.660"	1.660"
Wall thickness	0.109"	0.109"	0.109"	0.109"	0.109"	0.109"
Steam gap, first pass (cold)	0.096"	0.096"	0.096"	0.096"	0.096"	0.096"
Outer clad	304	304	304	304	304	304
O.D.	1.250"	1.250"	1.250"	1.250"	1.250"	1.250"
Wall thickness	0.049"	0.049"	0.028"	0.028"	0.028"	0.016"
UO_2 (% enrichment)	2.3%	2.3%	4.5%	3.5%	3.5%	4.0%
O.D.	1.151 $\pm$ .001	1.151 $\pm$ .001	1.194 $\pm$ .0005	1.190 $^{+\ 0.005}_{-\ 0.000}$	1.190 $^{+\ 0.004}_{-\ 0.000}$	Not compiled
I.D.	.750 $^{+\ .005}_{-\ .000}$	.750 $^{+\ .005}_{-\ .000}$	.755 $^{+\ .009}_{-\ .000}$	.753 $^{+\ 0.011}_{-\ 0.000}$	.757 $^{+\ 0.008}_{-\ 0.000}$	Not compiled
Weighted inside diametral fuel-clad gap (cold)	Not determined	Not determined	7.5 mils	5.4 mils	7.0 mils	Not determined
Inner clad	347	347	304	304	304	304
O.D.	.750"	.750"	.750"	.750"	.750"	.750"
Wall thickness	.035"	.035"	.028"	.028"	.028"	.016"
Steam gap, second pass (cold)	.153"	.153"	.097"	.097"	.097"	.109"
Instrument tube O.D.	.375"	.375"	.500"	.500"	.500"	.500"
Active fuel length	36"	36"	36"	36"	36"	36"
Power (KW)	50	50	100	100	73	78
Power density (KW/KG)	16.7	16.7	26.6	26.6	18.3	18.2

TABLE 3.1

DESIGN AND FABRICATION DATA (Page 2)

	SH-1	SE-2	SH-4B	SH-4	SH-4C	SH-5A
Fuel section inlet temp., °F	545	545	545	545	545	575
Max. clad temp. (STEADY), °F	1070	1070	1200	1200	1200	1200
Max. clad temp. (TRANSIENT) °F	--	--	1292	1292	1300	1300
Max. superheat temp., fuel exit (STEADY), °F	825	825	925	900	915	845
Max. superheat temp., heater exit (STEADY), °F	825	825	925	925	915	803
Max. superheat temp., fuel exit (TRANSIENT), °F	--	--	980	980	980	910
Max. heat flux (STEADY), Btu/hr-ft^2	200,000	200,000	332,000	332,000	276,000	289,000
Max. heat flux (TRANSIENT), Btu/hr-ft^2	--	--	332,000	332,000	276,000	289,000
Min. steam flow rate (STEADY), lbs/hr	730	730	1032	1032	795	1180
Min. steam flow rate (TRANSIENT), lbs/hr	--	--	915	915	690	1030
Max. fuel temp. (STEADY) °F	2080	2080	3030	3030	2700	2770
Max. fuel temp. (TRANSIENT) °F	--	--	3120	3120	2800	2860
Design drawing	141F657G1	141F607G1	141F785G2	141F785G1	762D438G1	762D437G1
Outer clad spacer	Fin (4)	Fin (4)	Fin (4)	Fin (4)	S. wire (3)	Pin (4) - Attached to process tube
Instrument tube or velocity tube spacer	Fin (4)	Fin (4)	Fin (4)	Fin (4)	Fin (4)	Fin (4)

TABLE 3.1
DESIGN AND FABRICATION DATA (Page 3)

	SH-1	SH-2	SH-4B	SH-4	SH-4C	SH-5A
Inert Z_r O_2 spacers	yes	yes	yes	yes	no	no
Bellows	none	yes	none	none	none	none
Gum-drop (UO_2 expansion monitor)	none	none	yes	yes	yes	none
Outer clad F = free standing, NF - non-free standing	F	F	marginal	marginal	marginal	NF

TABLE 3.2

IRRADIATION HISTORY

	SH-1	SH-2	SH-4B	SH-4	SH-4C	SH-5A
Total irradiation time, hrs.	Not compiled	Not compiled	617	864	492	845 to 1/1/62
Approximate irradiation period (START)	7-31-59	5-1-59	1-15 & 4-24-51	6-7-61	8-28-61	11-13-61
Approximate irradiation period (END)	9-15-59	6-30-59	1-29 & 5-25-51	8-20-61	9-23-61	on test
Exposure, MWD/T (APPROX)	440	440	327	456	371	346 to 1/1/62
Estimated max. clad temp. (STEADY), °F	≈950	≈1050	1350 to 1500*	1350 to 1500*	1200 to 1350*	1150 to 1300*
Max. superheat exit temp. (STEADY), °F	825	825	900	875	830	845
Estimated max. heat flux (STEADY), Btu/hr-ft^2 **	216,000	176,000	356,000	240,000	240,000	265,000
Estimated max. power (KW)**	54.5	44	94	68	64	75
Reason for termination of test	VBWR modification	Failure	Failure	Scheduled	Failure on test	1/1/62
Chloride corrosion detected	Not measured	Not measured	Yes	Cl detected in corrosion film	Yes	
Position and cause of failure	--	Crack in bellows - probably caused by inadequate or defective bellows.	Pinhole defects adjacent to middle spacer - longitudinal split defect about 2" below middle spacer - corrosion attack - predominantly intergranular.	--	Circumferential crack near the top of inside clad - brittle failure.	
Fabrication, irradiation & evaluation reports	GEAP-3211 GEAP-3387	GEAP-3211 GEAP-3387	GEAP-3796	--	--	

* Values take into account the lower fuel-to-clad contact coefficient of 150 Btu/hr-ft^2-°F, a flux skewing factor of approximately 1.3, and a film temperature correction on the steam film coefficient. The temperature exists over a length of about 4 inches and a circumferential arc of at least 30 degrees.

** The values given should be accurate to within ± 5%.

3.2 Post-Irradiation Examinations

3.2.1 SH-4 Evaluations

SH-4 is a .028", 304 stainless clad UO_2 fuel element which was exposed in SADE-VBWR for 36 days at significant power levels for an average accumulated exposure of 570 MWD/T. It was subjected to 31 power cycles but no failure occurred throughout the reactor exposure. No destructive examination was performed or is presently planned for this element. It is of particular significance that the chloride concentration on the surfaces approaches that found in SH-4B. X-ray diffraction analysis of the corrosion film removed from the clad surface exhibited a similar pattern to that found in Cl-1 heater tubes where iron, nickel, copper and chromium chlorides were identified.

Detailed pre- and post-irradiation dimensional measurements were given in the Ninth Quarterly report for SH-4.

After irradiation, three corrosion plus crud and one crud sample were taken for chloride ion analysis. The first three samples were removed by scraping a 4-inch section of the outer cladding around the complete periphery. The fourth sample, containing crud only, was removed from the entire I.D. bore using a cotton swab. Results are tabulated in Table 3.3.

Because a portion of each sample was lost in an accident, no sample weight was possible for the slight amount of sample remaining without risk of losing additional material. Thus, the same weights are rough estimates.

Table 3.3

CORROSION FILM AND CRUD ANALYSIS, SH-4 FUEL

Sample	Location	Type	Estimated Sample Wt - gms	gm Cl^- per Sample	Estimated ppm Cl^-	Crud Sampling Area - in^2
#1	8" to 12" from top weld on fuel section O.D.	corro. + crud	<1000	9.2	>9,000	~4.9
#2	0" to 4" below center fin, fuel section O.D.	corro. +	<1000	5.0	>5,000	~4.9
#3	0" to 4" above bottom fin, fuel section O.D.	corro. +	<1000	9.6	>9,000	~4.9
#4	Entire inner bore - I.D.	crud	<4000	38.2	>9,000	~15.2

It is significant that the "crud only" sample contained at least as much chloride ion as the "corrosion plus crud" samples. This suggests the crud layer is the collection area of the chloride ion as seen by the fuel element.

3.2.2 SH-4C Evaluations

Irradiation highlights for this fuel element are included in Table 3.2. During assembly in SADE, wire spacers used in this fuel element were filed sown to permit assembly. This occurrence minimized the value of performance information with regard to the fuel spacing technique. After removal from its process tube, two of the three spacer wires were found broken at the bottom of the fuel element just above, but away from, the weld. The third wire was broken about 6" from the bottom end. Since the fuel element had to be forcibly removed from the process tube after irradiation, it is not known when the wires broke. Two of the

wires had shiny ends, indicating failure after irradiation (during removal of fuel from tube). The other wire end was covered with loose crud, but this could have collected during removal as it was scraping the process tube interior walls.

No evidence of fretting corrosion was found on the surface of the fuel element, indicating that the spacing scheme of end plug attached wires was satisfactory from this point of view. The difficulty in inserting the fuel element in the process tube, and subsequent hand filing of the wire spacers to a depth of 0.015" made post-irradiation evaluation difficult. It may be summarized that:

1. The possible notch effects resulting from the hand filing operation on the wire spacers complicates evaluation of all the fractures, particularly the apparent complete break.

2. Partial fracture adjacent to the lower weld area indicates that this point is vulnerable to cyclic thermal and vibrational stresses. This indicates that the procedure of welding wire ends after passage <u>through</u> the end plug sockets is a proper corrective approach.

3. Apparent operation of the element <u>after</u> a complete break in one wire spacer (with no measurable flow or pressure drop differences) is encouraging with respect to gross flow blockage problems.

Post-irradiation examination of SH-4C included dimensional measurements, crud collection and analysis for chlorides and metallographic inspection of the failed section and the plenum void to measure UO_2 measurement.

Chemical analysis of the crud for chloride content indicated 6.9 gms/sample, removed from 0.2 $in.^2$, or 34.5 micrograms of chloride ion per square inch. Dimensional measurements show permanent bow of the fuel element of about 0.3 inches. Results are shown in Figures 3.1, 3.2 and 3.3. Visual examination disclosed the failure to be located in the inner clad wall, about 3" from the exit, the crack being circumferential around 360°. Figure 3.4. Chlorides were found in the vicinity of the failed portion, 35 micrograms of chloride per square inch of fuel element surface.

There was an overall increase in length of about 0.3 inches, a decrease in outside diameter of 10 mils due to uniform clad collapse over the pellets and no change in the inside diameter. There was a bow in the fuel element of about 0.25 to 0.3 inches maximum.

Metallographic examination of the defected region revealed severe intergranular attack, with many secondary adjacent cracks similar to those observed in SH-4B. Figures 3.5 and 3.6.

The gum-drop monitor, included in SH-4C to detect UO_2 measurement revealed the same results obtained from SH-4B, in that the UO_2 column was displaced downward approximately 0.050 inches. Figure 3.7.

3.3 Fuel Design and Fabrication

3.3.1 Fuel for SADE, SH-6

A rod cluster has been designed and fabricated for the SADE loop. This fuel rod cluster has been designated SH-6 and will be used

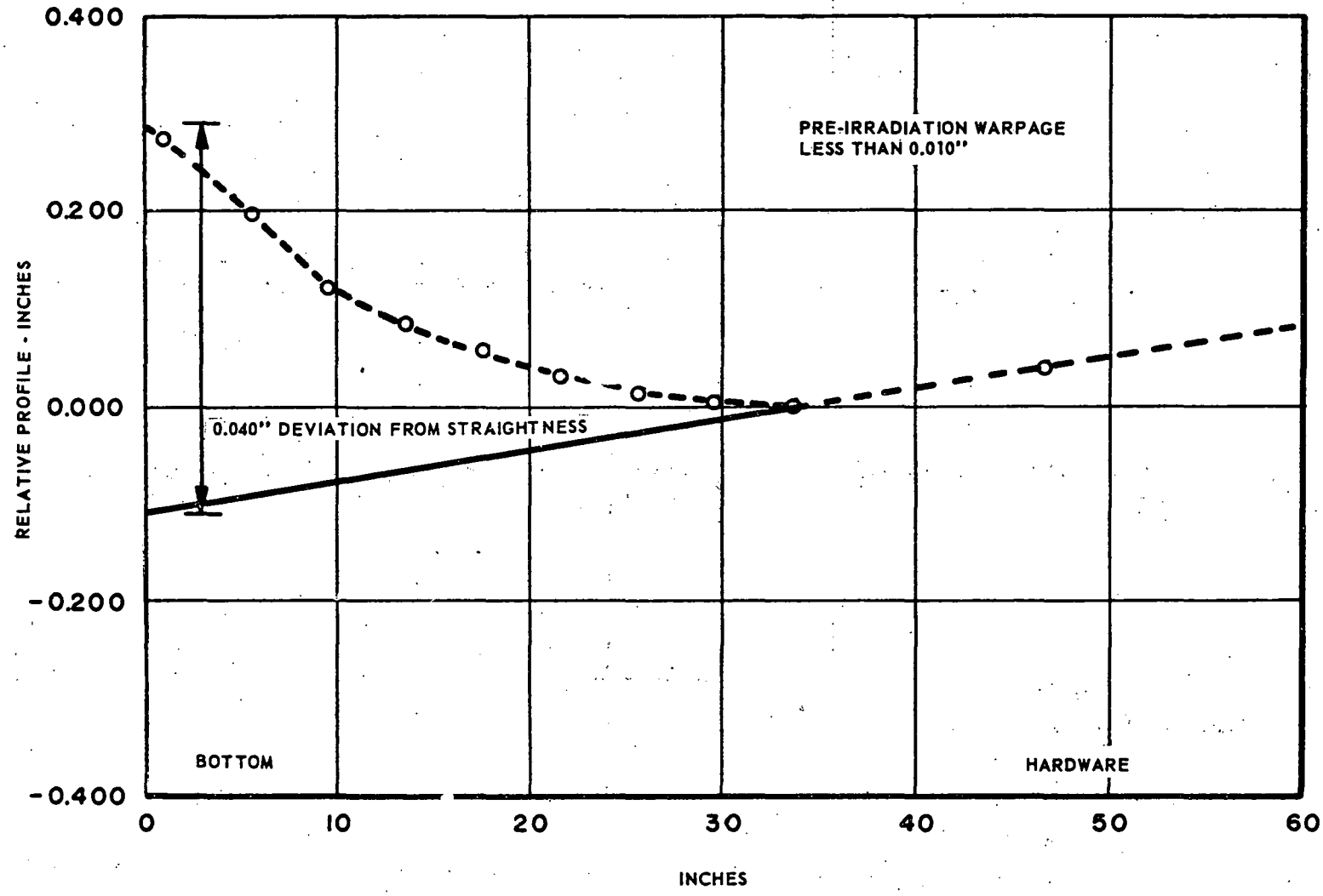

FIGURE 3.1
SH-4C
WARPAGE MEASUREMENTS
315°ORIENTATION-MAXIMUM BOW

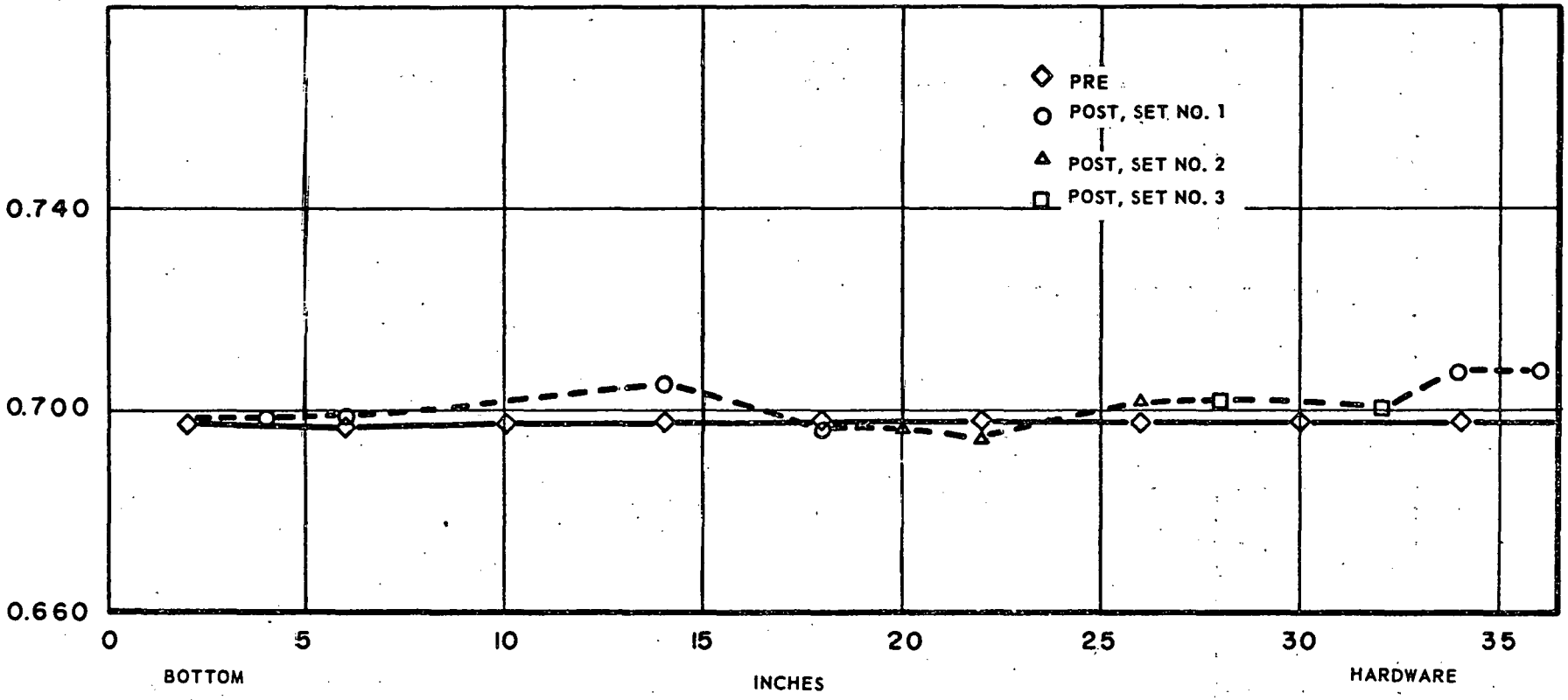

MEASUREMENTS IN INCHES

FIGURE 3.2
SH-4C
INSIDE DIAMETER MEASUREMENTS

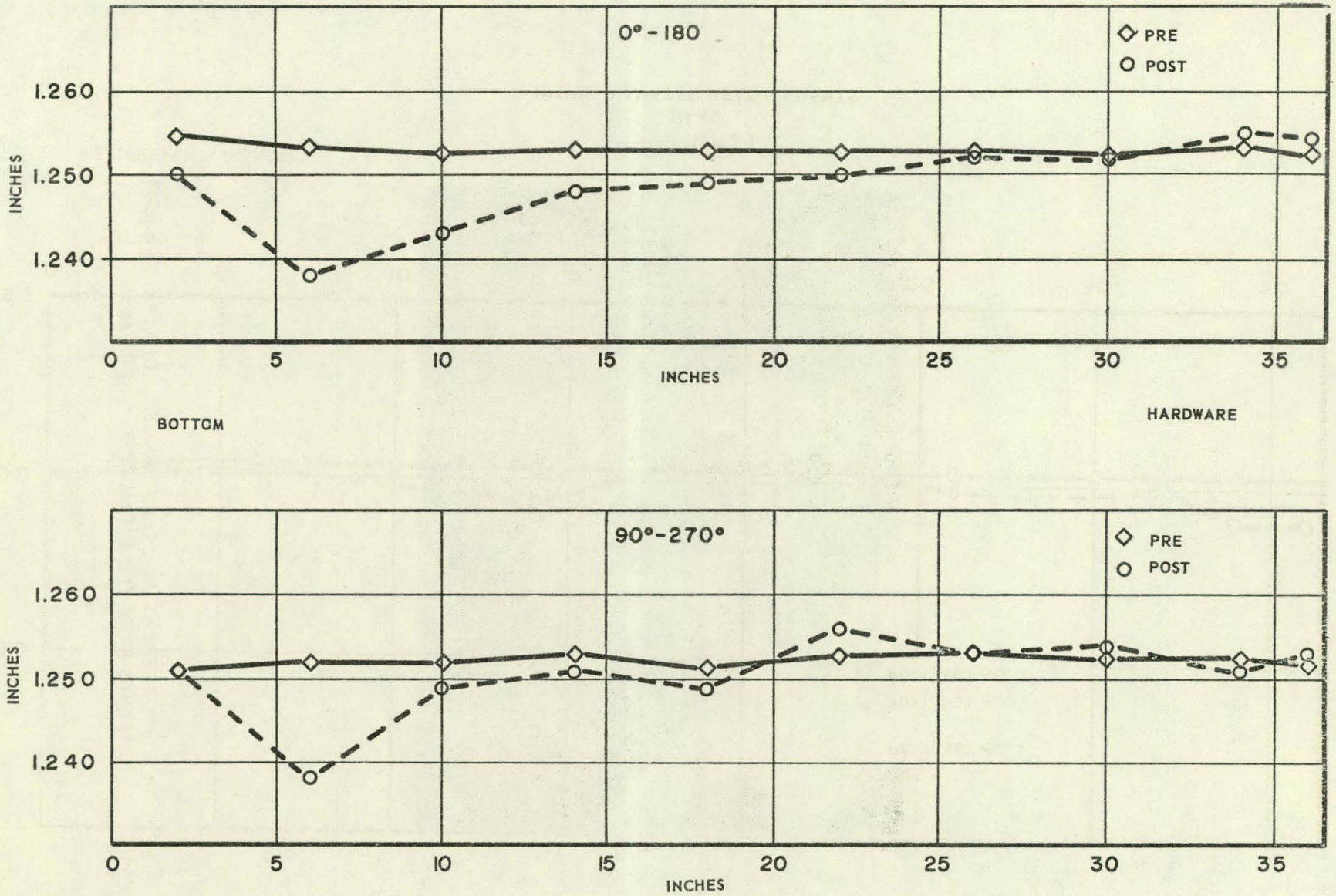

FIGURE 3.3
SH-4C

FIGURE 3.3
SH-4C
OUTSIDE DIAMETER MEASUREMENTS

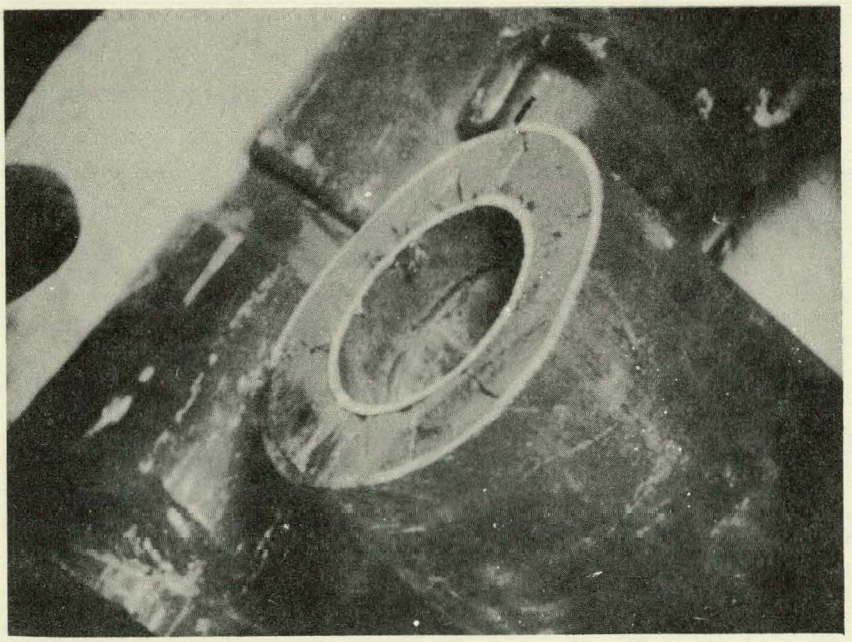

FIGURE 3.4 CIRCUMFERENTIAL CRACK IN SH-4C, LOCATED AT ABOUT 3 INCHES FROM THE STEAM EXIT, INNER PASS.

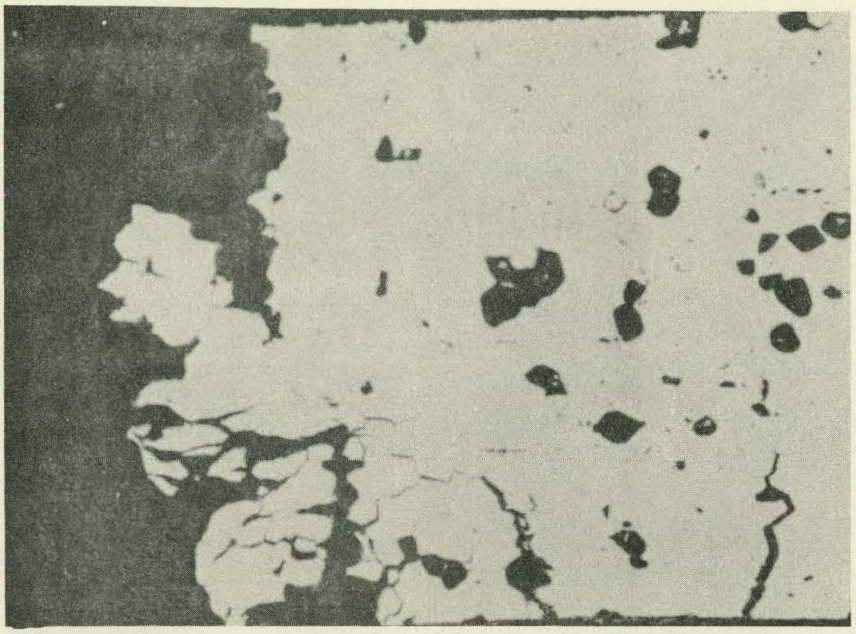

FIGURE 3.5 METALLOGRAPHIC EVIDENCE OF SEVERE INTERGRANULAR ATTACT, AND CRACKS EMANATING FROM THE STEAM-SIDE OF THE 0.028 INCH WALL. POROSITY IN MATRIX IS THE RESULT OF GRAINS REMOVED DURING SPECIMEN PREPARATION. CHLORIDE IMPURITIES IN CRUD SAMPLED NEAR DEFECT WERE 34.5 MICROGRAMS PER SQUARE INCH. 100X

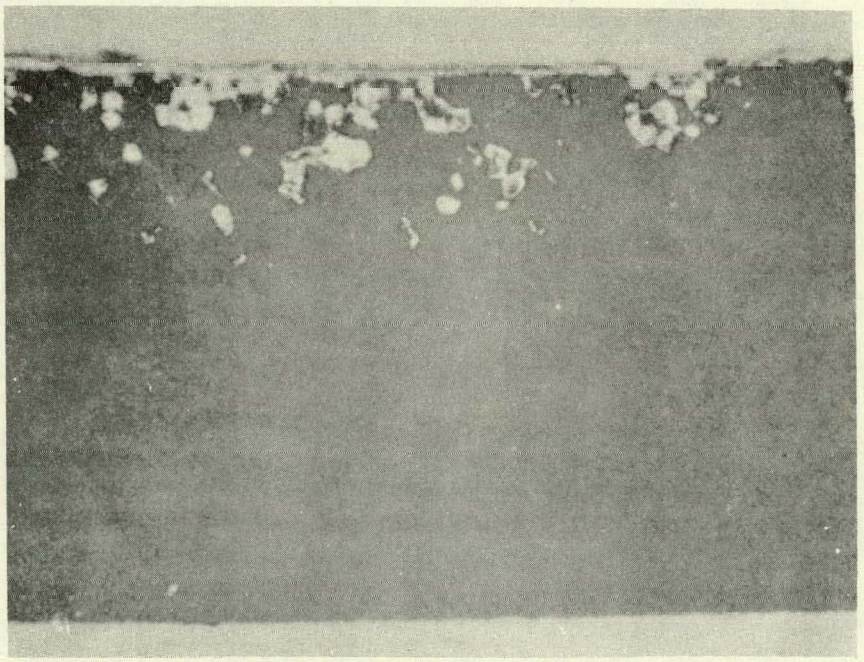

FIGURE 3.6 FUEL ELEMENT SH-4C INTERGRANULAR ATTACK OF CLAD AWAY FROM THE FRACTURE, SHOWING GRAINS MISSING FROM MATRIX
100X

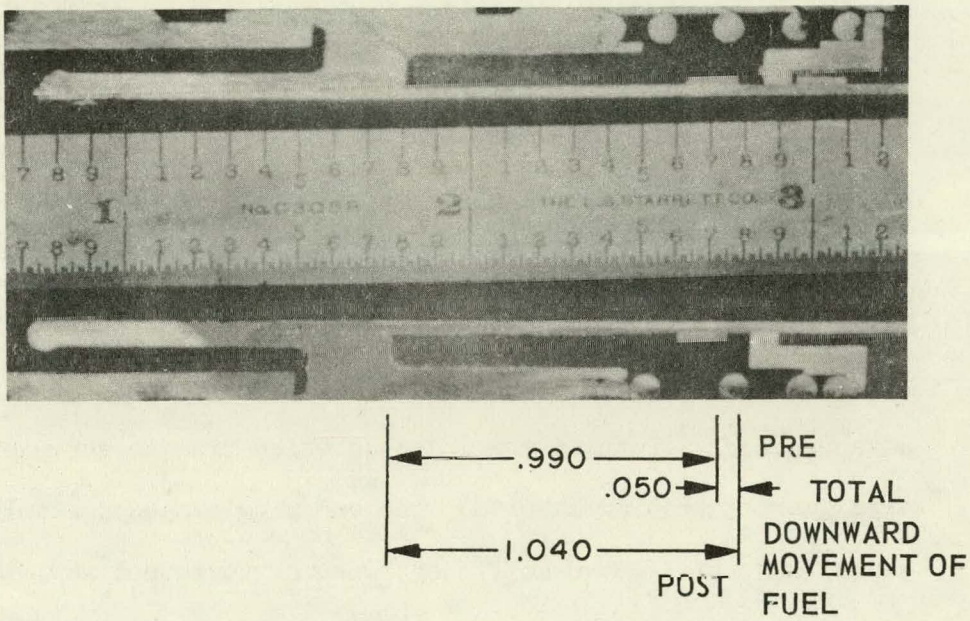

FIGURE 3.7 THE "GUMDROP" MONITOR FOR UO_2 EXPANSION RELATIVE TO THE CLAD, IN SH-4C. TOTAL DOWNWARD MOVEMENT OF UO_2 COLUMN, 0.050 INCHES.

as a back-up element for the remaining SADE test elements. Drawings 142F170 and 142F141 show the fuel cluster. The cluster is geometrically similar to the rod cluster being designed for ESH-2. The SH-6 cluster consists of six fueled rods surrounding a non-fueled center tube. A scalloped liner was used with the cluster to act as a velocity booster.

The fuel rod cluster is shown in Drawing 142F170 - as finally designed and fabricated. The design is conservative in that free-standing cladding is used. Each fuel rod has 5/16" O.D. x 0.020" wall 304 stainless steel cladding. Fuel is 3.9% enriched UO_2 pellets of 95% theoretical density. A two inch plenum is provided for fission gas, with a spring to keep the fuel pellets in place during handling. End plugs are tapered to assure a press fit between clad and end plug at the weld area and still permit easy assembly. The tapered end plug concept has another advantage. By slotting the end plug which fits in the plenum area (part 3 Drawing 142F170), the end plug can be partially seated and still leave sufficient opening to permit satisfactory gas flow during the outgassing procedure. Then the end plug can be fully seated with no concern about holes (for outgassing) to be plugged. Two spacer wires of 0.051" diameter, 304 stainless steel are attached to each fuel rod, as shown on Drawing 142F170. Final tightening of the wires is achieved by rotating spacer anchor, part 2, before welding to the end plug, part 3. Direction of wire wrap alternates so that the wires on adjacent rods do not interfere with each other.

142F170

UNLESS OTHERWISE SPECIFIED USE THE FOLLOWING—
APPLIED PRACTICES: 145A5481 | SURFACES: 63 | TOLERANCES ON MACHINED DIMENSIONS: FRACTIONS ± 1/64, DECIMALS ± .005, ANGLES ± 2½°

TITLE: FUEL ROD CLUSTER SH-6
FIRST MADE FOR: SADE VI
PL. ISSUED

FCF

(1) TUBING, 5/16 O.D. X .020 WALL X 41 9/16 LG

(14) .051 DIA. WIRE RIGHT HAND WRAP 3 TURNS (TOT. 3 RODS)

(10) CLAD 5/16 OD X .020 WALL X 38 1/2 LG

PELLET FUEL ACTIVE LGTH 36" ± 1/4

TYP EACH WIRE END

TYP EA. P5, P6 GTAW

GTAW EACH END EACH PIN

1/8 R MAX.

30°

1/2 DIA.

1 3/8

1 1/4

LEFT HAND WRAP 3 TURNS (TOT. 3 RODS) (SEE SECT "AA")

SECT "DD"

TYP 180° WELD AFTER WRAPPING WIRE

SECT "CC"

1/16 DIA-2 HOLES IN PART 1

20 ± 1/8

41 9/16 ± 1/16

"A" "B" "C" "D"

TYP GTAW

(2)

#54 (.055) DIA. 2 HOLES COUNTERSINK 90° BOTH ENDS EACH HOLE.

.175 ± .003 DIA.

.219 ± .001 DIA.

.298 ± .002 DIA.

BLEND RAD

1 5/8

(3)

.235 ± .005 DIA.

0° 30' ± 15'

.216 ± .001 DIA.

.275 ± .001 DIA.

.298 ± .002 DIA.

.030 ± .005

17/32

(9) DIFFERENT DRILLING OTHERWISE SAME AS P5

BLEND RAD.

DRILL #29 (.136 DIA)

1/16 DIA HOLE (ANGULAR ORIENTATION ARBITRARY)

15/16

(4) 1/16 THK.

.690 ± .005

3/16 x 45°

5/16 DIA HOLE

.800 ± .010

(5) AS SHOWN

(6) FOR P6 - THE 2 HOLES (.055 DIA) ARE DRILLED PARALLEL TO THE SLOT. OTHERWISE SAME AS P5.

#54 DRILL (.055 DIA) 2 HOLES & C'SK 90° BOTH ENDS DRILL HOLES PERPENDICULAR TO SLOT

.235 ± .005 DIA.

BLEND RAD.

.010 R MIN

.298 ± .002 DIA.

.275 ± .001 DIA.

.030 ± .005

1 7/16

(11)

.690 +.002 -.000 ID

.787 ± .002 DIA

TYP 2

(7)

.187 +.002 -.000 DIA TYP 12 LOOPS

60° ± 1° TYP

.475 ± .002 ID DIA

TYP 12

.035 DIA. WIRE

.535 ± .002 OD

(8)

.040

45° TYP

.081 DIA. WIRE

(12)

#29 DRILL (.136 DIA) C'SK BOTH ENDS 60° x 1/8 DEEP.

.270 +.000 -.002 DIA

BLEND RAD. (TYP)

LEFT HAND WRAP EVERY OTHER ROD (LOWER END PLUG P5)

RIGHT HAND WRAP (LOWER END PLUG P6)

SECT "AA"

VIEW "BB"

NOTES

1- ALL FILLER METAL E 308.

2- EACH FUEL ROD TO BE OUTGASSED AND BACKFILLED WITH HELIUM.

3- EACH FUEL ROD TO BE MASS SPECTROMETER LEAK CHECKED, MAXIMUM PERMISSIBLE HELIUM LEAKAGE 10^{-8} CC/SEC.

4- WELDING DETAIL PER ENGR. INSTRUCTION ALL WELDS GTAW.

REVISIONS | PRINTS TO

FP-815-P 2000 (11-56) 1 PRINTED IN U.S.A.

142F141

UNLESS OTHERWISE SPECIFIED USE THE FOLLOWING—
APPLIED PRACTICES | SURFACES ✓ | TOLERANCES ON FINISHED DIMENSIONS: FRACTIONS ± | DECIMALS ± .XX ± 1/64 | ANGLES ±

TITLE
FUEL ASM- SH-6
FIRST MADE FOR SADE VI

SIZE OF QUANTITY	QTY	PART NO.	DWG NO, DESCRIPTION, MAT'L.
	1	1	FUEL FL... 985C340G2
	1	2	THERMAL LINER 114B5248G4
	1	3	FUEL ROD CLUSTER 142F170 G1
	1	4	FLOW TUBE 985C882 G1
	1	5	PIN 149A4908P1
	1	6	INST. TUBE 985C825 G1
	1	7	COTT PIN. 1/8" DIA. x 1/2" LG. STN. STL.

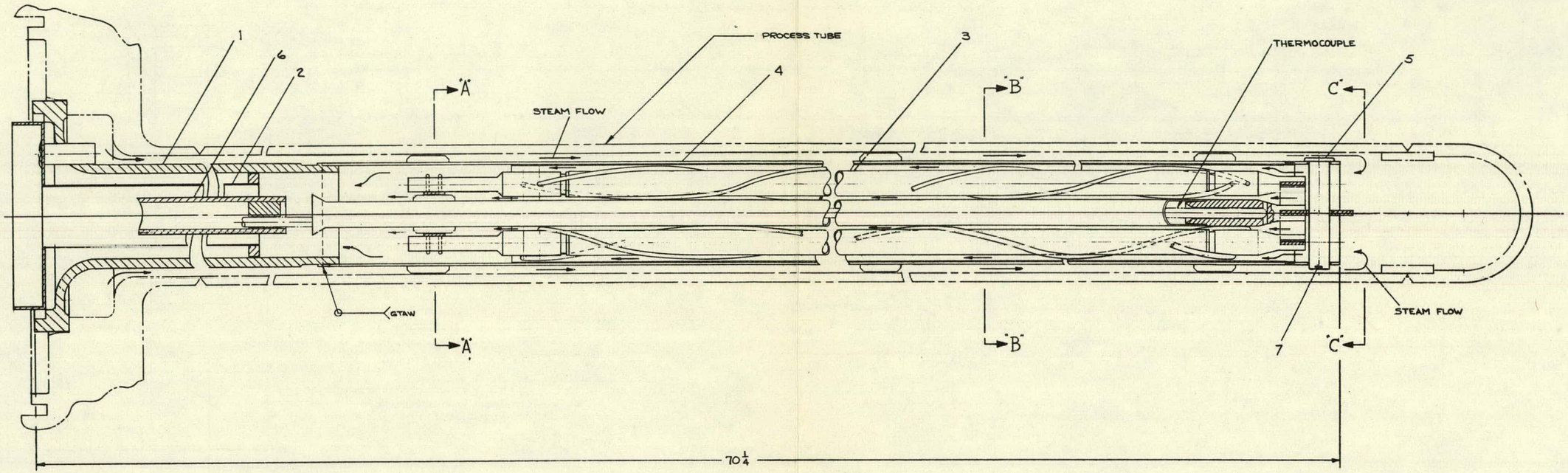

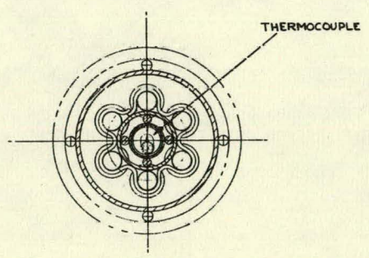

SECT."AA"

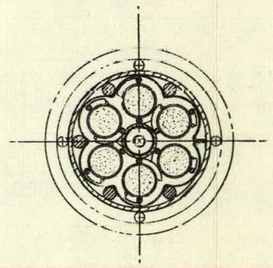

SECT."BB"

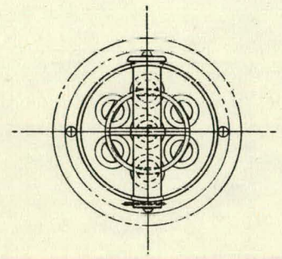

SECT. "CC"

REVISIONS | PRINTS TO

The lower end of each rod is welded to a ring which in turn is welded to a support plate to give a rigid assembly. Figure 3.8 shows the lower assembly before welding. The upper support assembly consists of a ring and wire arrangement which is welded to the center tube. This assemoly provides radial restraint only and permits free axial movement of the fuel rods to accommodate differential expansion and any axial growth which might occur. The upper assembly is shown in Figure 3.9.

The center tube serves the dual purpose of acting as a velocity booster and as a channel for placement of the thermocouple for indicating inlet steam temperature. The thermocouple seats in the center tube end plug (part 9, Drawing 142F170). Holes in this end plug allow a small amount of the inlet steam to bleed into thermocouple area. The thermocouple guide (part 12) also serves as a secondary throttling device for limiting the amount of steam leakage to the center tube. The enlarged upper end of the center tube facilitates proper thermocouple positioning.

Drawing 142F141 shows direction of steam flow, and the overall fuel assembly arrangement, including the scalloped-liner-flow-tube assembly. The flow tube consists of an outer circular tube and an inner scalloped liner. The outer tube is 1-1/4" O.D. x 0.035" wall 304 stainless steel tubing. This tube is welded to a SADE fuel flange (part 1, Drawing 142F141) and extends to below the cluster assembly. The rod cluster support pin is held at the lower end of this outer tube. The flow tube acts to direct the coolant steam down the outside and up through the inside of the flow tube so that satisfactory cluster cooling is achieved.

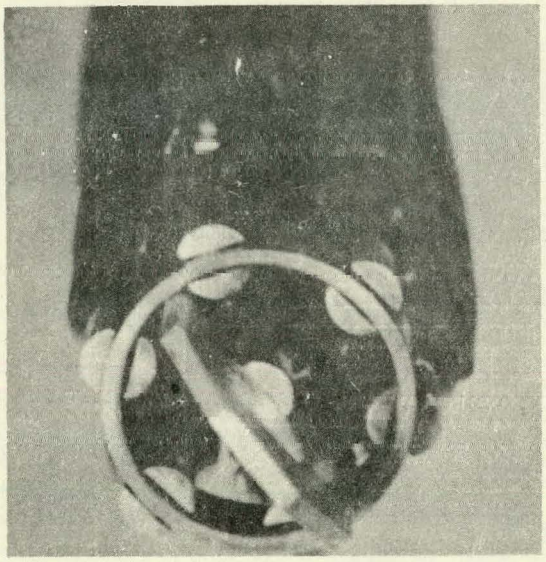

FIGURE 3.8 LOWER END OF FUEL ASSEMBLY PRIOR TO WELDING.

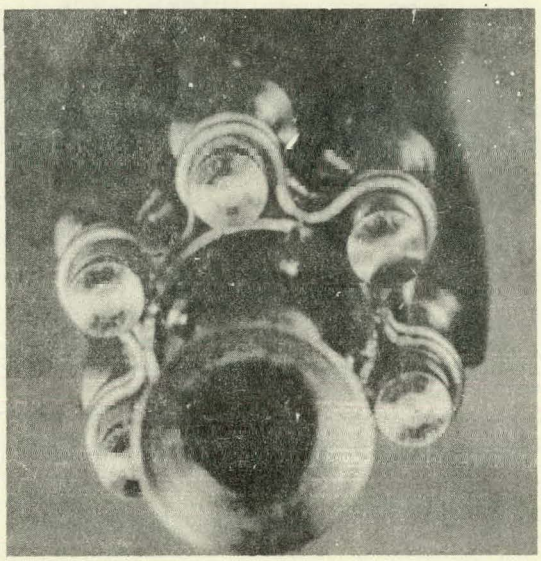

FIGURE 3.9 UPPER END OF FUEL ASSEMBLY.

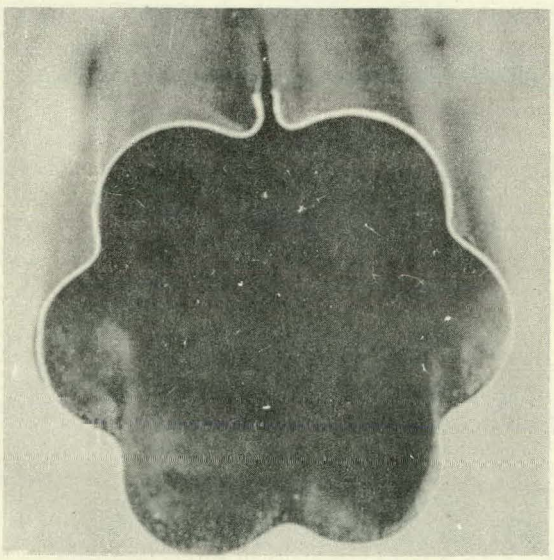

FIGURE 3.10 SCALLOPED LINER PRIOR TO WELDING.

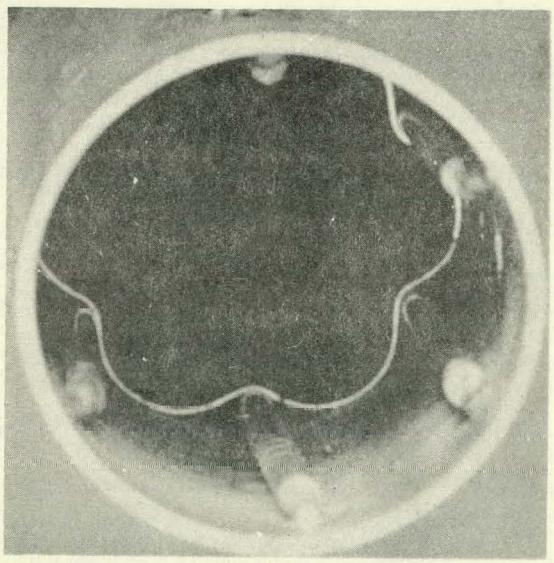

FIGURE 3.11 FLOW TUBE WITH REINFORCED SCALLOPED LINER IN PLACE.

In order to assure availability of the scalloped liner at the time of completion of the fuel rod assembly, the scalloped liner was formed from 0.010" 304 stainless steel strip stock and welded at the resultant seam. The appearance of the scalloped liner just before welding can be seen in Figure 3.10. The lower end of the scalloped liner is contoured to match the 1-1/4" tube and welded to prevent steam flow between the liner and tube. The liner is welded at the lower end only so that differential expansion of outer tube and liner will not cause thermal stresses.

Because it was necessary to use thin stock in order to satisfactorily form the scalloped liner, the allowable pressure differential across the liner is not great. Calculations indicated that expected pressure drops through the cluster would cause stresses in excess of the at-temperature yield point of the scalloped liner. It was decided to place rods between the outer tube and the scalloped liner for support, so that velocity boosting effect of the scalloped liner would not be reduced due to partial collapse. Figure 3.11 shows the scalloped liner and support rods in the outer flow tube.

After initial design was completed a prototype cluster was fabricated to determine fabrication problems and to check out the design. Construction of the prototype revealed that only minor changes needed to be made to make the cluster workable. After serving its original purpose, the prototype assembly was placed in the F-2 loop and pressure drop readings were taken. Results of the flow test are reported in Section 3.3.7 of this report.

3.3.2 Fuel Design for E-SADE, ESH-2

Few changes have been made in the ESH-2 annular fuel design, since the last quarterly report. Drawing 141F979 shows the latest drawing of the annular fuel. No change has been made in clad dimensions. Outer clad is 7/8" O.D. x 0.010 wall and 7/8" O.D. x 0.020 wall tubing. Inner clad is 7/16 O.D. x 0.016" wall tubing. The changes previously mentioned concerning the spring-loaded support plug in the plenum and the rings for attaching the spacer wires have been included in final drawings. The only other change of note is the decision to use dummy segments (for testing long wire spacers) on only two of the annular elements rather than on all.

The ESH-2 single rod element drawing has been issued and as shown in Drawing 762D660. No changes have been made from the previously reported 1/2 O.D. x 0.016 wall clad or other variables pertaining to this rod.

Design work has progressed on the ESH-2 rod cluster, which uses the mixed-spectrum-superheat-reactor-type fuel rods. The SH-6 rod cluster - reported in Section 3.3.2 of this report - is similar to the ESH-2 cluster; therefore, the information and experience gained in the design and fabrication of SH-6 can and has been applied in designing the ESH-2 cluster. For example, the SH-6 lower support assembly has been adapted to the ESH-2 rod cluster, thus greatly reducing the entrance region flow blockage problem which was present in the initial ESH-2 rod cluster design.

141F 979

UNLESS OTHERWISE SPECIFIED USE THE FOLLOWING:

APPLIED PRACTICES	SURFACES	TOLERANCES ON MACHINED DIMENSIONS: FRACTIONS	DECIMALS	ANGLES
145A5481	125√	± 1/64	± .003	± 2

ESH-2 FUEL ELEMENT

FIRST MADE FOR EXPANDED SADE EXPERIMENT

PLISSUED

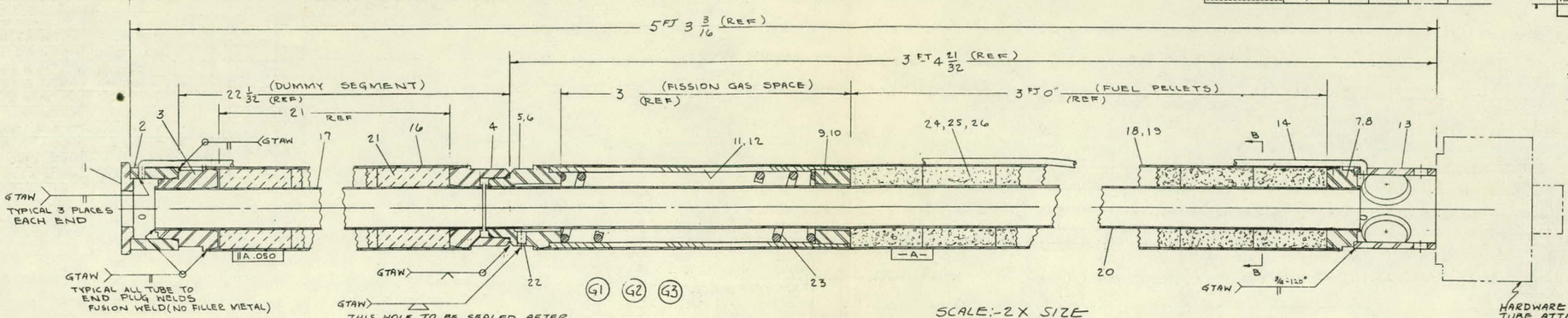

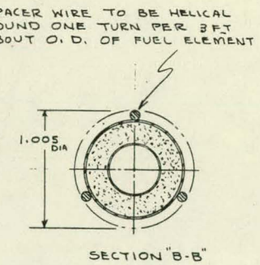

HARDWARE FOR PROCESS TUBE ATTACHMENT

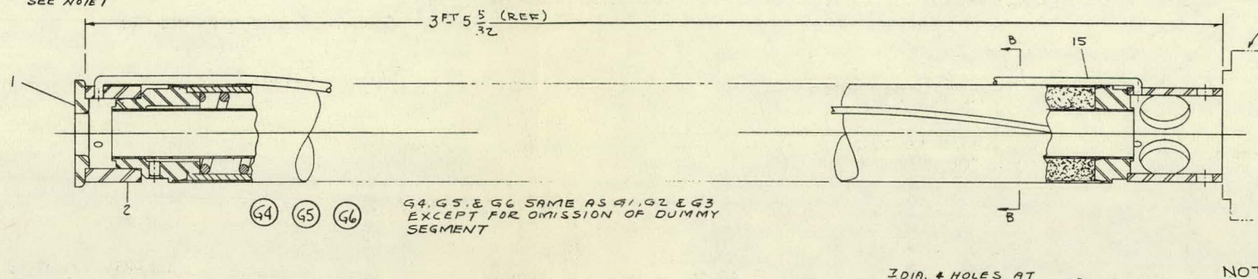

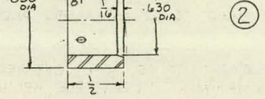

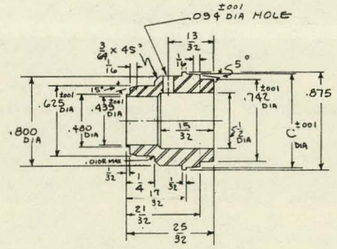

PART No.	C
5	.836
6	.856

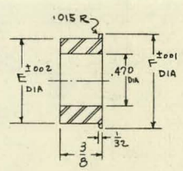

PART No.	E	F
9	.760	.824
10	.780	.844

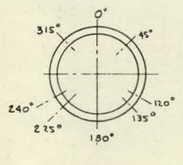

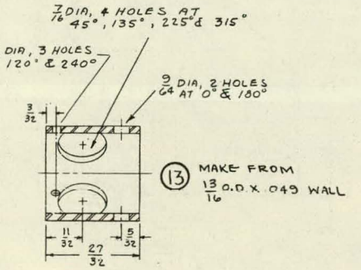

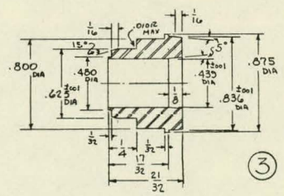

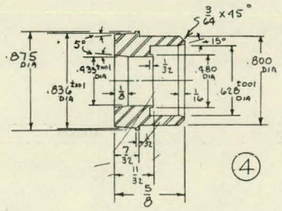

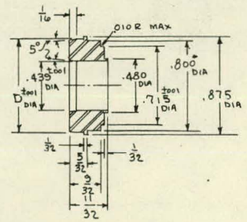

PART No.	D
7	.836
8	.856

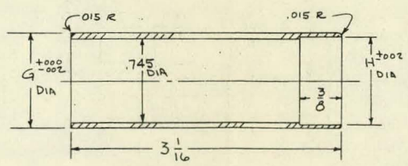

PART No.	G	H
11	.835 SEE NOTE	.770
12	.855 SEE NOTE	.790

NOTE:- INDICATED DIMENSION NOMINAL ONLY. MEASURE OUTER TUBE AND USE ACTUAL I.D. AS 'G' DIMENSION.

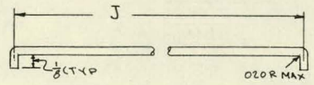

PART No.	J
14	5FT 2 1/2
15	3FT 4 3/8

MAKE FROM .065 DIA WIRE "J" DIMENSION APPROX ONLY TRUE LENGTH DETERMINED AT ASSEMBLY

NOTES:-
1. ACTIVE FUEL REGION TO BE OUTGASSED AND BACKFILLED WITH HELIUM.
2. FUEL ELEMENT TO BE LEAK CHECKED AFTER DUMMY SEGMENT (G1, G2, G3) OR P2 (G3, G4, G5) IS WELDED TO P5 OR P6. MAXIMUM PERMISSIBLE HELIUM LEAKAGE 10^{-8} CC/SEC
3. ALL FILLER METAL E-308

16 7/8 O.D. X .020 WALL X 2 1 5/16 LG

17 7/16 O.D. X .016 WALL X 22" LG

18 7/8 O.D. X .020 WALL X 3 FT 3 3/8 LG

19 1/8 O.D. X .010 WALL X 3 FT 3 3/8 LG

20 7/16 O.D. X .016 WALL X 3 FT 4 1/8 LG

21 .830 +.001 -.005 O.D. X .444 +.005 -.000 I.D. X 3/4 LG

REVISIONS	PRINTS TO

FF-815-P 2000 (11-50) 1 PRINTED IN U.S.A.

762D660

UNLESS OTHERWISE SPECIFIED USE THE FOLLOWING:—

APPLIED PRACTICES	SURFACES	TOLERANCES ON MACHINED DIMENSIONS: FRACTIONS	DECIMALS	ANGLES
145A5481	125	± 1/64	±.005	± 2 1/2°

TITLE ASM
ROD FUEL ELEMENT
FOR ESH-2 (SHNEE III)

GROUP NO.	AVE. QUANTITY	PART NO.	DRAWING NO., DESCRIPTION, MATERIAL, WEIGHT
	1	1	TOP PLUG ASTM A 276 TY 304
	1	2	BTM PLUG ASTM A 276 TY 304
	1	3	TUBE ASTM A 269 TP 304
	1	4	PLENUM ASTM A 269 TP 304
	1	5	RETAINER ASTM A 276 TY 304
	1	6	WASHER ASTM A167 TY 304
	3	7	WIRE TY 304 STN STL
	1	8	ORIFICE ASTM A167 TY 304
	AR	9	FUEL PER ENG INST.
	1	10	RETAINER ASTM A276 TY 304

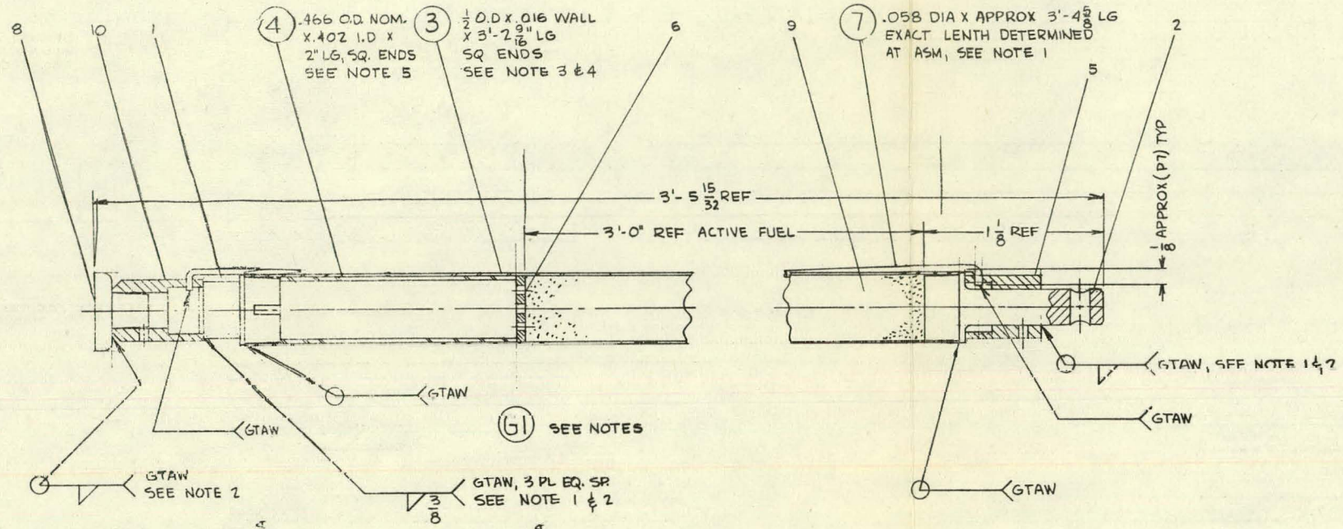

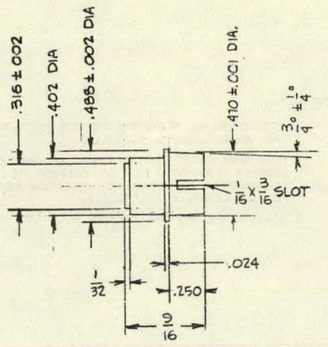

1

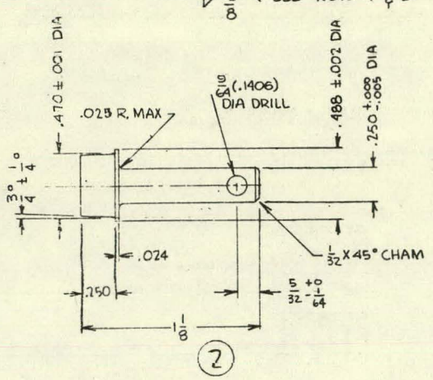

2

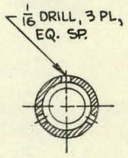

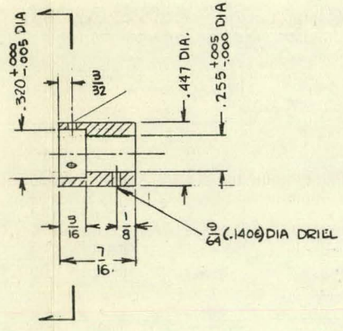

5

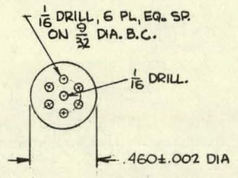

6 1/16 THK.

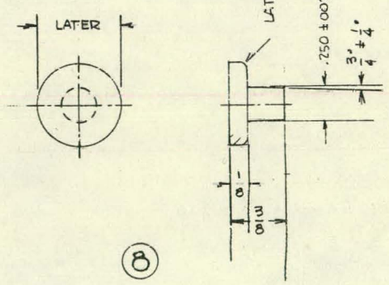

8

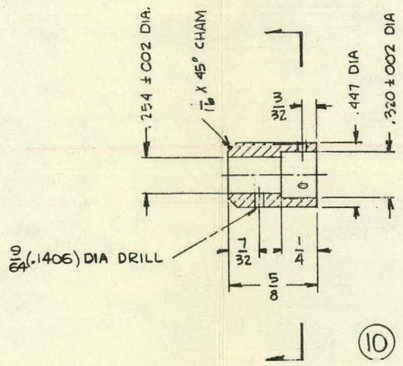

10

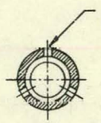

NOTES:

1. P7 TO TURN AROUND P3 ONE TURN PER 3'-0". TIGHTEN BY ROTATING P5 AND P10 IN OPPOSITE DIRECTIONS BEFORE WELDING
2. FILLER METAL E 308
3. FUEL ELEMENT TO BE OUTGASSED AND BACKFILLED WITH HELIUM
4. FUEL ELEMENT TO BE LEAK CHECKED BY MASS SPECTROMETER. MAXIMUM PERMISSIBLE HELIUM LEAKAGE 10^{-8} cc/sec
5. P4 TO FIT IN P3 WITH .003 MAX. DIA CLEARANCE, MEASURE I.D. OF P3 TO DETERMINE REQUIRED O.D. OF P4

DESCRIPTION OF GROUPS	REVISIONS	PRINTS TO

DRAWN BY BWILLIAMS 19 OCT 61

FF-811-P 6000 (8-56) PRINTED IN U.S.A.

3.3.3 Fuel Fabrication for ESH-1

Assembly of the nine fuel elements for this experiment was delayed to allow incorporation of new information, as it becomes available from SADE and laboratory tests. The delay will not affect the overall ESH-1 program but will allow the possible use of alternate clad materials and information gained from the irradiation of SH-5A. The status of the ESH-1 fuel assembly is as follows:

Fuel: All UO_2 ordered for this assembly has been received. Pellets are complete for 5 of the 9 elements.

Cladding and Hardware: All components required for the assembly of a 300 series stainless steel bundle are on hand.

Alternate Cladding Materials: Orders have been placed for the I.D. cladding tubes in both Inconel and Hastelloy-X. No bids have been received for the 1-1/4" O.D. cladding in any of the alternate alloys, but two promising prospective bids have been received and are now being evaluated.

3.3.4 Pellet Fabrication

In the production of annular fuel for the SADI and Trail Cable experiments, considerable problems were encountered in the control of pellet size, concentricity, integrity and density. A series of changes made prior to the production of the first expanded SADE fuel has resulted in a marked improvement in overall pellet quality. The changes are based primarily on the recognition of equipment limitations and improved process control.

A tight process control on "as pressed" density of the UO_2 pellet has resulted in the ability to sinter the internal diameters of

pellets to size. This eliminates the expensive and time consuming internal grinding operation. The size control has been accomplished by a unique method on a double action mechanical press. The press is equipped with a combination hydraulic-pneumatic accumulator for density control, but the sensitivity of this accumulator is not sufficient on large diameter annular pellets. It has been found, however, that the degree of response of the accumulator is directly related to as-pressed density of a pellet. The measurement of this response by either mechanical or electrical means allows an indication of the "as pressed" density for each pellet. An acceptance range is set up and pellets falling outside this range are rejected prior to the sintering operation. Reprocessing a small percentage of unsintered UO_2 at this point in the process is relatively cheap compared to the cost of grinding sintered pellets to size.

In the past a considerable number of annular pellets have been rejected because of radial cracks which occurred in the sintering operation. Other pellets have been rejected because of non-concentric internal and external diameters. The cause of both the cracking and the distortion in sintering has been identified as being radial density variations in the as-pressed pellet caused by a non-uniform fill of the die cavity. The condition has been corrected to a large extent by decreasing the height of the "as pressed" pellets. By this change radial cracking in sintering has been eliminated and the maximum pellet distortion reduced by a factor of five.

General pellet integrity has been improved by the changes mentioned above and also by lower sintering temperatures and the elimination of die lubricant additions to the powder. A sintering temperature os 1580°C ± 10°C has produced pellets with densities of 95% of theoretical or higher. The elimination of die lubricant additions to the powder has reduced internal porosity in the sintered product. Die lubrication is now accomplished through the lower punch on each ejection stroke of the press.

3.3.5 Non-Destructive Inspection

The conceptual design of an in-cell ultrasonic inspection station has been completed. It will be used to examine irradiated fuel elements for stress corrosion cracking. The tank has been designed so that the O.D. cladding can be scanned by a crystal mounted on a traveling bridge. I.D. cladding will be scanned by a crystal mounted on a bayonet which can transverse the entire internal length of the fuel element.

3.3.6 Fretting Corrosion Tests

The ESH-1 prototype element with spiral wire spacers has been tested for 178 hours. A thorough examination of this element after removal from the loop has revealed no evidence of fretting corrosion. The SH-6 prototype element was installed in the loop for pressure drop measurements. Steam flow was varied from 600 to 1100 lbs/hr. Preliminary data showed that the pressure drop across this element will fall into acceptable design limits. The ESH-1 prototype element has been re-inserted in the loop and will be tested for an additional 225 hours.

4.0 TASK C - MATERIALS DEVELOPMENT

4.1 Alternate Clad Program

4.1.1 Phase I - Literature Survey

A topical report, "Materials for Nuclear Superheat Applications - A Literature Survey," C. N. Spalaris, F. A. Comprelli, D. L. Douglass, and M. B. Reynolds, GEAP-3875, has been issued summarizing the findings in Phase I. The materials literature survey was initiated to investigate the possibility of developing an alternate clad for superheat fuel applications. The effort was divided into four categories as follows:

1. Oxidation behavior of alloys under superheated steam conditions.
2. Mechanical properties of alloys at temperature ranges of 800 to 1400°F.
3. Effect of neutron irradiation upon the physical properties of materials.
4. Practical applications of potentially promising alloys under superheat or intermediate superheat conditions.

The objectives of the literature survey were to review available data, visit individuals in laboratories engaged in related work and finally, prepare a document indicating a list of candidate alloys that should be investigated for possible superheat fuel clad applications. Three visits were made during November to laboratories engaged in high temperature alloy corrosion on other related work. No known work exists where the corrosion of promising alloys for superheat applications has been investigated either under high temperature steam or steam containing oxygen

nor chloride impurities and/or stresses. The highlights of the visits made to International Nickel Company, AEC, Washington (contacts with H. Pessel and N. Grant) and Oak Ridge National Laboratory are given below.

1. In comparative tests, Inconel, when properly prepared metallurgically, gave satisfactory and predictable performance in various corrosive media when other alloys such as 300 series steels yielded unsatisfactory results.

2. No data have been obtained which duplicate alloy environmental conditions such as those expected in nuclear superheat plants. It appears necessary that such data be obtained from experiments since no work is now being planned elsewhere.

3. Dispersion-strengthened, iron alloys exhibited higher stress rupture strength at room and high temperatures, in the experiments carried out at MIT. No corrosion work of any kind has been performed using these alloys and no joining (welding) methods are as yet available for these alloys. Although these alloys may be promising from the strength increase viewpoint, their corrosion resistance and fabricability must first be established before any serious consideration is given for their application in nuclear superheat hardware.

4. International Nickel Company is conducting an irradiation studies program, aimed at understanding basic mechanisms for deterioration in mechanical properties of alloys, such as loss of stress rupture strength due to irradiation. Progress

in this program should be followed, but initial experiments will not begin for another six months.

5. Recent data obtained at Oak Ridge suggested that boron content in Inconel is not the primary reason for loss in strength upon irradiation. This is in agreement with the interpretation of available data offered by Inco. The same tests, however, show a ten-fold reduction in average strain at a given rupture life due to irradiation. This effect was also independent of the boron content.

6. Grain size in Inconel has significant effect upon the mechanical properties such as elongation of rupture life. For material with an ASTM 1 grain size, the reduction of strain at failure (for a given life rupture) is 60% less than the same material which has a grain size of ASTM 6 or finer.

7. Both corrosion resistance and mechanical properties of Inconel improved upon reduction in grain size.

8. H. J. Pessl disclosed that stress corrosion tests were conducted at Hanford, using U bends of 406 material in 40% $MgCl_2$ (boiling) solution. After 6 - 7 days of testing, no stress marks appeared in AISI-406, which is in agreement with similar work done using other ferritic materials. (Work at APED with 406 is now in progress for determining its corrosion characteristics in high temperature 1050°F steam with oxygen and chloride ions present.)

9. Data at 1300°F show that for a given stress level, the life-to-

rupture for 304 is not affected by irradiation up to 4×10^{20} nvt. On the other hand, however, the tangential strain at rupture decreases by about a factor of four due to irradiation, in many cases to values less than 1%.

10. The irradiation experiments were done at ORR at temperatures of 1300°F and in air. (In cases where one may have intergranular attack due to corrosion, high stresses alone may be enough to cause failure of fuel clad in a brittle manner. In view of these data, failures in SH-4B and SH-4C may be partially due to high stresses alone, in addition to stress corrosion cracking in the presence of the chloride ions.)

During December a trip was made to Argonne National Laboratory to exchange information regarding corrosion of materials in oxygenated steam. High temperature steam corrosion tests were carried out in both low oxygen and oxygenated (15-20 ppm) steam at temperatures up to 1250°F. The experiments which are primarily designed for proof testing are being performed in small dynamic autoclaves. The specimens are 60 mil coupons about 1 x 1/2 inch and some flat plate assembly sections which were brazed with "Coast Metals 60" material. The brazed regions and braze material itself showed excellent corrosion resistance in steam. The 304 and 304L plates and coupons, however, showed erratic behavior with excessive scale formation on some samples. The scale thickness was on the order of 6 to 10 mils in 1000 hours, some of the scale exfoliating during the test. In some cases a rough, pit-like scale formed initially and subsequently "healed" during longer exposures. A

peculiar effect was observed on the brazed assembly which may be designated as an "outside-inside" effect. The outside plate, presumably the same material at the same temperature, exhibited a significantly higher corrosion rate than the inside surfaces of the plates. This assembly was produced at Atomics International as part of the prototype program for the Borax V fuel plate superheat section core.

Discussions were also held with ANL people in regard to steam corrosion of AISI-406 alloy, at 1200°F and 20 ppm of oxygen. The limited amount of information agrees with APED's preliminary data. The same conditions which produced erratic behavior on the 304 and 304-L samples resulted in a smooth adherent scale on 406. Samples to date have been stress free but future work will include studies on the effects of stress.

4.1.2 Conclusions of the Literature Survey

1. There is little prior experience, both industrial and experimental, upon which to base selection of materials for designing and/or fabricating components for use in nuclear superheat environments. A single alloy that will perform satisfactorily under all conditions in a nuclear superheat environment has not been located. Instead it is believed that a judicious combination of materials selection and proper design, with minimum inherent stresses, is required to minimize or eliminate the problems anticipated.

2. Based on information obtained as a result of the literature survey, most promising metallic alloys which can be considered

for investigation as likely candidates for nuclear superheat applications are: Incoloy, Inconel, modified 300 austenitic series such as 310, 304L types but with low nitrogen and carbon, Hastelloy-X, AISI 406, and RA-330. In addition, it is considered advisable to conduct preliminary screening tests, under superheat conditions, on the following alloys to study their feasibility for nuclear superheat applications: Hastelloy-N, Ni-O-Nel (modified), IN-102, R-20, Discaloy, and 17-14 CuMo. The use of one or more of the above candidates in critical components should be preceded by a development program where these materials are tested in laboratory and in-reactor experiments.

Further qualifications as to the general conclusions made above are as follows:

3. There is a certain element of risk in using any 300 series austenitic type alloy in nuclear superheat environments because of the possibility of failure due to localized stress corrosion attack. Improvement in service reliability of components fabricated with these alloys can be achieved by using an alloy containing minimum 20% chromium and 20-25% nickel. This alloy may be modified Type 310.

4. It was found that when Type 300 series austenitic alloys were modified to contain low nitrogen (0.01% or less) and low carbon (0.02% or less) their resistance to stress corrosion attack improved significantly. This can be achieved by suitable treatment during ingot fabrication such as vacuum melting or vacuum pouring.

5. Because the fabricability and availability of 310 stainless as it is stated in items 3 and 4 is not known, other more common types of 300 series stainless should be considered. Type 304, 304L or other special modifications of the 300 family should be investigated, since the fabrication, availability and irradiation properties of this alloy family are better known than others and component design allowances are possible. In any case, nitrogen content should be kept below 0.01% and carbon below 0.02% if 300 series austenitic type alloys are used.

6. Incoloy should be considered for use in nuclear superheat components because it is the best all-around "high" nickel alloy combining good mechanical and fabricability properties as well as tolerable corrosion resistance. In comparative tests, its resistance to stress corrosion attack is far better than regular austenitics but not as good as the high nickel alloys such as Inconel. Because long-term corrosion experience in oxygen containing steam is not available and irradiation results are non-existent for Incoloy, it is imperative than steps be taken immediately to gain such information.

7. Inconel is the best known high nickel alloy for use in high temperature service conditions. In addition, when properly heat treated, Inconel gave good service in media known to induce stress corrosion attack. In fact, the use of this alloy probably gives the highest assurance against stress corrosion attack, although some isolated cases of failure

through this mechanism have been encountered. Irradiation results show serious reduction of stress rupture, elongation and low cycle fatigue properties at high temperature.

8. Hastelloy-X should be considered because of its good fabricability and probably acceptable corrosion resistance. The high nickel content of this alloy provides good assurance for its use in stress-corrosion-promoting media. Exploratory work should be initiated immediately to determine its use and limitations in high temperature superheat reactor applications.

9. Ferritic type alloys, such as AISI-406 should be included in the program for immediate investigation because these combine low neutron cross section, adequate uniform oxidation and possible stress corrosion resistance characteristics.

10. Work should also be initiated for alloys such as Hastelloy-N, Ni-O-Nel, IN-102 and others which possess attractive high temperature mechanical properties.

11. None of the alloys recommended for consideration in Items 2 through 10 can be used in superheat reactors with adequate assurance, without prior basic developmental effort aimed at determining the properties and limitations of these alloys in high temperature steam environments.

4.1.3 Procurement of Alternate Cladding Materials

With the exception of Type 406 stainless steel, purchasing has been completed for all of the materials in the geometries necessary for preliminary corrosion and fabrication development screening

tests. Much of this material is now on hand and the remainder is scheduled for arrival by March, 1962. Purchasing efforts are continuing in an attempt to obtain Type 406 stainless steel in the required geometries. The following table summarizes the materials which are now on hand or which will be available by March.

Table 4.1

Application*	(a)	(b)	(c)	(d)	(e)	(f)	(g)
Fabricability Testing	X	X	X	X	X	X	X
General Corrosion Testing	X	X	X	X	X	X	X
Heaters for C1-1	X	X	X		X	X	X
Strain Cycle Tests	X	X	X				
ESH-1	X	X	X				
ESH-2	X	X	X				

Difficulties encountered in obtaining these materials have been due mainly to a lack of interest shown by the vendors because of the small quantities of speciality items involved. There appears to be no technical difficulty which would prevent the production of tubing or bar in quantities required for nuclear superheat applications.

4.1.4 Evaluation of 300 Series Stainless Steel Tubing

A total of 750 feet of tubing of various sizes and cold work conditions has been ultrasonically tested to determine number and level of defects. Tubing tested has been selected so data may be obtained to relate size and number of defects with manufacturer, degree of cold work and tube size. This information is needed to establish meaningful material specifications for 300 series stainless tubing.

* (a) Incoloy (e) Hastelloy N
(b) Inconel (f) RA-330
(c) Hastelloy X (g) Ni-O-Nel
(d) AISI 406

Included in the tubing tested are seven different sizes from four different manufacturers, and in three different cold work conditions. Ultrasonic testing information from this tubing will be correlated with existing tube burst test data to further establish levels of acceptable quality.

4.1.5 Fabricability Testing for Alternate Cladding Materials

A program was initiated to determine fabricability parameters for the candidate materials in support to fuel fabrication for E-SADE assemblies. Manufacturers of the various alloys have been contacted regarding available information and a welding program has been initiated in order to obtain specific information with regard to particular problems encountered in fuel element fabrication. Weld specimens are being prepared to establish integrity of welds of various geometries and materials. Also included will be an investigation of dissimilar metal joining consisting of the welding of these alloys to each other and to the reference alloy, Type 304 stainless steel. Corrosion behavior of welds will be tested in C1-1 coupon holders.

4.2 Strain Cycling Experiments

4.2.1 Strain Cycle Tests - Laboratory Experiments

Task C-3: The objective of this task has been the determination of low cycle strain fatigue life of thin wall Type 304 stainless steel tubing, so that these results can be compared with those obtained under irradiation. The tubular specimens used in these tests are alternately expanded and compressed by gas pressure between two fixed concentric mandrels. The strain range is

determined by the sizes of the mandrels relative to the specimen diameter and thickness. To date, a total of eleven specimens have been cycled to failure at 1300°F using argon as the activating gas, using identical cycling techniques to those planned in the reactor runs. The direction of the strain has been reversed every 15 minutes, i.e., two cycles per hour. At strain ranges above about one percent total (i.e., ± one-half referred to neutral position) specimens have been observed to deform by wrinkling parallel to the specimen axis. Failure has been found to be by intergranular fracture. In cases of specimen wrinkling, long fractures occur on the convex side of wrinkles. A study is underway to estimate the actual fiber strains at fracture by measuring the radii of curvature of the wrinkles in failed specimens. The results of tests to date are shown in Figure 4.1 in which total strain range is plotted against cycles to failure. Strain range as plotted is based on mandrel dimensions relative to specimen thickness and diameter and no allowance has been made for increase in actual fiber strain due to wrinkling. The probable correction for elastic strain is indicated by arrows, based on an estimated 15 kpsi elastic limit and 20 x 10^6 psi modulus at 1300°. When this series of tests is completed, the results will be reported fully including estimates of strain increase due to wrinkling.

4.2.2 Strain Cycling Under Irradiation

Capsule design was completed for all irradiation runs using 304 specimens, to test the effect of neutron exposure upon the low cycle fatigue properties at 1300°F. Two main experimental

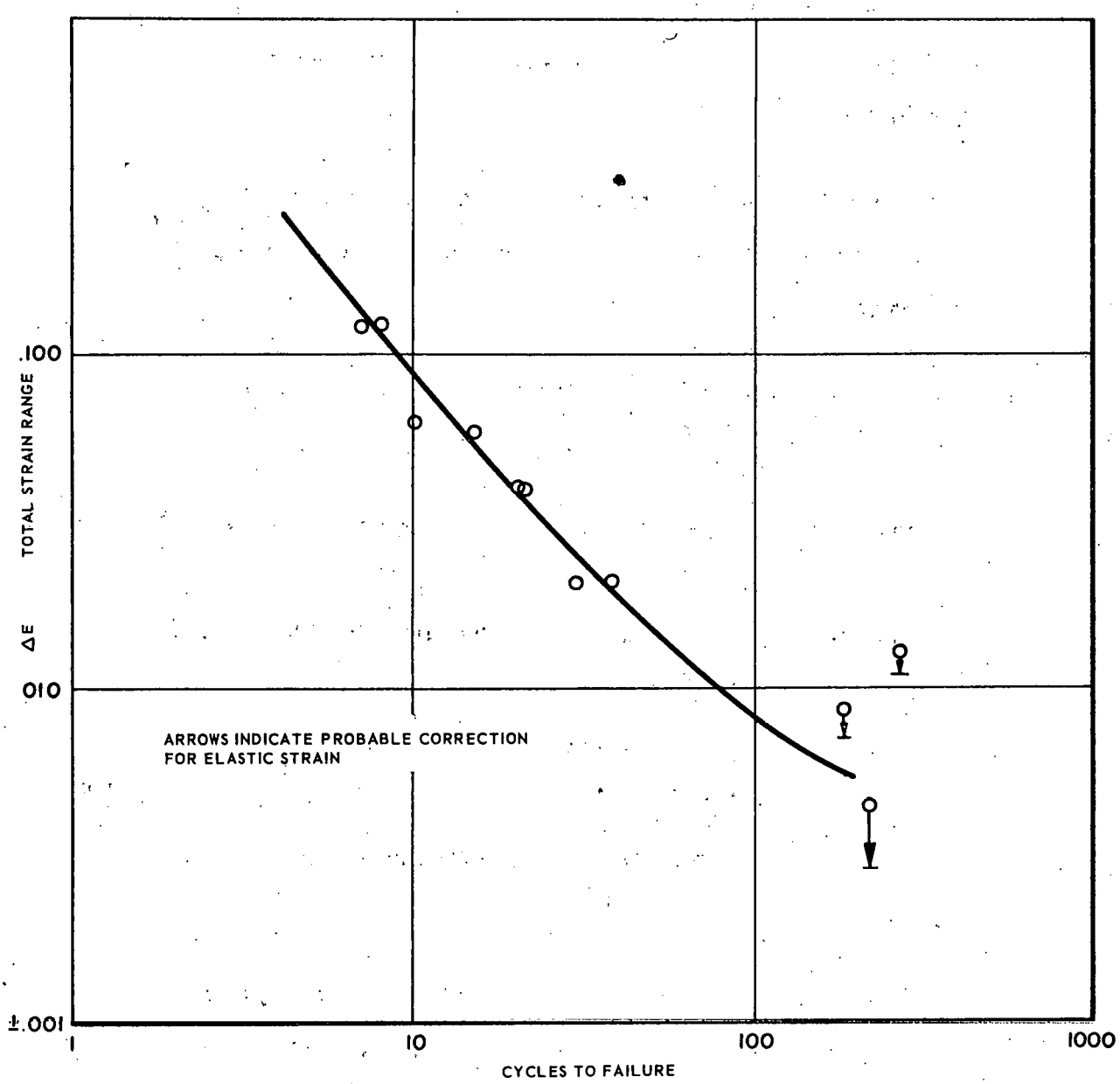

FIGURE 4.1
STRAIN-CYCLE TESTS, TYPE 304 STAINLESS STEEL
AT 1300° F

approaches are planned:

a. Determine low cycle fatigue properties of 304 where specimens are being cycled concurrently with irradiation exposure at 1300°F.

b. Determine low cycle fatigue properties of specimens cycled at 1300°F, after irradiation exposures at 1300°F were performed in static condition.

The results obtained from the tests shown above will then be compared to those obtained for non-irradiated specimens.

The groups of samples prepared for reactor exposure are as follows:

	No Heaters		With Heaters*	
Capsule #1:	2% specimen	Capsule #3:	2% specimen	
	1% "		1% "	
	1/2% "		1/2% "	
Capsule #2:	1/4% specimen	Capsule #4:	1/4% specimen	
	1/8% "		1/8% "	
	1/16% "		1/16% "	

*Heaters needed to perform tests at 1350°F after samples have been irradiated.

Irradiation experiments will commence with GETR cycle 30, during the first week of January, 1962. The irradiation schedule selected for these tests is shown in Table 4.2.

Table 4.2

IRRADIATION SCHEDULE

Strain Cycle Tests

Cycle 30	Cycle 31	Cycle 32	Cycle 33	Cycle 34
1. Insert capsule #1, and activate machines during the cycle.	1. Insert capsule #3, but do not activate any machines during the cycle.	1. Insert capsule #2, and activate machines during the cycle.	1. Insert capsule #4, but do not activate machines during the cycle.	1. At beginning of cycle, activate machines in capsule #4, in canal.
2. At end of cycle, send capsule #1 to RML.	2. At end of cycle, shift capsule #3 to GETR canal.	2. At end of cycle, send capsule #2 to RML.	2. At end of cycle, shift capsule #4 to GETR canal.	2. At end of cycle, send capsule #4 to RML.
		3. At beginning of cycle, activate machines in capsule #3 in canal.		
		4. At end of cycle, send capsule #3 to RML.		

As of December 31, 1961, capsule #1 with the test specimens indicated above was delivered to GETR along with the control console, for final installation.

The in-core berillium block was delivered, and mock-up tests were performed to determine dimensional compatibility of the parts to be positioned in the reactor core.

A flow test on the capsule bracket and control rod guide tube bracket was performed during the November shutdown. A review of the movies taken during the test indicate that a moderate amount of vibration is present, and that some rubbing on the guide tube bracket occurs. The bracket was damaged when it was removed. Another flow test will be run after the capsule is inserted to determine whether vibration of the capsule bracket with the capsule in place is excessive.

Irradiation of capsule #1 is expected to start during the first week in January, 1962.

5.0 TASK D - EXPERIMENTAL PHYSICS

5.1 AEC Superheat Critical Experiments

A topical report, GEAP-3882, "AEC Superheat Criticals - A Comparison of Experiment and Theory on Uniform Lattices" by G. T. Petersen and F. G. Warzek, is in the final stages of preparation. The following summary has been extracted from GEAP-3882.

5.1.1 Summary from GEAP-3882

Measurements were conducted with uniformly-spaced arrays of superheat fuel (no controls or water gaps) to obtain a direct measurement of the physical parameters within the fuel element cell. The element pitches of 1.800, 1.900, and 2.000 inches were utilized to cover a water-to-fuel volume ratio range of 1.47 to 3.67. The actual measurements were performed at the General Electric Vallecitos Atomic Laboratory in two phases.

Phase I

1. Critical Size
2. $(\partial\rho/\partial H)$ versus H (ρ = reactivity, H = water height)
3. Void Coefficient
4. Temperature Coefficient
5. Flux Distribution

Phase II

6. Thermal Utilization
7. Conversion Ratio

Phase I of the program covered the period October, 1960 through January, 1961. Phase II of the program covered the period May,

1961 through June, 1961. The primary reason for delaying the Phase II measurements was to provide the time necessary to develop a new and more accurate method of conversion ratio measurement, which was then applied to the superheat lattices.

The results of the Phase I measurements were compared to the predictions of an engineering design model that had demonstrated reasonable accuracy in treating BWR and PWR lattices. The resulting reactivity, void coefficients, and temperature coefficients are given in Table 5.1 for four representative cases. It can be seen that relatively large discrepancies in all three parameters exit. This model led to reactivity overpredictions of 2 to 5 percent $\Delta k/k$, and to more negative void and temperature coefficients than were measured.

Possible areas of uncertainty in the engineering design model included:

1. Thermal utilization,
2. Resonance escape, and
3. Neutron leakage.

Of these three, only thermal utilization appeared to offer a consistent explanation of the reactivity and reactivity coefficient discrepancies. Furthermore, it appeared that there was valid uncertainty as to the application of the zero-dimensional thermal spectrum calculation present in the model.

Based on the assumption that the thermal spectrum treatment in the thermal utilization calculation was the prime source of error, a

Table 5.1

AEC Superheat Criticals

Comparison of Engineering Design Model Predictions With Experiment

Fuel Configuration		Reactivity ("Just Critical" Size)	Void Coefficient (Moderator 20 C)	Temperature Coefficient (20 - 40 C)
Element Pitch (inches)	Flooding of Coolant Passages	k_{eff}	10^{-4} $\Delta k/k$ % Void	10^{-4} $\Delta k/k$ C
1.800	Unflooded	1.000* (1.022)** [1.001]***	-12.7 (-23) [-18]	+ 0.3 (-0.1) [+0.4]
1.800	Flooded	1.000 (1.037) [1.000]	- 5.7 (-10) [- 5]	+ 1.0 (+0.3) [+1.0]
1.900	Unflooded	1.000 (1.031) [0.998]	- 9.6 (-15) [-11]	+ 0.7 (+0.3) [+0.8]
2.000	Flooded	1.000 (1.050) [0.997]	+ 4.9 (- 1) [+ 3]	+ 2.1 (+1.1) [+1.9]

* Measured value.

** Calculated value using engineering design model.

*** Calculated value using modified engineering design model.

semi-empirical correction, normalized to the reactivity error in one case, was introduced to modify the calculational model. The resulting improvement in the experiment-theory correlation is striking. The largest reactivity discrepancy became 0.3 percent $\Delta k/k$ rather than 5 percent, and both the void and temperature coefficient discrepancies were markedly reduced. Part of the reactivity agreement is a result of normalizing the correction to give zero reactivity error in the 1.800-inch pitch flooded case, but it is quite significant that all of the other discrepancies dropped simultaneously and the previous trend toward larger error when the element pitch was increased or the outer coolant passage flooded, was removed.

To confirm the corrected thermal utilization as calculated by the modified engineering design model, calculations utilizing the SLO P-1 code were performed. SLO P-1 is a multi-thermal group code which permits scattering from each energy group to every other energy group, and solves the neutron transport equation by the P-1 approximation. Shortly after the SLO P-1 calculations had been completed, the Phase II thermal utilization measurements were made. Table 5.2 summarizes the results of the measurements, the SLO P-1 calculations, and both of the engineering design model calculations. The engineering design model, however, overpredicted thermal utilization by as much as 4.3 percent $\Delta f/f$, verifying the assumption that thermal utilization was the prime cause of the reactivity discrepancies.

In addition to the check of thermal utilization, resonance capture by U-238 received careful study. Calculations of the resonance escape probability utilizing the Monte Carlo code NYU-REP were performed. NYU-REP accurately treats the spatial capture in each of 55 resolved U-238 resonances. After a correction for the unresolved resonance contribution was made, the resonance escape probabilities as determined by Monte Carlo were compared to the predictions of the engineering design models. The agreement was excellent. The largest discrepancy was only $\pm$ 0.003 $\Delta p/p$ or $\pm$ 0.03 $\Delta(1-p)/(1-p)$, which indicates that resonance escape for U-238 is treated accurately by the engineering model for this fuel geometry.

Although the resonance escape probability for U-238 was not measured directly, the conversion ratio was. Since the resonance escape probability is directly related to the conversion ratio, an indirect measurement of the resonance escape probability was made. The calculated and measured conversion ratios were compared and good agreement was attained in all cases, with the largest discrepancy only 3 percent (ΔCR/CR), which would translate into less than 0.5 percent error in the resonance escape probability.

Table 5.2

AEC Superheat Criticals

Thermal Utilization

Fuel Element Pitch (inches)	Fuel Configuration	Measured f	Calculated f		
				Engineering Design Models	
			SLO P-1	Model A**	Model B**
1.800	Unflooded	0.763 ± 0.015*	0.760	0.769	0.759
1.800	Flooded	0.714 ± 0.015	0.717	0.737	0.719
2.000	Unflooded	0.716 ± 0.015	0.713	0.731	0.705
2.000	Flooded	0.667 ± 0.015	0.671	0.696	0.666

* 95 percent confidence limit.

** Model A = Engineering Design Model

Model B = Modified Engineering Design Model

5.2 ESADA-VESR Preliminary Critical Experiment Program

5.2.1 Summary

The ESADA-VESR critical program is being conducted at no cost to the AEC. The experimental measurements have been completed. The work during this period consisted of analyzing data and preparation of a topical report.

5.2.2 Comparison of Experimental Results with Predictions

Examination of measured (subcritical) reactivity for the flooded full core, center four rods inserted half-way,

indicates that the predicted reactivity was too high by about 1.4% Δk/k. The measured reactivity change due to flooding with the above rod pattern was -$1.09 at 80°C. The calculated value, however, was +$0.3, indicating a discrepancy of about $1.4 in predicting the cold flooding effect. This discrepancy was not apparent earlier since the measured value of -$1.09 was bracketed by calculated values of -$1.80 for the full core without controls and -$0.2 for the case with four inner control rods fully inserted. A recent two-dimensional analysis has shown that the calculated flooding effect passes through a maximum when the central four rods are partially inserted.

The observed reactivity discrepancies in the critical are being used to "correct" the Mark I design calculations in the following manner:

1. The cold unflooded k_{eff} is lowered 0.4% Δk.
2. The cold flooded k_{eff} is lowered 1.4% Δk.
3. The hot k_{eff} (flooded and unflooded) values are lowered 0.9% Δk.

In essence, those adjustments lower the slope of the unflooded reactivity versus temperature curve by 0.5% Δk (cold to hot) while increasing the slope of the flooded curve by 0.5% Δk. In addition, all reactivities are accordingly reduced by 0.4% Δk. Thus, the calculated temperature coefficients and cold flooding reactivity effect for the critical assembly are made to agree with measurements.

The circumferential power scalloping (azimuthal variations in power around the circumference of individual fuel rods) has been

calculated by two-dimensional techniques. These data, together with axial power distributions and values of integrated power for each fuel rod normalized to core average power, complete the analytical three-dimensional synthesis of power distribution in the critical experiment.

Experimental control worths were extracted from the measurements to be used to determine the appropriate adjustment to be applied to the calculated control worth.

The calculated control system worth (12 rods) is compared below to the best experimental value.

Controls (12 rod) Worth - 20°C - Unflooded	
Calculated (As Built)	Measured
15.1% Δk	12.5 ± 0.7% Δk

The "as built" control elements for the critical were slightly over-size and had on the average 2.8% more weight per linear inch than the actual EVESR control elements. In general, it is concluded that the total control worth is over-predicted by 2.6 ± 0.7% Δk.

6.0 TASK E - COOLANT CHEMISTRY

6.1 Out of Pile Evaluations

6.1.1 General Corrosion

A topical report, GEAP-3779 "Corrosion of Type 304 Stainless Steel in Simulated Superheat Reactor Environments", has been issued summarizing the work carried out through fiscal 1961.

6.1.2 Chloride Stress Corrosion Studies

The series of chloride stress corrosion tests started in the CL-1 facility on September 1, 1961 has been completed. The chloride in the recirculating water was maintained at 1.5 ± 0.5 ppm with sodium chloride. The Type 304 test sheaths were operated under stresses calculated to produce 0.1% creep in 1000 hours in the middle and exit superheaters. After 400 hours of exposure the entrance superheater (Q-1) with its multicolored salt deposit was removed and replaced. After an additional 400 hours the two entrance sheaths (Q-1 and Q-2) were inserted so that the salt deposits were operating at a metal temperature of 1100°F and 1300°F. After an additional 400 hours under these conditions examination indicated that the salts had affected the scale formation and was causing spalling in the deposit areas. There was some intergranular attack, with some grains completely removed, but the greatest attack had not progressed more than two grains below the surface. The application of stress caused spalling in the 1300°F areas which is not unusual. Descaling of the second superheater (Q-4) exposed for

Table 6.1

SUPERHEAT EXPOSURES IN CL-1
(Type 304 Stainless Steel)

Run No.	Dates	Exposure Time, Hours	Heater Sheath Location			Special Run Conditions
			Low 800-900°F*	Middle 900-1100°F*	High 1100-1300°F*	
40	7/21 - 9/30/60	1000	E	9	10	No control of O_2 and H_2 gas in steam
41-42	10/24 - 11/20/60	950	P-3	P-6	P-5	Normal Operation
43-45	11/22 - 3/30/61	2465	P-7	P-9	P-2	Normal Operation
45C-46A	4/27 - 5/25/61	1000	P-11	P-8	P-12	Normal Operation
46B	5/29 - 6/20/61	500	P-11	P-10	P-23	Normal Operation
47	6/23 - 6/30/61	200	P-17	P-14	P-24	Special gas recombination study
48	7/1 - 8/25/61	1000	X9**	X3**	X33**	Start of alternate material study
49	9/1 - 9/22/61	495	Q-1	Q-4	Q-3	Start of stress chloride study - 1.5ppm Cl^- added to recirculating water - Longitudinal stress placed on sheaths
49A	9/22 - 10/16/61	447	Q-2	Q-4	Q-3	Same
49B	10/23 - 11/15/61	433	Y-3	Q-1(Reversed)	Q-2(Reversed)	Same
50	11/22 - 12/ 2/61	210	Y-4	Y-5	Y-3(Reversed)	Same
50B	12/ 2 - 12/14/61	238	Y-8	Y-5	Y-3(Reversed)	Same
50D	12/18 - 12/31/61	242	Y-2	Y-5	Y-3(Reversed)	Same

* Calculated Metal temperature
** Type 347 Stainless Steel

800 hours at a metal temperature of 900-1100°F, indicated no material change in the corrosion rate but an increased loss of scale to system.

Two failures in the CL-1 facility have occurred which have been identified as stress cracking. Both of these failures occurred on stressed heater sheaths in low temperature regions (200°F to 250°F) of the electrically insulated sheaths opposite gasket seals. Operating data are included in Table 6.2. (Not in normal high temperature or steam flow path.) Additional work is in progress to provide more detailed evaluations of these failures.

Table 6.2

Out-of-Pile Stress Failures in CL-1 Heater Sheaths

Heater Location	Chloride in Loop Water ppm	Stress Level psi	Surface Temperature °F	Chloride in Gasket ppm	Time to Failure hr.
Boiler	1.5	22,000	200-250	5(soluble) 500(total)	1491
Entrance Superheater	1.5	23,000	200-250	1280(soluble) 12,700(total)	210

As a result of the two failures above and since it has not been possible to reproduce the chloride cracking at high temperature observed in case of SH-4B and SH-4C, the CL-1 loop is being programmed to operate under simulated SADE exposure conditions. The CL-1 superheat facility will be operated with the boilers producing steam at about 300-350°F and the superheaters operating with only about 1/10 their normal power load. The heaters would continue to have a

longitudinal stress applied and the recirculating coolant will contain about 1.5 ppm chloride. The facility will be cycled to result in one week of operation at normal high temperature and one week at the proposed low temperature for a period up to six weeks.

6.1.3 Inspection of Stress Corrosion Samples

Tubing stress corrosion specimens of Types 316, 347, and 406 stainless steels and of Inconel have been exposed under stress in a simulated nuclear superheat environment shown in Table 6.3.

Table 6.3

Steam Temperature: 1044°F	Flow: 438 lb/hr
pH: 6.5 $\pm$ 0.5	Chlorides in boiler water: $<$0.3 ppm
Oxygen in Steam: 29 ppm	Hydrogen in Steam: 4.57 ppm
Chloride in Steam: $<$0.02 ppm	
Chloride in boiler water during stressed beam exposure: 1.5 ppm	

After exposure, samples of each of these materials were sectioned and examined microscopically. Results of this inspection are summarized in Table 6.3, which includes comparable data obtained with type 304 stainless. Photomicrographs of the scales formed on the specimens are included in Figures 6.1 to 6.10.

No stress corrosion cracking was observed on any of the specimens. Corrosion scales formed are uniform and composed of two layers, as can be seen from the photomicrographs. The heaviest scale, 1.2 mils thick, was formed on the Type 406 as

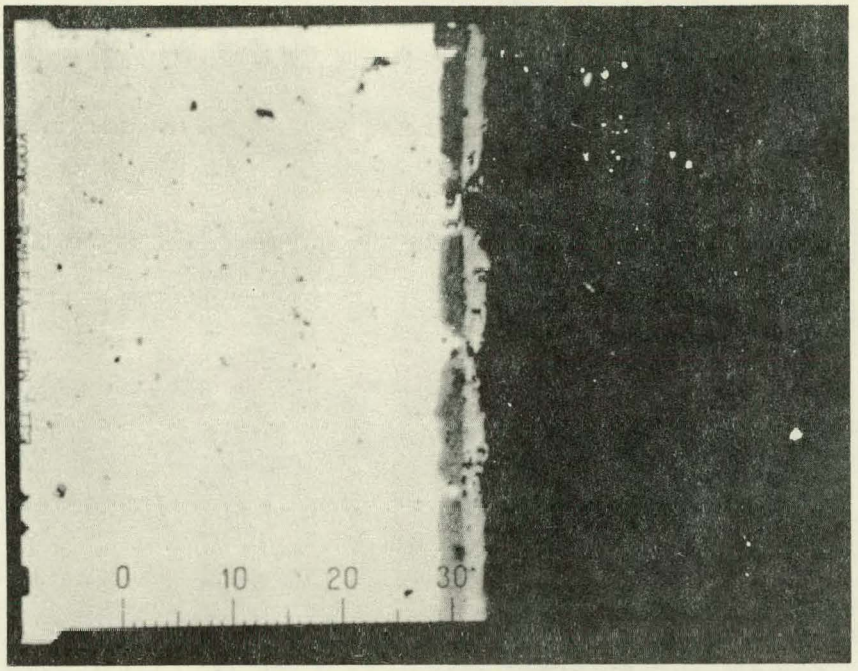

FIGURE 6.1
TYPE 316, 400X, UNETCHED

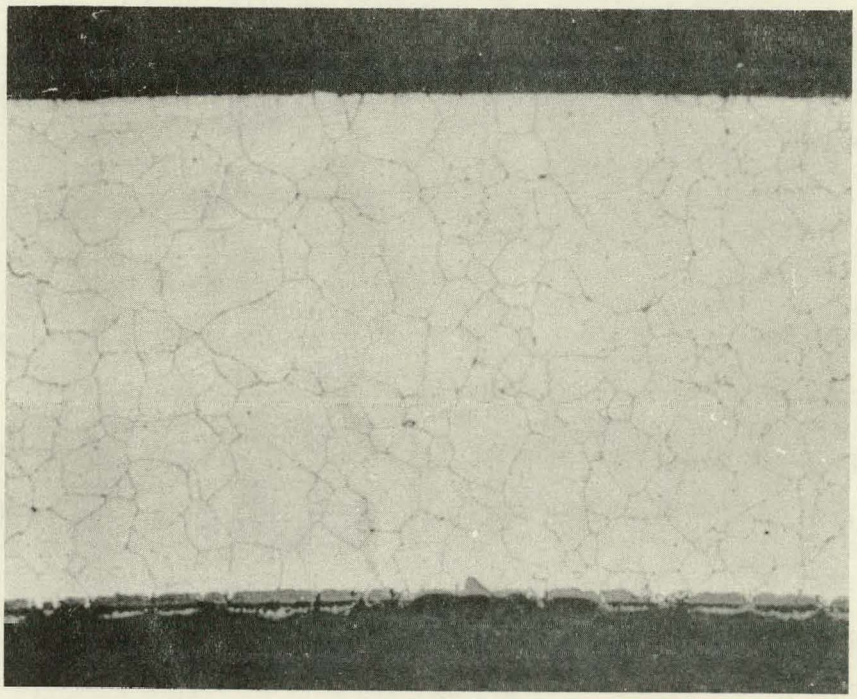

FIGURE 6.2
TYPE 316, 400X, VILELLA'S ETCH

CORROSION SCALE FORMED ON TYPE 316 STAINLESS STEEL IN 1000 HOURS OF EXPOSURE IN A SIMULATED NUCLEAR SUPERHEAT ENVIRONMENT UNDER CONSTANT STRESS.

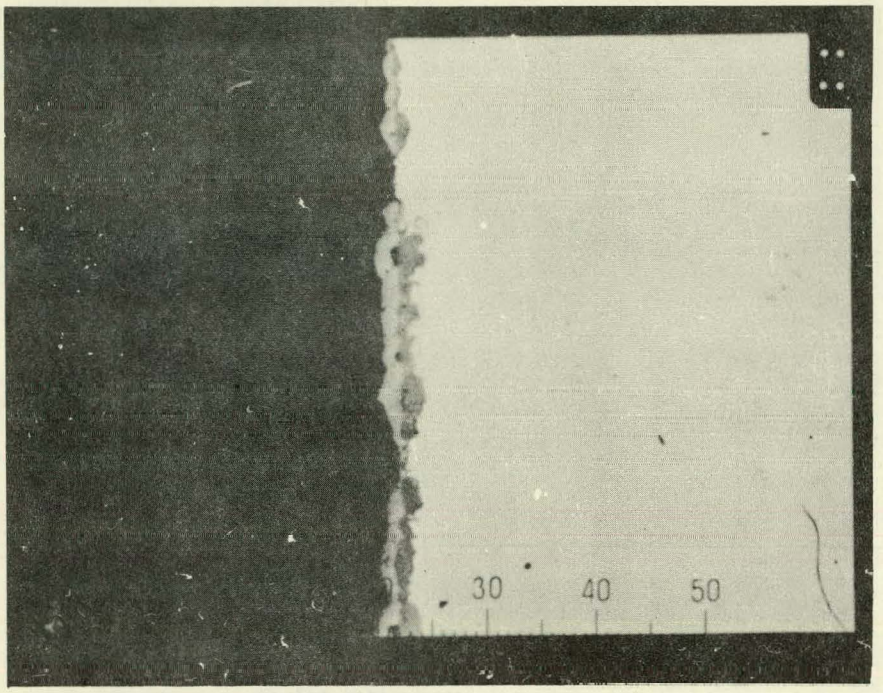

FIGURE 6.3
TYPE 347, 400X, UNETCHED

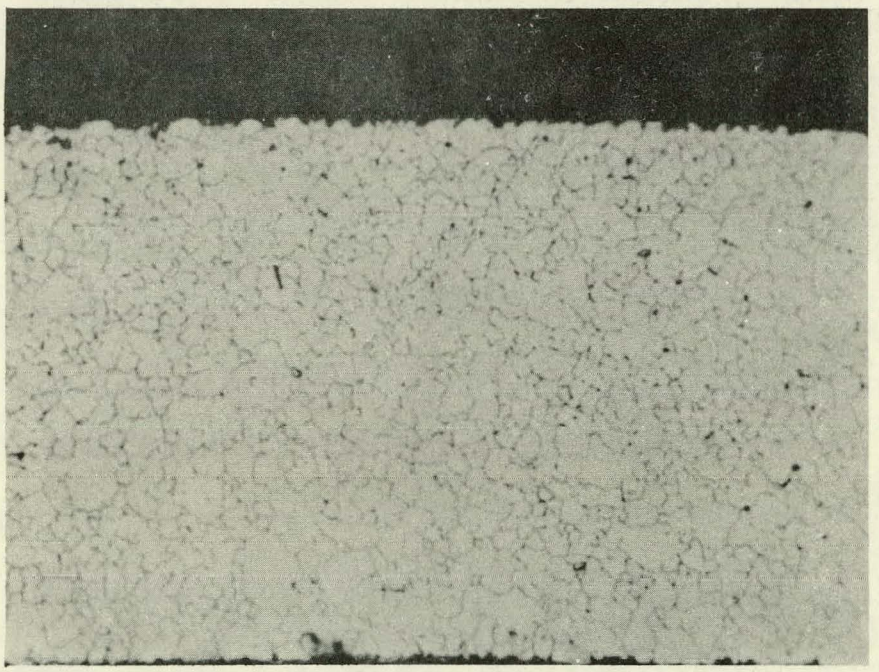

FIGURE 6.4
TYPE 347, 400X, VILELLA'S ETCH
CORROSION SCALE FORMED ON TYPE 347 STAINLESS STEEL IN 1000 HOURS OF EXPOSURE IN A SIMULATED NUCLEAR SUPERHEAT ENVIRONMENT, UNDER CONSTANT STRESS.

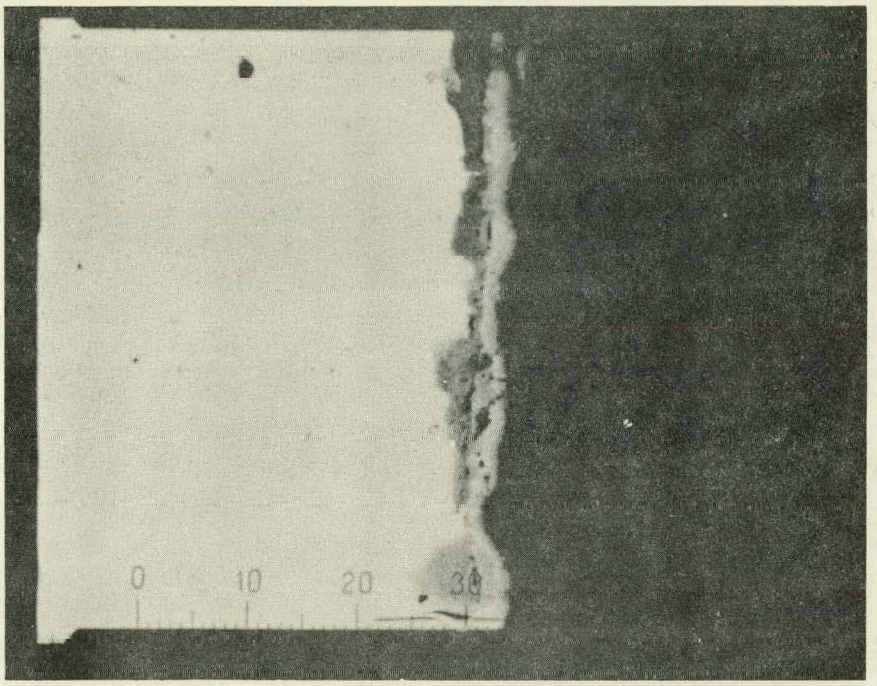

FIGURE 6.5
TYPE 406, 400X, UNETCHED

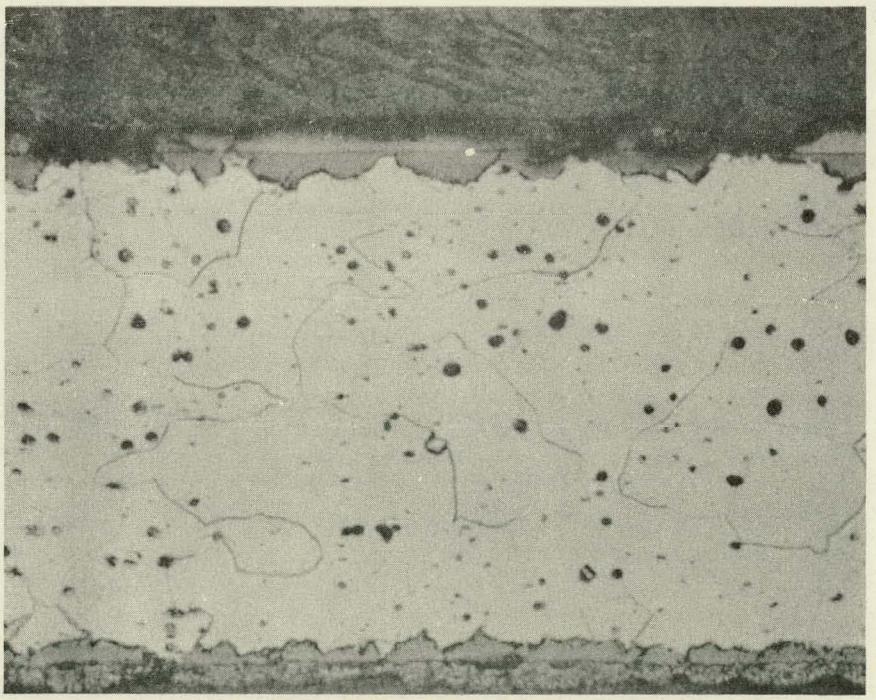

FIGURE 6.6
TYPE 406, 400X, VILELLA'S ETCH

CORROSION SCALE FORMED ON TYPE 406 STAINLESS STEEL IN 1000 HOURS OF EXPOSURE IN A SIMULATED NUCLEAR SUPERHEAT ENVIRONMENT.

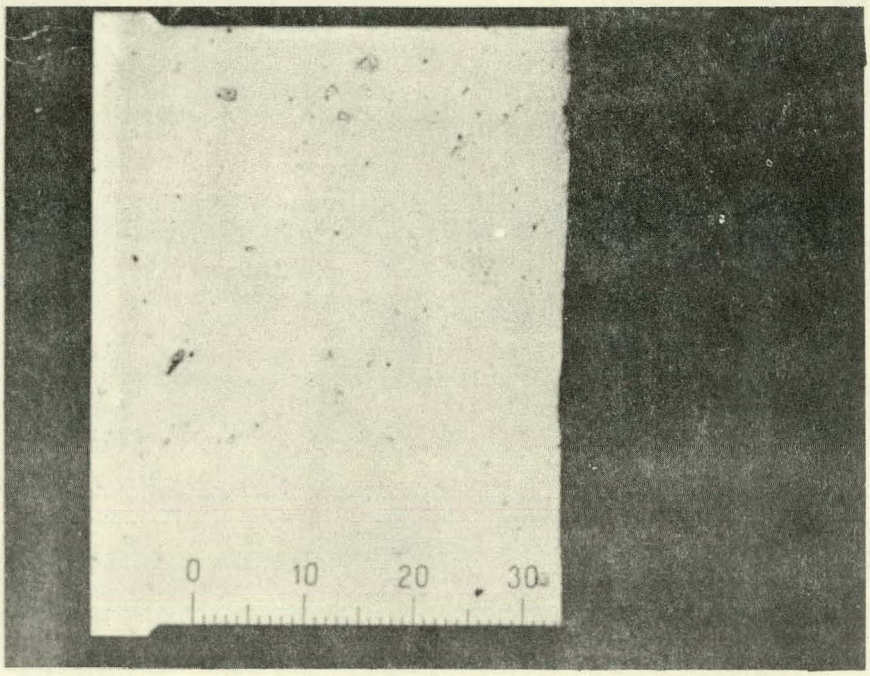

FIGURE 6.7
INCOLOY, 400X, UNETCHED

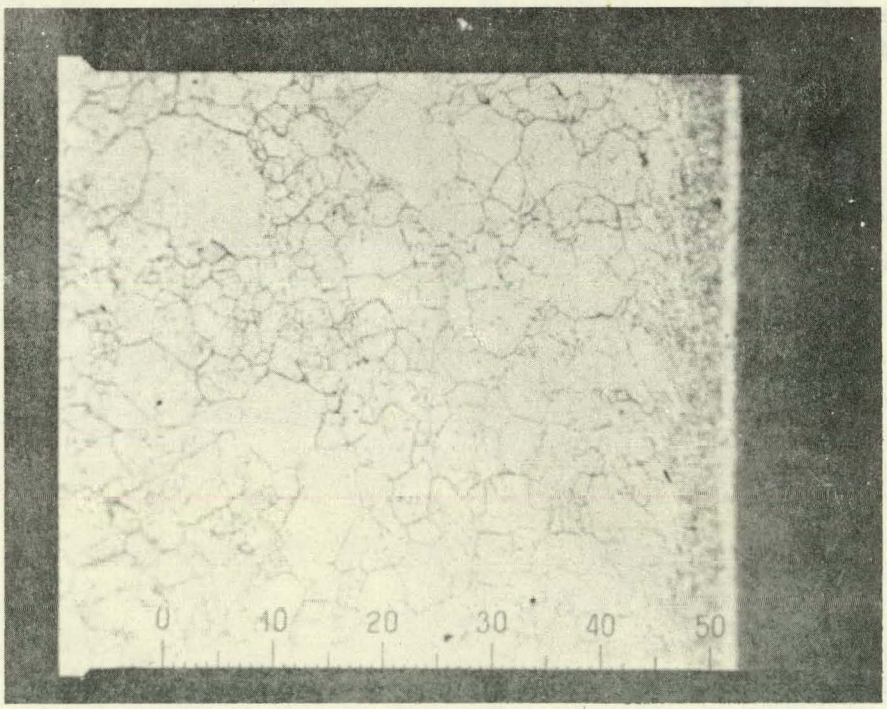

FIGURE 6.8
INCOLOY, 400X, MARBLE'S ETCH
CORROSION SCALE FORMED ON INCOLOY ALLOY IN 1000 HOURS OF EXPOSURE IN A SIMULATED NUCLEAR SUPERHEAT ENVIRONMENT UNDER CONSTANT STRESS.

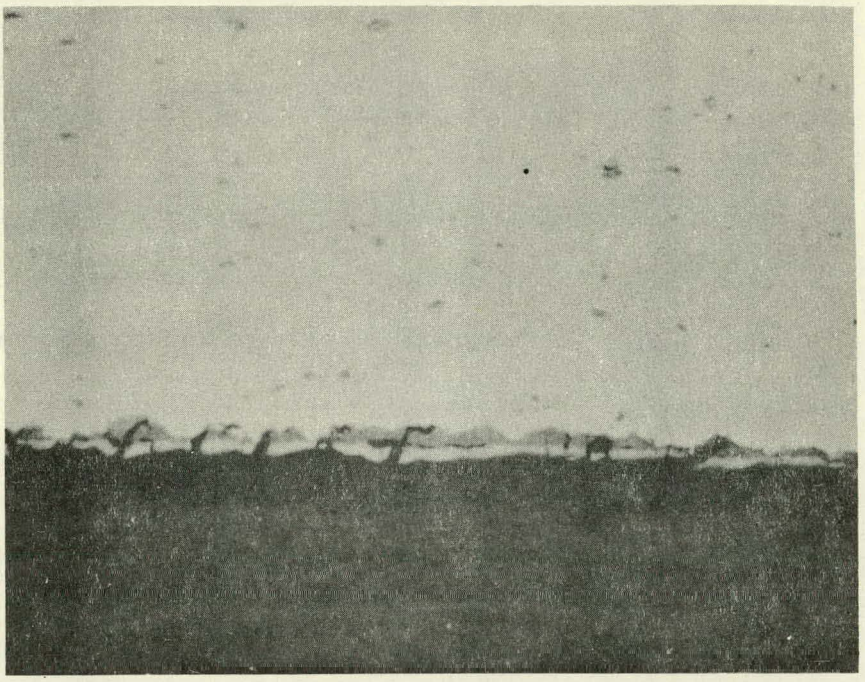

FIGURE 6.9
TYPE 406, 400X, UNETCHED

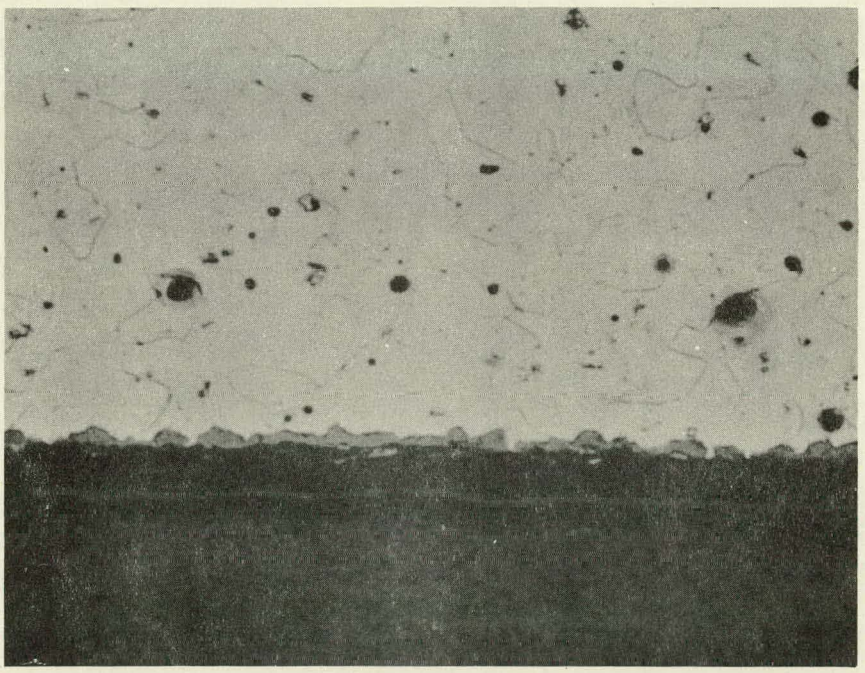

FIGURE 6.10
TYPE 406, 400X, VILELLA'S ETCH

CORROSION SCALE FORMED ON 406 AFTER EXPOSURE IN SIMULATED NUCLEAR SUPERHEAT ENVIRONMENT, FOR 443 HOURS UNDER CONSTANT STRESS.

compared to the Incoloy on which there was no observable scale. The Incoloy sample had been severely cold worked at the surface by a reaming operation during specimen preparation, Figures 6.7 and 6.8. Corrosion scales formed on the type 316 and 347 materials compare closely to those previously observed on type 304 stainless steel.

Table 6.4

Tubular Constant Stress Fixtures Exposed to Nuclear Superheat Environment

Material	Condition	Exposure Hrs.	Applied Stress psi	Scale Thickness mils	Remarks
304 S.S.	Annealed	1000	21,000	1.0	Two phase uniform scale
316 S.S.	Annealed	1000	21,000	0.6	Two phase uniform scale
347 S.S.	As Rec'd	1000	21,000	0.6	Two phase uniform scale
406 S.S.	As Rec'd	1000	32,000	1.2	Two phase uniform scale
Incoloy	As Rec'd	1000	29,000	No Visible Scale	The exposed surface was severely cold worked due to reaming of the tube I.D. during specimen preparation.
406 S.S.	As Rec'd	443	26,000	0.4	Two phase uniform scale
406 S.S.	As Rec'd	443	7,000	0.4	Two phase uniform scale

Stressed beam specimens of Incoloy, AISI 406 and RA-330 were inserted into the superheat coupon section of the CL-1 loop and exposed for various lengths of time. Four coupons of each material were exposed.

The test loop started September 27, 1961, and operated continuously until October 17, 1961, for a total exposure period of 443 hours. At that time, one Incoloy and one RA-330 coupon were

removed from the beam holder, weighed and prepared for metallurgical examination.

The 406 specimens exhibited complete stress relaxation and had fallen from the coupon holder. Only three of the 406 coupons were recovered; they were all weighed and prepared for metallographic examination. The recorded weight gains for the various coupons are listed in Table 6.5.

Table 6.5

Material		Exposure hrs.	Weight Gain mg/dm^2	Scale Thickness inches
Incoloy		443	6.58	None Observed
RA-330		443	60.2	.0004
AISI 406	#1	443	246.5	.0005
	#2	443	244.0	.0005
	#3	443	238.0	.0005

Figure 6.11 shows the general surface attack on the RA-330 coupon and reveals the typical "alligator hide" effect. Figure 6.12 is an unetched cross section showing the scale formation and subscale attack. The attack is non-uniform but shows no preference for transgranular or intergranular attack. This is clearly seen in Figure 6.13 in which the specimen has been etched for microstructure.

The same pictoral presentation is shown in Figures 6.14, 6.15, and 6.16 for Incoloy, and Figures 6.17 through 6.19 for a representative 406 coupon. The Incoloy coupon showed a very small amount of scale or oxide formation. The very small

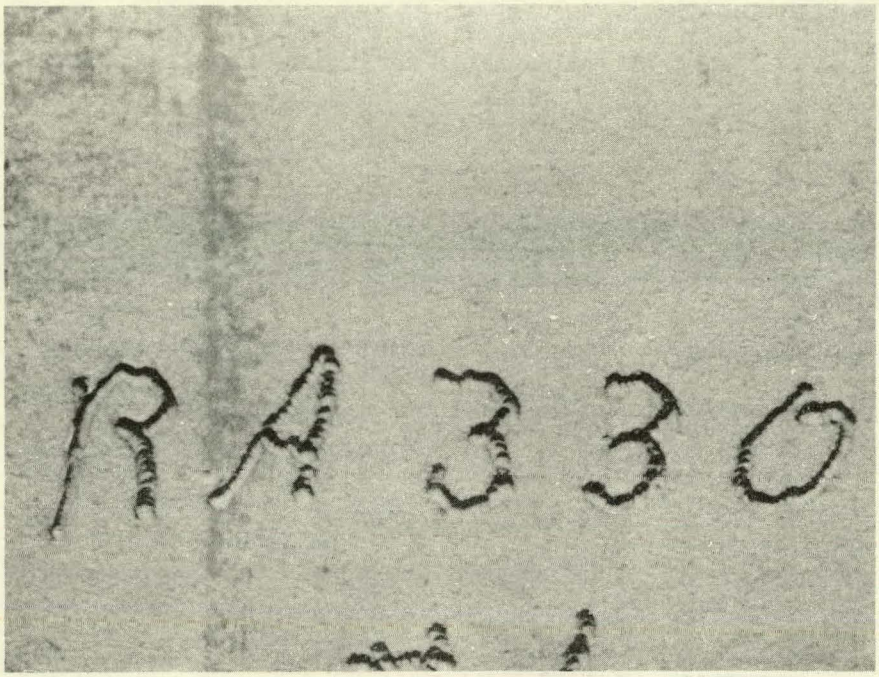

FIGURE 6.11
TYPE RA330 SURFACE CONDITION AFTER 443 HOURS
EXPOSURE (STRESSED BEAM)

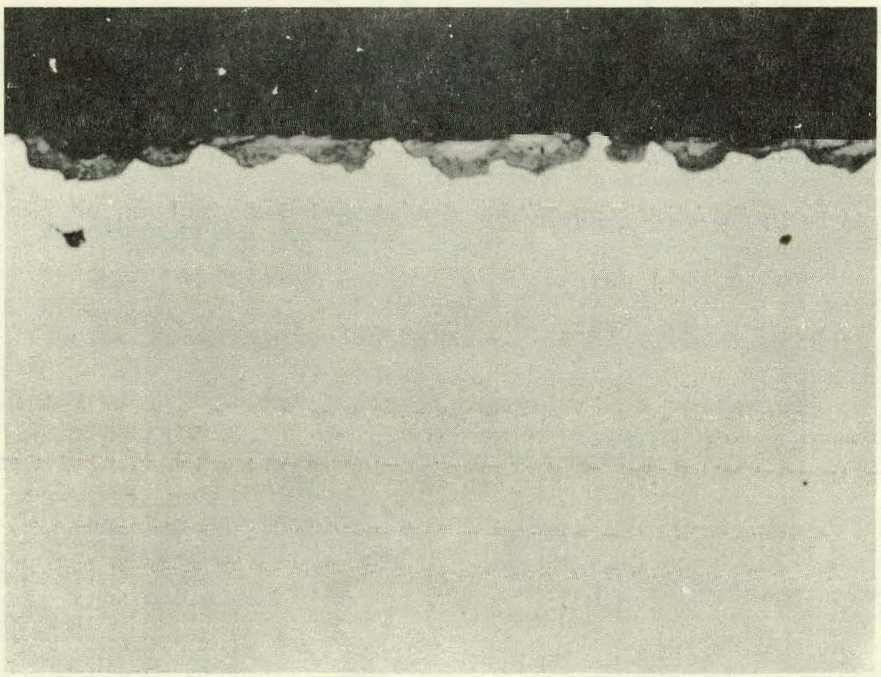

FIGURE 6.12
TYPE RA330 SCALE FORMATION AFTER 443 HOURS
EXPOSURE (STRESSED BEAM) UNETCHED, 400X

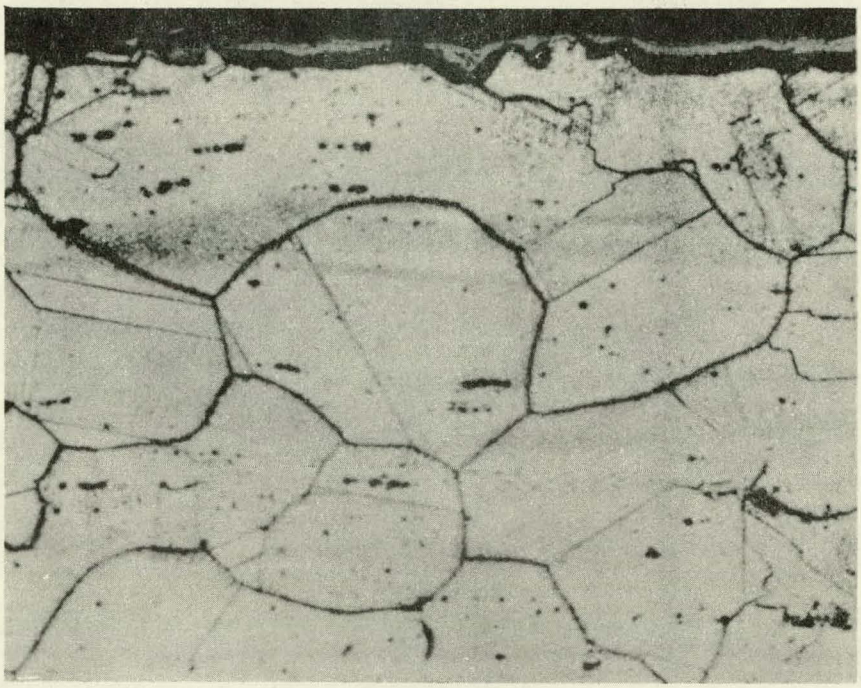

FIGURE 6.13
TYPE RA330 MICROSTRUCTURE AND SCALE FORMATION
AFTER 443 HOURS (STRESSED BEAM). OXALIC ETCH. 400X.

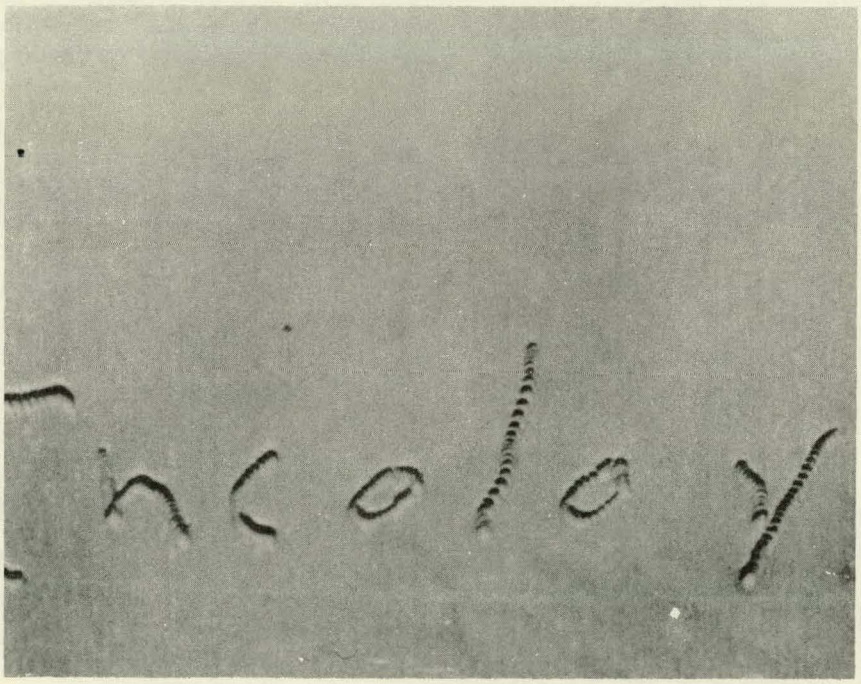

FIGURE 6.14
INCOLOY SURFACE CONDITION AFTER 443 HOURS
EXPOSURE (STRESSED BEAM) 11X

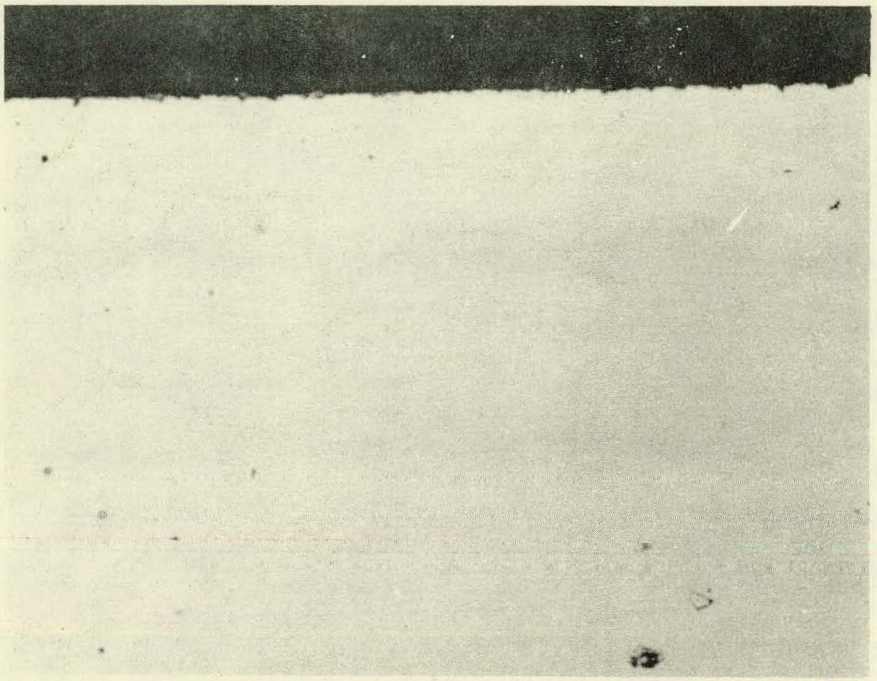

FIGURE 6.15
INCOLOY SCALE FORMATION AFTER EXPOSURE OF
443 HOURS (STRESSED BEAM). UNETCHED. 400X

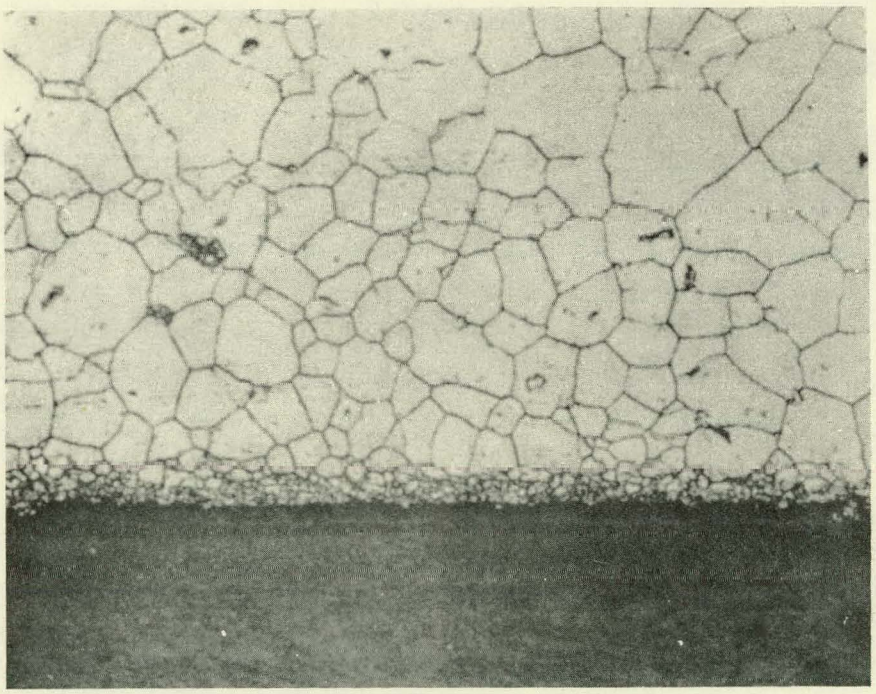

FIGURE 6.16
INCOLOY MICROSTRUCTURE AND SCALE FORMATION AFTER
443 HOURS EXPOSURE. SMALL GRAINS AT SURFACE DUE
TO HEAVY COLD WORKING (STRESSED BEAM).
MARBLE'S ETCH, 400X.

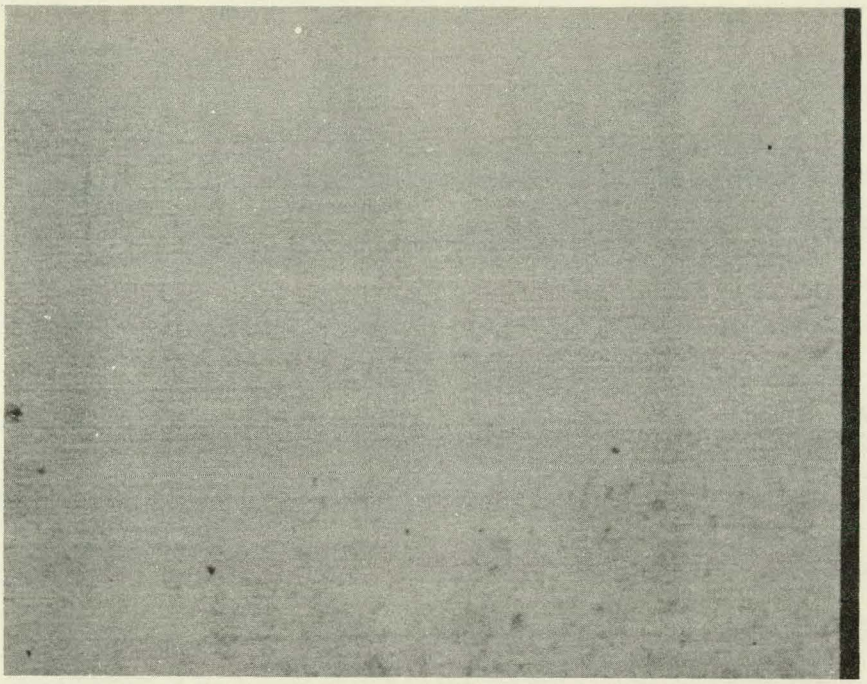

FIGURE 6.17
TYPE 406 SURFACE CONDITION AFTER 443 HOURS
EXPOSURE (STRESSED BEAM) 11X

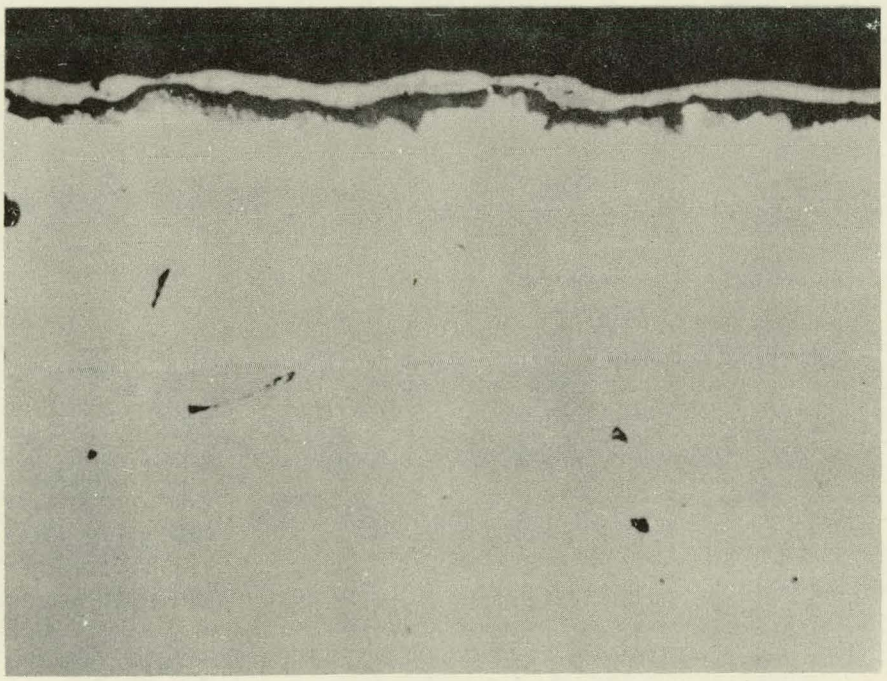

FIGURE 6.18
TYPE 406 SCALE FORMATION AND SUBSCALE ATTACK
AFTER 443 HOURS EXPOSURE (STRESSED BEAM)
UNETCHED, 400X

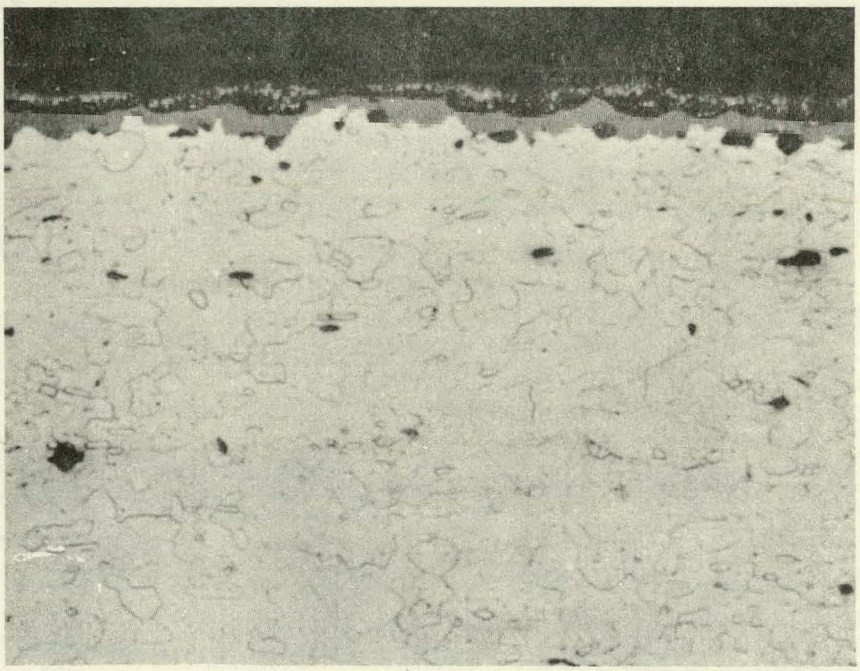

FIGURE 6.19
TYPE 406 MICROSTRUCTURE AND SCALE FORMATION
AFTER 443 HOURS EXPOSURE (STRESSED BEAM).
VILELLA'S ETCH, 400X

grains at the surface of the coupon are not believed to be due to exposure but rather due to heavy cold working.

AISI 406 exhibited the most uniform surface and subscale oxidation. No oxide fingers were observed and the grain boundary structure at the oxide interface was normal.

The loop chemistry conditions are listed in Table 6.3. The chloride additions for this test were made to the boiler water about 4 hours after loop startup. Since the only chlorides in the superheated steam are present in moisture carryover, it is doubtful that any moisture, and hence chlorides, existed beyond the first heater test unit of the superheater section in the CL-1 loop. Therefore chloride attack was not a factor in the oxidation of these coupons.

A test has been undertaken to determine the relative susceptibility of several materials to intergranular attack by NaCl and heavy metal chlorides as identified in the deposits on SADE fuel elements and CL-1 test sheaths. Unstressed specimens of Type 304 and 406 stainless steels, Inconel, RA330 and Hastelloy X were exposed in air to NaCl for 1400 hours at 1100°F. All the alloys were subject to surface attack. Type 406 showed the greatest surface attack while RA330 showed the greatest intergranular attack ($\sim$.009"). Type 394 was similarly exposed to the chlorides of copper, iron, chromium and nickel. The $CuCl_2$ was the most aggressive with intergranular attack of 0.003". The other three salts produced an intergranular attack of 0.003". The other three salts produced

an intergranular attack of 0.001". The tests are being continued with stressed specimens of the various materials.

6.1.4 Oxygen-Hydrogen Recombination Studies

An evaluation of the data collected relative to studying the recombination characteristics of the oxygen and hydrogen to water at the high metal temperatures present on the sheaths under test has been completed. Although basic trends were indicated as reported in GEAP-3778[1], the procedures are not yet adequately refined to justify more quantitative evaluations. It is planned to defer the proposed recombination study report until the analytical equipment can be rebuilt to permit the accuracy required for such a study.

---

[1] Fitzsimmons, M.D., Pearl, W. L. Siegler, M., A Simulated Superheat Reactor Corrosion Facility, August 14, 1961.

6.2 SADE Evaluations

6.2.1 Summary

The SADE loop was not operated during October because of the VBWR shutdown for E-SADE equipment installation. The remainder of the reporting period was involved with measurements made during operation of SH-5A.

6.2.2 In-Pile Evaluations on SH-5A

The SH-5A fuel element design features, operating characteristics and irradiation history are shown on Table 3.1 and 3.2. The SADE installation for SH-5A was modified to provide both a mass spectrometer tight assembly and a seal weld on the under water

flange. These precautions were taken to ensure minimum in-leakage of VBWR water to the superheat fuel region.

During November, SH-5A appeared to be releasing small amounts of fission gases and radio-iodines but the data was variable and difficult to interpret. Unusual amounts of radio-iodine have appeared intermittently in both the inlet and outlet steam condensate samples. The most recent of these showed a different distribution of iodine isotopes from that in the reactor water and hence cannot be attributed to unexpectedly high reactor water carryover. Outlet steam samples have occasionally shown more fission gas radioactivity than inlet samples but not consistently. Both inlet and outlet steam samples have had significantly more fission gas radioactivity than would correspond to the amount seen in the reactor off-gas.

The carryover of reactor water into the SADE loop with the inlet steam has been measured using Na-24 tracer with the following results:

Power, MWt	Water Level, Ft.	Separation Factor Na-24
28	- 0.2	16,000
26	+ 0.5	5,000
20	+ 1.0	6,500

Chloride in the reactor water averaged less than 0.026 ppm and had a measured peak of 0.043 ppm during November, 1961.

An apparatus for measuring the oxygen content of the steam based on the reaction of oxygen with thallium metal has been installed at the SADE steam sample station. The first measure-

ments showed 19 ± 3 ppm of oxygen in the steam entering SADE. Sources of the variability in the measurements are being investigated further.

The unknown isotope (gamma ray = 103 Kev, $t_{\frac{1}{2}}$ - 65 hours) present on coupons exposed to the exit steam during the SH-4C irradiation has been identified as Np-239 (E = 106 Kev, $t_{\frac{1}{2}}$ = 56.3 hours). Identification was by chemical separation and detection of the alpha activity of its daughter, Pu-239. Chemical separations also indicated the presence of measurable quantities of radioactive cerium, barium, and zirconium deposited on the coupons.

Calculations of the radioactivity buildup to be expected in a turbine utilizing steam from a superheat reactor have been extended to include the possibility that a fraction of the activity deposited is subsequently washed from the surface. Measurements of the relative deposition concentrations of iodine isotopes on SADE coupons during the SH-4C exposure and of cobalt isotopes during the SH-4B exposure qualitatively support this hypothesis that a portion of the deposited radioactivity later leaves the surface. Current data are inadequate to estimate the radiation levels in a superheat turbine after long exposure, but do give reason to believe the buildup will not be as severe as was calculated on the basis that all radioactivity was irreversibly deposited.

Irradiation of SH-5A continued during December, 1961. The fission gas content of the steam leaving the loop has generally been within plus or minus twenty percent of the amount entering

the loop. Any leakage of fission gases from the SADE fuel has been less than about 0.5 μc/sec (six gases) during steady power operation and could have been much smaller. The high background activity contributed by other leakers in the VBWR core prevented more precise measurement of fission gas release from the SADE fuel.

Measurements of the radio-iodine in SADE condensate were refined. At 15 MWt VBWR power, the release of radio-iodines from the SADE fuel was measured as being approximately as follows:

	μc/Sec
I-134	4×10^{-3}
I-132	3×10^{-4}
I-135	5×10^{-4}
I-133	2×10^{-4}
I-131	2×10^{-5}

Whether this very small release was from a defect or from surface contamination has not been determined.

The chloride concentration in the reactor water averaged less than 0.03 ppm and had a peak of 0.16 ppm prior to December 30. On December 30, a peak chloride concentration of 0.6 ppm was observed while the reactor was operating at 25 MWt. Valving in of a new condensate demineralizer brought the chloride concentration back to normal, but the concentration was apparently above 0.1 ppm for about thirty hours.

7.0 TASK F - HEAT TRANSFER

7.1 Summary

Work in Heat Transfer and Fluid Flow consisted of operating various steam superheating assemblies for heat transfer data; exposure of prototype fuel assemblies to superheated steam atmospheres; and obtaining pressure drop data in the prototype fuel assemblies with superheat steam flow.

Twenty additional heat transfer data runs have been made. Preliminary reduction of the data from four of these runs is shown in Table 7.1, and appears consistent with similar data obtained at Argonne. Difficulty has been experienced in obtaining steady accurate heater temperature measurements; however, a few of the additional 16 runs are expected to yield valid heat transfer data.

7.2 Task F-2, Heat Transfer to Superheated Steam

A tubular flow test section, 0.370 in I.D. and 10 ft. long, was assembled and operated with 5 clamps, each holding 3 thermocouples against the heater tube's outer surface, at nominal levels of 0, 2, 4, 7, and 10 ft. from entrance to the heater.

Four runs were obtained before operations were stopped by an electrical short, between the clamp and support structure, at the 0 ft. level. Good data was not obtained at the 0, 7, and 10 ft. levels due to loosening of the clamps and resultant error in readout temperature, or an oscillatory temperature readout due to variation of electrical pickup by the couple.

Data from the above 4 runs, at the 2 and 4 ft. levels, was reduced without refinement of flow, tube wall temperature drops and longitudinal

heat flux variation, all of which would contribute approximately 5-10% variation in results. The results of these runs are tabulated below[1] and compared to the Argonne superheat data on Table 7.2.

Table 7.1

Heat Transfer Data for 0.370 in. I.D. Tube 10 ft. Long

Run No.	Test Section Level-In. From Inlet	Pressure psi	Exit Temp. °F	Steam Flow Lb/Sec	Mass Velocity lb/hr ft^{2}X10^{-6}	$\left(\frac{hD}{k}\right)_{(1)(2)} Pr^{-1/3}$	Reynold[2] No. X10^{-6}
29	21	800	812	0.252	1.22	1790	0.753
	45					1745	.718
30	21	800	875	0.255	1.23	1578	.740
	45					1420	.703
31	21	800	895	0.216	1.04	1210	.626
	45					1110	.592
32	21	800	905	0.140	0.68	832	.403
	45					758	.396

(1) An error in the Nusselt numbers, reported in the Nov. 1961 Monthly Report, has been corrected.

(2) Arithmetic mean of heater wall and steam properties used to evaluate steam properties.

Sixteen additional runs were made with a new heater assembly similar to the one above, except that the clamps were spring loaded. The springs on the clamps were spring loaded. The springs on the clamps were designed to result in a load of 4-5 lbs. holding the thermocouple against the outer heater wall. Heater temperature data was erratic, but a few indicative results are expected after data reduction is completed.

Although the spring loaded clamps appeared to result in better thermocouple contact, trouble was still experienced with warping and loss of thermocouple contact.

Further analysis has indicated that the 100 cycle Choppers, used to remove A.C. pickup in the couples due to contact with the electrical heater surface, may not be operating fast enough to remove the A.C. pickup and induced voltage pickup to which the couples are exposed. A new heater assembly design will be tried in which the thermocouples are not in direct contact with the electrically heater superheater tube.

7.3 Fretting Corrosion

The superheat facility, used for Task F-2 above, was operated several times to provide a typical steam environment for prototype fuel elements.

Steam exposure was made on two elements during this quarter. Times of exposure and range of conditions are tabulated below.

Table 7.2

Exposure Conditions for ESADE Prototype (General Electric Drawing 124F761)

		Range of conditions during operation with	
		Water	Steam
Temperature,	°F	70/540	600/902
Pressure,	PSI	0/1000	775/1207
Flow Rate,	Lbs/Hr.	Low(1)	0/1242
Exposure Time To Date,	Hrs.	55.2	178.5

Table 7.3

Exposure Conditions for Dummy Cluster (3 Wire) Element

		Range of conditions during operation with	
		Water	Steam
Temperature	°F	-	647/836
Pressure	PSI	-	957/1008
Flow Rate	Lbs/Hr.	0	623/1165
Exposure Time To Date	Hrs.	0	21.3

(1) Not Monitored

7.4 Superheated Steam Pressure Drops - ESADE Element

A total of 30 pressure drop runs have been logged on this element to date.

Preliminary reduction of the overall pressure drop show it to be consistent, within about 10%, and varying with the mass flow to the 1.79 power.

Overall pressure drop ranged from 9.9 psi at 0.103 lb/sec (371 lb/hr), with inlet steam at 845°F and 813 psi, to 124 psi at 0.345 lb/sec (1243 lb/hr) with inlet steam at 677°F and 801 psi.

7.5 Superheated Steam Pressure Drops - Dummy Cluster (3 Wire) Element

Five pressure drop runs were made and preliminary reduction shows overall drop to be consistent in trend and within 10%.

Overall drop varied from 4.5 psi at 0.185 lb/sec (666 lb/hr) with inlet steam at 836°F and 993 psi, to 10.2 psi at 0.324 lb/sec (1165 lb/hr) with inlet steam at 660°F and 999 psi.

8.0 TASK G - MECHANICAL DEVELOPMENT

8.1 Steam Separator Development

8.1.1 Summary

During this report period efforts were devoted to procurement and air-water testing of the full circle radial separator model. Results of these tests continue to be favorable, but further testing to give more quantitative results on downcomer flow profiles and steam-water carryover are required.

8.1.2 Discussion

The full circle radial vane separator model tested during this period is made up of 36 vanes of 130° arc of 4-inch radius mounted on a 10-inch diameter plenum. The vanes are mounted on the plenum to provide 18 active pairs alternating with 18 inactive pairs around the full circle. Inlet nozzles 1/2" wide x 3/4" long x 18" high are provided. These nozzles can be restricted in height by appropriate plugs. The reduced number of nozzles (18 instead of 36) and the restriction of nozzle height are required to insure design liquid and gas velocities at the flow capabilities of the test loops.

The model as tested is equipped with three different diameter shrouds. These shrouds perform the function of the reactor vessel wall in that the vane discharge streams impinge on the shroud to form a downcomer vortex. The three shrouds used allowed an annular downcomer space between the vane ends and the shroud of 1-$\frac{1}{2}$", 2, and 3". Tests showed all three shrouds to be satisfactory from a carryunder standpoint. However, combined quantitative carry-under and visual carryover results indicated the 2" annulus to be

the most satisfactory. With the 2" annular gap the model operated with a 6" high inlet nozzle at 760,000 lb/hr of water and 2,170 lb/hr of air with a resulting carryunder void fraction of less than 0.02% and no water overflow at the top of the vanes.

8.1.3 Test Program

8.1.3.1 Air-Water Testing

Based on the results described above, a transparent plastic shroud to give a 2" annulus has been designed and is presently being fabricated. This shroud will allow visual and photographic study of the vortex formation on the wall. Pitot tubes in this shroud will be used to determine the flow profile in the annulus. The profile data will be used in analytical studies of the separator.

8.1.3.2 Steam-Water Testing

After the above air-water testing, the model with steel shroud will be run on steam-water mixtures in the Moss Landing loop. In these runs, carryunder will be measured as a check on the air-water, steam-water carryunder correlation that has previously been observed. Carryover data will also be obtained because the air-water testing gives no correlation with steam-water on carryover.

8.2 Seal Development

8.2.1 Leak Test of Superheat Seal

During October the autoclave test facility to measure seal leak rates was set up.

In November six test runs were conducted in the leak test facility. A summary of the average leakage rates is given below.

The superheat seal performed satisfactorily for one position in the test capsule, (Runs 1-3). The seal didn't perform as well for two other positions, (Runs 4-6). The summary below shows that the maximum leak rate of 2.2 lb/hr from saturated water to saturated steam and 8.3 lb/hr from saturated steam to superheated steam was exceeded only during Run 4.

Average Leak Rates

	1	2	3	4	5	6
Sat. Steam Leak Rate (lb/hr)	0.0	0.0	0.0	2.38	1.10	0.79
Superheated Steam (lb/hr)	0.58	0.4	0.0	8.51	7.30	6.33

8.2.2 Leak Test of Superheat Seal

The leak tests showed that the seal idea is feasible. However, a slight modification of the test chamber was planned to take advantage of the seal formed in Runs 1-3.

In the month of December, a modification to the test capsule was made, and another seal was being fabricated for testing in the modified capsule.

8.2.3 Corrosion Test

The corrosion test was started on October 20, 1961. The sealed capsules containing the solder and stainless steel specimens were placed in a furnace maintained at a temperature of 800-840°F.

The test was terminated on December 18, 1961. None of the specimens subjected to 10,000 psi and 15,000 psi bending stress

failed during the test. Visual examination of the test specimens showed that some surface corrosion had occurred. No conclusions regarding intergranular corrosion or cracking can be made until the metallurgical examination is completed.

9.0 TASK H - SADE AND E-SADE

9.1 SADE

9.1.1 Summary

The SADE irradiation during this reporting period was limited to SH-5A since the VBWR reactor was down from October 5 to October 31 for E-SADE installation. Tables 3.1 and 3.2 provide a complete summary of SADE fuel irradiations.

9.1.2 SH-4C Irradiation

SH-4C fuel element was removed from the loop in late September when steam samples indicated that the element was adding significant radioactivity to the steam, probably from a cladding defect. The element was forwarded to RML for examination. RML results are reported in Section 3.2.2.

9.1.3 SH-5A

9.1.3.1 SH-5A Facility Preparation

Because of the concern about chloride stress corrosion of the stainless steel cladding which has been employed on test superheat fuel elements, including SH-5A, the installation of this element was carefully evaluated to determine the significance of leakage of reactor water into the test section. It was decided that the leakage should be held to as low a value as possible for test of this fuel element to determine if optimum conditions, with regard to chloride contamination, would result in failure of the cladding. The internal seal surfaces were carefully reworked and lapped to assure minimum internal leakage. This rework included both lower and upper flanges even though the upper flange is in the steam dome of the reactor. A static pressure leak check

of the process tube, tube bundle assembly showed a total gas leakage of this assembly of 0.12 cu. in. per minute of air at a pressure differential of 10 psig. If reactor water with chlorides at a level of 0.02 ppm leaked into the assembly at the same gaseous volume rate, and the chlorides were to deposit uniformly over the surface of the fuel element, the rate of deposit on the element would be 0.366×10^{-2} mg/sq. dm. per month.

The seals were repaired by the following sequence of operations on each seal surface.

1. Removal of the oxide present on the seal surfaces of the reused flange and tube bundle, by a power driven soft wire brush.

2. Hand lapping of the seal surfaces starting with coarse diamond dust and then progressively finer grit and emery paper using lapping plates specifically made for the work.

3. Careful cleaning to remove all traces of abrasive.

4. Remachining and/or hand grinding of the flange seating surfaces to preserve the original dimensional relationships between the seal surfaces and the seating surfaces.

The seals were lapped sufficiently to remove all traces of the indentations and machining marks. The final surface produced was essentially a "mirror" finish estimated to be less than 6 microinches RMS and flat within .0002 in. The lapping was carefully controlled to maintain the seal surface parallel to the flange seat surface, and is estimated to be within 1.5 mils. In addition, the Skinner

seal ring was gold plated with approximately 0.0005 thickness pure gold to assist in providing a leak tight seal.

Because of the critical significance which will be attached to the test of SH-5A, with regard to stress chloride corrosion of the fuel element cladding, it was decided that the lower flange, which is located below the water level inside the reactor, should be seal welded. This has not been done in the past since it would then be necessary to cut the process tube in order to remove the installation from the reactor. However, leakage through this flange has increased significantly on some past installations during the irradiation period. Although the lapped seals of this assembly for SH-5A have achieved a satisfactorily tight assembly, the decision was made to seal weld the flange to assure maintenance of satisfactory leak tightness throughout the test period. Since no equipment was available to cut the assembly after it is welded and irradiated, the assembly was not installed at the start of the fuel cycle runs to permit time to obtain suitable equipment.

A guillotine cutter was procured to cut the process tube and upper extension of the fuel element to permit removal when test of this element is completed.

This cutter was tested on a dummy assembly. A close fitting collar was made to fit directly under the cutter section to minimize distortion to the process tube and possible damage to the fuel section during cutting. The test was successful and seemed to indicate that negligible disturbance of the fuel element section would occur during the cutting process. With this

cutter available, fuel element SH-5A was installed in the SADE loop and irradiation of the element started on November 13. Pressure test of the in-core assembly, prior to installation in the reactor, showed essentially zero leakage.

9.1.3.2 SH-5A Operating Conditions

The fuel element design was changed to provide a pre-heat section for the incoming steam to help assure that dry steam is in contact with the fuel element. This has been accomplished by removing the thermal liner in the upper "hardware" section of the fuel element, permitting regenerative heat transfer from the superheated (outlet) steam to the inlet steam. Thus, only dry superheated steam would be in contact with the element during normal power operation of the element. The heat transfer is sufficient to dry about 4% moisture in the inlet steam at normal power. Table 9.1 lists the design operating conditions for this element and is based upon dry steam entering the heater section of the fuel element. These values are based upon an estimated power of 78 KW for the element which has been predicted by physics calculations for this element at a VBWR power of 33 MW.

Table 9.1

Inlet temperature - heater section - ^{o}F	545
Inlet temperature - fuel section - ^{o}F	575
Maximum steam temperature - fuel exit - ^{o}F	857
Maximum steam temperature - heater exit - ^{o}F	803
Maximum clad temperature - ^{o}F	1,200
Maximum heat flux - Btu/hr-ft^2	289,000
Maximum fuel temperature - ^{o}F	2,770
Minimum steam flow rate - lb/hr	1,180

Figure 9.1 shows the final design of the SH-5A fuel element. Figure 9.2 gives the process tube design employed with this element. (The G-3 assembly was employed with SH-5A.) Figure 9.3 gives the power plot for this element.

Irradiation of superheat fuel element SH-5A continued through the end of this report period. Superheat discharge temperatures above 800°F, corresponding to clad temperatures from 1100 to 1200°F, were maintained for a considerable portion of the operating period. Some evidence of a slight defect in the fuel cladding has been obtained from steam samples and from the SADE radiation monitor, but the release rate is very low and inconsistent. Details of radiochemistry measurements for SH-5A operation are reported in Section 6.2.2.

Calculations of power output of SH-5A based upon test data give a power for this element of 2.79 KW for each one MW reactor power. This is an average of a number of different data sets which were employed to minimize uncertainties in reactor power level in these calculations.

9.1.3.3 SH-5A Operating Data

Operation of this element, up to January 1, 1962, has been as follows:

Superheat Discharge Temp.	Hours of Operation
800°F and higher	175
725°F to 800°F	310
Below 725°F	360

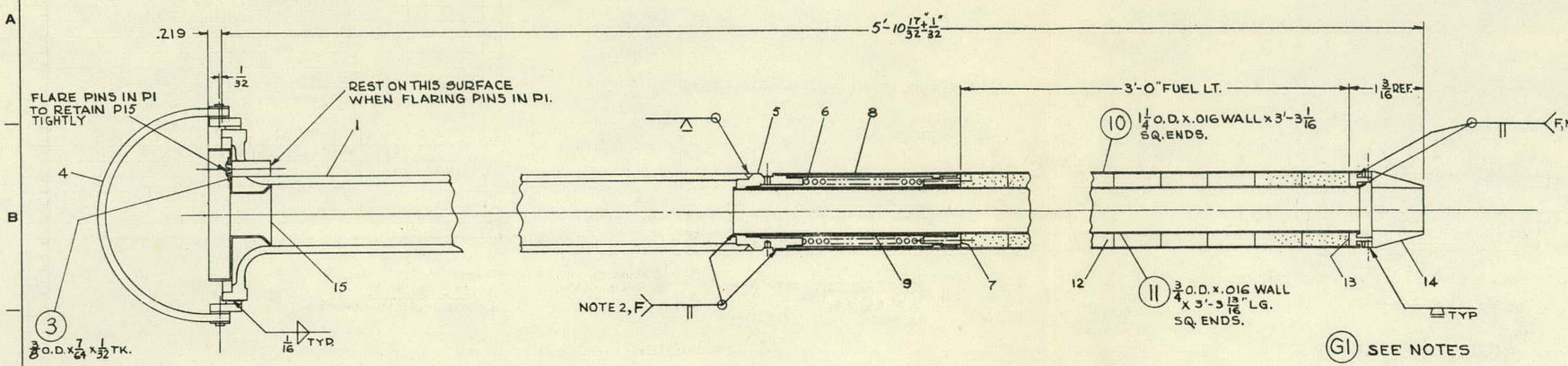

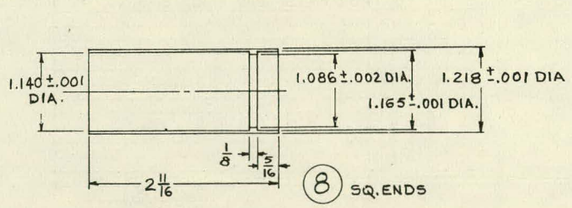

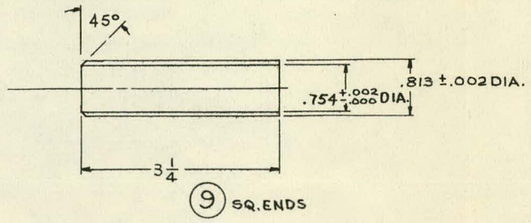

UNLESS OTHERWISE SPECIFIED USE THE FOLLOWING:—				
APPLIED PRACTICES	SURFACES	TOLERANCES ON MACHINED DIMENSIONS		
		FRACTIONS	DECIMALS	ANGLES
145A5481	63	± 1/64	± .005	± 1°

762D437

REV. NO. Ø1

TITLE: FUEL ELEMENT SH5A

FIS MADE FOR SADE FCF 221L140

GROUP NO. AND SUFFIX	G1	PART NO.	NAME	DRAWING NO., DESCRIPTION, MATERIAL, WEIGHT
	1	1	FUEL FLANGE	985C340 G1
		2	THERMAL LINER	114B5248G3
	3	3	WASHER	AISI TP 304
	1	4	BAIL	114B5252G1
	1	5	END PLUG	149A4522P1
	1	6	SPRING	149A4523P1
	1	7	SLEEVE	149A4524P1
	1	8	TUBE	ASTM A 269 TP 304
	1	9	TUBE	
	1	10	OUTER CLAD	WD
	1	11	INNER CLAD	ASTM A269 TP 304 WD
	X	12	FUEL	PER ENG. INSTR.
	1	13	END PLUG	149A4525P1
	1	14	CONE	149A4526P1
	1	15	LINER	149A4809G1

NOTES:

1. FOR INTERPRETATION OF GEOMETRIC TOLERANCING REFER TO DWG. 219B402.
2. THESE WELDS TO BE CHECKED FOR LEAKAGE WITH MASS SPECTROMETER EQUIP. MAXIMUM PERMISSIBLE LEAKAGE NOT TO EXCEED .005 MICRON CU. FT. / HR.
3. OTHER WELDS TO BE TESTED PER SEPARATE ENGINEERING INSTR.
4. F = AWGT FUSION WELD.
5. FOR WELD. ROD USE E308 WHERE REQ.

Figure 9.1

UNLESS OTHERWISE SPECIFIED USE THE FOLLOWING:— APPLIED PRACTICES | SURFACES 125 | TOLERANCES ON MACHINED DIMENSIONS: FRACTIONS ± 1/64, DECIMALS ± .005, ANGLES ± 1° | SCALE FULL | 141F786

TITLE: PROCESS TUBE
FIRST MADE FOR SADE V

P.L. ISSUED

6'-0 15/16 ± 1/16

.005

G1
G2 DIFF NO. & LOCATION OF SCREWS OTHERWISE SAME AS G1.
G3 OMITTED P3 & C6 OTHERWISE SAME AS G2

BEND OVER D7 AS SHOWN TYP. 2 PL. 10

DETAIL E

7 3/4
6.250 BASIC
3.125
60° TYP.
.750 +.005 −.000 DIA 2 HOLES
⊕ .002 R
3 1/2 DIA
5 1/2
3/32 R
G
3/4 TYP
3/4 R, TYP.
3/8-16 UNC 2B x 1/2 DP. DO NOT BREAK THRU. TYP. 2 PL.

1 SEE NOTE 1.

SECTION H-H TYP. SEE NOTE 4.

5'-9 3/32
37 1/2 ± 2 1/2, TYP.
1/32 TYP.
19 1/8
2
17
2 13/16
6-32 UNC2B 4 HOLES EQ. SP AT EACH LOCATION.

2 1 1/4 SCH. 10 PIPE

22 1/2
22 1/2
SECTION K-K
LOCATE HOLES AS INDICATED

1 3/8 DIA.
5/8-10 STUB ACME 2G BLUNT START
5 BREAK SHARP CORNERS

1.442 DIA.
5/16
4 1 1/2 STD. BUTT WELD PIPE CAP

37 1/2 ± 2 1/2 TYP.
6-32 UNC2B 4 HOLES EQ. SP AT EACH LOCATION
21 5/8
18 1/2
1 3/8
5'-9 3/32
13 1 1/4 SCH. 10 PIPE SQ. ENDS

.875 DIA.
1/16
1/8
1/2
1

STAMP 3/64 HIGH 1/64 DEEP
SH-5
29/64 DRILL, 2 HOLES
2 3/4 R
1/4
3/8 R
11 1/4 x 3/4 x 12 1/8 DEV. LT. (APPROX.)

25/64 DRILL
1/4
5/8
15/16
13/16
3/32
3/4
1 1/2
10 1 11/16 DEV. LT. (APPROX.)

©A .002 T I R
4.770 ± .002 DIA
4.545 DIA.
4 1/4 DIA.
2.755 +.002 −.000 DIA.
2 7/16 DIA.
15°
1/63 R, MAX.
-A-
-B-
-C-
2.50 ± .001
15/650 ± .002
⊥ A .002
⌒ .002 B
Ⓜ B .010
Ⓜ B .001
17/32
2 7/32
1/4 R
1.442 DIA.
1.660 DIA.
37 1/2 ± 2 1/2
6 SEE NOTE 2.
3, SEE NOTE 3
SECTION G-G

.010 R MAX. TYP
DETAIL C

MAX. RADIUS 1/2"
33/64
1 1/32
3/32
VIEW D

1/16 SAWCUT, TYP.
1/4
7/8
6 1" O.D. x .049 WALL (ANNEALED)

GENERAL ELECTRIC — PARTS LIST FOR 141F786

PARTS LIST FOR 141F786				TITLE: PROCESS TUBE, FIRST MADE FOR SADE V		
G3	G2	G1	PART NO.	NAME	DRAWING NO., DESCRIPTION, MATERIAL, WEIGHT	
	1	1	1	FLANGE	ASTM A 167 TP 304L	
		1	2	PIPE	ASTM A 312 TP 304L	
	1	1	3	BACKING RING	FOR 1 1/4 SCH. 40 PIPE, ASTM A167 TP 304L, NUB TYPE	
	1	1	4	CAP	ASTM A 403 TP WP 304L	
	2	2	5	NUT	SEE DETAIL	
	2	2	6	RETAINER	SEE DETAIL	
2	2	2	7	BOLT, HEX. HD.	3/8-16 UNC 2A x 3/4 LG. STN. STL.	
2	2	2	8	WASHER	1" O.D. x .391 I.D. x 1/16 THK. STN. STL.	
2	2	2	9	BUSHING	7/16 O.D. x .028 WALL x .130 ± .002 LG. AISI 304 STN. STL.	
2	2	2	10	LOCKWASHER	AISI 304 STN. STL.	
1	1	1	11	BAIL	AISI 304 STN. STL.	
16	16	16	12	SET SCREW	OVAL POINT, 6-32 UN 2A 1/4 LG TP 304	
	1	1	13	PIPE	ASTM A 312 TP 304L	

DESCRIPTION OF GROUPS

REVISIONS: 1 GEN. REV. 2 NE 613 3 NE 1647

PRINTS TO

APPROVALS: APED SAN JOSE — PARTS LIST FOR 141F786

Figure 9.2

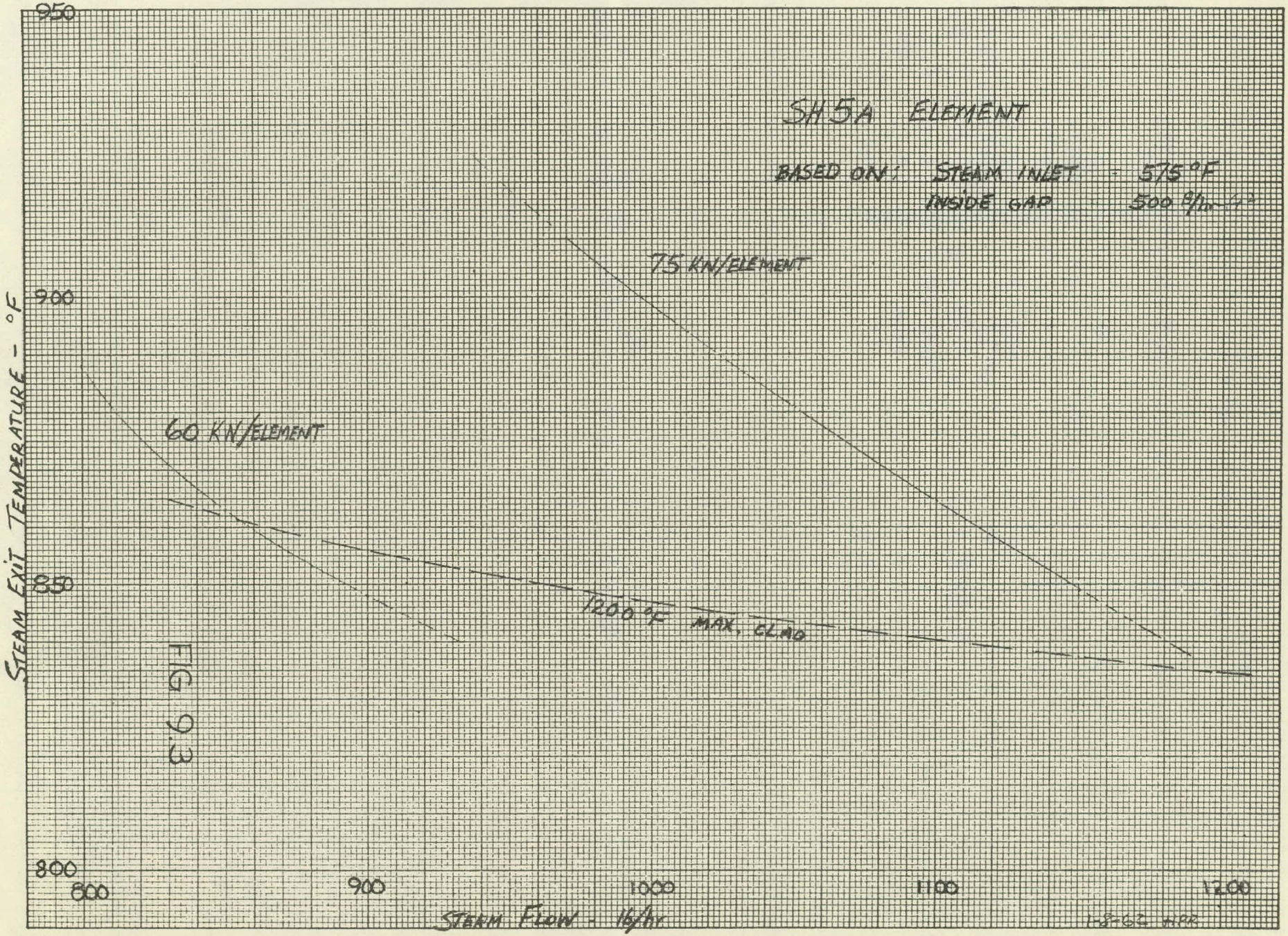
SH 5A ELEMENT
BASED ON: STEAM INLET = 575 °F
INSIDE GAP = 500 B/hr-ft²
75 KN/ELEMENT
60 KN/ELEMENT
1200 °F MAX. CLAD
950
900
850
800
800
900
1000
1100
1200
STEAM EXIT TEMPERATURE - °F
STEAM FLOW - lb/hr
11-8-62 WER

FIG 9.3

Reactor power levels were varied during this period as follows:

Reactor Power Level	Hours of Operation
0 to 15 MW	180
15 to 20 MW	225
20 to 25 MW	300
Above 25 MW	140

Total burnup to this date for the element has been 346 MWD per ton and the heat generation has been 38.9 MW hours thermal.

Reactor Power	H_2O Level, Ft.	Separation Factor Reactor Water / Inlet Steam Na-24	Iodine
28	- 0.2	16,000	
26	+ 0.5	ca. 5,000	
20	+ 1.0	6,500	
15	0		1,500
21	- 0.3		900
25	- 0.3		1,400

The difference in the measurements using iodine as a tracer and those using Na-24 may be due either to volatilization of iodine from the reactor or to partial deposition of droplets in the steam or sampler piping. It is not known which tracer gives a more reliable measurement of the carryover of chloride to the superheat fuel.

9.1.4 NUSU Irradiation

9.1.4.1 NUSU Summary

Planning for the installation of the NUSU element was completed. Design conditions for the element were established, the SADE system revisions necessary for the installation of this element were determined, and fabrication of the necessary in-core hardware was completed. The NUSU element was received from General Nuclear Engineering Corporation on December 23, 1961. The element appeared to be in satisfactory condition with no apparent shipping damage. Upon further examination, however, it was found that the element was not leak tight. Checking on a mass spectrometer leak detector revealed a leak or leaks in excess of the saturation limit of this equipment (saturation occurs at 10^{-3} cc/sec). General Nuclear was notified of our findings. They are sending their representative to review our findings and direct repair work on the element.

9.1.4.2 NUSU Design Conditions

Since a sizeable portion of the power output of the NUSU fuel element is to the reactor water side of the element, and there is no means of measuring the output to this side, the actual operating power of the element must be calculated. A plot giving element power and clad temperatures as a function of measured steam flow and temperature on the superheated steam side has been prepared. However, the inside gap conductance between the fuel and the cladding must be assumed in the preparation of such a

plot, and variation in the value assumed for this conductance causes sizeable changes in the plot. The value selected for thermal conductivity of the UO_2 also has a significant effect on the heat split of this element. A detailed study of the factors affecting the heat split has showed that the most accurate estimate of the operating power of the element is obtained from the final reactor core physics calculations. The design conditions for the element have been finalized upon this power estimate. Figure 9.4 gives a plot of steam flow and steam exit temperature for various element powers with inside gap conductances of 100, 150, and 300 Btu/hr-ft^2-^{o}F.

Physics calculations for the power of the NUSU boiling-superheat fuel element indicated that this element will produce 105 KW at 36 MW reactor power. Design calculations have been completed for this element at 90 KW and at 102 KW and a set of curves has been prepared, based upon linear interpolation, to provide alarm and scram set points for a range of element powers from 90 KW to 105 KW. For the range of power involved in these curves, the difference between the values resulting from linear interpolation and code calculations is very small, and is far less than effects resulting from uncertainties in gap conductivity, UO_2 thermal conductivity, and other variables which occur in the heat transfer analysis. (See Figure 9.5)

A reference scale for reactor power has been included on the curves for alarm and scram set points. This reference

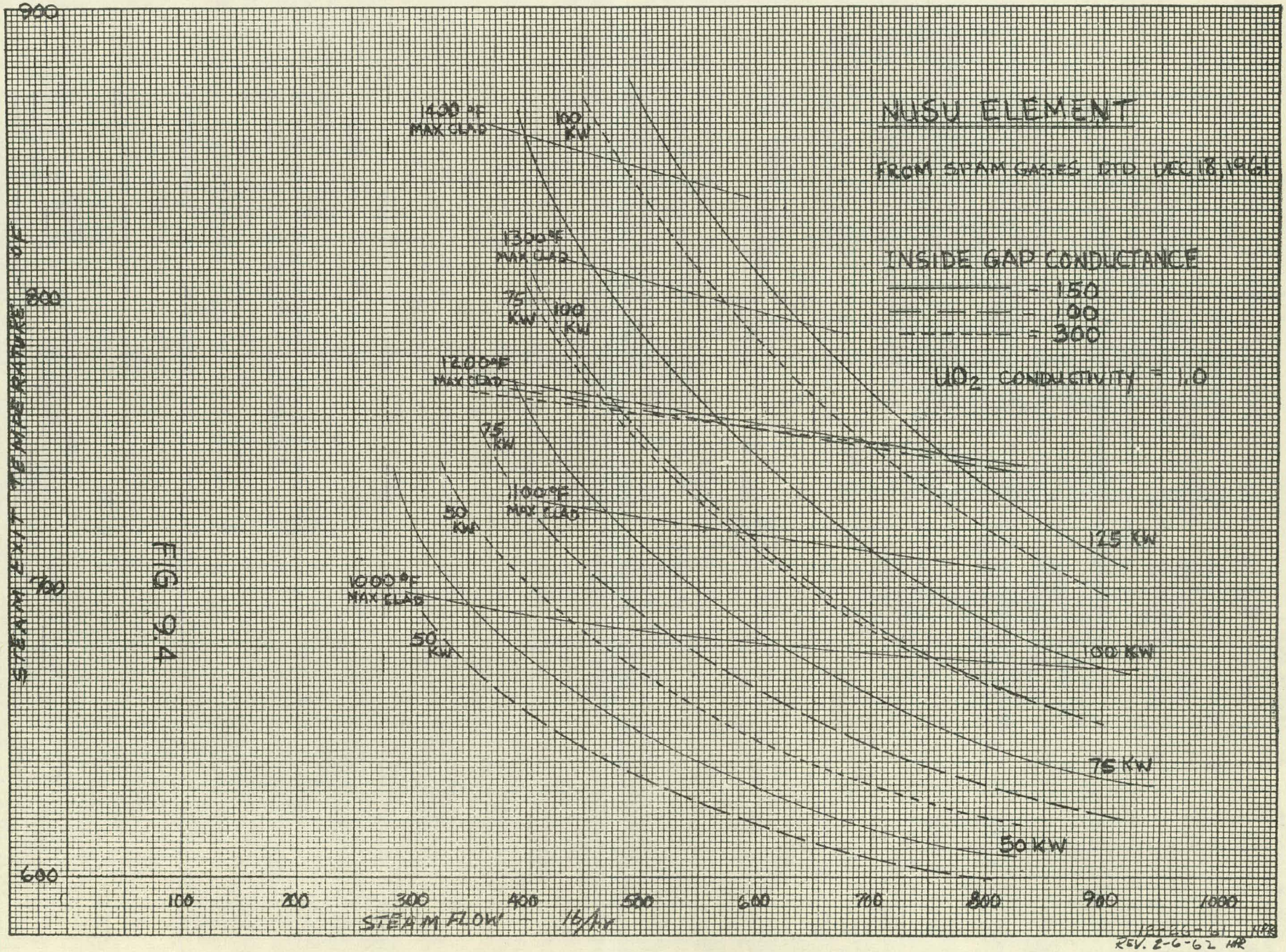
NaSU ELEMENT
FROM STEAM GASES DTD. DEC. 18, 1961
INSIDE GAP CONDUCTANCE
= 150
= 100
= 300
UO_2 CONDUCTIVITY = 1.0
1400 °F MAX CLAD
100 KW
1300 °F MAX CLAD
75 KW
100 KW
1200 °F MAX CLAD
75 KW
1100 °F MAX CLAD
50 KW
125 KW
1000 °F MAX CLAD
50 KW
100 KW
75 KW
50 KW
900
800
700
600
STEAM EXIT TEMPERATURE °F
100
200
300
400
500
600
700
800
900
1000
STEAM FLOW lb/hr
REV. 2-6-62 HR

FIG. 9.4

NUSU SUPERHEAT FUEL ELEMENT

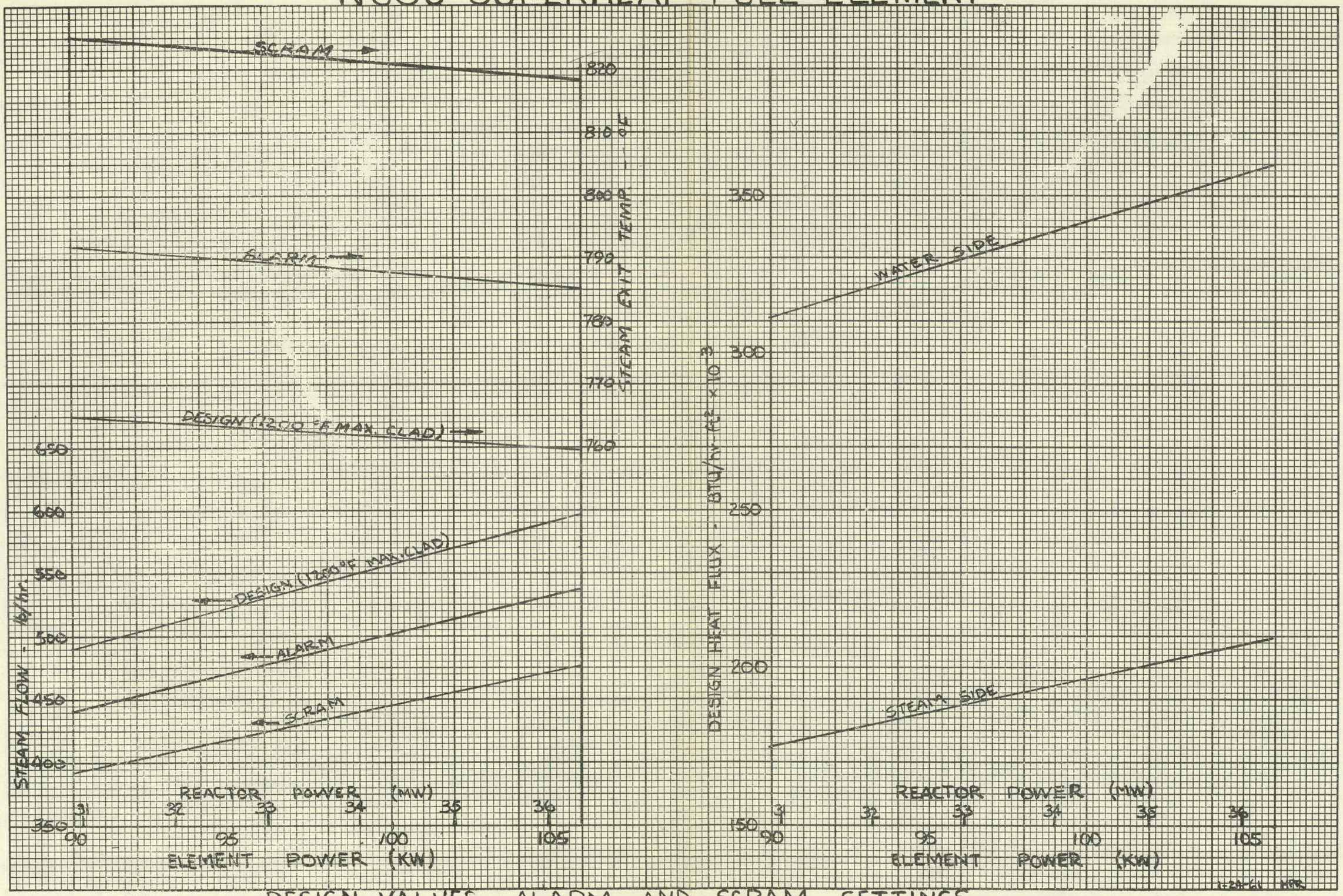

DESIGN VALUES, ALARM AND SCRAM SETTINGS

Figure 9.5

scale is based upon the predicted power for NUSU of 105 KW at 36 MW reactor power. If later information shows the power ratio between the reactor and the NUSU fuel element is different from this predicted value, the same curves may be employed as long as the power generated by the NUSU element is used for the reference scale.

Table 9.2 gives the information for the two design calculation conditions.

Table 9.2
NUSU Operating Conditions

Fuel enrichment	3.5% U^{235}
Steam pressure	1000 psia
Active fuel length	34.5"
Outer clad, outside diameter	1.50"
Outer clad thickness	0.028"
Outer clad material	347 S.S.
Inner clad, outside diameter	1.072"
Inner clad thickness	0.025"
Inner clad material	Inconel X
Outer steam supply tube, outside diameter	0.814"
Water flow tube, outside diameter	2.00
Water flow tube thickness	0.049"
Fuel (UO_2) % theoretical density	95%
Total fuel loading (UO_2)	4.25 kg
Inside clad-to-fuel contact coefficient	150 Btu/hr-ft^2-^oF
Outside clad-to-fuel contact coefficient	1000 Btu/hr-ft^2-^oF
Axial peaking factor	1.58
Linear radial flux depression factor	1.10
Thermal conductivity (UO_2)	1.0 Btu/hr-ft^2-(^oF/ft)

Fuel element power	90 KW	102 KW
Predicted reactor power	30.9 MW	35 MW
Maximum clad temperature (STEADY)	1200°F	1200°F
Maximum superheat exit temperature (STEADY)	765°F	761°F
Maximum steam side heat flux (STEADY)	175,000 Btu/hr-ft^2	201,000

Max. steam side heat flux (STEADY)	311,000 Btu/hr-ft^2	348,000
Min. steam flow rate (STEADY)	490 lbs/hr	570 lbs/hr
Min. burnout ratio (STEADY)	3.22	2.87
Max. fuel temperature (STEADY)	2675°F	2915°F
Max. clad temperature (TRANSIENT*)	1300°F	1300°F
Max. superheat exit temperature (TRANSIENT*)	819°F	807°F
Max. steam side heat flux (TRANSIENT*)	169,000 Btu/hr-ft^2	195,000
Max. water side heat flux (TRANSIENT*)	315,000 Btu/hr-ft^2	352,000
Min. steam flow rate (TRANSIENT*)	400 lbs/hr	480 lbs/hr
Min. burnout ratio (TRANSIENT*)	3.18	2.84
Max. fuel temperature (TRANSIENT)	2725°F	2962°F

* The transient conditions may be achieved for short intervals to obtain test data; extended operation will be in accordance with the limits for steady conditions.

Set points for 36 MW reactor power (105 KW NUSU power) are given in Table 9.3.

Table 9.3

		Alarm	Scram
FIS-1101	Steam flow indicator	530 lbs/hr	470 lbs/hr
TE-1102 (TRS-1102)	Superheat temperature, fuel exit*	875°F	819°F
TE-1103 (TRS-1103)	Superheat temperature, fuel exit*	785°F	819°F
TE-1101 (TRS-1101)	Superheat temperature, reactor outlet	655	675
TIS-1103	Superheat temperature, reactor outlet	655	675
FCV-1112	Throttle valve by-pass	Set to close in 2 min. minimum following scram.	

9.1.4.3 NUSU Facility Preparation

Figure 9.6 gives the final schematic drawing of the SADE loop system for the NUSU installation.

The final arrangement of the SADE control and safety circuits is given in Figure 9.7.

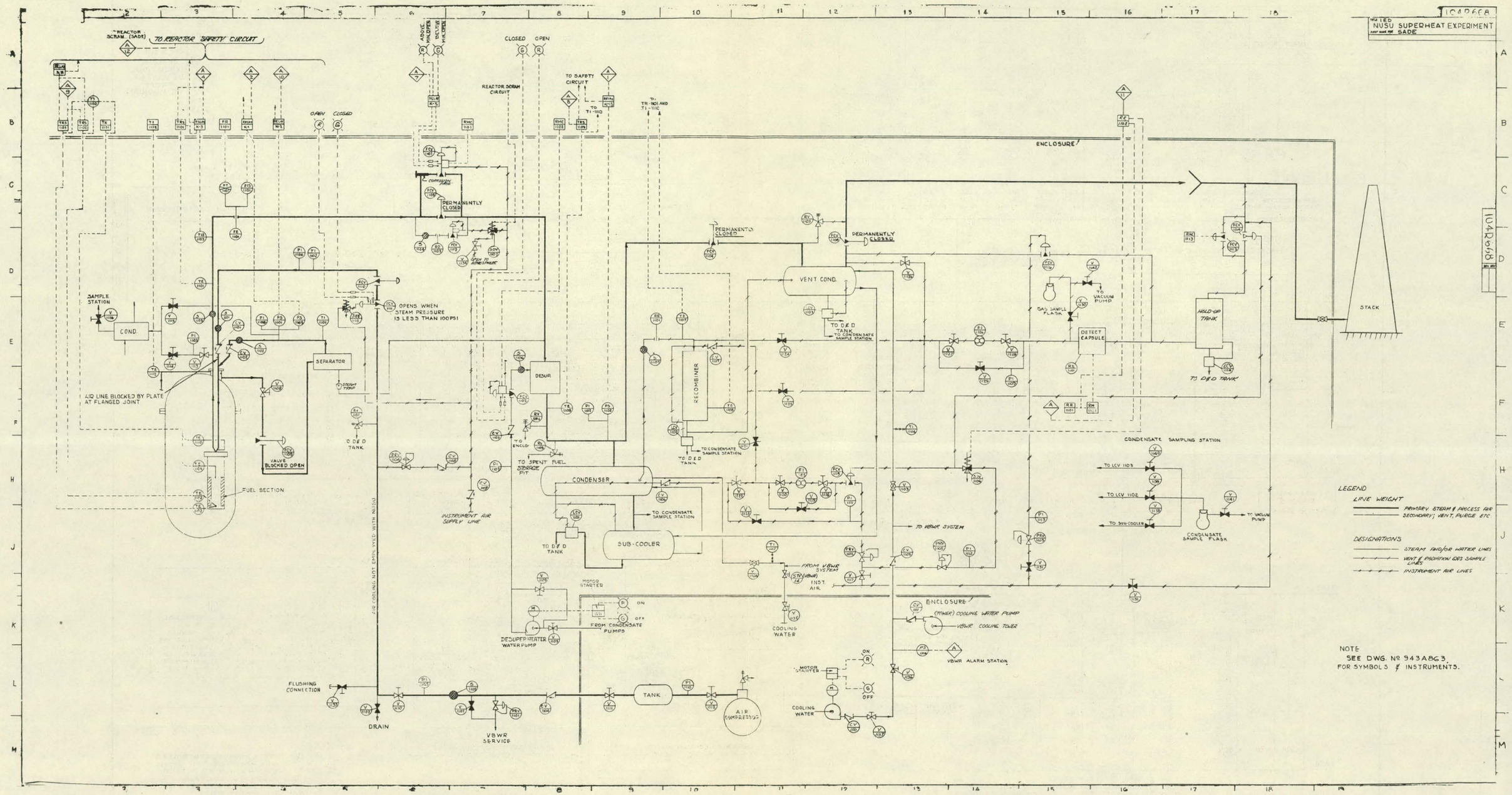
NUSU SUPERHEAT EXPERIMENT
SADE
104R668
REACTOR SCRAM (SADE)
TO REACTOR SAFETY CIRCUIT
ABOVE HALDEN
BELOW HALDEN
CLOSED
OPEN
REACTOR SCRAM CIRCUIT
TO SAFETY CIRCUIT
TO TR-1101 AND TI-1110
ENCLOSURE
PERMANENTLY CLOSED
SAMPLE STATION
COND.
OPENS WHEN STEAM PRESSURE IS LESS THAN 100PSI
SEPARATOR
STEAM TRAP
AID LINE BLOCKED BY PLATE AT FLANGED JOINT
VALVE BLOCKED OPEN
FUEL SECTION
TO D & D TANK
TO ENCLO.
TO SPENT FUEL STORAGE PIT
DESUP.
CONDENSER
TO CONDENSATE SAMPLE STATION
INSTRUMENT AIR SUPPLY LINE
SUB-COOLER
RECOMBINER
VENT COND.
TO VBWR SYSTEM
FROM VBWR SYSTEM
INST. AIR
STACK
GAS SAMPLE FLASK
TO VACUUM PUMP
DETECT CAPSULE
HOLD-UP TANK
CONDENSATE SAMPLING STATION
TO LCV 1103
TO LCV 1102
TO SAM-COOLER
CONDENSATE SAMPLE FLASK
MOTOR STARTER
FROM CONDENSATE PUMPS
DESUPP. HEATER WATER PUMP
COOLING WATER
(OTHER) COOLING WATER PUMP
VBWR COOLING TOWER
VBWR ALARM STATION
FLUSHING CONNECTION
DRAIN
VBWR SERVICE
TANK
AIR COMPRESSOR
FOR COOLING NOT EMPLOYED WITH NUSU
LEGEND
LINE WEIGHT
PRIMARY STEAM & PROCESS AIR
SECONDARY; VENT, PURGE ETC.
DESIGNATIONS
STEAM AND/OR WATER LINES
VENT & PROVISION GAS SAMPLE LINES
INSTRUMENT AIR LINES
NOTE
SEE DWG. Nº 943A863
FOR SYMBOLS & INSTRUMENTS.

Figure 9.6

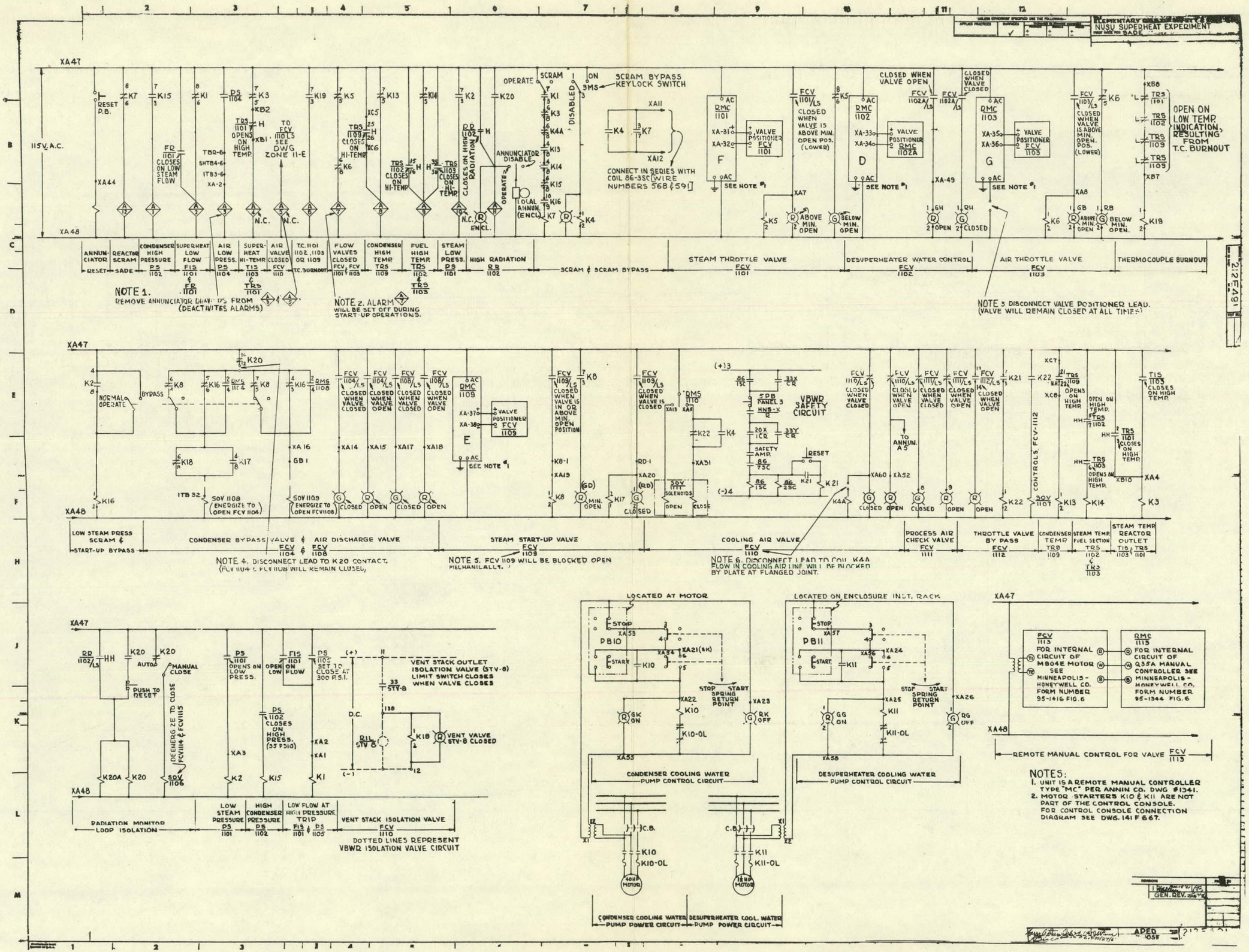
NUSU SUPERHEAT EXPERIMENT
XA47
XA48
115V A.C.
RESET P.B.
OPERATE
SCRAM
DISABLED
ON
SCRAM BYPASS KEYLOCK SWITCH
CONNECT IN SERIES WITH COIL 86-3SC [WIRE NUMBERS 568 & 591]
ANNUNCIATOR DISABLE
LOCAL ANNUN. (ENCL.)
OPEN ON LOW TEMP. INDICATION, RESULTING FROM T.C. BURNOUT
CLOSED WHEN VALVE OPEN
CLOSED WHEN VALVE CLOSED
CLOSED WHEN VALVE IS ABOVE MIN. OPEN POS. (LOWER)
CLOSED WHEN VALVE IS BELOW MIN. OPEN POS. (LOWER)
ANNUNCIATOR RESET
REACTOR SCRAM SADE
CONDENSER HIGH PRESSURE PS 1102
SUPERHEAT LOW FLOW FIS 1101 & FR 1101
AIR LOW PRESS. PS 1104
SUPERHEAT HI-TEMP TIS 1103 & TRS 1101
AIR VALVE CLOSED FCV 1110
TC 1101 1102 1103 OR 1109 TC. BURNOUT
FLOW VALVES CLOSED FCV 1101 & 1103
CONDENSER HIGH TEMP TRS 1109
FUEL HIGH TEMP. TRS 1102 & TRS 1103
STEAM LOW PRESS. PS 1101
HIGH RADIATION RR 1102
SCRAM & SCRAM BYPASS
STEAM THROTTLE VALVE FCV 1101
DESUPERHEATER WATER CONTROL FCV 1102
AIR THROTTLE VALVE FCV 1103
THERMOCOUPLE BURNOUT
NOTE 1. REMOVE ANNUNCIATOR BRANCHES FROM (DEACTIVATES ALARMS)
NOTE 2. ALARM WILL BE SET OFF DURING START UP OPERATIONS.
NOTE 3 DISCONNECT VALVE POSITIONER LEAD. (VALVE WILL REMAIN CLOSED AT ALL TIMES)
NORMAL OPERATE
BYPASS
SOV 1108 (ENERGIZE TO OPEN FCV 1104)
SOV 1109 (ENERGIZE TO OPEN FCV1108)
FCV 1104 CLOSED WHEN VALVE CLOSED
FCV 1104/LS CLOSED WHEN VALVE OPEN
FCV 1108 CLOSED WHEN VALVE CLOSED
FCV 1108/LS CLOSED WHEN VALVE OPEN
FCV 1109/LS CLOSED WHEN VALVE IS IN OR ABOVE MIN. OPEN POSITION
FCV 1109/LS CLOSED WHEN VALVE CLOSED
VBWD SAFETY CIRCUIT
SAFETY AMP.
RESET
FCV 1110/LS CLOSED WHEN VALVE CLOSED
FCV 1110/LS CLOSED WHEN VALVE OPEN
FCV 1111/LS CLOSED WHEN VALVE CLOSED
FCV 1111/LS CLOSED WHEN VALVE OPEN
FCV 1112/LS CLOSED WHEN VALVE OPEN
TO ANNUN. A5
CONTROLS FCV-1112
OPENS ON HIGH TEMP.
OPEN ON HIGH TEMP.
CLOSES ON HIGH TEMP.
LOW STEAM PRESS SCRAM & START-UP BYPASS
CONDENSER BYPASS VALVE & AIR DISCHARGE VALVE FCV 1104 & FCV 1108
STEAM START-UP VALVE FCV 1109
COOLING AIR VALVE FCV 1110
PROCESS AIR CHECK VALVE FCV 1111
THROTTLE VALVE BY PASS FCV 1112
CONDENSER TEMP TRS 1109
STEAM TEMP FUEL SECTION TRS 1102 & TRS 1103
STEAM TEMP REACTOR OUTLET TIS & TRS 1103 & 1101
NOTE 4. DISCONNECT LEAD TO K20 CONTACT. (FCV 1104 & FCV 1108 WILL REMAIN CLOSED)
NOTE 5. FCV 1109 WILL BE BLOCKED OPEN MECHANICALLY.
NOTE 6. DISCONNECT LEAD TO COIL K4A FLOW IN COOLING AIR LINE WILL BE BLOCKED BY PLATE AT FLANGED JOINT.
AUTO
MANUAL CLOSE
PUSH TO RESET
DEENERGIZE TO CLOSE FCV1114 & FCV1115
SOV 1106
VENT STACK OUTLET ISOLATION VALVE (STV-8) LIMIT SWITCH CLOSES WHEN VALVE CLOSES
VENT VALVE STV-8 CLOSED
RADIATION MONITOR LOOP ISOLATION
LOW STEAM PRESSURE PS 1101
HIGH CONDENSER PRESSURE PS 1102
LOW FLOW AT HIGH PRESSURE TRIP FIS 1101 & PS 1105
VENT STACK ISOLATION VALVE FCV 1110
DOTTED LINES REPRESENT VBWD ISOLATION VALVE CIRCUIT
LOCATED AT MOTOR
LOCATED ON ENCLOSURE INST. RACK
STOP
START
SPRING RETURN POINT
CONDENSER COOLING WATER PUMP CONTROL CIRCUIT
DESUPERHEATER COOLING WATER PUMP CONTROL CIRCUIT
CONDENSER COOLING WATER PUMP POWER CIRCUIT
DESUPERHEATER COOL. WATER PUMP POWER CIRCUIT
FCV 1113 FOR INTERNAL CIRCUIT OF MB04E MOTOR SEE MINNEAPOLIS-HONEYWELL CO. FORM NUMBER 95-1416 FIG. 6
RMC 1113 FOR INTERNAL CIRCUIT OF Q35A MANUAL CONTROLLER SEE MINNEAPOLIS-HONEYWELL CO. FORM NUMBER 95-1344 FIG. 6
REMOTE MANUAL CONTROL FOR VALVE FCV 1113
NOTES:
1. UNIT IS A REMOTE MANUAL CONTROLLER TYPE "MC" PER ANNIN CO. DWG #1341.
2. MOTOR STARTERS K10 & K11 ARE NOT PART OF THE CONTROL CONSOLE. FOR CONTROL CONSOLE CONNECTION DIAGRAM SEE DWGS. 141 F 867.
GEN. REV.
APED 105F

Figure 9.7

Detailed operating instructions for the SADE loop with the NUSU element installed were prepared and incorporated with the VBWR operating instructions. Operating personnel were indoctrinated in the design features of the installation, and in the changes in the SADE system to accommodate this element.

Because the outside of the NUSU element functions as a boiling water element in the VBWR core, the standard operating procedure for new boiling water elements in the VBWR core are to be observed during the test program for this element. This procedure requires visual inspection of the element after operating at a heat flux of 250,000 Btu/hr-ft^2, and after this inspection for increases in power of the reactor to be in 250,000 Btu/hr-ft^2 step increases in heat flux of the new element, with one-half hour or longer operation at each point before further power increases. The following test instructions have been prepared to comply with these procedures.

The NUSU superheat fuel element is to be tested in the SADE loop in accordance with the following procedure.

1. Start the reactor and the NUSU test in accordance with the operating instructions prepared for the SADE loop with the NUSU fuel element installed. Increase reactor power and pressure in accordance with these operating instructions until normal reactor operating pressure is reached.

2. Reactor power may be increased as desired up to a maximum of 25 MW. The water-side heat flux of the NUSU element is 250,000 Btu/hr-ft^2 at this power and reactor power may not be increased above 25 MW until the inspection as required in Section 5.5.9, step 4, of SG-VAL 2 is completed. At 25 M_W, set the SADE steam flow rate as low as practical to obtain as high a superheat steam temperature as possible. Hold reactor power and steam flow for a minimum of 1 hour at this setting, and until all SADE operating conditions are stabilized. Read and record all SADE data. Increase steam flow in the SADE loop by 10% from the above setting, let operating conditions stabilize, and repeat readings of all SADE data.

   Reactor operation at or below 25 MW may be continued as desired, until the reactor is shut down to permit inspection of the NUSU fuel element.

3. Shut down and depressurize the reactor to permit inspection of the water side of the NUSU element as required in SG-VAL 2. To accomplish this insepction, do not disconnect the in-core assembly and tube bundle from the refueling port flange. Lift the refueling port and in-core assembly as a unit with the crane, raising the fuel element above the reactor channels enough to permit inspection of the outside surface of the fuel element through the refueling port. Inspect

for visible evidence of damage, distortion and bowing. If no serious damage is evident, replace element in channel, reassembly refueling port flange, steam piping, and thermocouple connections, and resume reactor operations.

4. After reactor operation is resumed and normal reactor pressure is reached, reactor power may be increased in compliance with Section 5.5.9, step 5 of SG-VAL 2. The initial step-wise power increase is to 27.5 MW, which is to be held for a minimum of one-half hour before proceeding to the next power level. Complete SADE data is to be recorded at each power step, with SADE steam flow set to the practical minimum (near steam flow alarm setting for FIS-1101) to obtain as high a superheat steam temperature as possible. (When a superheat steam temperature of 760 F is achieved, the steam flow rate is to be adjusted as necessary to hold this temperature at each power step.) After holding power at this level for a minimum of one-half hour and after the data have been recorded, increase reactor power in similar steps to 30.0 MW, to 32.5 MW, to 35.0 MW, and to 36 MW, halting the step power increases at the maximum planned reactor operating power level.

5. After maximum reactor power has been reached, SADE steam flow is to be controlled, within the practical

limits of the low steam flow scram trip, to maintain steam outlet temperature as close to design temperature (750 to 760 F) as possible for the maximum operating time.

6. Because of the configuration of the NUSU fuel element, an accurate estimate of the total NUSU element power from steam flow and temperature measurement is not possible. A moderate change in the value assumed for the inside clad gap conductivity (within the range of expected values for this factor) causes an appreciable change in the steam-side power level. The most accurate figure for the power of this element is obtained from the reactor core physics calculations which predict 105 KW for NUSU at 36 MW reactor power. For reactor powers other than 36 MW, the NUSU power may be taken as a direct proportion of the 105 KW calculated for 36 MW operation.

9.1.5 SH-1 Irradiation

Initial design information for the test program of SH-1 defected element test was given in the Eighth Quarterly Progress Report, GEAP-3785.

New operating conditions for operation of the defected element SH-1 have been calculated based upon the analysis of data from previous elements, and revisions to the calculational code to improve accuracy, to incorporate radial flux depression and to include a revised axial flux distribution. The instrument tube

diameter was reduced from 1/2" to 3/8" for the revised conditions to provide a better temperature balance between inside and outside cladding. The revised conditions are given in Table 9.4. (The power of 70 KW is expected at a reactor power of 33 MW, based on latest physics core estimates.)

Table 9.4

Fuel enrichment	2.3% U^{235}
Fuel (UO_2) % theoretical density	95%
Fuel conductivity	1.1 Btu/hr-ft-^oF
Radial flux depression	1.12
Axial peaking	1.58
Steam pressure	1000 psia
Outer clad:	
O.D.	1.25"
Thickness	0.049"
Material (weld-drawn tubing)	304 SS
Inner clad:	
O.D.	0.75
Thickness	0.035"
Material (weld-drawn tubing	347 SS
Active fuel length	36"
Instrument tube, O.D.	0.375"
Outer clad-to-fuel conductance	1000 Btu/hr-ft^2-^oF
Inner clad-to-fuel conductance	150 Btu/hr-ft^2-^oF
STEADY STATE	
Power	70 KW
Maximum clad temperature	1200^oF
Maximum superheat exit temperature	795^oF
Maximum heat flux	264,500 Btu/hr-ft^2
Maximum fuel temperature	2960^oF
Minimum steam flow rate	1120 lb/hr
LOW FLOW TRANSIENT	
Power	70 KW
Maximum clad temperature	1300^oF
Maximum superheat exit temperature	835^oF
Maximum heat flux	263,600 Btu/hr-ft^2
Maximum fuel temperature	3060^oF
Minimum steam flow rate	975 lb/hr

Plots of steam flow versus superheat exit temperature at various power levels are given in Figure 9.8. A plot of steam temperature and cladding temperature versus fuel element position for the

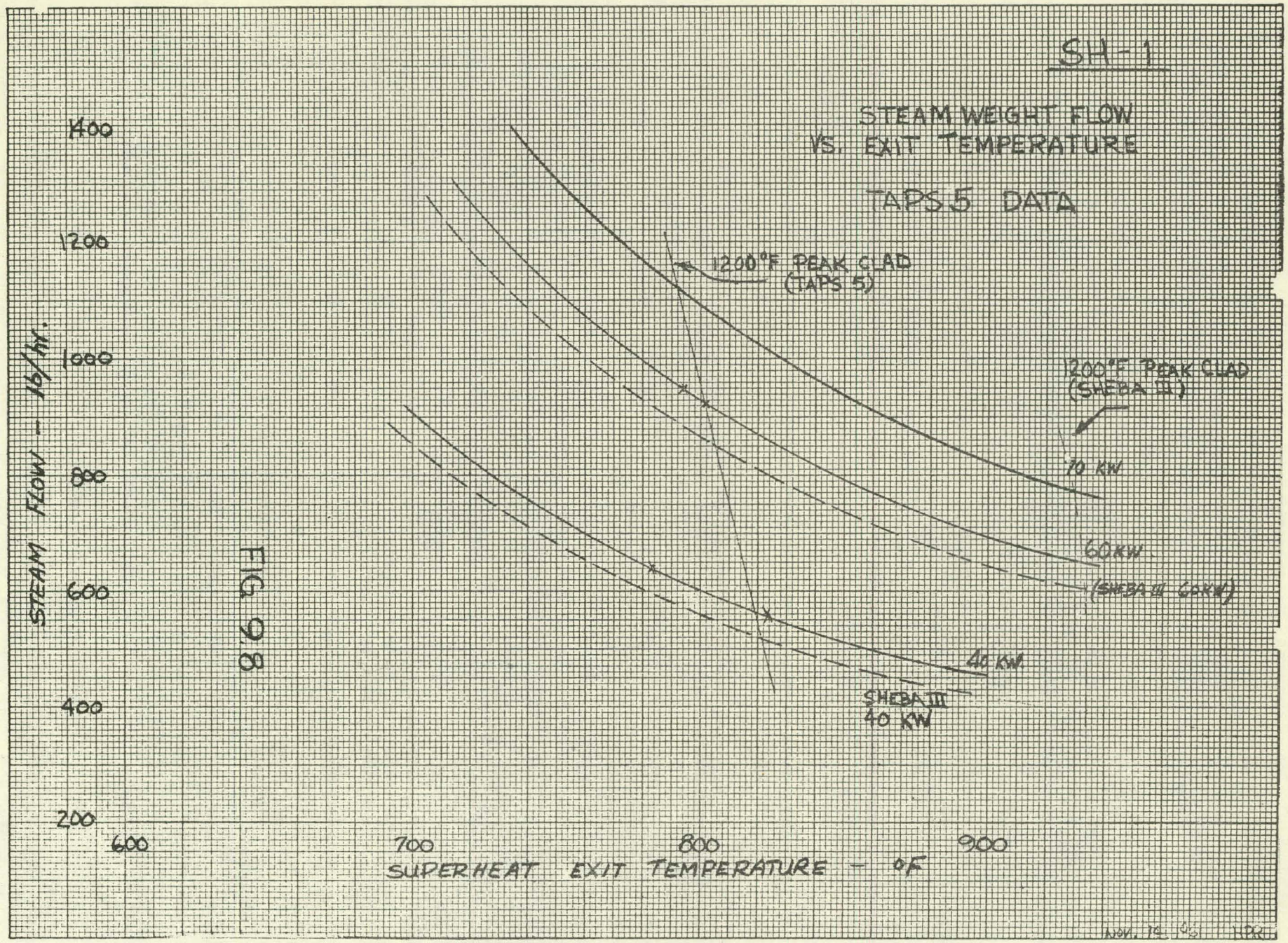
SH-1
STEAM WEIGHT FLOW
VS. EXIT TEMPERATURE
TAPS 5 DATA
1200°F PEAK CLAD
(TAPS 5)
200°F PEAK CLAD
(SHEBA III)
70 KW
60 KW
(SHEBA III 60KW)
40 KW
SHEBA III
40 KW
STEAM FLOW - lb/hr.
1400
1200
1000
800
600
400
200
600
700
800
900
SUPERHEAT EXIT TEMPERATURE - °F

FIG 9.8

steady-state design condition is given in Figure 9.9. Figure 9.10 gives a plot of the heat loss to the process tube for various operating conditions for this fuel element.

A.E.C. safeguards approval for conducting the testing of an intentionally defected fuel element in the SADE loop was received during this period. Concern about the adequacy of the loop to handle radioactive discharges for routine tests of such defected elements had been expressed. Additional information about test program to be conducted on such elements, and the monitoring system and special sampling program which would be conducted during such a test, was furnished to the A.E.C. In addition, a filter for the off-gas system, to greatly reduce possible iodine release, was incorporated in the system.

9.1.6 SH-6 Design Conditions

Design and fabrication of a six-rod fuel cluster (SH-6), which would be installed in a standard SADE process tube, is complete. A "re-entry" tube is incorporated in the fuel element assembly to adapt this single pass type element to the annular flow configuration of the SADE loop.

Physics calculations have predicted the design fuel element power of 60 KW at a reactor power of 36 MW. Table 9.5 gives design conditions for 60 KW output for this element.

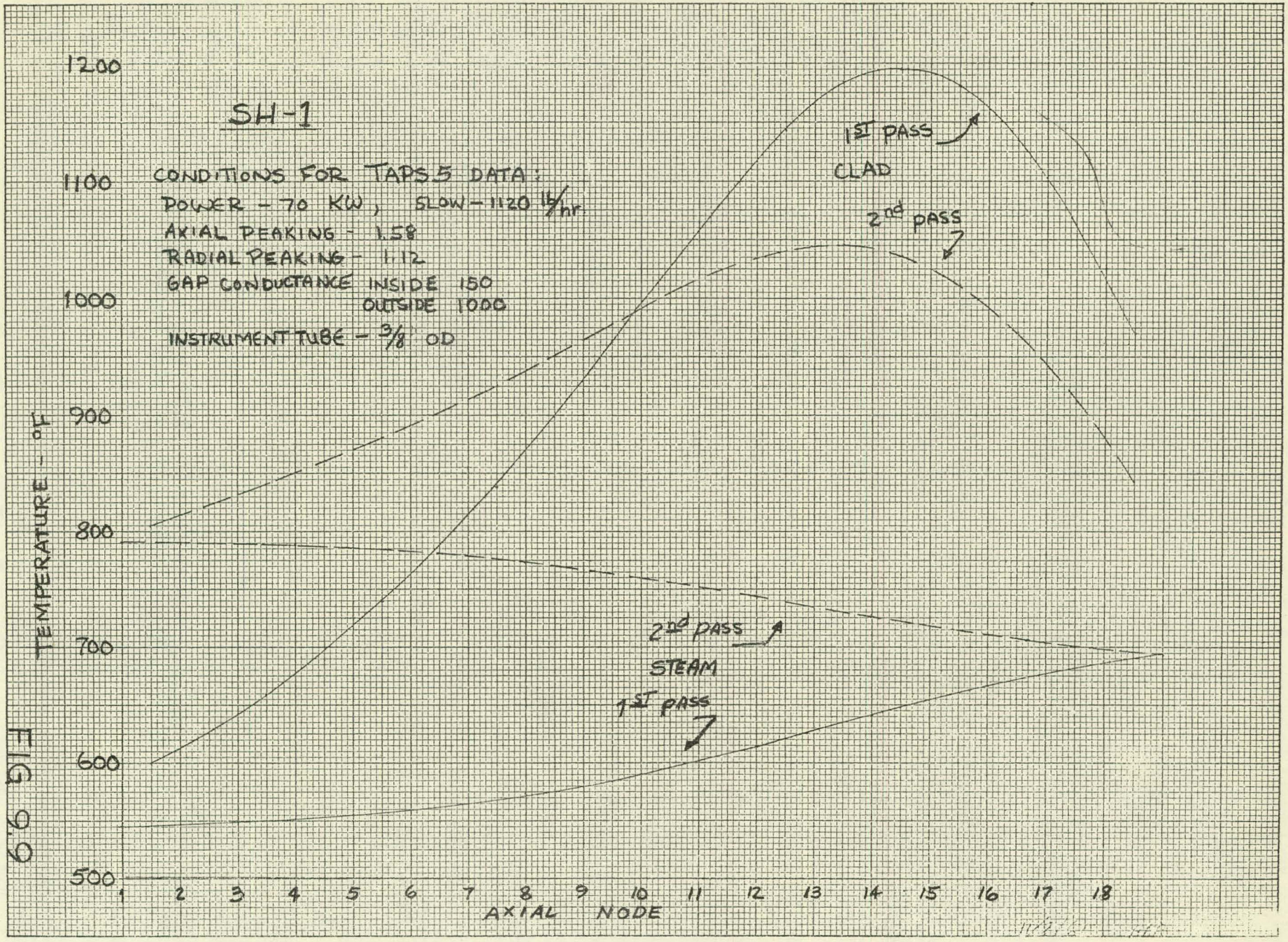
SH-1
CONDITIONS FOR TAPS 5 DATA:
POWER - 70 KW, FLOW - 1120 lb/hr
AXIAL PEAKING - 1.58
RADIAL PEAKING - 1.12
GAP CONDUCTANCE INSIDE 150
OUTSIDE 1000
INSTRUMENT TUBE - 3/8 OD
1ST PASS CLAD
2ND PASS
2ND PASS STEAM
1ST PASS
TEMPERATURE - °F
AXIAL NODE
1200
1100
1000
900
800
700
600
500
1 2 3 4 5 6 7 8 9 10 11 12 13 14 15 16 17 18

FIG 6.6.9

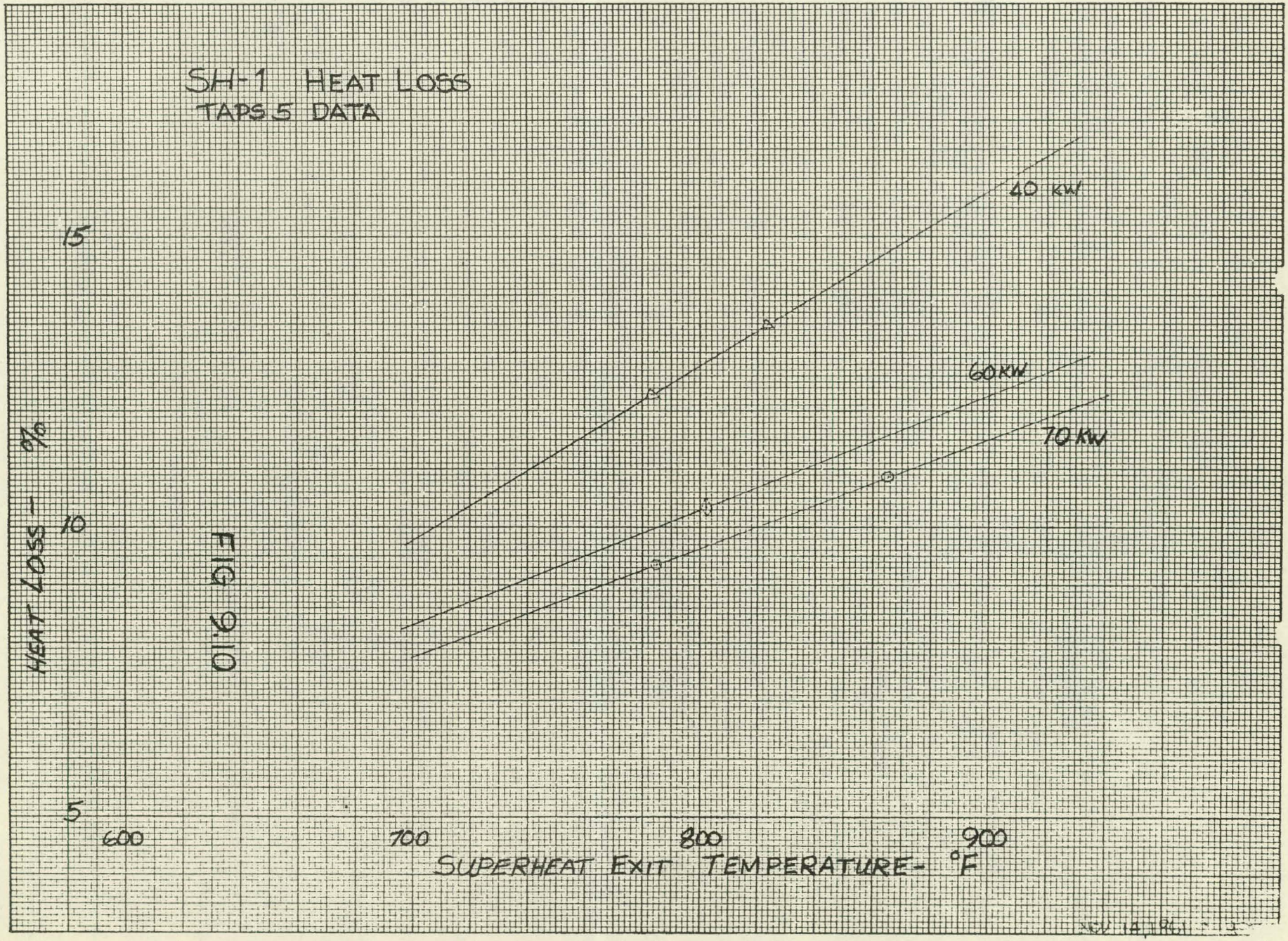
SH-1 HEAT LOSS
TAPS 5 DATA
40 KW
60 KW
70 KW
15
10
5
% HEAT LOSS
600
700
800
900
SUPERHEAT EXIT TEMPERATURE - °F

FIG 9.10

Table 9.5

Operating Conditions

Power	60 KW
Fuel enrichment	3.9% U^{235}
Steam pressure	1000 psia
Active fuel length	36"
Clad, outside diameter	5/16"
Clad thickness	.020"
Clad material	304 L and 304 S.S.
Instrument tube, outside diameter	5/16"
Spacer wire diameter	.051"
Flow tube, outside diameter	1.25"
Flow tube thickness	.035"
Scalloped liner thickness	.010"
Pitch to diameter ratio	1.18
Number of rods	6
Number of spiral wire spacers	12
(Fuel (UO_2) % theoretical density	95%
Axial peaking factor	1.58
Radial peaking factor	1.10
Contact coefficient, fuel-to-clad	500 Btu/hr-ft^2-^oF
UO_2 conductivity	1.10 Btu/(hr-ft^2)(^oF/ft)
Total fuel loading (calculated)	2.06 Kg
Inlet steam temperature	560^oF
Maximum clad temperature (STEADY)	1200^oF
Maximum superheat exit temperature (STEADY)	913^oF
Maximum heat flux (STEADY)	241,000 Btu/hr-ft^2
Minimum steam flow rate (STEADY)	833 lbs/hr
Maximum fuel temperature (STEADY)	2960^oF
Maximum clad temperature (TRANSIENT*)	1300^oF
Maximum superheat exit temperature (TRANSIENT*)	981^oF
Maximum heat flux (TRANSIENT*)	241,000 Btu/hr-ft^2
Minimum steam flow rate (TRANSIENT*)	713 #/hr
Maximum fuel temperature (TRANSIENT*)	3060^oF

* The transient conditions may be achieved for short intervals to obtain test data; extended operation will be in accordance with the limits for steady conditions.

Settings for the SADE loop which vary with different test elements are given in Table 9.6.

Table 9.6

Alarm and Scram Settings for SH-6

		Alarm	Scram
FIS-1101	Steam flow indicator	750 lbs/hr	667 lbs/hr
TE-1102 (TRS-1102)	Superheat temperature,* fuel exit	957°F	1020°F
TE-1103 (TRS-1103)	Superheat temperature,* fuel exit	957°F	1020°F
TE-1101 (TRS-1101)	Superheat temperature, reactor outlet	720°F**	740°F**
TE-1103	Superheat temperature, reactor outlet	720°F**	740°F**
FCV-1112	Throttle valve bypass	Set to close in 1 hour following scram.	

* Note that both TE-1102 and -1103 both measure the fuel exit temperature.

** The setting of FCV-1112 listed in Table 9.6 (valve remains open for 1 hour after scram) was arrived at from an analysis that predicted a peak clad temperature of 1400°F for the case of no steam flow one hour after a scram - following continuous operation of the loop for 30 days at full power of 60 KW. The VBWR water temperature is conservatively assumed to be 545°F. SH-6 design is shown in Figures 9.11 and 9.12.

9.2 E-SADE

9.2.1 E-SADE Installation and Construction Status

Installation work was performed on E-SADE during the VBWR shutdown October 5 to October 31, 1961. Work outside the enclosure has been essentially completed, except where it is dependent upon SADE equipment which will be used in the E-SADE system, and for control room work which must be done after delivery of control and instrument consoles. Work within the enclosure is restricted to periods when the reactor is not operating and therefore, has been limited. Careful planning of work during reactor shutdowns has provided maximum utilization of time during these periods, but enclosure basement activities, which are higher than expected when initially

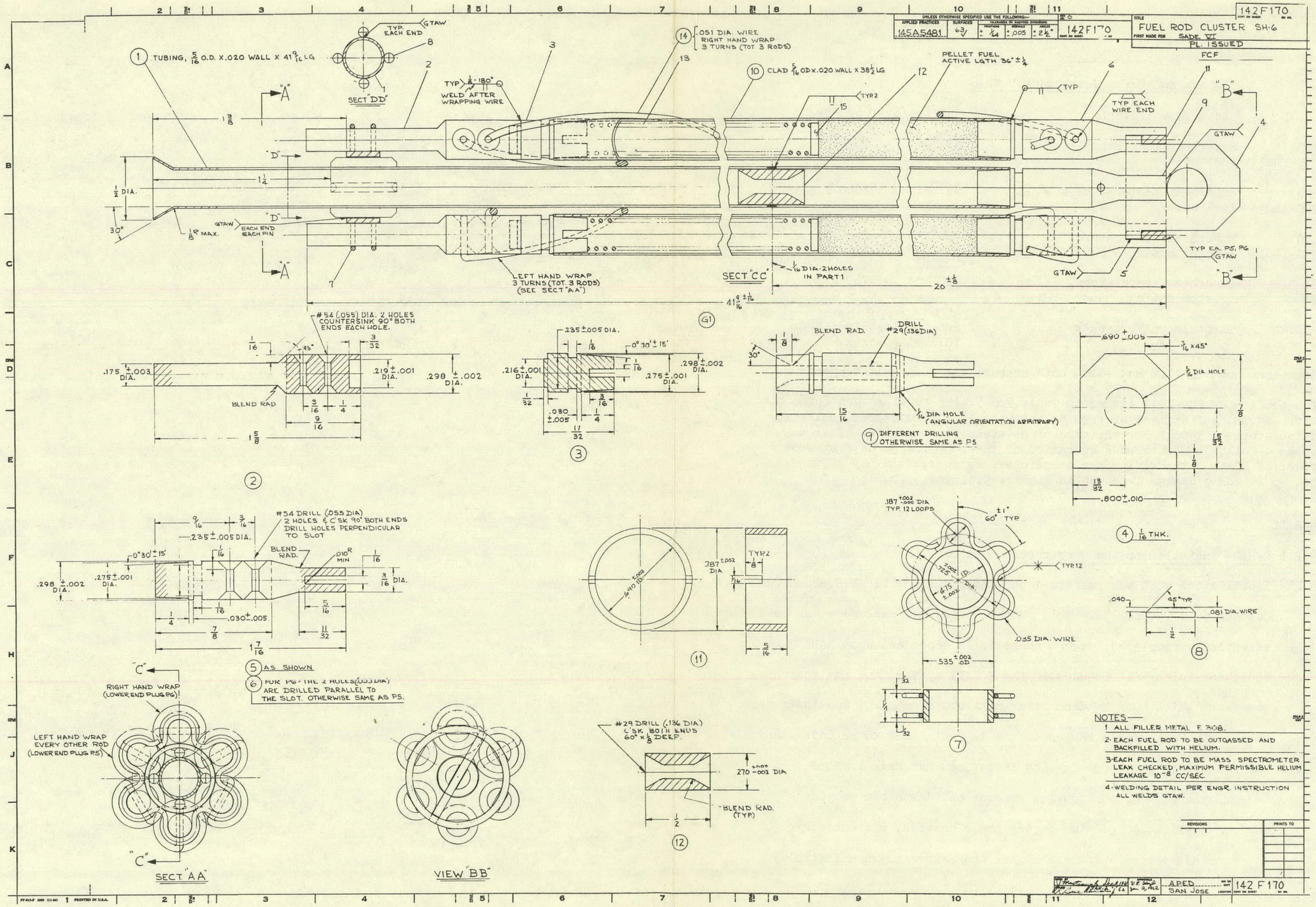
UNLESS OTHERWISE SPECIFIED USE THE FOLLOWING:
APPLIED PRACTICES 145A5481
SURFACES 63
TOLERANCES ON MACHINED DIMENSIONS: FRACTIONS ± 1/64, DECIMALS ± .005, ANGLES ± 2½°
142F170
TITLE FUEL ROD CLUSTER SH-6
FIRST MADE FOR SADE VI
PL. ISSUED
142F170
1 TUBING, 5/16 O.D. X.020 WALL X 41 9/16 LG
TYP. EACH END
GTAW
SECT "DD"
TYP 180° WELD AFTER WRAPPING WIRE
14 .051 DIA. WIRE RIGHT HAND WRAP 3 TURNS (TOT 3 RODS)
10 CLAD 5/16 OD X.020 WALL X 38½ LG
PELLET FUEL ACTIVE LGTH 36" ± ¼
TYP2
TYP
TYP EACH WIRE END
"A"
"B"
"D"
1 3/8
1 1/4
½ DIA.
30°
1/8 R MAX.
GTAW EACH END EACH PIN
LEFT HAND WRAP 3 TURNS (TOT. 3 RODS) (SEE SECT "AA")
SECT "CC"
1/16 DIA-2 HOLES IN PART 1
20 ± 1/8
41 9/16 ± 1/16
TYP EA. P5, P6 GTAW
GTAW
#54 (.055) DIA. 2 HOLES COUNTERSINK 90° BOTH ENDS EACH HOLE.
.175 ± .003 DIA.
.219 ± .001 DIA.
.298 ± .002 DIA.
BLEND RAD
1 5/8
2
.235 ± .005 DIA.
0° 30' ± 15'
.216 ± .001 DIA.
.298 ± .002 DIA.
.275 ± .001 DIA.
.080 ± .005
17/32
3
BLEND RAD.
DRILL #29 (.136 DIA)
30°
15/16
1/16 DIA HOLE (ANGULAR ORIENTATION ARBITRARY)
9 DIFFERENT DRILLING OTHERWISE SAME AS P5
.690 ± .005
7/16 x 45°
5/16 DIA HOLE
7/8
15/32
1/8
13/32
.800 ± .010
4 1/16 THK.
#54 DRILL (.055 DIA) 2 HOLES C'SK 90° BOTH ENDS DRILL HOLES PERPENDICULAR TO SLOT
9/16
3/16
.235 ± .005 DIA.
0° 30' ± 15'
BLEND RAD.
.010 R MIN
.298 ± .002 DIA.
.275 ± .001 DIA.
.030 ± .005
7/8
11/32
1 7/16
5 AS SHOWN
6 FOR P6 THE 2 HOLES (.055 DIA) ARE DRILLED PARALLEL TO THE SLOT. OTHERWISE SAME AS P5.
.640 ± .002 DIA
.787 ± .002 DIA
TYP2
5/16
11
.187 +.002 -.000 DIA TYP. 12 LOOPS
±1°
60° TYP
.705 ± .002 DIA
.475 ± .002 DIA
TYP12
.035 DIA. WIRE
.535 ± .002 OD
7
.040
45° TYP
.081 DIA. WIRE
1/2
8
RIGHT HAND WRAP (LOWER END PLUG P6)
LEFT HAND WRAP EVERY OTHER ROD (LOWER END PLUG P5)
"C"
SECT "AA"
VIEW "BB"
#29 DRILL (.136 DIA) C'SK BOTH ENDS 60° x 1/8 DEEP.
.270 +.000 -.002 DIA
BLEND RAD. (TYP.)
12
NOTES
1 ALL FILLER METAL E 308.
2 EACH FUEL ROD TO BE OUTGASSED AND BACKFILLED WITH HELIUM.
3 EACH FUEL ROD TO BE MASS SPECTROMETER LEAK CHECKED, MAXIMUM PERMISSIBLE HELIUM LEAKAGE 10⁻⁸ CC/SEC.
4 WELDING DETAIL PER ENGR. INSTRUCTION ALL WELDS GTAW.
REVISIONS
PRINTS TO
APPROVED
SAN JOSE
142 F 170

Figure 9.11

UNLESS OTHERWISE SPECIFIED USE THE FOLLOWING:						142F141
APPLIED PRACTICES	SURFACES	TOLERANCES ON MACHINED DIMENSIONS				
		FRACTIONS	DECIMALS	ANGLES		
	✓	±	± .1/64	±		

QTY	PART NO	NAME	DWG NO. DESCRIPTION. MAT'L.
1	1	FUEL FLG.	985C340G3
1	2	THERMAL LINER	114B5248G4
1	3	FUEL ROD CLUSTER	142F170 G1
1	4	FLOW TUBE	985C852 G1
1	5	PIN	149A4908P1
1	6	INST. TUBE	985C828 G1
1	7	COT PIN.	1/32 DIA x 1/2 LG. STN STL

TITLE: FUEL ASM- SH-6
FIRST MADE FOR SADE VI

142F141

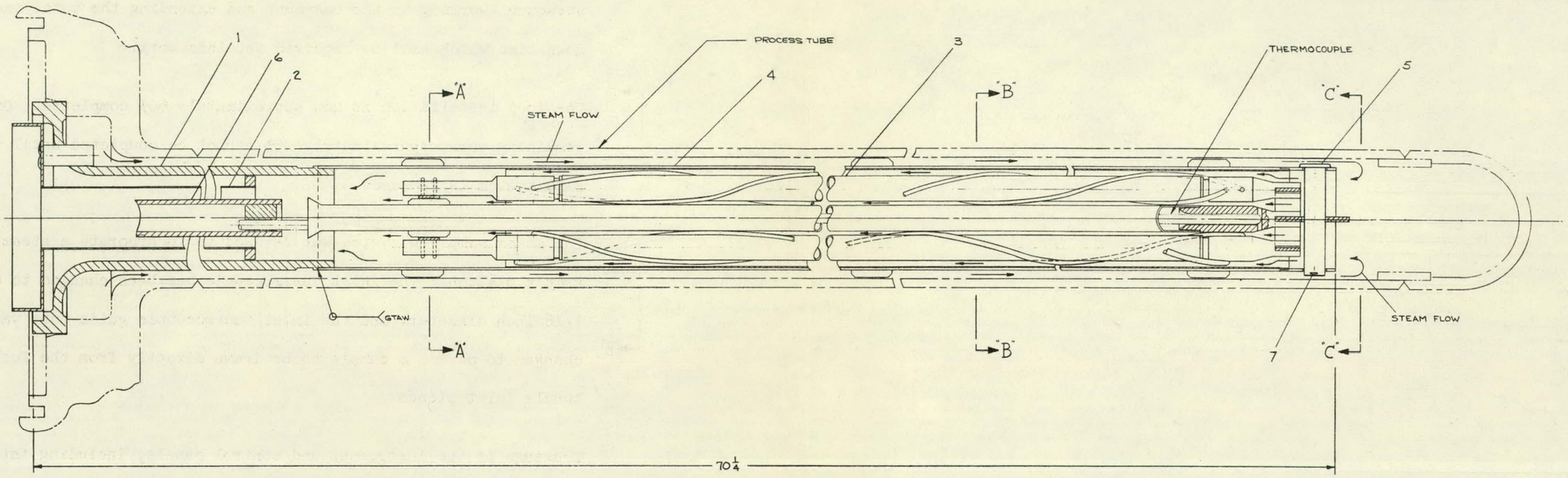

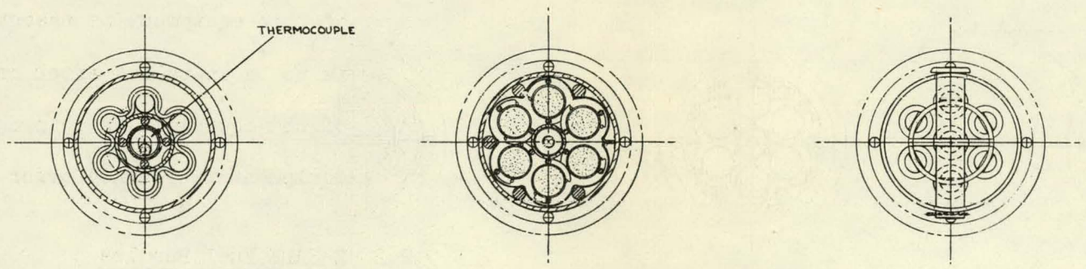

SECT."AA"

SECT."BB"

SECT."CC"

REVISIONS | PRINTS TO

APED. SAN JOSE | 142F141

Figure 9.12

planning the installation, have resulted in a burn-up problem for personnel working in the basement and extending the total reactor down-time which will be required for this work.

The loop installation is now approximately 60% completed. Of the remaining work, approximately 15% cannot be completed until the SADE system is removed.

The steam sampling system was revised to incorporate a steam inlet sample station. The inlet thermocouple has been changed to a 1/16 inch diameter, and the inlet thermocouple guide tube was changed to permit a sample to be drawn directly from the fuel bundle inlet plenum.

Drawings of the instrument and control panels, including interconnection diagrams, have been completed. Fabrication and assembly of this equipment is essentially complete except for equipment which is to be installed after removal from the SADE system. Check-out of the equipment is in progress and a system simulation test of all equipment is planned prior to delivery to the reactor site.

9.2.2 E-SADE Fuel Bundles

Test results of elements in the SADE loop indicated that a re-evaluation of the significance of leakage of reactor water into the test section was necessary. Failures of fuel cladding, which apparently resulted from chloride stress corrosion, indicated that such leakage should be held to the very lowest practical level. The lower flange coupling design for E-SADE was revised to provide a duplex seal such that any seal leakage will be diverted past the

fuel section into the superheat exit line. Figure 9.13 shows the arrangement of the fuel bundle as revised to provide this seal.

A test fixture to check the duplex seal arrangement has been designed and is now being fabricated. The fixture will be tested in an autoclave chamber to simulate temperature effects on the coupling. Figure 9.14 shows this test fixture.

Design and heat transfer studies for ESH-2 assembly, employing a re-entry tube arrangement to obtain single pass flow for the elements, has continued during this period. It has been determined that the arrangement is compatible with reactor limitations if the maximum power per element is limited to approximately 60 KW. A 3-hour post-scram cooling period is required with this arrangement to limit the maximum clad temperatures to the license limitations. Design of the coupling was revised to incorporate the duplex seal arrangement, and drawings have been released to the shop for fabrication of the equipment necessary for the installation of ESH-2. Figure 9.15 shows the fuel bundle assembly for this assembly.

9.2.3 Power Scalloping - ESH-1 Fuel Bundle

A two-dimensional analysis has been completed which predicts the power scalloping on the inside and outside surface of each of the nine ESH-1 fuel annuli.

The VBWR core configuration was assumed to be that shown in Figure 9.16. The method used in this analysis was to specify each fuel region in ESH-1 discretely rather than homogenized over a one rod cell.

198E282

UNLESS OTHERWISE SPECIFIED USE THE FOLLOWING—
APPLIED PRACTICES | SURFACES ✓ | MACHINED TO NOMINAL DIMENSIONS SHOWN: FRACTIONS ± 1/64, DECIMALS ±

TITLE: NINE ELEMENT FUEL ASSEMBLY
FIRST MADE FOR SHNEE II FCF 7176E79

PL ISSUED

198E282 REV NO. 4

6'-8 11/16"
10 3/4
6 1/2
5'-9 13/16" REF.
8'-0" ACTIVE FUEL LT.
3 3/8 REF.
SEE NOTES AT SECT. D-D & VIEW K-K
TYP
1/16
3/8
1/16 LG. 4 PL. EQ. SP. TYP.
.030
24, TYP.
SEE NOTES
SEE NOTE AT VIEW K-K
23
21
20
16, FLATTEN HEAD & ENDS TO FIT I.D. OF PROCESS TUBE
1/16 MIN. TYP.
1/16 MIN. TYP. 4 PL.
TYP. 2 PL., POS. B + H
3/8 3 PL., EQ SP.
5'-9 1/2"

SECTION B-B

NOTES: F: TIG FUSION WELD.
ALL WELD FILLER METAL TO BE E308
BEND LIP TO RETAIN P20; 3 PL., EQ. SP.

TYP. 4 PL.
VIEW A-A

SECTION C-C
DO NOT WELD PT OR B TO P15

BEND TO FIT, IF NECESSARY, INTO P5
SECTION H-H

VIEW M-M
SAME AS VIEW A-A WITH P1, 2, 3 & 4 REMOVED
TYR & PL UPPER EDGE ONLY

WELDED PROJECTIONS ON CORNER PROCESS TUBES MUST BE ALIGNED AS SHOWN, TO LOCATE AND HOLD PARTS 18 & 19.
SECTION D-D

SLOT IN SLEEVE OF PROCESS TUBE P11 & V NOTCHES ON PLUG OF VELOCITY BOOSTER TO BE ALIGNED TO FACE DIRECTION AS INDICATED BY LETTER "E" ON SIDE OF ELEMENT SPACER, P14.
VIEW K-K

4PL EQ SP AT EACH TUBE LOCATION
SECTION G-G

SECTION J-J

C B A
F E D
I H G
REF FUEL ELEMENT LOADING LOCATIONS, SEE SEC. D-D (VIEW FROM BELOW)

REVISIONS		PRINTS TO
4 Master NE 2115	1 NE 1596	
	2 NE 1822	
	3 NE 2037	

APED SAN JOSE 198E282

Figure 9.13

985C824 CONT ON SHEET SH NO.

UNLESS OTHERWISE SPECIFIED USE THE FOLLOWING:—

APPLIED PRACTICES	SURFACES	TOLERANCES ON MACHINED DIMENSIONS		
		FRACTIONS	DECIMALS	ANGLES
145A5481	125	± 1/64	± .005	±

REV NO. O

985C824 CONT ON SHEET SH NO.

TITLE: TEST COUPLING

FIRST MADE FOR SHNEE FCF 105X328

GROUP NO. AND QUANTITY G1	PART NO.	NAME	DRAWING NO., DESCRIPTION, MATERIAL, WEIGHT
1	1	FLANGE	AISI TYPE 304 STN. STL.
1	2	FLANGE	AISI TYPE 304 STN. STL.
1	3	SEAL	CAT. 12195 PA5500 BY HARRISON
		MFG. CO. OR ENGRG. APPD. EQUIV.	
1	4	SEAL	CAT. 12150 PA5500 BY HARRISON
		MFG. CO. OR ENGRG. APPD. EQUIV.	
2	5	BOLT, HEX. HD.	N50P25028
2	6	NUT, HEX.	N201P25
1	7	TUBE	ASTMA269 TYPE 304
1	8	SET SCREW, FL. PT.	8-32UNC2A × 5/16 LG. STN. STL.
1	9	TUBE	AISI TYPE 304 STN. STL.

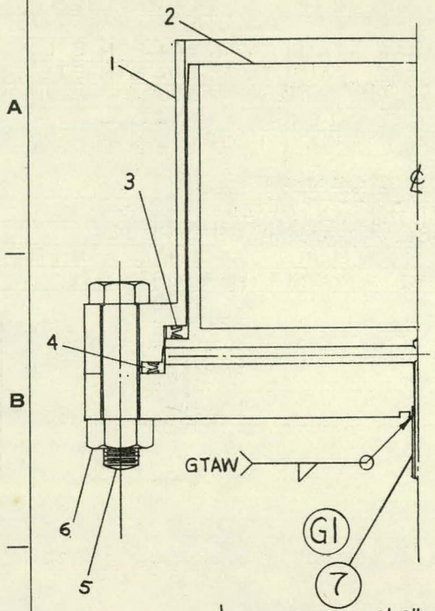

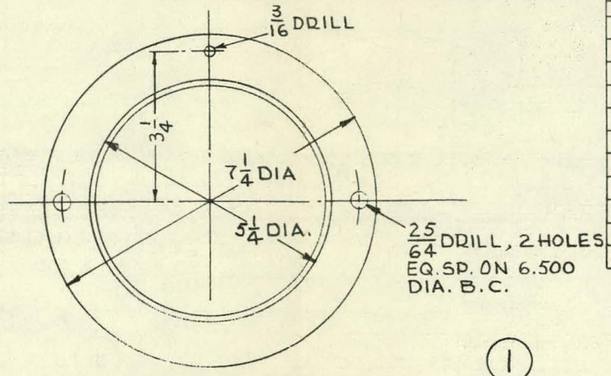

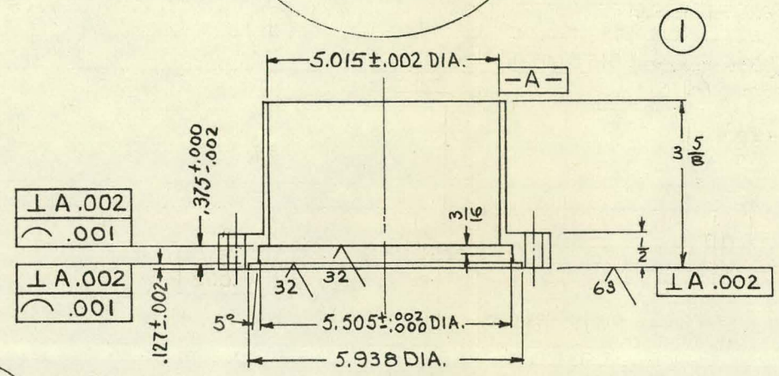

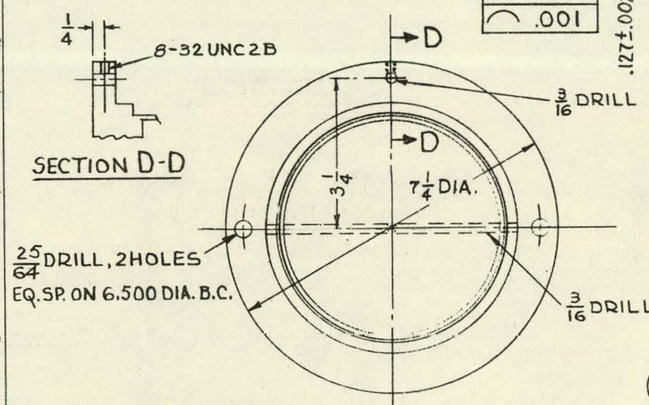

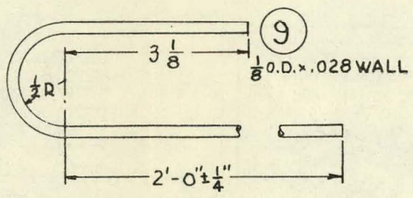

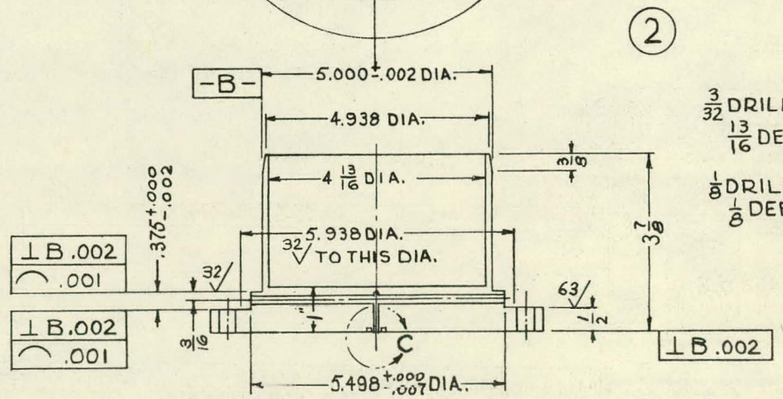

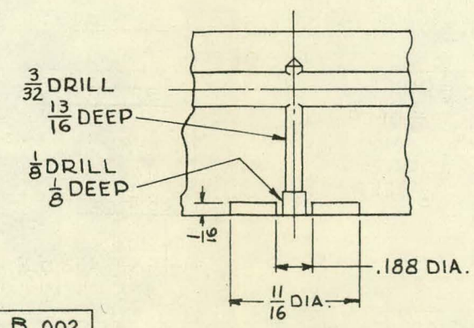

DESCRIPTION OF GROUPS	REVISIONS	PRINTS TO

DRAWN BY Jerry C. Stern Oct. 30, 1961 — APPROVALS HHP 11/30/61 — APED DIV OR DEPT — SAN JOSE, CALIF. LOCATION — 985C824 CONT ON SHEET SH NO.

DRAWING NO. 985C824 CONT ON SHEET SH NO. REV NO. O

FF-808-P 7M (7-56) PRINTED IN U.S.A.

Figure 9.14

TITLE: NINE ELEMENT FUEL ASM (SINGLE PASS) FIRST USED FOR SHNEF III FCF 7178E79

PL ISSUED

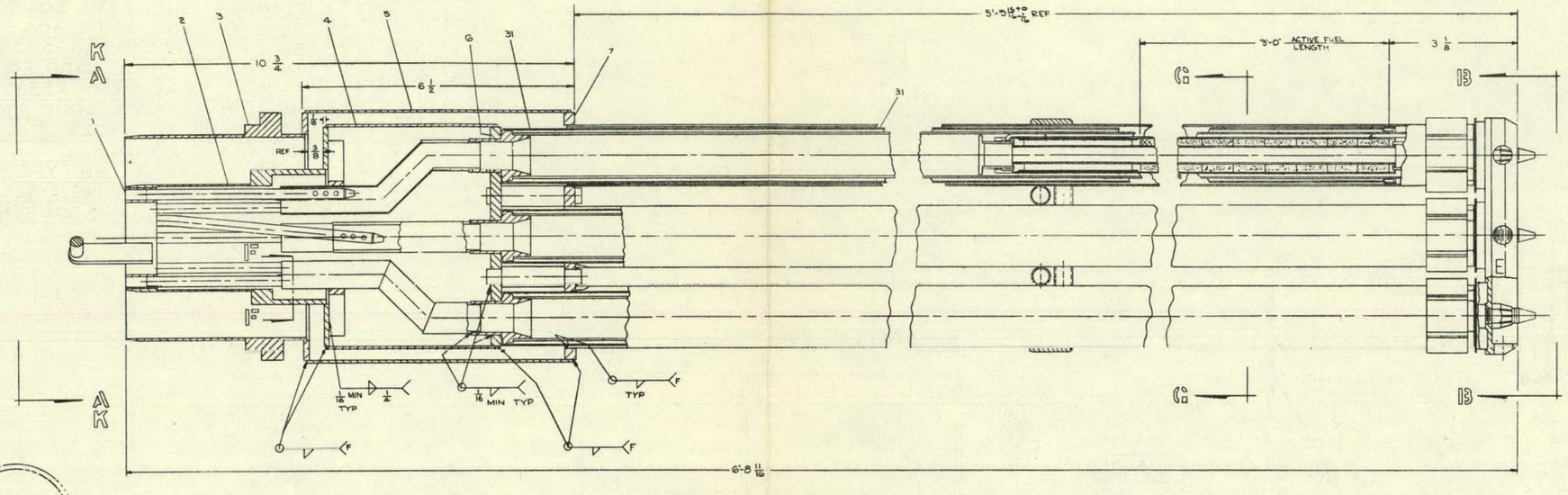

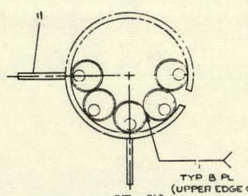

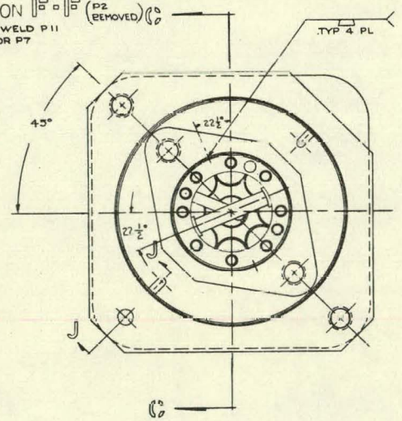

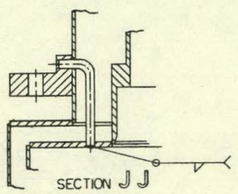

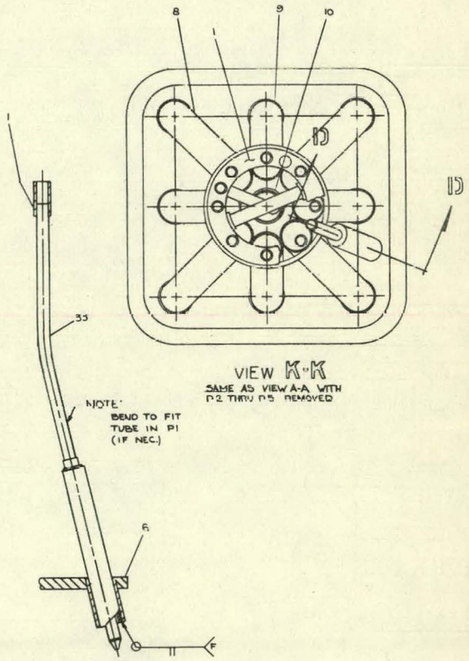

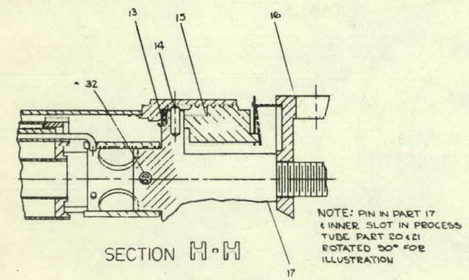

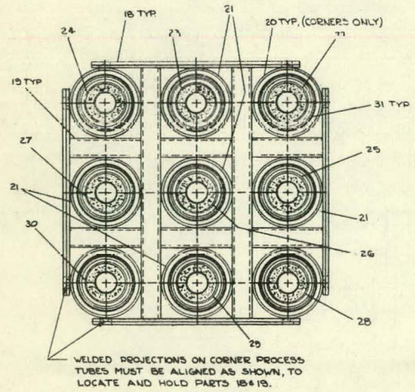

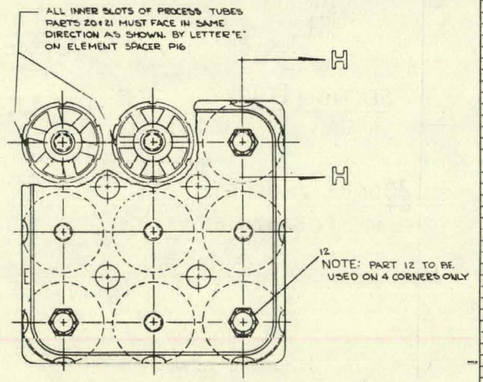

NOTES
1. ALL WELDING FILLER METAL TO BE E 308
2. F = GTAW FUSION WELD

APED SAN JOSE 212E449

Figure 9.15

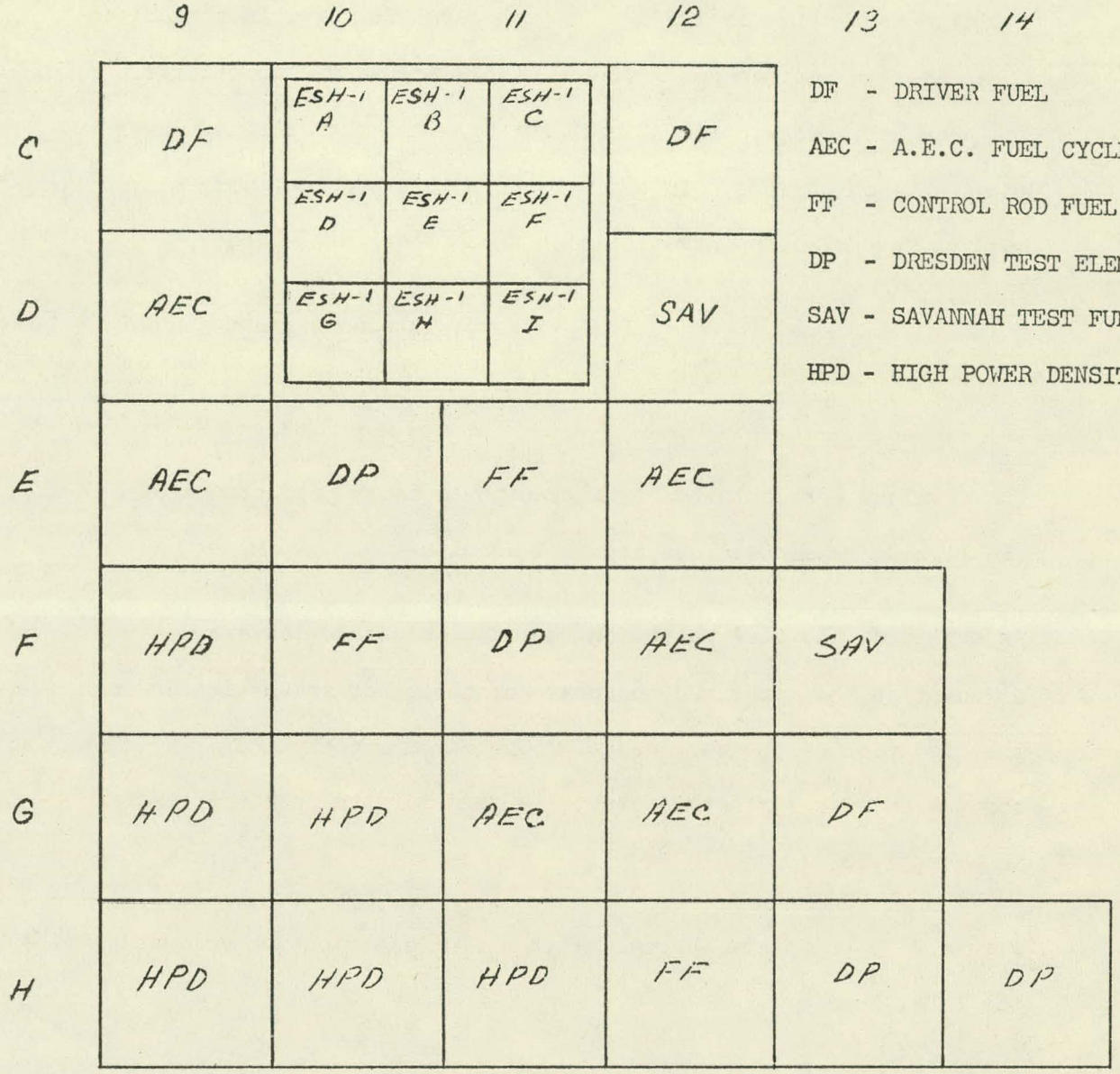

ASSUMED VBWR CORE CONFIGURATION, ESH-1

FIG. 9.16

Results of this analysis are shown in Figures 9.17 - 9.35. A power profile is presented for the inside and outside surface for each of the nine assemblies in ESH-1. In each case the power is normalized to an average surface power of 1.0. This allows one to observe the peak to average power of both surfaces and the relative power shape on each surface. In order to normalize the two surface powers, the following normalization factors are presented:

Enrichment	Power-inside surface / Power-outside surface
6	0.784
8	0.690
10	0.561

These values were obtained from transport theory predictions of the flux depression across the fuel annuli.

As expected, the peak values on the outside assemblies are adjacent to the water and the peak for the other assemblies is in the direction of the core center. The maximum peak to average for the outside surface is about 1.40 and for the inside surface is about 1.20.

Figure 9.35 shows the thermal neutron flux distribution across the ESH-1 bundle.

9.2.4 E-SADE Special Handling Equipment

Design of the special equipment required for handling of the E-SADE fuel assembly, to lift the assembly from the fuel channel and to transfer the assembly from the NE refueling port to the

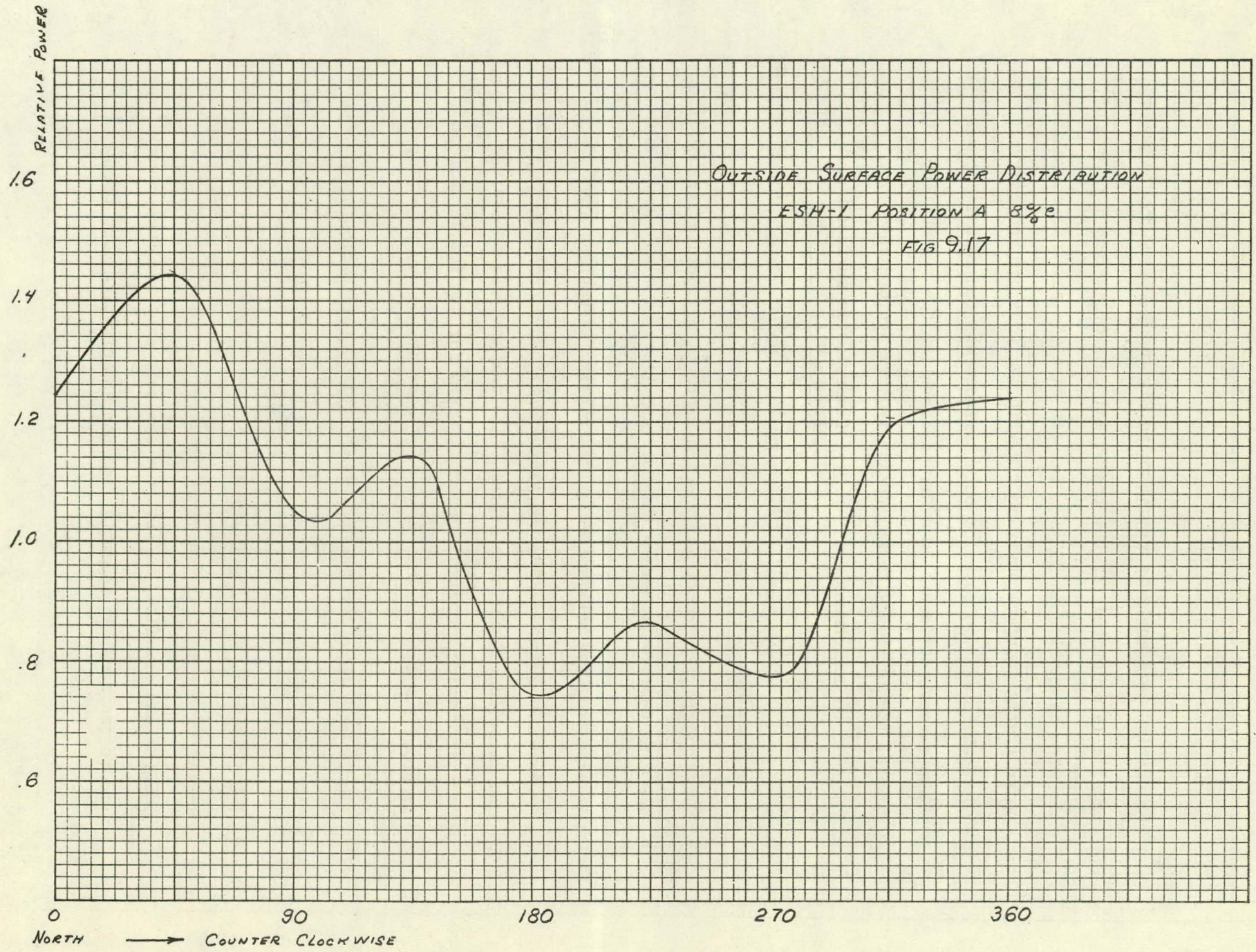

OUTSIDE SURFACE POWER DISTRIBUTION
ESH-1 POSITION A 8% e
FIG 9.17

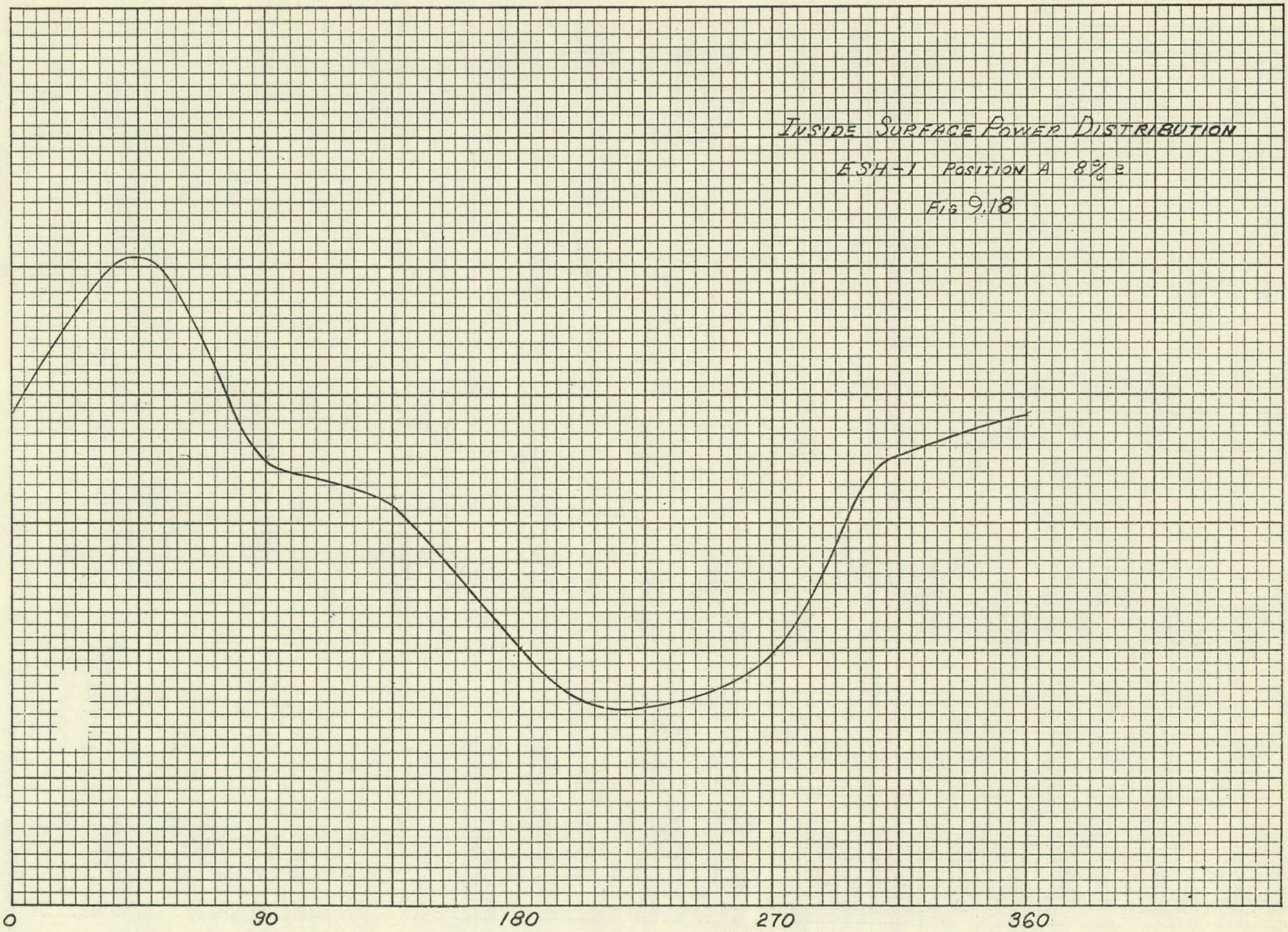
INSIDE SURFACE POWER DISTRIBUTION
ESH-1 POSITION A 8½ ε
FIG 9.18
RELATIVE POWER
1.2
1.0
.8
0
90
180
270
360

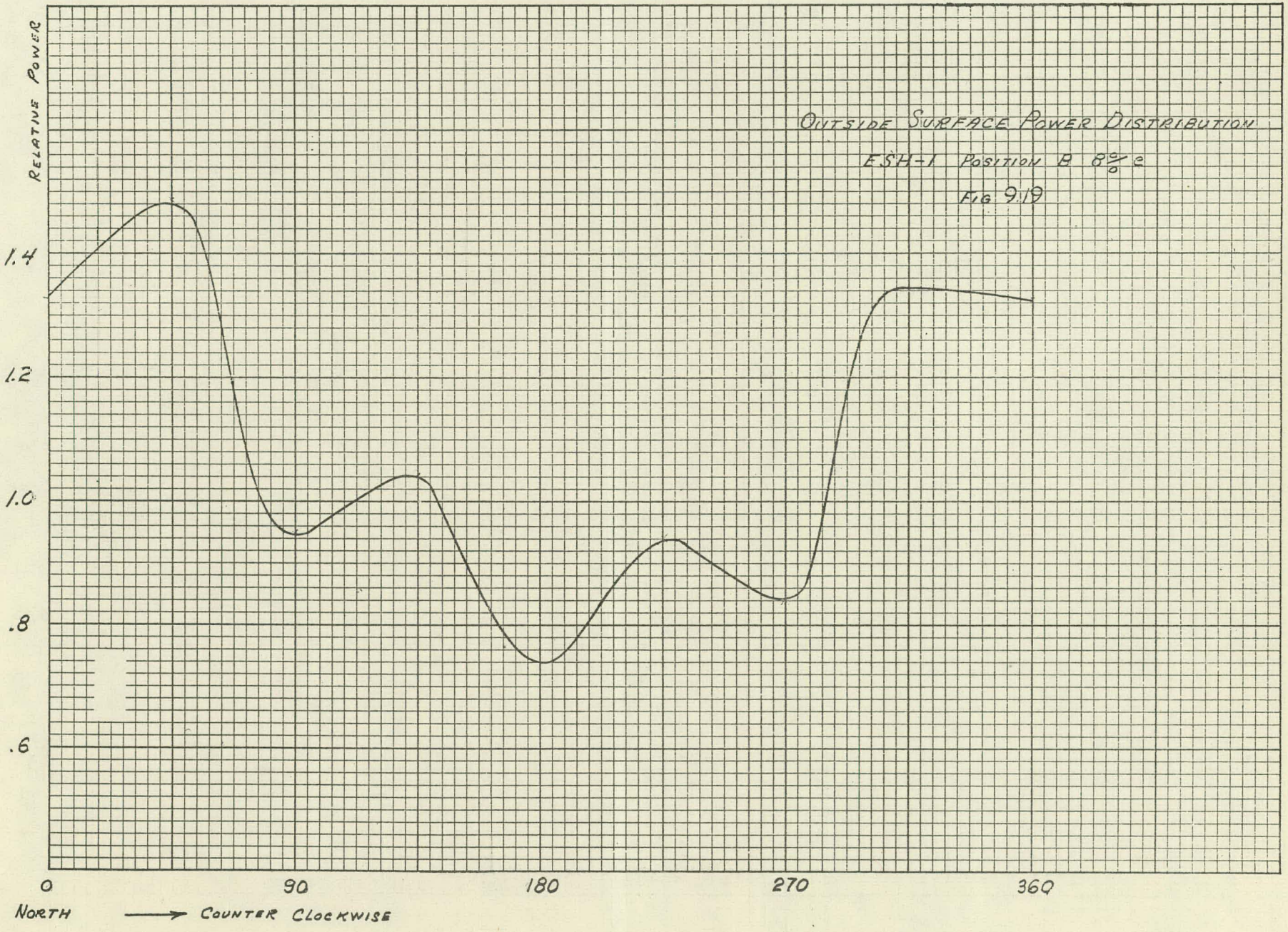

OUTSIDE SURFACE POWER DISTRIBUTION

ESH-1 POSITION B 8% ℄

FIG 9.19


INSIDE SURFACE POWER DISTRIBUTION
ESH-1 POSITION B R.P.F.
FIG 9.20
RELATIVE POWER
1.2
1.0
.8
0
90
180
270
360
NORTH → COUNTER CLOCKWISE

OUTSIDE SURFACE POWER DISTRIBUTION

ESH-1 POSITION C 10% E

FIG 9.21


INSIDE SURFACE POWER DISTRIBUTION
ESH-1 POSITION C 10% e
FIG 9.22
RELATIVE POWER
1.2
1.0
.8
0
90
180
270
360
NORTH
COUNTER CLOCKWISE

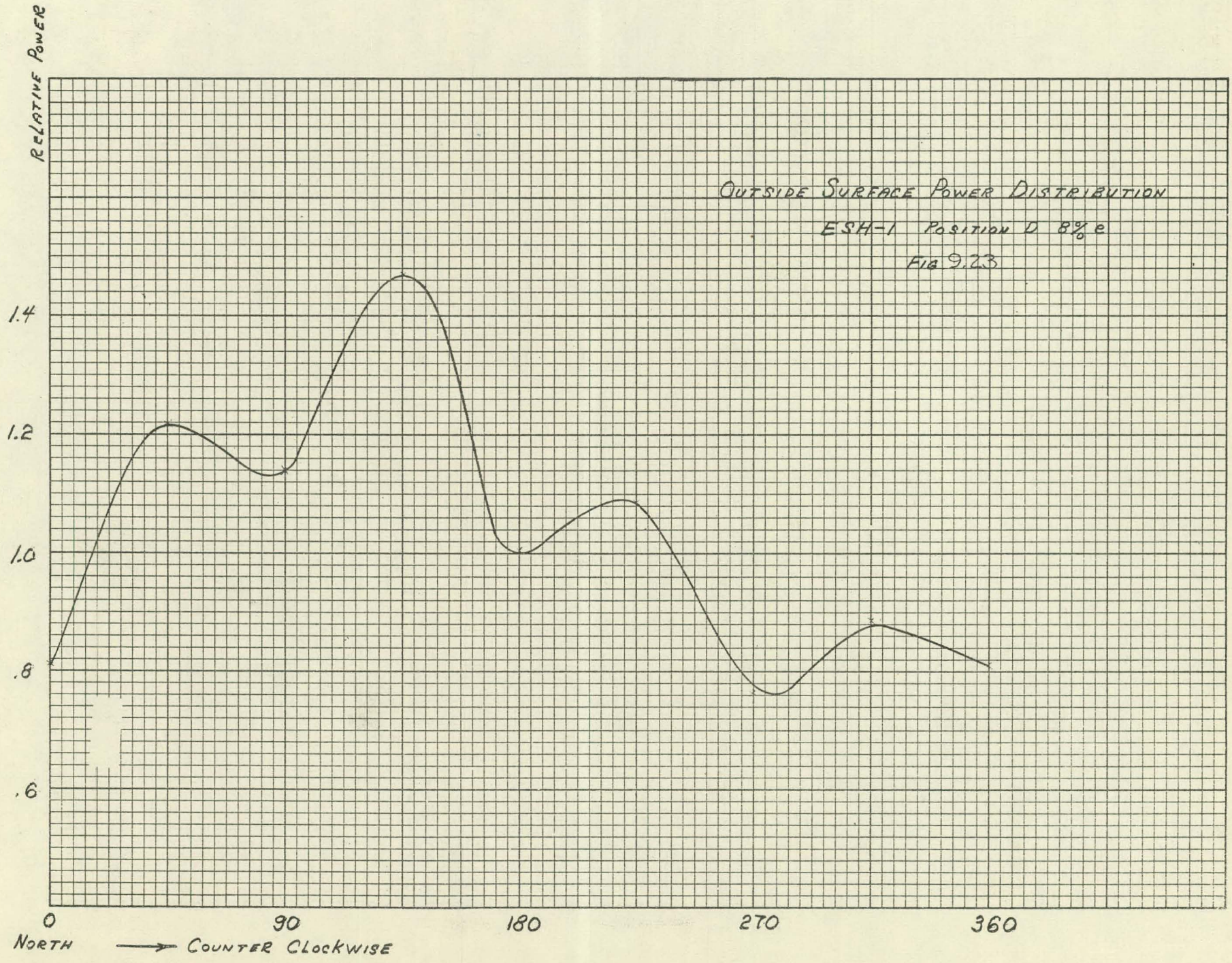

OUTSIDE SURFACE POWER DISTRIBUTION

ESH-1 POSITION D 8% e

FIG 9.23

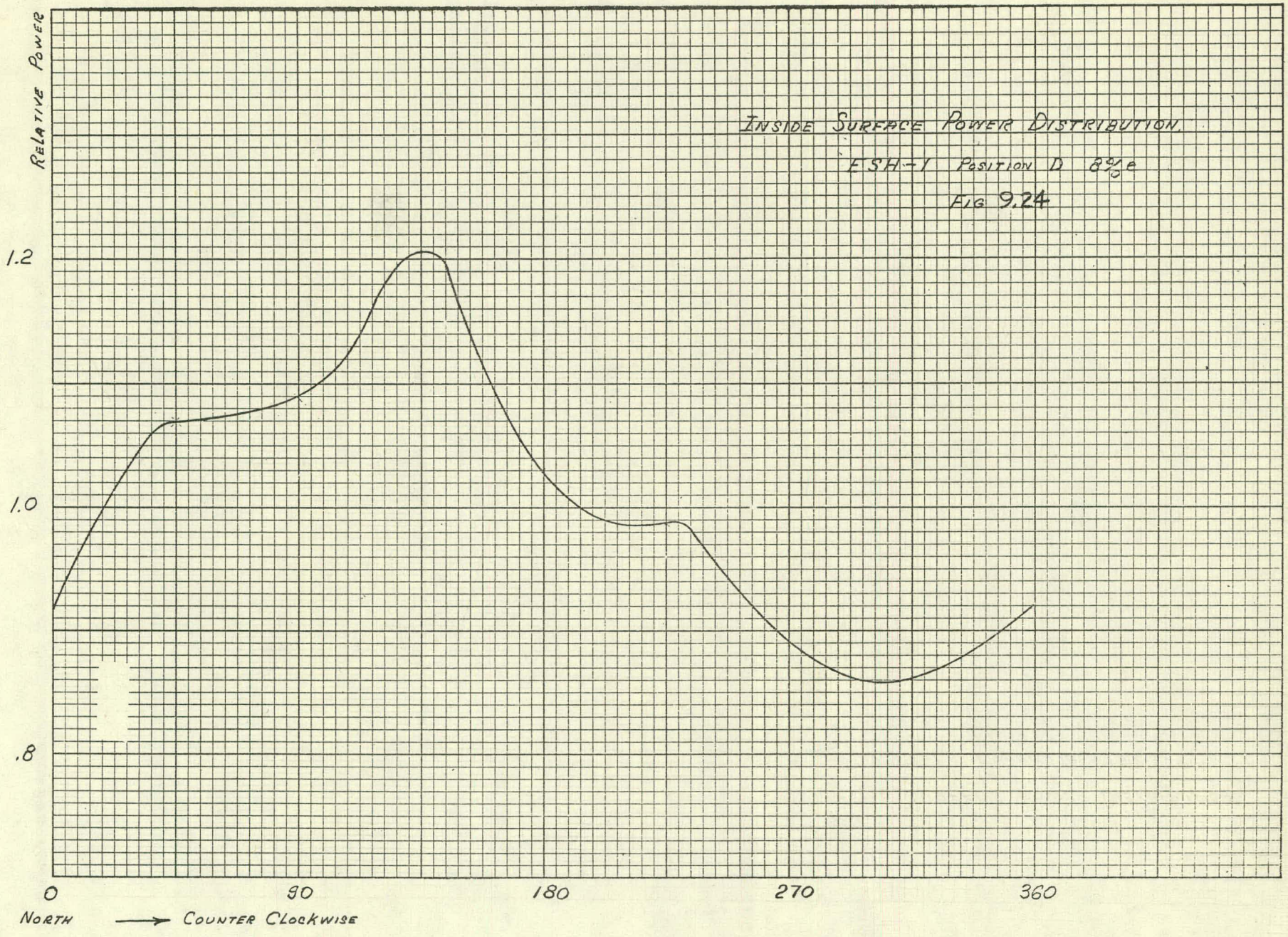

Inside Surface Power Distribution

ESH-1 Position D 8 2/3 e

Fig 9.24


Relative Power
1.4
1.2
1.0
.8
.6
0
90
180
270
360
North
Counter Clockwise
Outside Surface Power Distribution
ESH-1 Position E 10% E
Fig 9.25

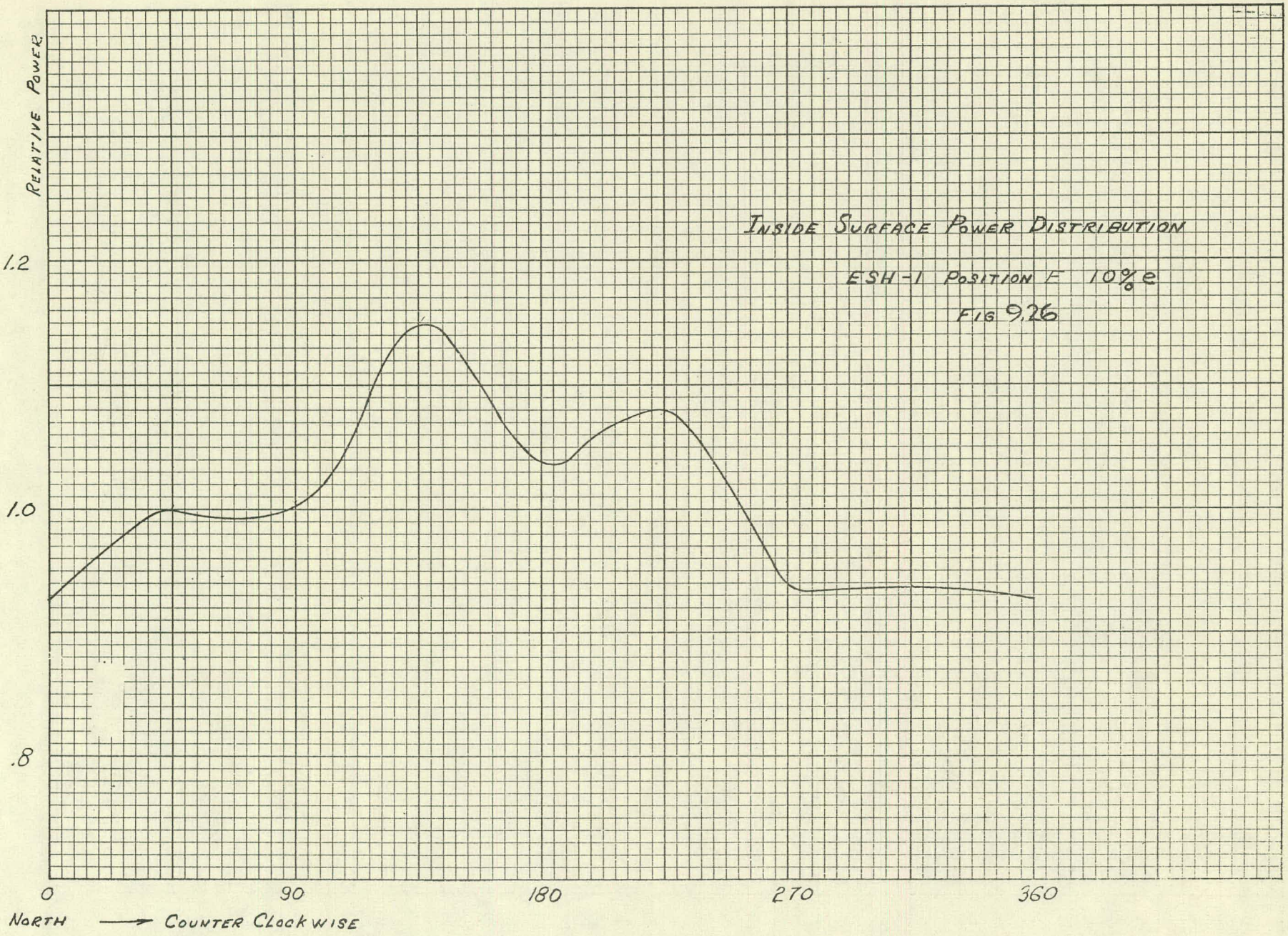
RELATIVE POWER
1.2
1.0
.8
0
90
180
270
360
NORTH → COUNTER CLOCKWISE
INSIDE SURFACE POWER DISTRIBUTION
ESH-1 POSITION F 10% e
FIG 9.26

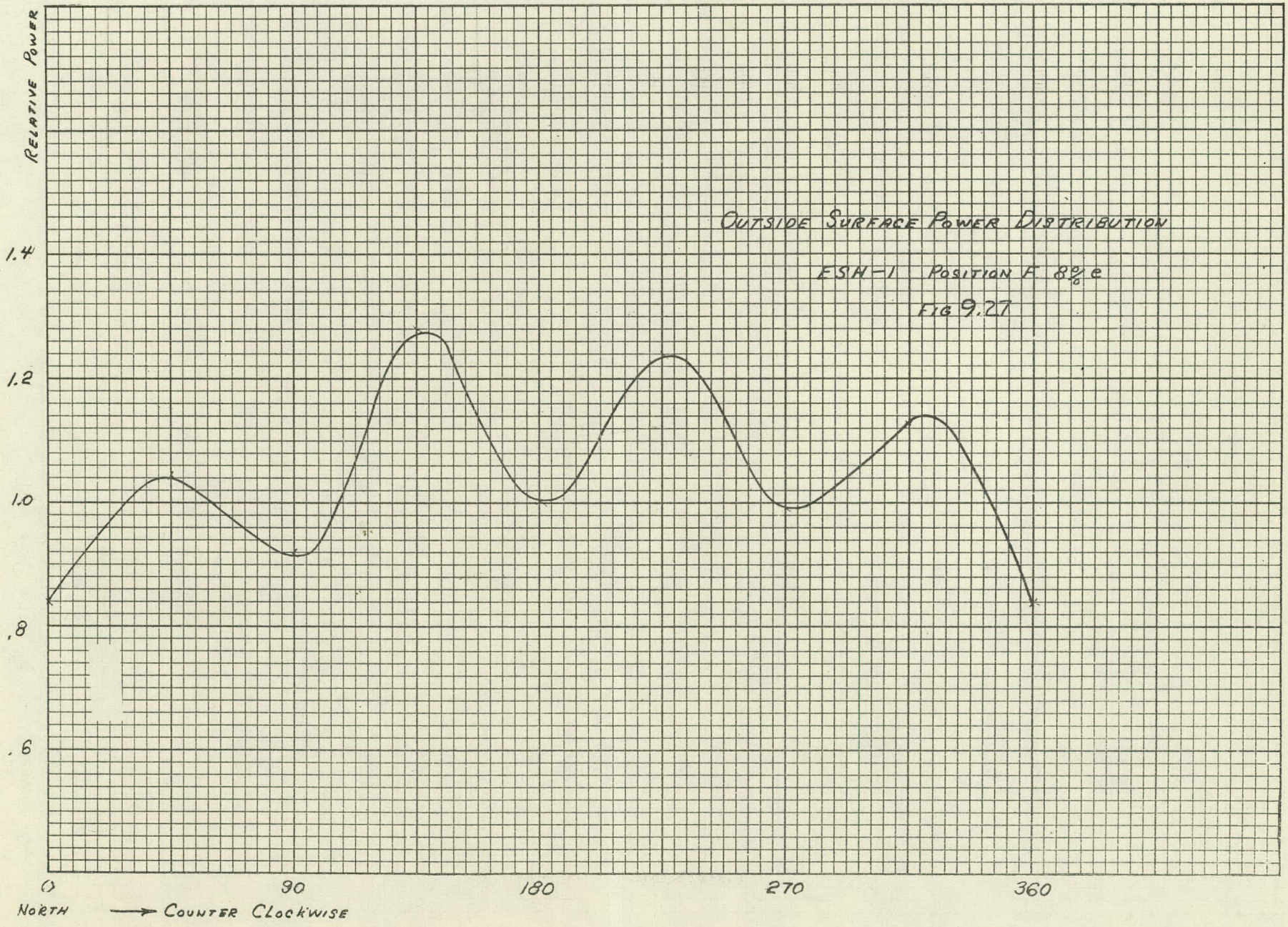

OUTSIDE SURFACE POWER DISTRIBUTION

ESH-1 POSITION F 8% e

FIG 9.27

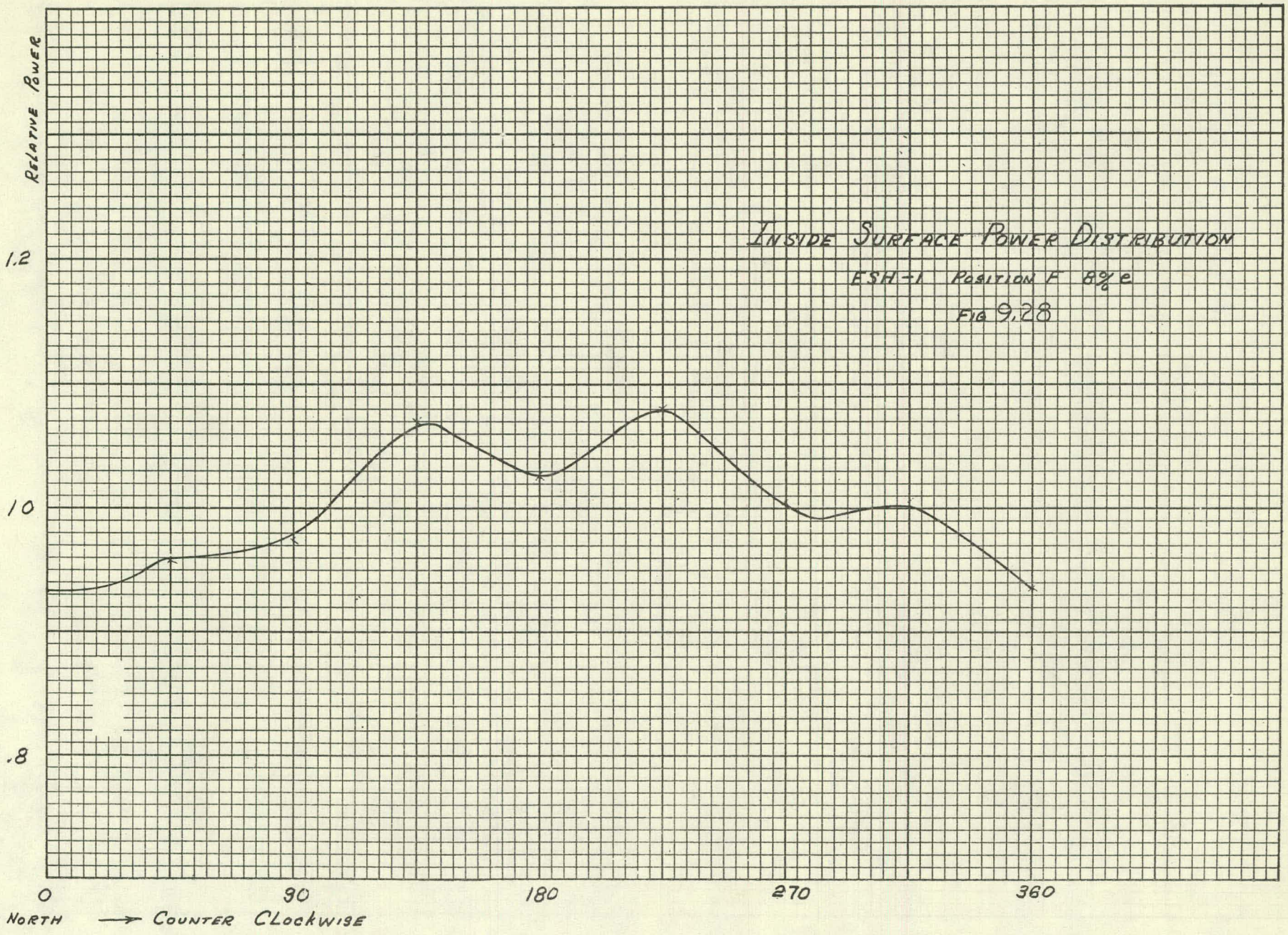
RELATIVE POWER
1.2
1.0
.8
0
90
180
270
360
NORTH → COUNTER CLOCKWISE
INSIDE SURFACE POWER DISTRIBUTION
ESH-1 POSITION F 8% e
FIG 9.28

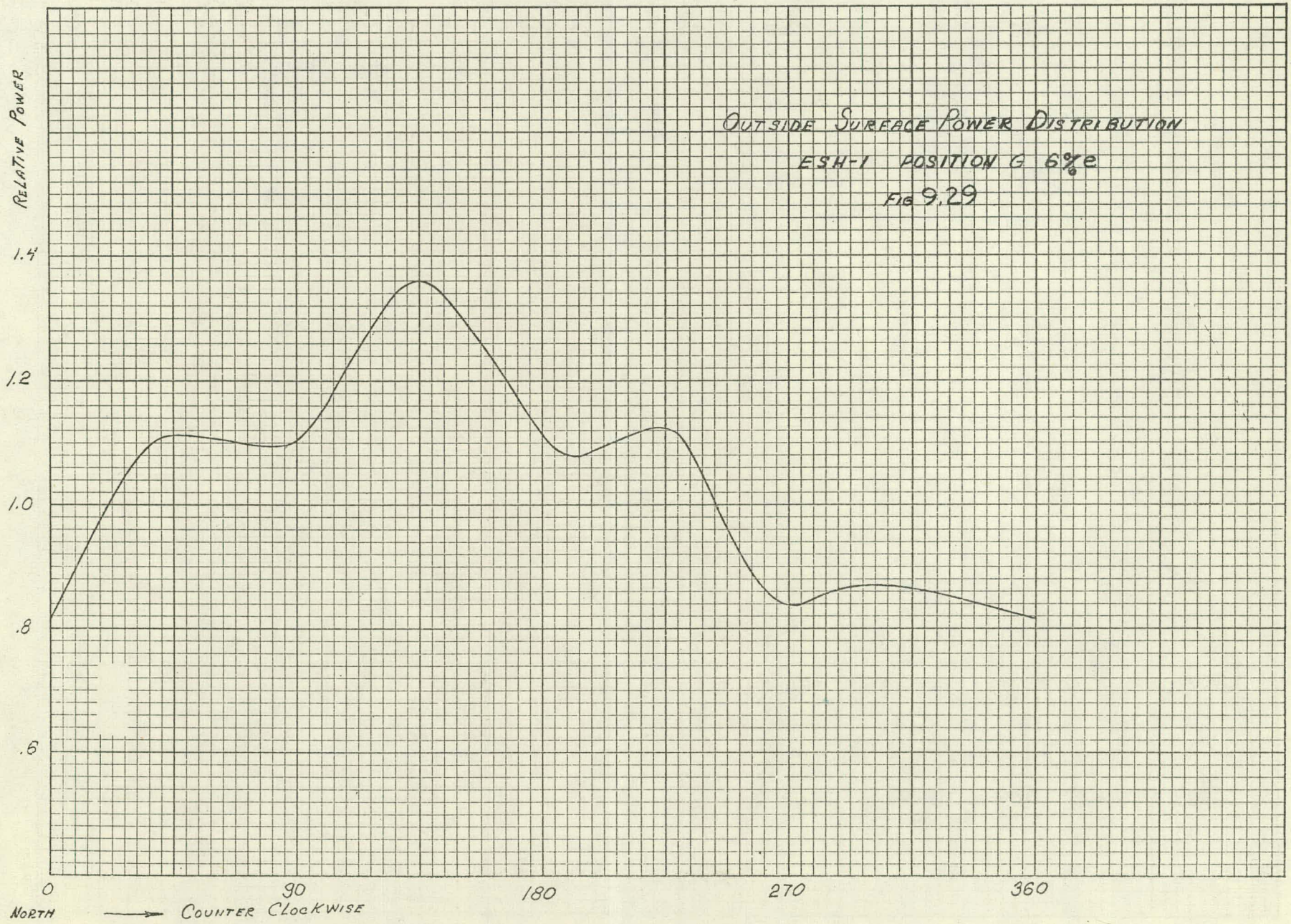
OUTSIDE SURFACE POWER DISTRIBUTION
ESH-1 POSITION G 6%e
FIG 9.29
RELATIVE POWER
1.4
1.2
1.0
.8
.6
0
90
180
270
360
NORTH
COUNTER CLOCKWISE

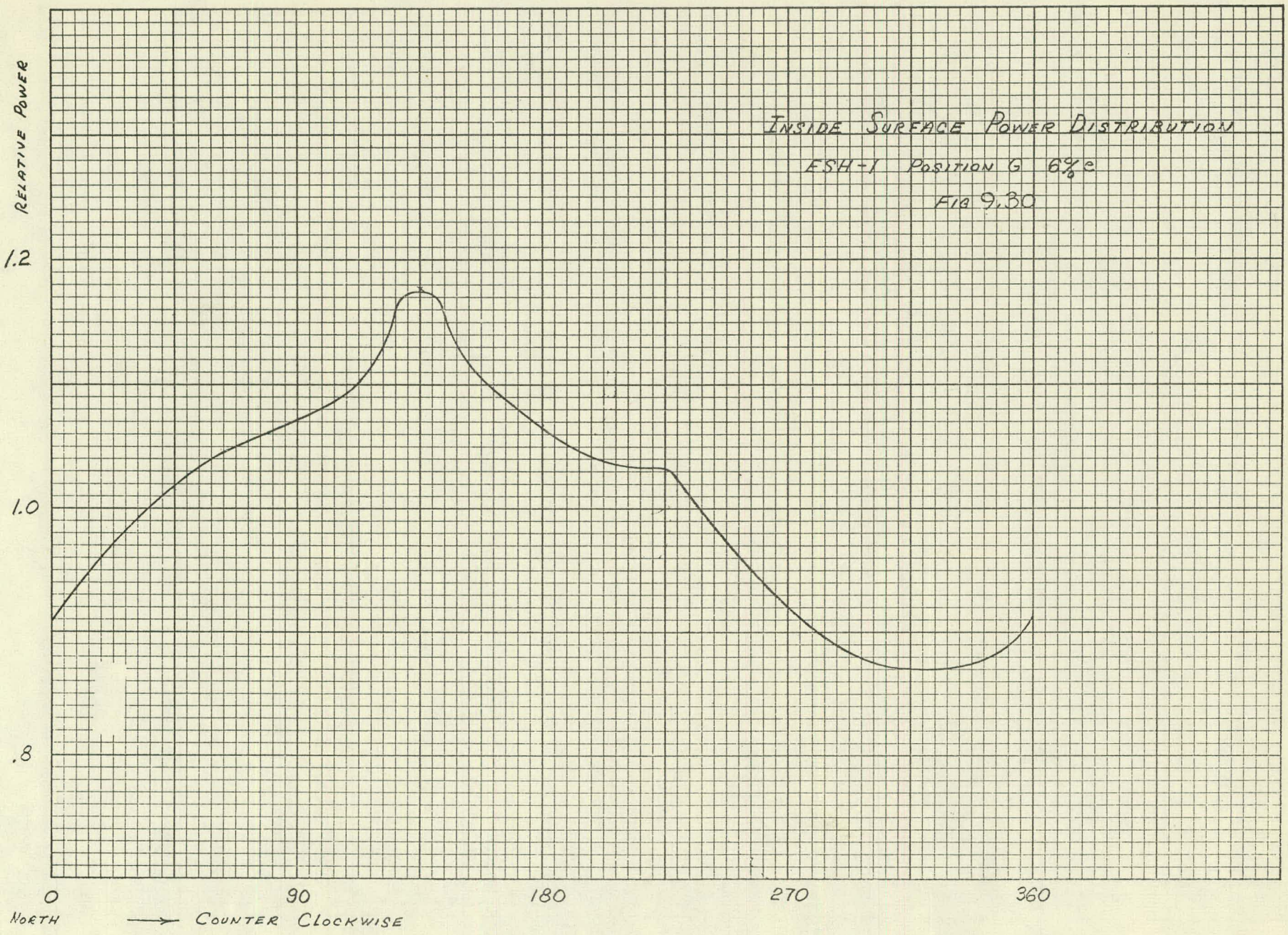
INSIDE SURFACE POWER DISTRIBUTION
ESH-1 POSITION G 6% e
FIG 9.30
RELATIVE POWER
1.2
1.0
.8
0
90
180
270
360
NORTH
COUNTER CLOCKWISE

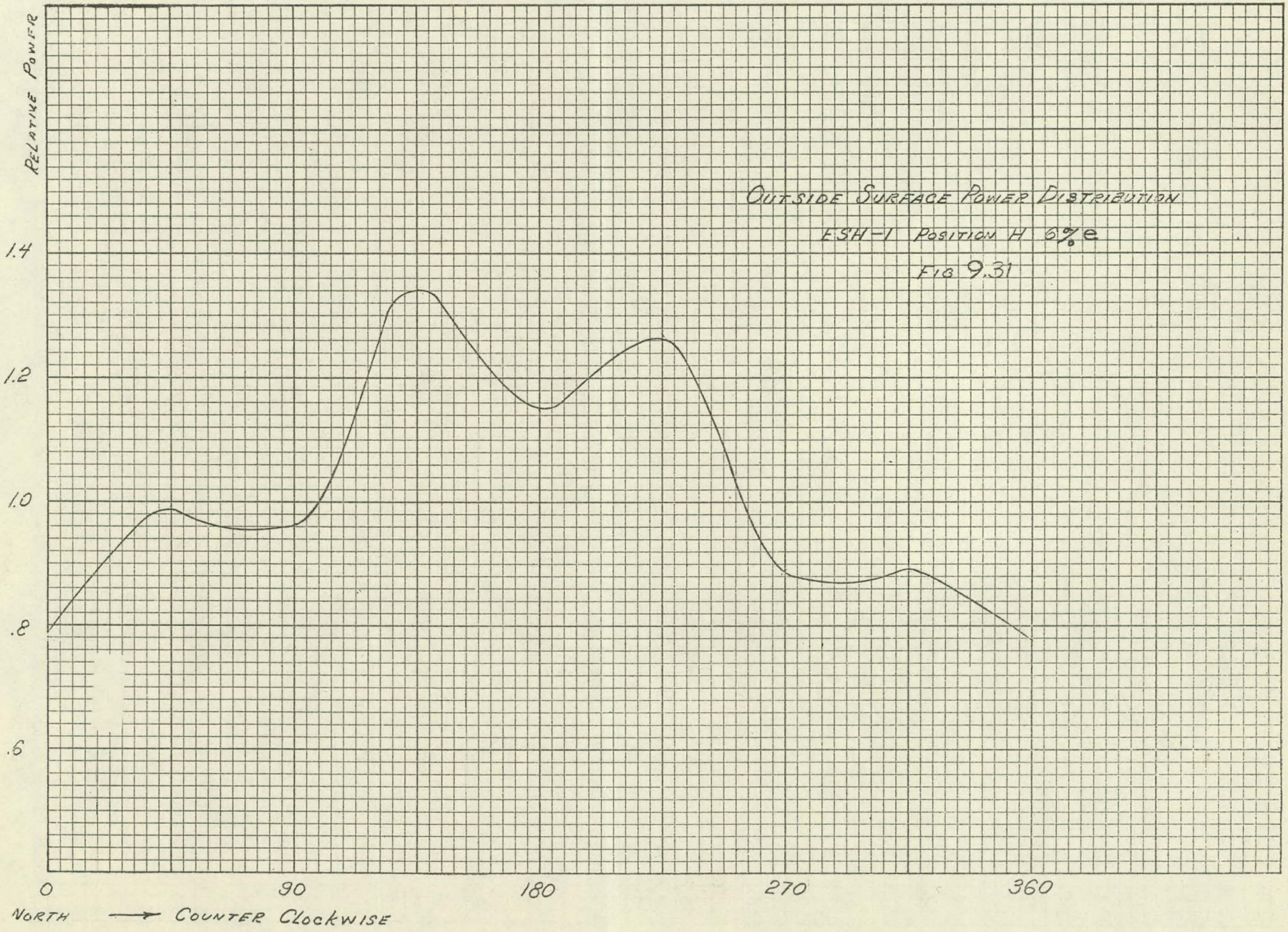

Outside Surface Power Distribution

ESH-1 Position H 6% e

Fig 9.31

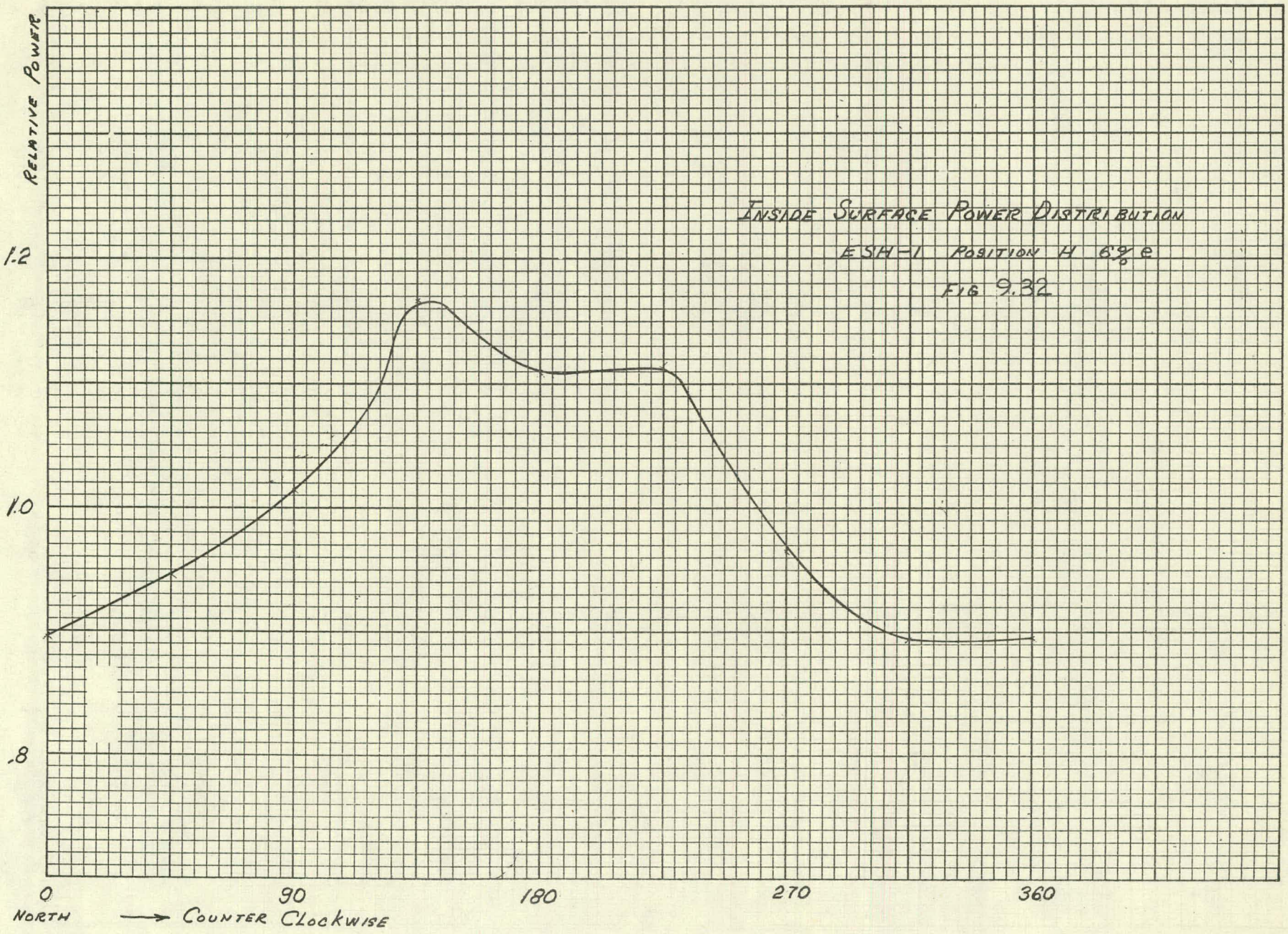

INSIDE SURFACE POWER DISTRIBUTION
ESH-1 POSITION H 6% E
FIG 9.32

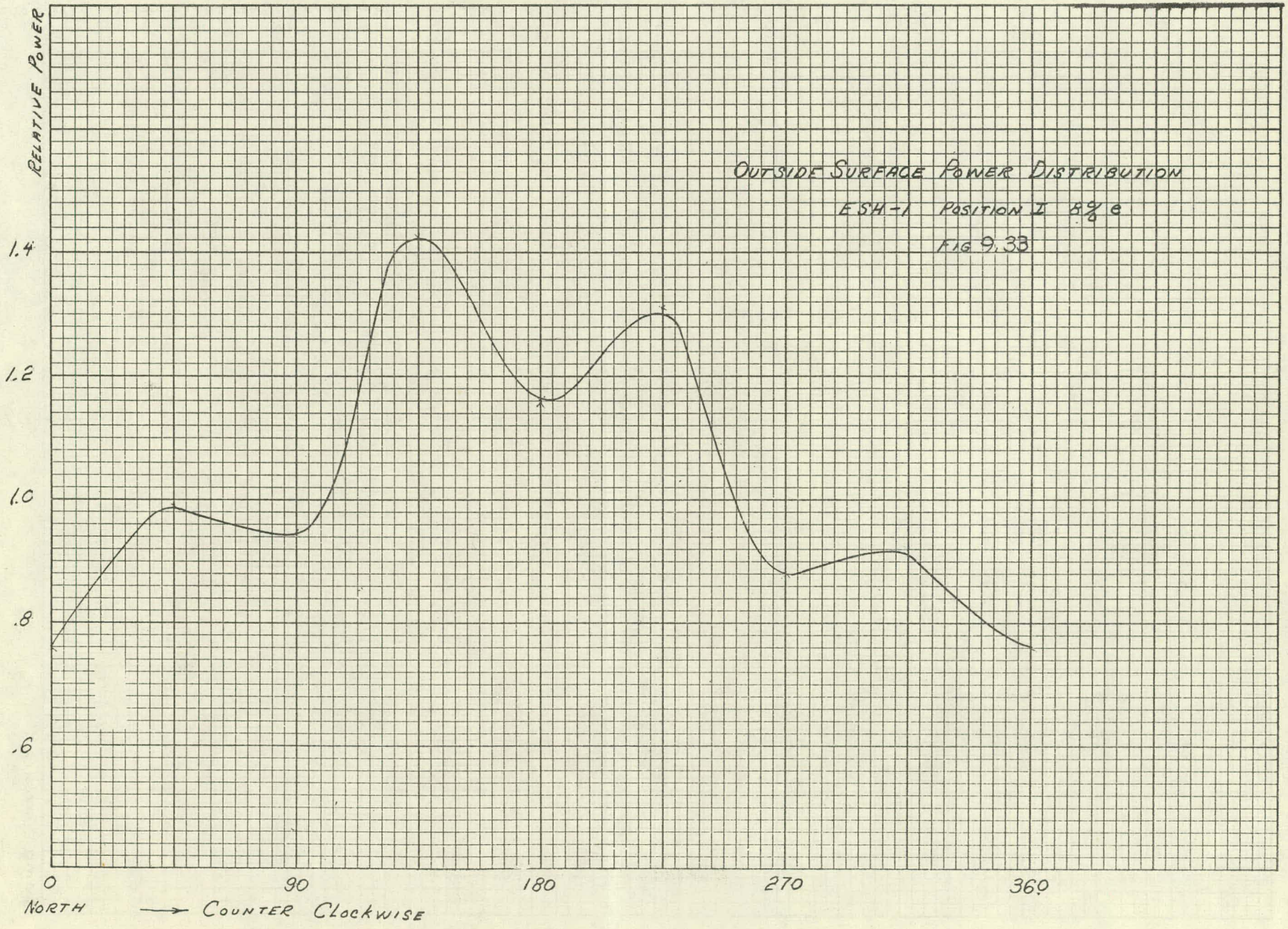

OUTSIDE SURFACE POWER DISTRIBUTION

ESH-1 POSITION I B & C

FIG. 9.33

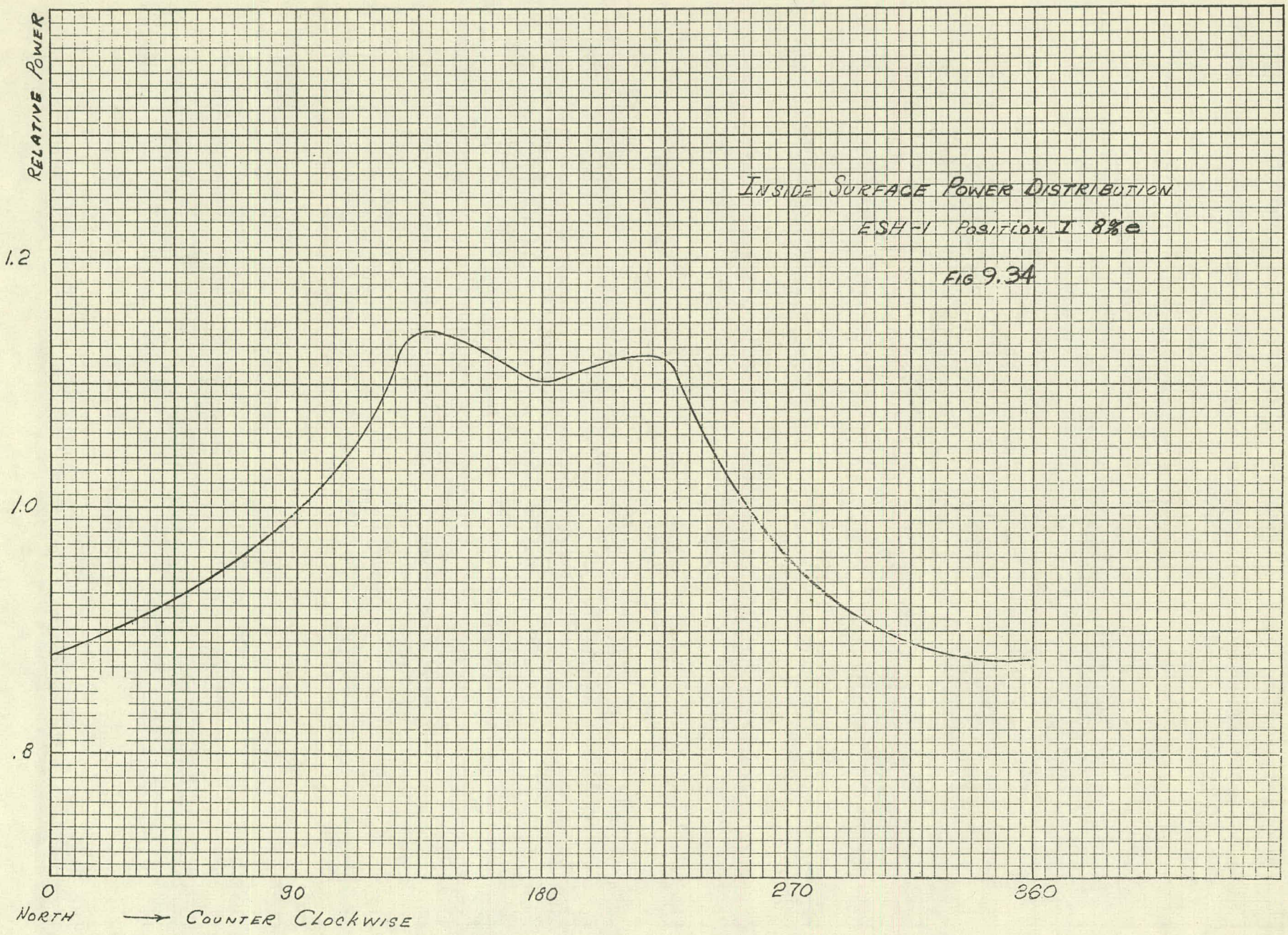
RELATIVE POWER
1.2
1.0
.8
0
90
180
270
360
NORTH
COUNTER CLOCKWISE
INSIDE SURFACE POWER DISTRIBUTION
ESH-1 POSITION I 8%e
FIG 9.34

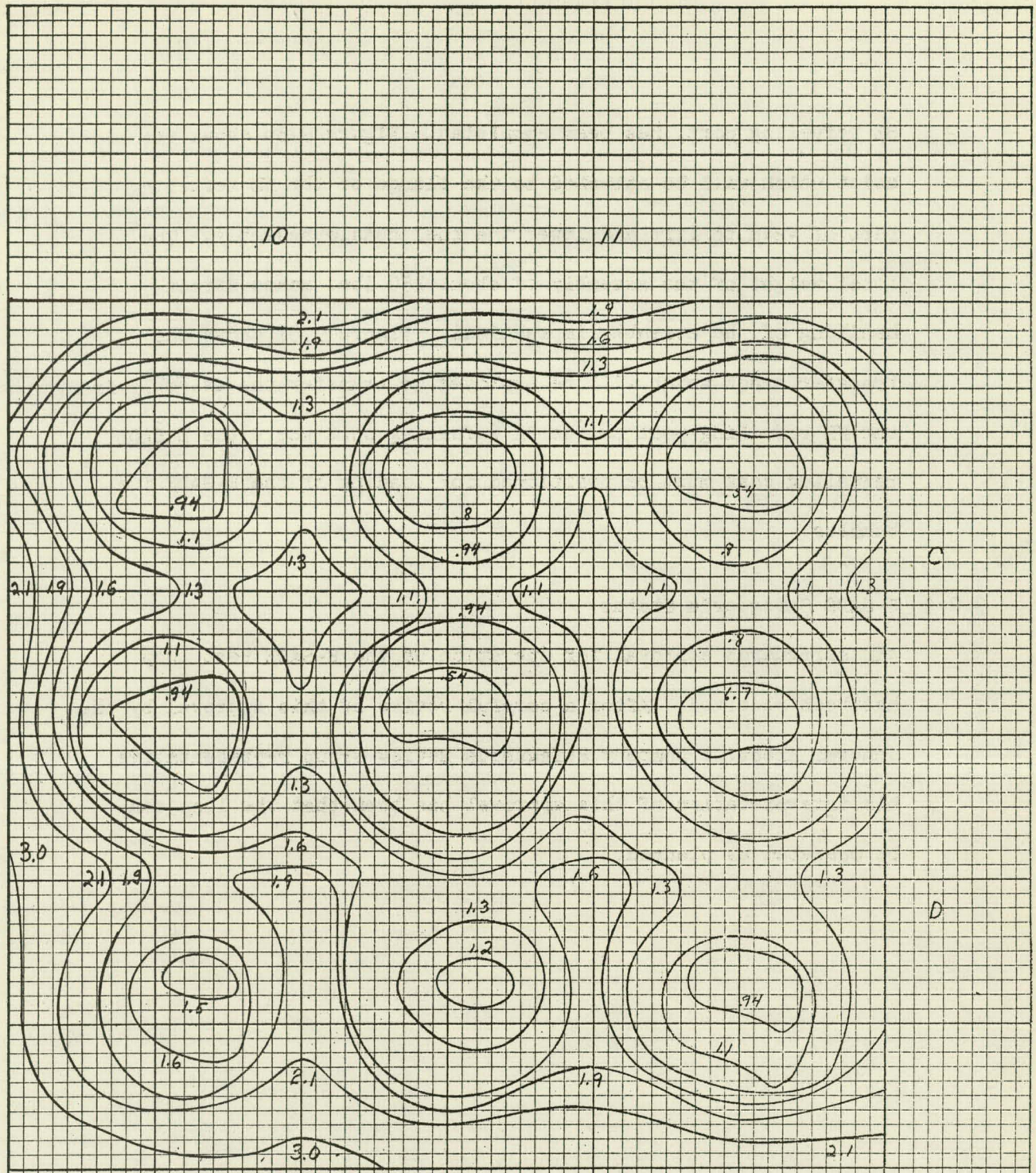

ESH-1 THERMAL NEUTRON FLUX DISTRIBUTION ($\times 10^{13}$)

VBWR POWER – 36 MW

FIG 9.35

SE refueling port, has been completed. Figure 9.36 shows the hoist which will be attached to the flange of the NE refueling port of VBWR to lift and lower the fuel bundle assembly. The total weight of the assembly of about 150 lbs. makes direct handling of the assembly impractical. Figure 9.37 shows the transfer track which will be employed to transfer the assembly from the NE refueling port to the SE refueling port where the E-SADE refueling cask must be positioned for loading of the E-SADE fuel bundles.

9.2.5 E-SADE Safeguards Status

AEC safeguards approval for operation of the E-SADE test loop has been received. After a careful review of this approval by the General Electric Company Safeguards Review Group representative, his interpretation of this approval has been that the loop can be operated as planned.

UNLESS OTHERWISE SPECIFIED USE THE FOLLOWING —
APPLIED PRACTICES | SURFACES | DECIMALS ± | ANGLES ±
√ | 64 | .005 |

TITLE ASM HOIST
FIRST MADE FOR JSNEE
FCF 105x328

212E515

PL ISSUED

.750±.001 DIA HOLE P1

1.175

.187 +.005 −.000 2 HOLES AS SHOWN

.187 +.005 −.000 DIA 2 HOLES AT ASM ROTATED 90° OUT OF POSITION THRU PART 5 AND 12

BRAZE SECURELY

VIEW E

NOTE: LOCATE P26 & 31 SO THAT CABLE HOLES IN DRUM ARE NOT UNOBSTRUCTED

28,29 (USED AT SITE)

BRAZE

SECTION A-A

SECTION B-B

VIEW C-C

SECTION D-D

NOTE
1. PAINT STEEL PARTS PER P30 TYP I ASA 49

REVISIONS | PRINTS TO

APED SAN JOSE 212E515

Figure 9.36

762 D689

UNLESS OTHERWISE SPECIFIED USE THE FOLLOWING:—
APPLIED PRACTICES: 145A5481 | SURFACES: 125 | TOLERANCES ON MACHINED DIMENSIONS: FRACTIONS ± 1/64, DECIMALS ± .005, ANGLES ± 2°

REV NO. Ø1 — 762 D689 — CONT ON SHEET — SH NO.

TITLE: TRANSFER TRACK

F. FOR SHEET FCF 105×328

G1	PART NO.	DRAWING NO., DESCRIPTION, MATERIAL, WEIGHT	
	2	1	AISI 1018 STL.
	4	2 ANGLE	ASTM A7-56 STL.
	2	LUG	AISI 1018 STL.
	6	PIN	ASTM B139-52 ALLOY BI HARD
	5	WASHER	N400P45 STL.
	6	BAR	AISI 1018 STL.
	2	7 BLOCK	AISI 1018 STL.
	2	8 COUPLING	AISI 1018 STL.
	1	9 RAIL	6061-T6 ALUM
	2	10 PIN	ASTM B139-52 ALLOY BI HARD
	16	11 COTTER PIN	N504P916 STL
	2	12 BOLT	HEX. HD 1⅜-6UNC-2A×6 LG STL.
	2	13 NUT	HEX. 1⅜-6UNC-2B STL.
	1	14 TROLLEY	762D686
	1	15 BAR	AISI 1018 STL.

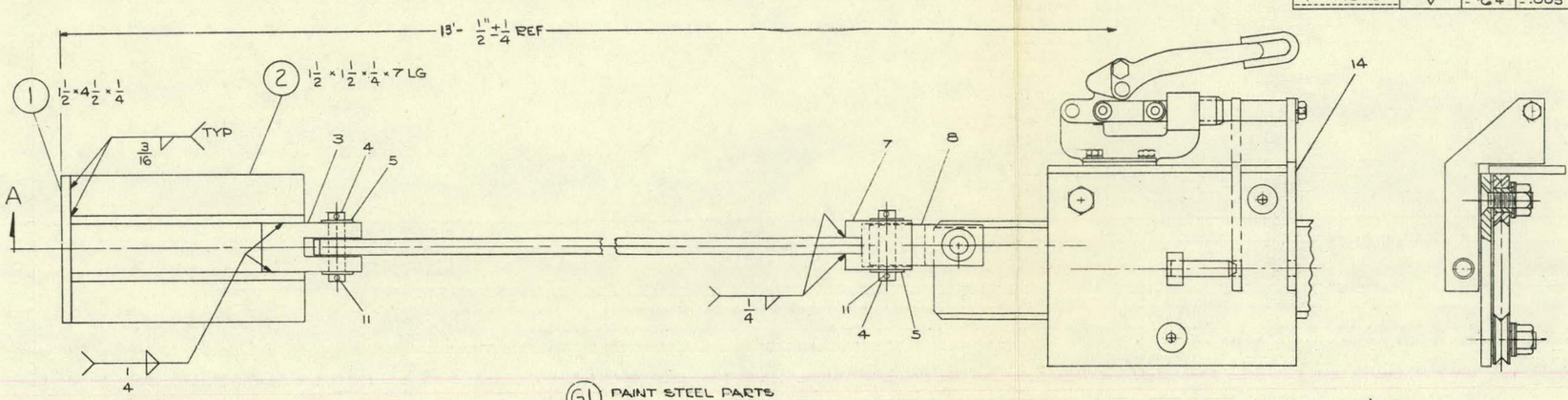

(G1) PAINT STEEL PARTS PER R50YR1 ASA 49

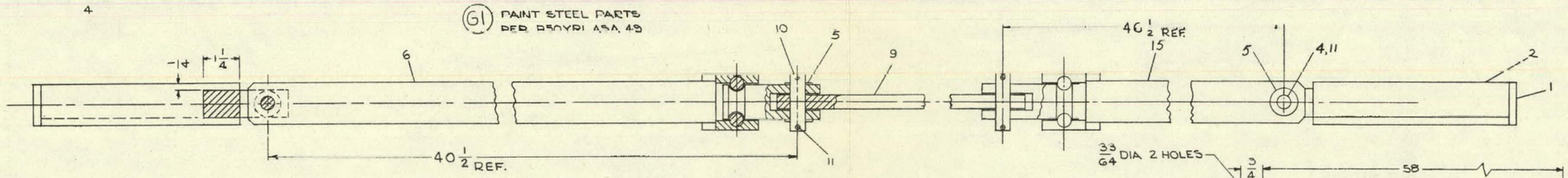

SECTION A-A

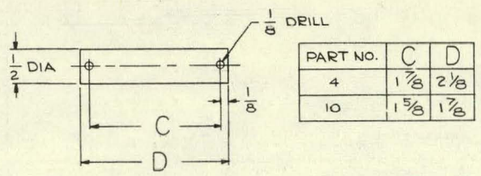

PART NO.	C	D
4	1 7/8	2 1/8
10	1 5/8	1 7/8

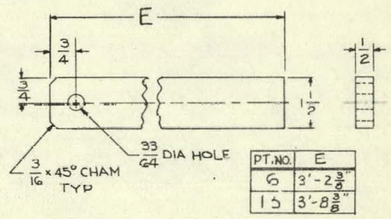

PT. NO.	E
6	3'-2 3/8"
15	3'-8 3/8"

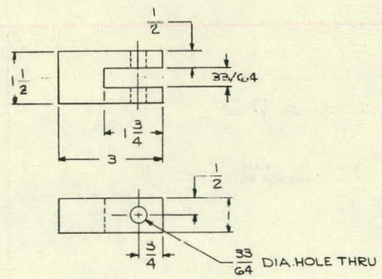

③

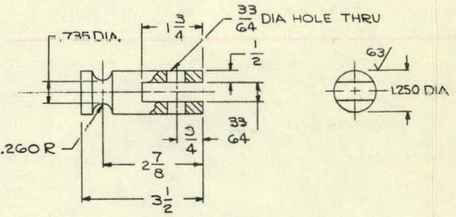

⑧

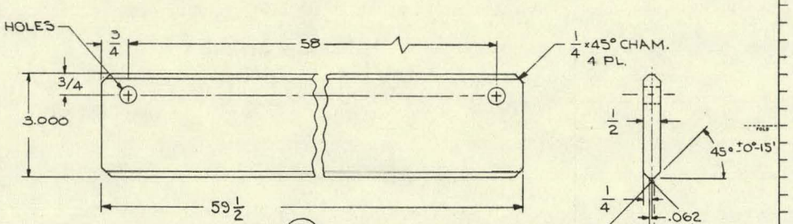

⑨

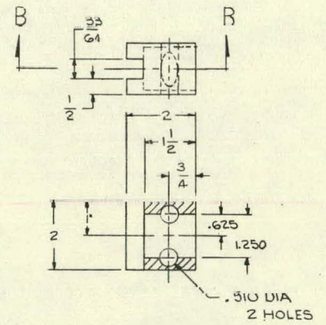

SECTION B-B

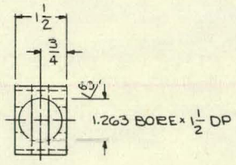

⑦

DESCRIPTION OF GROUPS	REVISIONS	PRINTS TO
	1 NE 1983	

MADE BY E. NOV. 24, 61 | ISSUED 4-12-64 | APPROVALS | A P E D DIV OR DEPT. | SAN JOSE LOCATION | 762 D689 SH NO. | CONT ON SHEET

FF-811-P 6000 (8-56) PRINTED IN U.S.A.

Figure 9.37

10.0 TASK J - MIXED SPECTRUM SUPERHEATER DESIGN STUDY

10.1 Prototype Design

The primary effort during this reporting period was spent in accumulating the design, performance, and cost information on the 75 MWe MSSR prototype. This information will be presented in a conceptual design report now under preparation. This report will be issued on February 25, 1962. Table 10.1 summarizes the essential features of the plant with the details left to be published in the design report.

Table 10.1

Summary of 75 MWe MSSR Reactor Data

General	
Gross MWe	75
Thermal MW	200
Steam flow (lb/hr)	570,000
Vessel inside diameter (ft)	11
Vessel inside height (ft)	36
Boiling Water Core	
Core flow (lb/hr)	$10.7 - 10^6$
Inlet subcooling - based on 1% carryunder (Btu/lb)	9
Pressure (psia)	1015
Cycle	Natural
Lattice	D
No. of assemblies - Thermal core	128
- Thermal buffer	16
Effective active fuel length (in)	80
Equivalent core diameter (in)	92.9

Circumscribed core diameter (in)	101.4
Overall core power density(kw/l)	20.4
Heat transfer area (ft^2)	6340

Superheat Core

Inlet temperature (^oF)	545
Outlet temperature (^oF)	950
Outlet pressure (psia)	925
Lattice - close packed, triangular array	Rods
No. of assemblies - Fast core	60
- Fast core control	4
- Fast buffer	32
No. of rods per assembly - Fast core	52
- Fast core control	42
- Fast buffer	26 in each of 28 42 in each of 4
Rod outside diameter (in)	0.438
Clad thickness (in)	0.030
Pitch to diameter ratio	1.05
Fast core dimensions (fueled region)	$31\frac{1}{2}$" x $31\frac{1}{2}$" x 30" high
Control elements	4 fuel bundles in fast core 8 coupling control blades between superheater & boiler
Overall core power density (kw/l)	98.5
Maximum heat flux (Btu/hr-ft^2)	386,000
Hot channel average velocity (FPS)	151
Maximum clad surface temperature (^oF)	1230
Maximum fuel temperature based on K = 1.3 (^oF)	4320

10.2 Safety-Core Meltdown Studies

During this reporting period, the detailed equations were formulated for analyzing the possible consequences of a fast core meltdown. A description of the proposed method of analysis (FARM I)is included in Section 10.3.

To avoid duplication, some of the work on the meltdown analysis is being utilized in the AEC Fast Ceramic Reactor Program where similar analysis is required. In particular, the specifications for the meltdown accident analysis developed under the MSSR program will be used as the basis for a computer program developed under the Fast Ceramic Program. The computer code will be available for both MSSR and FCR work.

After completion of coding and application of code to MSSR safety analysis, it is expected that a detailed description of the analytical method will be published in topical report form.

10.3 Test Reactor Meltdown Excursions and Resultant Energy Releases (FARM I)

10.3.1 Introduction

The following contains extracts from the FARM I analytical method which describes a problem setup for the determination of the reactor transients and energy releases during a fast reactor meltdown excursion. A description of the Problem is contained in Section 10.3.2, Problem Approximation in Section 10.3.3, Equations in Section 10.3.4, Boundary Conditions and Initial Conditions in Section 10.3.5. Numerical Approximations have not been included to conserve space in the Quarterly report.

As set up, the problem solution provides a continuous monitoring of the reactor transients from the original homogeneous state, through the melting and compaction states to an eventual sub-critical condition. Coupled nuclear, inertia and energy equations provide a basis for the problem solution.

10.3.2 Problem

In evaluating the hazards associated with a fast power reactor accident leading to meltdown, one should have some knowledge of the energy released during the accident transient. The problem being set up for computer solution in this report represents a continuous evaluation of the following "accident transient steps":

A. Steady state operation of reactor.

B. Sudden loss of coolant with or without control transients.

C. Resultant heating up of fuel elements.

D. Melting and redistribution of nuclear materials.

E. Nuclear excursion resulting from material redistribution.

F. Shutdown of the excursion as a result of a subsequent sub-critical redistribution of materials.

Evaluation of the above transient steps results in a knowledge (within the limitations imposed by the approximations used in solving the problem) of the energy release history during the accident transient.

10.3.4 Problem Approximation

The approximations used in describing the accident transient steps are described in the following "problem solution steps".

A. The reactor configuration and initial conditions are assumed to be approximated by a homogeneous sphere.

B. The transient nuclear characteristics are followed for the homogenized sphere utilizing the transient diffusion equation[1] considering both delayed neutrons and doppler.

C. The temperature transients are followed assuming no conduction[2] or radiation.

D. When melting transpires, it is assumed that the molten material is propelled toward the center with a force equivalent to the free-fall force of gravity,[3] filling in the existing voids (flow area between fuel elements).

E. In the center molten sphere, formed in D above, in addition to the transient nuclear characteristics considered in B above, the equations for the conservation of momentum, conservation of mass, conservation of energy and equation of state are also assumed to hold. In these calculations, the nuclear cross-sections and the diffusion coefficient are modified to account for the time dependent changes in density.

F. The process described in steps A through E above, continues until such a time as the configuration becomes sub-critical.

---

1. Initially, the problem will be looked at using a one-group approximation. Provision will be made for the future insertion of more groups.
2. Provision will be made for inserting the conduction equations into the program at a later date if it appears to be warranted.
3. Provision will be made in the program to provide arbitrary force causing the material to compact.

At any point in time during the "problem solution steps", it is possible to determine the total energy of the system.

10.3.5 Equations

The equations required to describe the "problem solution steps" were set up assuming spherical symmetry and using Lagrangean coordinates (i.e., a particle is followed in Lagrangean coordinates as opposed to looking at the flux flowing past a fixed point in Eulerian coordinates).

10.3.5.1 Conservation of Neutrons

The nuclear diffusion equation representing one group and accounting for delayed neutrons, change in density effects on the diffusion coefficient and cross-sections, and the temperature effects (doppler) can be shown as follows:

$$V \frac{D_o}{V_o} \nabla^2 Q + \frac{V_o}{V} (\nu \Sigma_f - \Sigma_a - \Sigma_{D_N} - \Sigma_D) Q - \frac{1}{V} \frac{\partial Q}{\partial t} = \lambda C \Pi \Sigma_f \quad (1)$$

where Q, the heat generation, has replaced the usual neutron flux and density terms.

The delayed neutron equation is of the form:

$$\frac{dC}{dt} = + \frac{1}{\Pi \Sigma_f} \Sigma_{DN} Q - \lambda C \quad (2)$$

10.3.5.2 Conservation of Momentum

The conservation of momentum equation has the form:

$$\frac{1}{\mathcal{H}} \frac{\partial^2 R}{\partial t^2} = -V_o \left(\frac{R}{r}\right)^2 \frac{\partial p}{\partial r} \quad (3)$$

The appropriate equation of state has the form:

$$p = \left(\alpha + \beta T + \gamma V\right)\left(\frac{V_R}{V}\right)^n + q \tag{3a}$$

where the coefficients are described in Section 10.3.5.7 From (3) and (3a) the following three forms of the momentum equation result:

1. Liquid phase with $V/V_R \geq 1.0$

$$\frac{1}{\mathcal{H}}\frac{\partial^2 R}{\partial t^2} = -V_0\left(\frac{R}{r}\right)^2\left[\beta\frac{\partial T}{\partial r} + \gamma\frac{\partial V}{\partial r} + \frac{\partial q}{\partial r}\right] \tag{4a}$$

2. Liquid phase with $V/V_R < 1.0$

$$\frac{1}{\mathcal{H}}\frac{\partial^2 R}{\partial t^2} = -V_0\left(\frac{R}{r}\right)^2\left[\beta\left(\frac{V_R}{V}\right)^2\frac{\partial T}{\partial r} - \frac{V_R^2}{V^3}\left(2\alpha + 2\beta T + \gamma V\right)\frac{\partial V}{\partial r} + \frac{\partial q}{\partial r}\right] \tag{4b}$$

3. Vapor phase

$$\frac{1}{\mathcal{H}}\frac{\partial^2 R}{\partial t^2} = -V_0\left(\frac{R}{r}\right)^2\left\{\beta\left[1 + \frac{0.712\beta V_0}{R^*}\left(\frac{T_c}{T}\right)^2\right]\frac{\partial T}{\partial r} - \frac{\beta^2 T}{R^*}\frac{\partial V}{\partial r} + \frac{\partial q}{\partial r}\right\} \tag{4c}$$

10.3.5.3 Conservation of Energy

The conservation of energy equations, derived from the equation of state, (3a) (See Section 10.3.5.7) are as follows:

1. Liquid phase with $V/V_R \geq 1.0$

$$\kappa_{VL}\frac{\partial T}{\partial t} + (\alpha + \gamma V + q)\frac{\partial V}{\partial t}\mathcal{R} = VQ + Vk\nabla^2 T \tag{5a}$$

2. Liquid phase with $V/V_R < 1.0$

$$\kappa_{VL}\frac{\partial T}{\partial t} + \left[\left(\frac{V_R}{V}\right)^2(\alpha + \gamma V) + q\right]\frac{\partial V}{\partial t}\mathcal{R} = VQ + Vk\nabla^2 T \tag{5b}$$

3. Vapor phase

$$\kappa_{VV}\frac{\partial T}{\partial t} = VQ + Vk\nabla^2 T - q\frac{\partial V}{\partial t}\mathcal{R} \tag{5c}$$

4. Solid (original) phase

$$c_{vs}\frac{\partial T}{\partial t} = VQ + Vk\nabla^2 T \qquad (5d)$$

10.3.5.4 Conservation of Mass

The conservation of mass equation has the form:

$$V = V_0\left(\frac{R}{r}\right)^2\frac{\partial R}{\partial r} \qquad (6)$$

10.3.5.5 Pseudo-viscous Pressure - (1) *

During a violent excursion a shock wave will move through the configuration. In order to spread the shock front out over a large area for numerical calculations, a pseudo-viscous pressure term is introduced which obeys the following equations and ranges of applicability:

$$q = \frac{(a\Delta r)^2}{V_0^2 V}\left(\frac{\partial V}{\partial t}\right)^2\left(\frac{r}{R}\right)^4 \qquad \text{if } \frac{\partial V}{\partial t} < 0 \qquad (7)$$

$$q = 0 \qquad \text{if } \frac{\partial V}{\partial t} \geq 0$$

10.3.5.6 Melting

It is assumed that melting occurs at constant temperature (T_m). During the constant temperature process heat is being added as a result of the nuclear characteristics described by (1) and (2). (5) is not utilized during the melting process since $\frac{\partial T}{\partial t} = 0$.

Once that an amount of heat equal to the heat equal to the heat of fusion $\left(Q_F \leq \sum_{j=m}^{n} Q_j^{\ell *}\right)$ has been added the material is assumed to have completed the melting process.

* See Reference in Bibliography.

10.3.5.7 Vaporization

It is assumed that once the molten material has exceeded its critical temperature (T_c) that a transition has been made from the liquid (molten) phase to the vapor phase. In addition, when the liquid phase pressure exceeds the value [2]:

$$p > 10^{\left[2.72 + \log_{10} p_c - 2.72\left(\frac{T_c}{T}\right)\right]} \qquad (8)$$

(liquid saturation line) a transition takes place between the liquid and vapor phases. This transition is approximated during a discrete time interval by a heat addition at constant temperature. The heat addition at constant temperature, as a result of the coupled equations (1), (4), and (2) yields a new pressure at the end of the time interval.

A new temperature, constant for the next discrete time interval, is found by inserting the new pressure into the liquid saturation line equation [8]:

$$T = \left[\frac{2.72\, T_c}{2.72 - \log_{10}\left(p/p_c\right)}\right] \qquad (8a)$$

The percent of the total volume vaporized during the time interval can be represented by the equation:

$$\% = \frac{\sum_{\ell=v}^{n} Q_j^{\ell *}}{Q_v} \times 100 \qquad (9)$$

where Q_v is the heat of vaporization and Q_j^n represents heat added during the discrete time interval.

The incremental vaporization process described above is shown schematically in Figure 10.1.

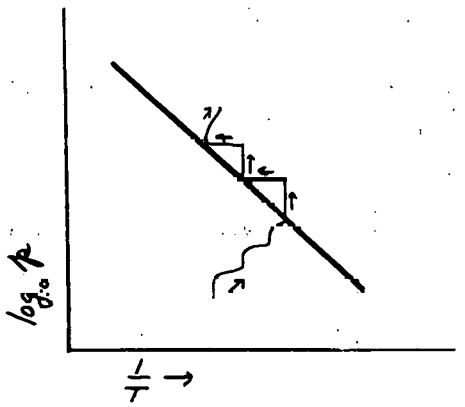

FIGURE 10.1

10.3.5.7 Equation of State

The equation of state for the liquid and vapor phases is assumed to have the form (2), (3), (4), (5):

$$p = \left[\alpha + \beta T + \gamma V\right]\left(\frac{V_R}{V}\right)^n + g \qquad (10)$$

where n = 0 for the vapor phase

n = 0 for the liquid phase when $V/V_R \geq 1.0$

n = 2 for the liquid phase when $V/V_R < 1.0$

Coefficients of (10) for the liquid phase have the form (3):

$$\alpha = \frac{1 - \bar{\alpha} T_R}{\kappa_T}, \quad \beta = \frac{\bar{\alpha}}{\kappa_T}, \quad \gamma = -\frac{1}{V_R \kappa_T} \qquad (11)$$

Coefficients of (10) for the vapor phase have the form [2]:

$$\alpha = \gamma = 0 \quad , \quad \beta = \frac{R^*}{\left[V + 0.356\, V_c \left(\frac{T_c}{T} \right)^2 \right]} \tag{12}$$

where

$$V_c = R^* T_c / p_c$$

From thermodynamics we have the relationship:

$$c_v = \left(\frac{\partial e}{\partial T} \right)_v = \phi + \varepsilon T \tag{13}$$

where ϕ and ε are constants.

Integrating (13) we obtain:

$$e = \phi T + \frac{\varepsilon T^2}{2} + f(V) \tag{14}$$

From the second law of thermodynamics we have:

$$\frac{1}{T} (de + p\, dV) = ds \tag{15}$$

Substituting values from (10 and (14) into (15) we obtain for a constant entropy process:

$$f(V) = \int_{V_0}^{V} \left[\frac{\alpha V_R^n}{V^n} + \frac{\gamma V_R^n}{V^{n-1}} + g \right] dV \tag{16}$$

For the liquid phase with $V/V_R \geq 1.0$ (16) becomes

$$f(V) = \alpha V + \frac{1}{2} \gamma V^2 + g V + \text{Const.} \tag{17a}$$

For the liquid phase with $V/V_e < 1.0$ (16) becomes:

$$f(V) = -\alpha \frac{V_e^2}{V} + \gamma V_e^2 \ln V + g V + \text{Const.} \tag{17b}$$

For the vapor phase (16) becomes:

$$f(V) = g V + \text{const.} \tag{17c}$$

Substitution of (17) and (14) into the conservation of energy equation:

$$\frac{\partial e}{\partial t} = VQ + kV\nabla^2 T \tag{18}$$

yields (5) of Section IV-C above.

10.3.5.8 Transient Nodes

In the numerical approximation of the coupled, spherically symmetric, set of equations, the space coordinates will be divided into a series of radial intervals or nodes. Each node represents a spherical segment of thickness Δr. Each spherical segment will be represented by an average temperature, specific volume, pressure, heat generation, delayed neutron density and pseudo-viscous pressure. Once that a node (spherical segment) has reached the melting temperature and had heat equal to the heat of fusion added, that node is considered to be in the liquid phase. The molten node makes a transition from the original homogeneous state to a center molten sphere, either immediately, or (through a time delay option) at a specified time after melting has occurred. This

transition is made either under the force of a free fall acceleration (the gravitational constant being specified) or, (under the influence of a constant velocity option) at constant velocity (see also time delay option). The transient node is in motion, inward, until such a time as contact is made with the center molten sphere. Once that contact has been made the node acts under the influence of the coupled momentum equation.

Equations relating the transient node to the coupled equation coordinate system are:

1. Transient Node Radius

$$R = R_o - g\,(t^n - t_j^m)^2/2 \qquad (19a)$$

where t^m is the time of melting and t^n a point in time after melting.

2. Transient Node Radius with Options

a. Constant velocity option

$$R = R_o - I\,(t^n - t_j^m) \qquad (19b)$$

b. Time delay option

$(t^n - t_j^m)$ in (19a) and (19b) are replaced with:

$$\begin{aligned} & t^n - (t_j^m + t_j^{DT}) && \text{for } t^n > t_j^m + t_j^{DT} \\ & R = R_o && \text{for } t^n \le t_j^m + t_j^{DT} \end{aligned} \qquad (19c)$$

3. Transient Node Gap

The value of the difference between the inside

diameter of the transient node and the outside diameter of the center sphere can be calculated from the following relationships:

a. Acceleration node

$$G_j^n = R_j^o - g\frac{(t^n - t_j^m)^2}{2} - \left(\frac{V_j^n}{V_j^o}\right)\frac{(R_j^o)^2(R_{j+1}^o - R_{j-1}^o)}{\left[2R_j^o - g(t^n - t_j^m)^2\right]^2} - \quad (20a)$$

$$- R_{j-1}^n - \frac{1}{4}\left(\frac{V_{j-1}^n}{V_{j-1}^o}\right)\left(\frac{R_{j-1}^o}{R_{j-1}^n}\right)^2(R_j^o - R_{j-2}^o)$$

b. Constant velocity option

$$G_j^n = R_j^o - I(t^n - t_j^m) - \left(\frac{V_j^n}{V_j^o}\right)\frac{(R_j^o)^2(R_{j+1}^o - R_{j-1}^o)\ 1/4}{\left[R_j^o - I(t^n - t_j^m)\right]^2} - \quad (20b)$$

$$- R_{j-1}^n - \frac{1}{4}\left(\frac{V_{j-1}^n}{V_{j-1}^o}\right)\left(\frac{R_{j-1}^o}{R_{j-1}^n}\right)^2(R_j^o - R_{j-2}^o)$$

c. Time delay options

(19a) holds for both (20a) and (20b)

4. Equation of State

The transient node specific volume for the gap equations (20a), (20b), (20h), (20hh) and (20s) will be determined from the ambient pressure ($p_{amb.}$) and the equation of state for a liquid with

$$V_j^n = \frac{p_{amb} - \alpha - \beta T_j^4}{\gamma} \quad (10a)$$

5. Velocity

The transient node velocity at any point in time t^n after melting has the value:

a. Acceleration node

$$\frac{\partial R}{\partial t} = g\left(t^n - t^m\right) \tag{20d}$$

b. Constant velocity option

$$\frac{\partial R}{\partial t} = I \tag{20e}$$

c. Time delay option

(20d) changes to

$$\frac{\partial R}{\partial t} = g\left[t^n - \left(t_j^m + t_j^{DT}\right)\right] \quad \text{for } t^n > t_j^{DT} + t_j^m$$

$$\frac{\partial R}{\partial t} = 0 \quad \text{for } t^n \leq t_j^{DT} + t_j^m \tag{20f}$$

6. Transient Node Specific Volume

The specific volume for the transient node, to be used in equations (1), (5a) and (2) will have the form:

$$V_j^n = V_j^0 \left(\frac{R_j^n}{R_j^{n-1}}\right)^2 \left(\frac{R_{j+1}^{n+1} - R_{j-1}^{n+1}}{R_{j+1}^n - R_{j-1}^n}\right) \tag{20g}$$

10.3.5.9 Center Sphere Nodes

A transient node compacts to fill the void or flow areas. The specific volume (V) of the transient node is determined by (10a). The change between a transient node and the center sphere node takes place when the gap (20a) $G_j^n \leq G_{Lim}$.

The velocity for the transient node meeting the conditions $G_j^n \le G_{Lim}$ is given by (20d) at time t^n when the gap limit G_{Lim} is reached.

Node number 1 (the innermost node) in making a transition toward the center of the sphere has a gap check against R = o. The equation for this relationship has the form:

$$G_1^n = R_1^o - g\frac{(t^n - t_j^m)^2}{2} - \left(\frac{V_1^n}{V_1^o}\right)\frac{(R_1^o)^2 R_2^o}{[2R_1^o - g(t^n - t_1^m)^2]^2} \qquad (20h)$$

for the normal node. The constant velocity option has the form:

$$G_1^n = R_1^o - I(t^n - t_1^m) - \left(\frac{V_1^n}{V_1^o}\right)\frac{(R_1^o)^2 R_2^o}{4[R_1^o - I(t^n - t_1^m)]^2} \qquad (20hh)$$

Modification of (20h) and (20hh) for the time delay option is described in Section 10.3.5.8 above.

10.3.5.10 Total Energy

1. Heat Generated

The total heat generated from time t = o to t^N has the form:

$$Q_T = \sum_{n=1}^{N} Q_T^n \qquad (20i)$$

where

$$Q_j^{n*} = Q_j^n (t^n - t^{n-1}) V_j^{n-1} \tag{20ij}$$

$$Q_j^n = \sum_{j=1}^{J} Q_j^{n*} W_j^o \tag{20j}$$

and

$$W_j^o = \frac{4\pi}{3 V_j^o} \left\{ \left(\frac{R_{j+1}^o + R_j^o}{2} \right)^3 - \left(\frac{R_{j-1}^o + R_j^o}{2} \right)^3 \right\} \tag{20k}$$

2. Kinetic Energy

The total kinetic energy present at the end of time interval t^n is:

$$K_T^n = \frac{1}{2MM} \sum_{j=1}^{J} W_j^o \left(\frac{R_j^n - R_j^{n-1}}{t^n - t^{n-1}} \right)^2 \tag{20l}$$

10.3.5.11 Variable Cross-Sections

1. The absorption cross-section Σ_{aj} in (22) and (32) has the form:

$$\Sigma_{aj}^n = A_j \qquad \text{for} \leq t_{aj}^{DT}$$

$$\Sigma_{aj}^n = A_j + B_j (t^n - t_{aj}^{DT}) \qquad \text{for } t^n > t_{aj}^{DT} \tag{20m}$$

where A_j and B_j are input quantities.

2. Doppler cross-section Σ_{Dj} in (22) and (32) has the form:

$$\Sigma_{Dj}^{n+1} = \frac{1}{E_j + F_j \ln T_j^n} \tag{20n}$$

where $A_j = 0$ (in 20 m)

$$E_j = \frac{1}{\Sigma^o_{aj}}\left[b \ln T^o_j + 1\right]$$

$$F_j = -\frac{b}{\Sigma^o_{aj}}$$

and b represents the coefficient in the Doppler coefficient equation $\frac{\Delta k}{k \cdot \Delta T} = \frac{-b}{T}$ (k is the reactivity).

10.3.5.12 Outer Gap Check

When an overlap exists between the inside diameter of the lowest numbered node not yet melted (j = x) and the outside diameter of node j = x-1 the normal mode of operation will be to stop the problem. An option will assume that all non-melted nodes are governed by the conservation of momentum equation. The following equations hold for the option.

1. (34a) with

$$\alpha = \frac{\mu}{\kappa_T}\left(1 - \bar{\alpha} T^o_j\right)$$

$$\beta = \frac{\bar{\alpha}\mu}{\kappa_T} \qquad (20q)$$

$$\gamma = -\frac{\mu}{\kappa_T V^o_j}$$

where μ is an input constant.

2. (33a) with (20q) and κ_{VS} replacing κ_{VL}.

3. (32), (26), (27), (35), (36), and (37)

No node checks will be necessary on nodes x, x + 1, ··· , J for equation of state considerations (i.e. no check of V/V_e, T^m or liquid saturation line evaluation). Initial conditions for option:

$$\frac{\partial R_j^n}{\partial t} = 0$$

$$V_j^n = V_j^o \qquad \text{(20r)}$$

for all nodes x, x + 1, ··· , J.

Boundary conditions for the option

$$V_J^n = V_J^o \quad \text{for all time.}$$

The outer gap check equation has the form:

$$U_x^n = \frac{1}{2}\left(3R_x^o - R_{x+1}^o\right) - R_{x-1}^n - \frac{V_{x-1}^n W_{x-1}^o}{\rho\pi\left(R_{x-1}^n\right)^2} \qquad \text{(20s)}$$

and the option limits are:

$$-U_{Lim} > U_x^n \qquad \text{(20t)}$$

10.3.6 Initial and Boundary Conditions

10.3.6.1 Initial Conditions

1. Nuclear Equations (1) and (2) - Initial conditions for (1) and (2) are derived from the reactor operating point just prior to the excursion. Values of

V, Q, T, C and R will be given for each node in the configuration.

2. Energy Equation (5) - Initial conditions for (5) will be derived from the reactor operating point just prior to the excursion. Values of V, Q, T and R will be given for each node of the configuration.

3. Momentum Equations (4) - Initial conditions for (4) will be derived from the conditions

V_j^n (10a), T_j^n , $\frac{\partial R_j^n}{\partial t}$,

and Q_j^n of the transient node at the point in time when the gap $G_j^n \leq G_{lim.}$ for a transient node.

4. Pseudo-viscous Pressure (7) - Initially $q_j^n = 0$ for all molten nodes.

10.3.6.2 Boundary Conditions

1. Nuclear Equations (1) and (2)

   a. $Q_{J+1} = M$ at the outer diameter of the initial homogenized sphere. M is a constant prescribed in the input. Also

   $R_{J+1} = 1/2(3R_J - R_{J-1})$, $q_{J+1} = o$, $V_{J+1} = o$,

   $T_{J+1} = 1/2\ (3T_J - T_{J-1})$.

   b. Symmetry about the spherical coordinate origin

   $Q_o = Q_1$, $T_o = T_1$, $V_o = V_1$, $q_o = q_1$, $R_o = -R_1$

2. Energy Equations (5) - In the form of (5) with $\nabla^2 T = o$ (i.e., no heat conduction) the only boundary condition required for (5) is symmetry about the origin. $Q_o = Q_1$, $T_o = T_1$, $V_o = V_1$, $q_o = q_1$, $R_o = -R_1$.

3. Momentum Equations (4)

   a. Symmetry about the origin $Q_o = Q_1$, $T_o = T_1$, $V_o = V_1$, $q_o = q_1$, $R_o = -R_1$.

   b. The outermost center molten sphere node specific volume is determined from the equation of state for the liquid and the specified ambient pressure $p_{amb.}$ (eqn. (10a)).

   Also $T_{D+1} = 1/2\ (3T_D - T_{D-1})$, $V_{D+1} = o$, $q_{D+1} = o$, $R_{D+1} = 1/2\ (3R_D - R_{D-1})$, where the subscript D represents the outermost node of the center molten sphere.

4. Pseudo-viscous Pressure (7)

   a. Symmetry about the origin $q_o = q_1$, $R_o = -R_1$.

   b. The outermost center molten sphere Pseudo-viscous pressure $q_D^n = 0$.

10.3.7

Notation:

a Pseudo-viscous pressure coefficient n. d.

A,B Absorption coefficient constants

C Delayed neutrons Neutrons/in^3 (Neutrons/Cm^3)*

c_v Specific heat at constant volume Btu/#-^oR (Cal/kgm-^oK)

c Speed of sound in/sec. (Cm/sec)

D Diffusion coefficient in. (Cm)

e Internal Energy Btu/# (Cal/kgm)

G Limiting inner gap in. (Cm)

g Acceleration constant in/sec^2 (Cm/sec^2)

H Generation shutdown limit Btu/in^3-sec (Cal/Cm^3-sec)

I Compaction velocity in/sec. (Cm/sec)

K Kinetic energy in. # (kgm Cm)

k Thermal conductivity Btu/in-^oR-sec (Cal/Cm-^oK-sec)

M Boundary heat generation rate Btu/in^3-sec (Cal/Cm^3-sec)

p Pressure #/in^2 (kgm/Cm^2)

Q Heat generation rate Btu/in^3-sec (Cal/Cm^3-sec):

q Pseudo-viscous pressure #/in^2 (kgm/Cm^2)

r Fixed radial coordinate in. (Cm)

R Moving radial coordinate in. (Cm)

R* Universal gas constant $R^* = R^\Delta / \mu$ where $R = \frac{\text{in-\#}}{\text{\# mol-}^oR}$ $(\frac{\text{Cm-kgm}}{\text{kgm mol-}^oK})$, μ = molecular weight.

s Entropy Btu/#-^oR (Cal/kgm-^oK)

T Temperature ^oR (^oK)

t Time sec.

U Outer gap limit in. (Cm)

v Mean neutron velocity in/sec (Cm/sec)

V Specific volume in^3/# (Cm^3/kgm)

---

* kgm, Cm, Cal, ^oK, sec. units may be used throughout with the proper designation of Ж, Д, and Я.

W Weight # (kgm)

X,Y,Z Option numbers

α, β, γ Equation of state coefficients

$\bar{\alpha}$ Coefficient of thermal expansion for liquid phase in/in-^{o}R (Cm/Cm-^{o}K)

∇ Del operator

κ_T Isothermal compressibility $in^2/\#$ (Cm^2/kgm)

λ Decay constant

ν Multiplication coefficient

ϕ, ε Specific heat constants

Σ Macroscopic cross-section in^{-1} (Cm^{-1})

Π Conversion factor (2.75×10^{-14} for U^{235}) Btu/fission (6.93×10^{-12} Cal/f for U^{235})

$\mathcal{H}$ Gravitational constant (386) in/sec^2 (980.7 Cm/sec^2)

$\mathcal{K}$ Compressibility modification constant n.d.

$\mathcal{J}$ Equivalent energy constant (1.072×10^{-4}) Btu/in-# (0.0266 Cal/Cm-kgm)

Subscripts:

a Absorption

amb. Ambient

c Critical

D Doppler

DN Delayed Neutron

f Fission

j Space interval

J Total nodes

Lim Coefficient limit

L Liquid phase

O Initial phase

R Reference

S Solid Phase

T Total

v Vapor phase

Superscripts:

m Melting time index

n Time index

DT Time delay period

10.4 Critical Facility Design

During this reporting period, the conceptual design of the Mixed Spectrum Critical Facility was initiated for the purposes of cost estimating and preliminary hazards reviews. The proposed design has been reviewed by the Vallecitos Safeguard Council. A description of the facility and hazards evaluation follows:

10.5 Mixed Spectrum Superheater Critical Experiment Preliminary Hazards Evaluation

10.5.1 Description of the Core

The Mixed Spectrum Superheater reactor will consist of a two region core. The inner region will be made up of UO_2 fuel enriched to approximately 20% in U-235 and clad with stainless steel. The volume fraction of UO_2 will be approximately 50%. The outer region will be made up of a conventional boiler design utilizing 3% enriched UO_2 fuel, stainless steel clad, moderated with light water.

The reference design for the Mixed Spectrum Superheater Power Reactor calls for the steam which is generated in the outer boiler region to be superheated by passing downward through the fast core.

Not shown in Figure 10.1 are the fast buffer region and the thermal buffer region which are included to prevent peaks at the fast-thermal interface. These regions will be included in the critical experiment core.

The critical experiment (MSSCE) will operate at less than 200 watts and will not be pressurized. The MSSCE core support structure and fuel element will be designed to make the conventional fast core accidents incredible. The fast core fuel elements are supported from above (rather than resting on a solid support plate) so that falling objects cannot compress the core and so that melting fuel cannot accumulate in a high density configuration. Fuel element loading is from below and by a loading machine so that the maximum rate of fuel addition is mechanically limited. The fuel bundles are supported by fusible links of U-235 metal which melt in an accident and permit the fuel to fall from the reactor. A cone directly under the core prevents reassembly on impact. Sketches of the proposed equipment are attached.

Control of the fast core is by motion of six fuel bundles in and out of the bottom of the fast core (4 safety - 2 control). The thermal core is regulated by water height and/or control rods. Procedures and interlocks will require going critical on fast core control rods after water is in thermal core. Detailed loading and operating procedures will be reviewed by VALSG prior to operation of the facility.

The fast core can and thermal core can will be separated by a small air gap so that water cannot leak into fast region.

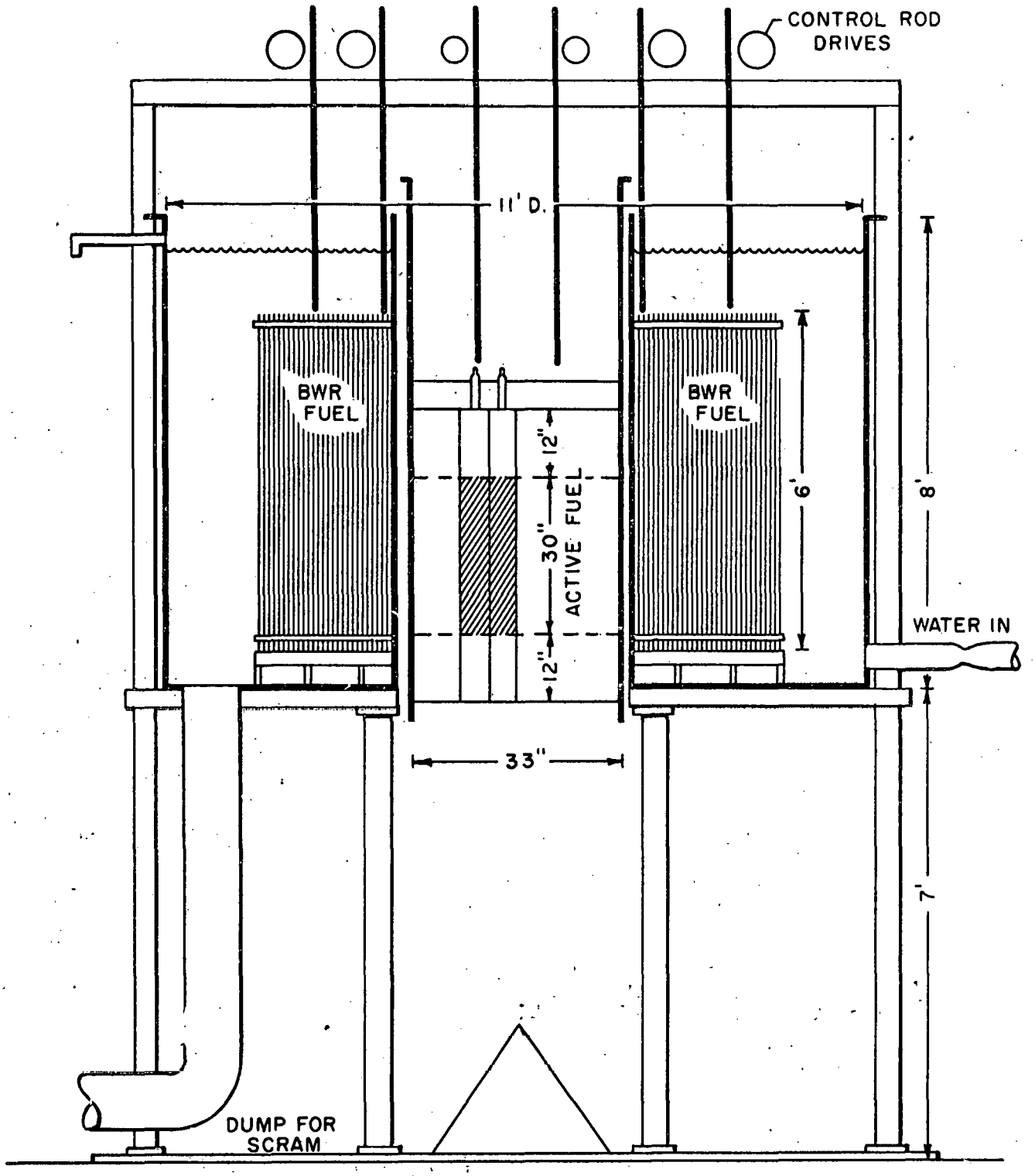

FIGURE 10.2 SKETCH SHOWING ELEVATION OF PROPOSED MSSR CRITICAL EXPERIMENT FACILITY.

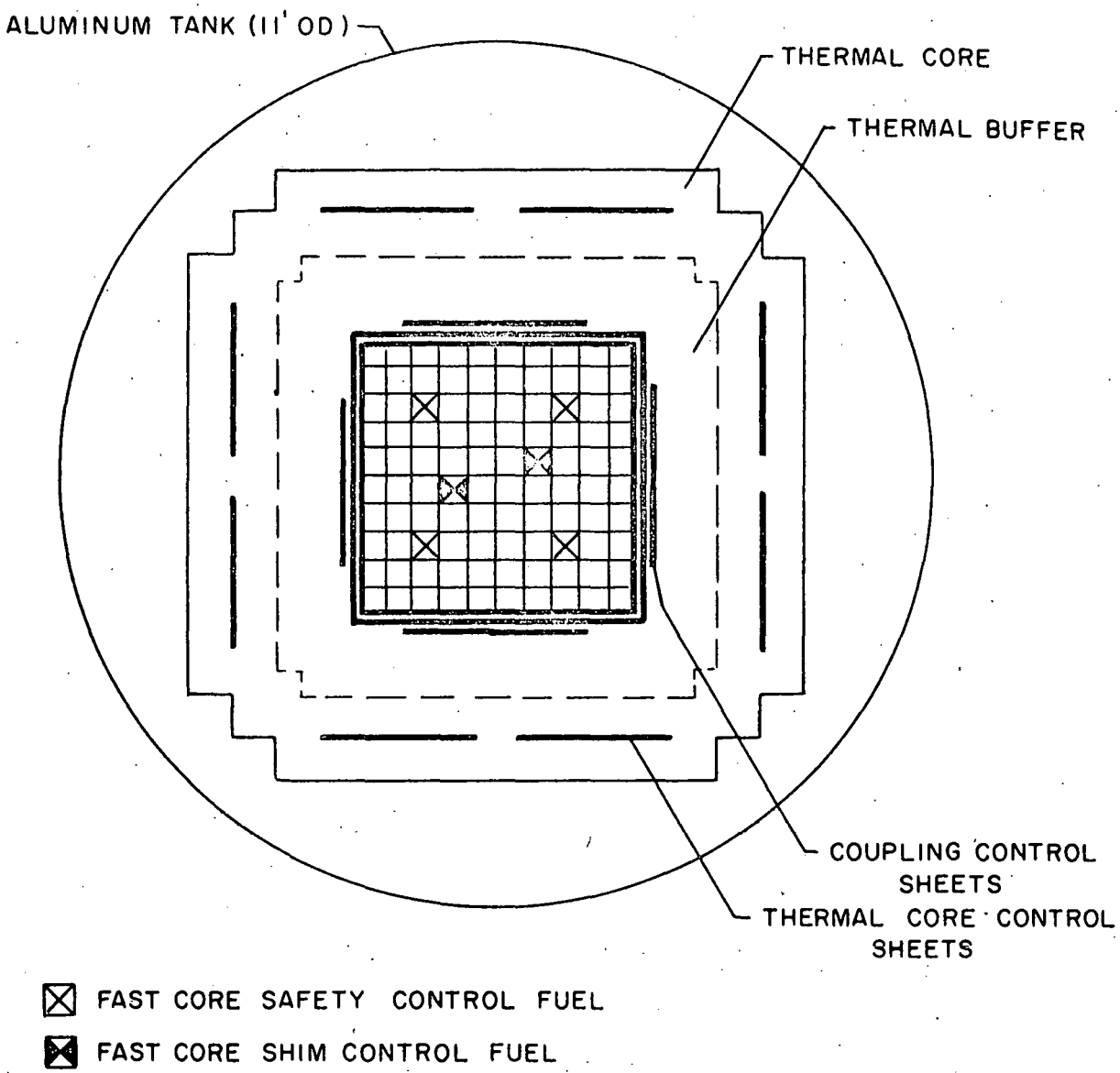

FIGURE 10.3 CORE CROSS SECTION OF PROPOSED MSSR CRITICAL EXPERIMENT FACILITY

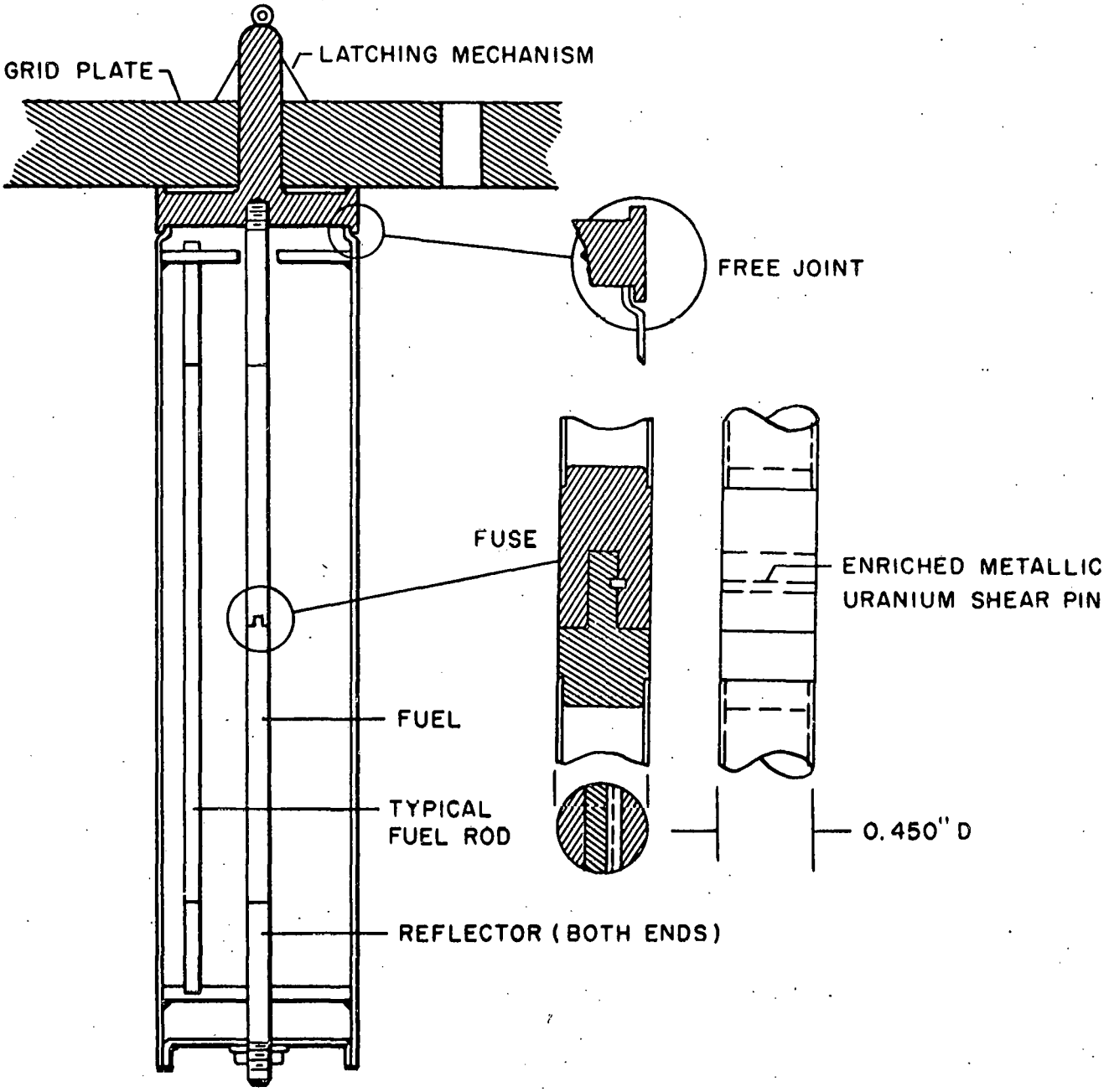

FIGURE 10.4 SCHEMATIC DIAGRAM OF FAST CORE FUEL ELEMENT FOR MSSR CRITICAL EXPERIMENT.

10.5.2 Differences Between the New Core and the Old Core

The differences between the hazards associated with the Mixed Spectrum Superheater core and the previously run cores are due to the presence of a fast region in the center of the core. This region is not cooled, it has a smaller Doppler coefficient and a shorter lifetime than the old cores. Further, because it is a fast core the plausibility of a catastrophic explosion accident of the type possible in a small metal assembly must be investigated in detail. This point in discussed in the next section.

In evaluating the maximum credible accident for the old cores the ultimate shutdown was always boiling; the clad integrity was maintained; and the reactor, if not completely shut down after the excursion, could operate indefinitely in the boiling condition, self-controlled and at a relatively low power.

For the new core there is no moderator in the fast region; hence, the ultimate shutdown is disassembly of the core, although clad integrity is maintained. Because there is no cooling in the fast region there is no steady state operation corresponding to the boiling condition in the old cores.

Although the Mixed Spectrum Superheater core does have a light water moderated region, the reactivity effects in that region have only a small effect on the over-all reactivity

of the core. It follows that if excess reactivity is added to the thermal region the reactor will shut down like a water moderated reactor. If, however, excess reactivity is added to the fast region the boiling of the water in the thermal region cannot be relied upon to shut down the reactor. This memorandum deals only with reactivity additions to the fast region.

10.5.3 Excursion Types

Nuclear excursions are caused by reactivity addition. The discussion of maximum credible accidents falls naturally into two parts. The first part (10.5.4) covers the effects of reactivity additions, and the second part (10.5.5) covers the credibility of high rates of reactivity additions.

The effect of reactivity addition depends upon the initial power level of the reactor. At very low initial power levels the statistical assembly accident becomes possible. This refers to an accident which can occur with a small metal assembly which has a very small inherent source of neutrons. In such a reactor a large amount of reactivity can be added during the time in which no neutrons happen to be present. The source of neutrons in a small fast assembly due to spontaneous fission of U-238 and U-235 is about 10^{-3} of the source present in the Mixed Spectrum Superheater critical core. Therefore the time required to establish a persistent chain reaction in the Mixed Spectrum Superheater critical

core will be about 1/1000 that of a small fast assembly. For small fast assemblies the time between reactivity addition and beginning of neutron multiplication has been observed to be as long as a few seconds. This means that the statistical lag between reactivity addition and the following of this by the neutron flux will be of the order of a few milliseconds in the Mixed Spectrum Superheater core. Thus the statistical assembly accident cannot occur in the Mixed Spectrum Superheater core.

We will consider accidents which are caused by ramp additions of reactivity. The inherent source of neutrons is small. Hence the reactor will remain at a very low power level for some time after the initiation of the ramp. By the time the power reaches a level high enough to heat the fuel the reactivity may exceed prompt critical. The maximum power of the resulting excursion is limited by the prompt negative fuel temperature coefficient, i.e., the Doppler effect.

Accidents which are caused by a very rapid ramp, i.e., a step increase in reactivity, can be tolerated if only a limited amount of reactivity can be inserted. The amount which can be safely inserted is approximately equal to the maximum reactivity which results from the fastest permissible ramp. For the Mixed Spectrum Superheater this amount is likely to be specified as a limitation on experimental apparatus such that only $1.00 can be credibly inserted rapidly.

10.5.4 Calculated Excursions

The maximum tamperature of the fuel is a function of the ramp rate and the Doppler coefficient. Three ramp rates have been investigated with the TER code to determine the history of the power during excursions. For these calculations the Doppler coefficient at room temperature was assumed to be 10×10^{-6} k/°C and 1/T dependence of Doppler coefficient was assumed.

The only shutdown mechanism assumed in the calculation is the Doppler effect. Actually, the reactor will shut down by disassembly of the core due to melting of a U-235 metal pin in each fuel bundle. Part of the core will fall thereby decreasing reactivity. Approximately 0.1 second after melting the fuel pin is required for 2 inches of motion, at which point the reactivity decrease becomes significant. The three ramp rates, which were investigated, are .05, 1, and 10 $ per second. The Table below summarizes the results of the TER problems.

Ramp Rate	Time to 500°F	Temperature 0.03 seconds after 500°F	Temperature 0.1 seconds after 500°F
.05 $/sec	20.5 sec	530°F	600°F
1 $/sec	1.2 sec	12000°F	15000°F
10 $/sec	.16 sec	120000°F	160000°F

The 10 $/sec accident is included for completeness but is not considered credible.

We can see from the above Table that there is not a great difference between the temperature at .03 seconds and at .1 seconds so that spring loading to obtain an acceleration of 10 g would not significantly increase the safety of the reactor.

The vaporization temperature is the upper limit to the safe temperature of the fuel. Above that temperature an explosion is possible. For UO_2 the vaporization temperature is approximately 5700°F. Hence, we estimate that, for a Doppler coefficient of 10×10^{-6} k/°C, a ramp of approximately 6$/sec would not cause an explosion. For some experimental core loadings, the Doppler coefficient at room temperature may be as low as 5×10^{-6} k/°C; then, a ramp of approximately 2$/sec would not cause an explosion. It is expected that, in the AEC License Application Amendment, the maximum credible accident will have a ramp rate of 0.5 $/sec and the minimum negative calculated value of the Doppler coefficient at room temperature will be 5×10^{-6} k/°C.

10.5.5 Maximum Credible Accident

The credibility of rapid insertion of reactivity depends on consideration of the mechanisms of reactivity addition in light of the proposed design.

Large rates of reactivity addition require large velocities. These velocities can conceivably arise from falling objects. Heavy equipment falling on the core from heights greater

than about 10 ft. could cause rapid compression for a core supported from below; however, the Mixed Spectrum Superheater core has no bottom support. The fuel will be hung from an upper grid sheet. The possibility of the entire core falling intact on a flat surface and compressing is not considered to be credible because of concrete cone under the core.

Objects falling on top of the core do not add reactivity by improved neutron reflection because the fast core has a thick U-238 reflector on top and bottom.

Fuel elements cannot be inserted from above through the upper support plate so that falling fuel cannot enter the core intact. Fuel elements will be loaded from below and inserted with a mechanical lift due to their heavy weight (about 100 lbs.). Maximum ramp is limited by the mechanical limitation of the lift.

Because of the core design the conventional fast reactor meltdown accident in which a small accident melts the core which flows into a supercritical configuration is not considered credible.

Falling water can enter the fast core only by leaking around the guide pins in the upper grid sheet. The resulting ramp is small.

The assumption is made that a core can be designed which cannot be jammed. Clearances will be large enough to allow for all plausible warpages and distortions. The loading

machine will be driven by a torque limited motor. Several tentative designs have been suggested which appear to satisfy the requirements. However, the final design will be justified before the VALSG.

All intentional reactivity addition such as fuel loading, control rod loading, etc., can be mechanically limited to less than 0.1 $/sec.

Consideration of several plausible sequences of events has led to the following Maximum Credible Accident:

1. By violation of procedure, the fast core has been changed unknowingly to be near critical in the shutdown condition.
2. As water is pumped into the thermal core for a standard start up, the reactor goes critical (not possible without violation of procedures). The thermal buffer is worth about $10 over a 20 cm region of the fast core. The water fill rate is 1.1 cm/sec. This amounts to a ramp of 0.5 $/sec.
3. It is assumed that period and power level scrams fail, but that the water pump continues adding water.
4. The resulting accident is less severe than the calculated accident of $1.0/sec ramp in the above Table. In that accident, reactor reached $1.16 reactivity when appreciable heating began. Doppler limited the fast rise in temperature to 1200°F at

1.2 sec after reactor became critical. The U-235 fuses melted and released the fuel bundles at about 1.2 seconds. The accident is terminated by falling fuel about 0.1 seconds later, by which time the fuel temperature has risen to 1500°F.

5. The accident size is approximately 1000 MWS.
6. There is no explosion.
7. The fuel clad does not melt (MP 2500°F). Fission product release is limited to that of the melted fuses (amounting to less than 0.3% of the U-235 in the core). The small amount of fission product contamination is contained in cell by standard particulate filter with the exception of the inert gases and iodine. The dispersed fission products in the cell amount to about one curie after one week.
8. The U-235 fuse pins are at the mid-plane of the core. In this relatively fast accident, the heat generated in the pins by fission does not have time to dissipate and the temperature of the pins is related to the temperature of the oxide fuel simply be the respective enrichments and heat capacities. When the fuel reaches 5000°F, the pins reach the melting temperature of uranium metal.

10.5.6 Conclusions

This discussion considers only those aspects of the MSSR hazards which may be different from existing hazards in the Critical Experiment Facility. The primary difference between

the maximum credible accident for the MSSCE and our other cores is that no moderator is present to carry away heat generated by the accident. Further, there is no steady state operating level comparable to the boiling condition. To circumvent this detail, the MSSCE is fused so that the core drops after reaching the fuse temperature to terminate an excursion. As in our other cores, the accident size is limited by Doppler coefficient. Our analysis indicates that for the range of accidents considered the shorter lifetime of the fast core does not contribute to the nuclear hazard. The analysis presented in this memorandum indicates that Mixed Spectrum Superheater Critical Experiments can be safely done in the VAL Critical Experiment Facility.